Universidad de Granada

Departamento de Física Teórica
y del Cosmos

Nuclear activity and interstellar medium in a sample of isolated galaxies

José Sabater Montes
Departamento de Astronomía Extragaláctica,
Instituto de Astrofísica de Andalucía-CSIC

Tesis Doctoral

CONSEJO SUPERIOR
DE INVESTIGACIONES
CIENTÍFICAS

Editor: Editorial de la Universidad de Granada
Autor: José Sabater Montes
D.L.: GR 2282-2009
ISBN: 978-84-692-3071-8

Departamento de Física Teórica
y del Cosmos
Universidad de Granada

Departamento de Astronomía Extragaláctica
Instituto de Astrofísica de Andalucía - CSIC

Nuclear activity and interstellar medium in a sample of isolated galaxies

Memoria presentada por:

José Sabater Montes

para optar al grado de

Doctor por la Universidad de Granada

Dirigida por:

Lourdes Verdes-Montenegro Atalaya (IAA-CSIC)
Stephane Leon Tanne (IRAM)

Granada, 28 de abril de 2009

Como directora de la tesis titulada *Nuclear activity and interstellar medium in a sample of isolated galaxies*, presentada por **D. José Sabater Montes**,

Dña. Lourdes Verdes-Montenegro Atalaya, Doctora en Ciencias Físicas y Científico Titular del Departamento de Astronomía Extragaláctica del Instituto de Astrofísica de Andalucía - CSIC, y **D. Stephane Leon Tanne**, Doctor en Ciencias Físicas.

DECLARAN:

Que la presente memoria, titulada *Nuclear activity and interstellar medium in a sample of isolated galaxies* ha sido realizada por **D. José Sabater Montes** bajo su dirección en el Instituto de Astrofísica de Andalucía - CSIC. Esta memoria constituye la tesis que **D. José Sabater Montes** presenta para optar al grado de **Doctor por la Universidad de Granada**.

Granada, a 28 de abril de 2009

Fdo:
Lourdes Verdes-Montenegro Atalaya

Fdo:
Stephane Leon Tanne

A Yolanda

Nuclear activity and interstellar medium in a sample of isolated galaxies

José Sabater Montes

28 de abril de 2009

Índice general

Resumen

La evolución de las galaxias depende del entorno. En particular la actividad nuclear, producida por la acreción de materia en el agujero negro supermasivo central, podría verse afectada por dicho entorno. Se piensa que la interacción entre galaxias disminuye el momento angular del gas, provocando su caída hacia el agujero negro central, alimentándolo de este modo. Según esta hipotesis se esperaría un aumento de la actividad nuclear en las galaxias en interacción, sin embargo se encuentran resultados contradictorios. En unos estudios se encuentra que la tasa de actividad nuclear aumenta con la interacción mientras que en otros es independiente de ésta.

Gran parte de las diferencias entre los distintos estudios podría deberse tanto al uso de distintos criterios para la selección de las muestras como a la ausencia de una muestra de referencia. El proyecto AMIGA (Análisis del Medio Interestelar en Galaxias Aisladas; http://amiga.iaa.es/) ofrece una muestra estadísticamente significativa de galaxias aisladas libres de interacción durante un tiempo significativo de su vida. Esta muestra constituye la base para estudiar el efecto de las interacciones sobre la actividad nuclear, el medio interestelar y la formación estelar. El primero de estos aspectos constituye el objeto de estudio de la presente tesis.

Para llevar a cabo el estudio de la actividad nuclear en la muestra AMIGA de galaxias aisladas, hemos usado distintos métodos. Por una parte hemos estudiado la correlación entre la emisión en infrarrojo lejano y en radiocontinuo de las galaxias de la muestra. Pues un exceso de radiocontinuo en esta correlación indica la presencia de un núcleo activo emitiendo a longitudes de onda de radio. También hemos usado el color entre la emisión en infrarrojo medio y lejano, que nos indica la presencia de un candidato a núcleo activo. Asimismo hemos determinado el origen dominante de la ionización del núcleo usando los espectros en visible del Sloan Digital Sky Survey (SDSS). Por último hemos realizado una busqueda en la bibliografía existente del tipo de actividad nuclear que pudieran presentar las galaxias de nuestra muestra.

Se pueden destacar los siguientes resultados. No encontramos galaxias aisladas que muestren un valor superior a un factor 5 de exceso de radio con respecto a la correlacion radio continuo-infrarrojo lejano. Usando el límite más permisivo de un factor 3, encontramos tan solo un 2 % de galaxias con actividad nuclear tipo radio, las tasas más bajas encontradas con respecto a cualquier otra muestra. Comparando con muestras de galaxias situadas en entornos más densos se observa un aumento de la tasa de actividad en longitudes de onda de radio conforme aumenta el número de galaxias en interacción o la cercanía al centro de un cúmulo. Se ha descartado que este cambio en la tasa de actividad provenga de la relación entorno-morfología o entorno-luminosidad. Adicionalmente se ha cuantificado la precisión del método de selección de candidatos a galaxias activas usando el color infrarrojo obteniendo una tasa de acierto del 72.2 % para este método. El número de galaxias activas seleccionadas en base a los datos del Sloan Digital Sky Survey alcanza una tasa del 21.7 % y no muestra

una dependencia tan alta con el entorno en comparación con las galaxias activas tipo radio. El número de galaxias activas que muestran líneas de emisión anchas (Seyfert 1) con respecto al total de galaxias activas es del 10.2 %. Se ha creado un catálogo de candidatos a núcleos activos de galaxias en la muestra de galaxias aisladas. Este catálogo servirá para futuros estudios de los efectos del entorno sobre la actividad nuclear.

Del trabajo realizado en esta tesis doctoral podemos concluir que el entorno es fundamental para producir el fenómeno de la actividad nuclear de tipo radio, observándose un aumento de la actividad conforme aumenta la interacción (galaxias en interacción, pertenencia a un cúmulo, cercanía al centro del cúmulo) para todos los tipos morfológicos y todos los rangos de luminosidades. La muestra AMIGA de galaxias aisladas se confirma como la muestra de galaxias, incluidas las de tipo temprano, más libre de efectos de la interacción, con una tasa de actividad nuclear tipo radio casi nula.

Part I

Introduction

Chapter 1

Introduction to the thesis work

1.1. Active Galactic Nuclei

In 1909 Fath discovered emission lines in one spectrum of the "spiral nebula" NGC 1068. The spectrum was composed of absorption lines ans emission lines like the ones found in gaseous nebulae. Seyfert discovered in 1943 that some galaxies have a point-like nucleus which is the origin of these emission lines. This was the first systematic study looking for this kind of galaxies. Optical emission from these galaxies was similar to the emission of a planetary nebula plus the emission of a typical star like the Sun (spectral type G). Seyfert believed that the width of the emission lines was produced by Doppler widening. With this assumption the velocity of the source of the emission lines in the nuclear region would be of about 8 500 km s^{-1}. This velocity is compatible with a very hot gas moving at high velocities in comparison with the mean value of the velocity of stars and gas in a typical galaxie which is of about 300 km s^{-1}. These galaxies were called Seyfert galaxies.

In the sixties and seventies of the XXth century active galactic nuclei (AGN) took an important role in astronomy studies that is maintained till nowadays. After the initial development of radioastronomy by the pioners like Jansky and Reber the first surveys of the sky looking for accurate possitions of astronomical sources and their optical counterparts started. Smith (1951) obtained accurate positions for Cyg A, Cas A and other sources. Baade & Minkowski (1954) identified using these positions the optical counterparts of Cyg A and Cas A. With these optical identifications it was possible to determine their distances from their optical spectra. The origin of the radio emission was very distorted galaxies with very high radio luminosities, even larger than their optical luminosities. Later, is was discovered a type of galaxies with very bright galactic nuclei in radio, the *radio-stars*. After checked that they were extragalactic sources they were called quasars. Quasars are galaxies similar to Cyg A and Cas A but located at very high distances.

Sandage (1965) found a large population of objects similar in all the aspects to quasars but without a strong radio emission. These objects presents a high emission in the ultraviolet (UV) with respect to the optical. They are called QSO (Quasi-Stellar Objects). It was found a parallelism between QSOs and quasars, located in distant galaxies, and Seyfert galaxies. Later there were new discoveries like a kind of radio-emiting galaxies called BL Lac, galaxies with low ionization nuclear emission regions (LINERs) and other types of galaxies with similar characteristics. All the common features between these galaxies indicates a similar origin of the characteristics for

these objects belonging all to the wide concept of AGN.

The emission of an AGN can be explained by the presence of a supermassive compact nuclear object within the nucleus of the active galaxy. Now it is widely accepted that the origin of the emission comes from a supermasive black hole. This supermasive black hole has to be fed by some mechanism that removes angular momentum from the gas to produce the nuclear activity (see review of Wada 2004, and references therein).

A wide number of different types of AGN exist. A first attempt to classify the types of galaxies has been possible based on the presence or not of broad emission lines and on the presence or not of strong radio emssion. Seyferts 2 and Narrow Line Radio Galaxies (NLRG) have only narrow lines while Seyferts 1, QSO, quasars and Broad Line Radio Galaxies (BLRG) present wide lines. BL Lac objects (blazars), NLRG, quasars and BLRG present strong radio emission and blazars show a unusual optical spectrum. Blandford & Rees (1978) proposed that BL Lac objects were radiogalaxies viewed just in the same axis of the radio-jet emission. Rowan-Robinson (1977) proposed that wide lines were not present in Seyfert 2 galaxies because they were obscured and not due to their absence. Antonucci & Miller (1985) detected the wide emission in the polarized light of the Seyfert 2 galaxy NGC 1068. The unified model for AGN tries to explain all these facts adding the presence of a dust torus around the supermasive black hole and its acretion disk. The presence of wide emission lines would only depend on the point of view of the observer with respect to the orientaion of the dust torus. The strong radio emission would depend on the presence of a radio jet. Hence, all the types of AGN would be explained with an unified model (see Antonucci 1993).

It is usefull to clarify some concepts. The word "activity" is sometimes used to denote both an enhancement in the star formation (usually a starburst) and the effect of the feeding of a supermassive blak hole. The presence of a supermassive black hole does not imply the presence of an AGN. The black hole could be in a quiescent state or the level of activity could be undetectable due to several reasons like a low signal to noise ratio in the measurements. Hence, a non detection in a diagnostic method would not necessarily imply the absence of the black hole nor even the absence of activity. Although some AGN are called radio-quiet the emission at radio frecuencies is a typical characteristic of an AGN. The concept radio-loud AGN is somewhat arbitrary. Some authors define a radio-loud AGN as one with a radio luminosity of more than 10^{23}W Hz^{-1}, others as one with a "significant" presence of radio emission and others as an AGN located at one of the sides of the bimodal population found in the histograms of $L_{\rm B}/L_{\rm radio}$ (Hooper et al. 1995; Kellermann et al. 1989). Due to this ambiguity we will always deffine the physical properties of the AGN with radio emission that we study, avoiding as possible the concept radio-loud.

1.2. Evolution of galaxies and environment

Galaxy evolution depends strongly on the environment. In particular, galaxy-galaxy interactions can induce nuclear activity by removing angular momentum from the gas and, in this way, feeding the central black hole. Hence, a higher rate of nuclear activity would be expected in interacting galaxies. However, different studies of this topic lead to contradictory results. Some works conclude that galaxies hosting an active galactic nucleus (AGN) have a higher number of companions than those with nonactive galactic nuclei (Petrosian 1982; Dahari 1985; MacKenty 1989, 1990;

Rafanelli et al. 1995; Alonso et al. 2007), while others do not find this excess of interacting companions or find it only marginally (Bushouse 1986; Laurikainen & Salo 1995; Schmitt 2001). Miller et al. (2003) find that the fraction of AGN is independent of the environment even in clusters. Fuentes-Williams & Stocke (1988) found only a marginal excess of similarly-sized galaxies but a clear excess of faint companions for Seyfert galaxies. Most recent works find a different result depending on the type of Seyfert galaxy (Dultzin-Hacyan et al. 1999; Krongold et al. 2003). Recently Alonso et al. (2007) found for a sample of isolated galaxies a lower fraction of Type 2 AGN (23%) than for close galaxy pairs (30%). The proportion of galaxies hosting an AGN in extreme environments as compact groups was reported by Coziol et al. (2000) to be 70%, while 50% was reported by Shimada et al. (2000). More recently Martinez et al. (2006b,a) studied a sample of 215 compact groups from the UZC (Updated Zwicky Catalog), and 42 galaxies belonging to compact groups from the Hickson Catalogue. They found in the first case 43% of AGN and 20% of transition objects (objects with spectroscopic properties between pure AGN and pure star forming), while in the second subset 57% showed characteristics consistent with low-luminosity AGN with a low-ionization nuclear emission-line region (LINER) type and 16% were transition objects.

Selection of AGN candidates using the radio-FIR correlation is also found in the literature. This correlation is very tight and can be used to distinguish galaxies for which their radio continuum emission is due to star formation and which follow the correlation, and those with an AGN causing an enhancement of the radio continuum emission that lie above the correlation. It is known that all AGN are radio sources at some level, e.g., Ho & Ulvestad (2001) find that 85% of the nuclei of Seyfert galaxies are detected at radio wavelengths, with a wide range of intensities and morphologies (from compact cores to jet-like features). According to Reddy & Yun (2004) a significant fraction of radio-excess objects are associated with luminous AGN. For their sample of 114 galaxies in nearby clusters, they find that 70% of the radio-excess galaxies are AGN based on different indicators, such as the presence of radio jets, X-ray emission, or optical emission lines. Reddy & Yun consider this percentage as a lower limit of AGN among the radio-excess galaxies. They also analyse the sample of Miller & Owen (2001) and find that 80% of the radio-excess galaxies in their sample of local Abell clusters are spectroscopically-confirmed AGN. Far-infrared (FIR) colours have also been demonstrated as useful to identify AGN candidates (de Grijp et al. 1985).

The contradictory results reached in previous studies might be due to the design of the surveys, sometimes focused on galaxies with emission lines, or due to different selection criteria of the samples. For example, although the sample in Alonso et al. (2007) was selected with a well-defined isolation criterion (i.e., no companions within a radius of 100 kpc and a velocity difference of 350 km/s) these parameters are not restrictive enough to ensure that a galaxy has been isolated for a significant fraction of its life. Hence, a well-defined sample of really isolated galaxies, which have remained isolated for a significant part of their life, is needed. The goal of the AMIGA project (Analysis of the interstellar Medium of Isolated GAlaxies, `http://www.iaa.csic.es/AMIGA.html`; Verdes-Montenegro et al. 2005) is, therefore, to identify a statistically-significant sample of the most isolated galaxies in the local Universe and to quantify the properties of the interstellar medium in these galaxies and its relationship to the star formation and nuclear activity.

1.3. Thesis outline

From here on we will present the work developed by J. Sabater for this PhD. In Chapter 2 we present the AMIGA project which is the frame where the thesis study was carried on. The definition of the sample of isolated galaxies and the description of the data is made in Chapter 3. In Chapter 4 we show part of the work developed by J. Sabater for the study of the properties of the radio emission of the AMIGA galaxies that was presented in Leon et al. (2008). Then we make use of different methods to select the AGN-candidates: the radio continuum to far infrared correlation in Chapter 5, the far infrared colour in Chapter 6, and the optical spectra in Chapter 7. In Chapter 8, we present the final catalogue of AGN-candidates. We compared the accuracy of the different methods used in Chapter 9. We discuss and compare our results to other studies from the literature in Chapter 10. Finally, we present our conclusions and the future work in Chapter 11 (a version in Spanish is presented in Chapter 12).

Chapter 2

AMIGA project

It is well known that galaxy evolution is strongly affected, or even driven, by the influence of nearby galaxies (nurture), but a well defined baseline for assessing its frequency and amplitude is lacking. AMIGA project (Analysis of the interstellar Medium of Isolated GAlaxies) started at Instituto de Astrofísica de Andalucía (IAA) to provide such a baseline by quantifying the properties of a well defined sample of nature dominated galaxies and involves currently more than 30 participants from ~ 15 international institutions. As a result we have built a multifrequency database for ~ 1000 isolated galaxies, public through a Virtual Observatoty-interface in our Web page (`http://amiga.iaa.es/` or `http://www.iaa.csic.es/AMIGA.html`), and studied their global properties.

The main aims of the AMIGA project are:

- to compare and quantify the properties of different phases of the interstellar medium in this sample, as well as the level of star formation and nuclear activity.
- to quantify the role of nature versus nurture, distinguishing between environmental density and one-on-one interactions.
- to use this control sample as template in the study of star formation and galaxy evolution with respect to denser environments.

The starting sample for the AMIGA project is based on the Catalogue of Isolated Galaxies (CIG; Karachentseva 1973) which is composed of 1050 galaxies. In previous works we have:

1. revised all of the CIG positions (Leon & Verdes-Montenegro 2003);
2. optically characterised the sample (Verdes-Montenegro et al. 2005);
3. performed a revision of the morphologies (Sulentic et al. 2006);
4. derived mid-infrared (MIR) and FIR basic properties (Lisenfeld et al. 2007);
5. performed a careful reevaluation of the degree of isolation of the CIG (Verley et al. 2007c,b); and
6. derived radio continuum properties (Leon et al. 2008).

The following outline tries to clarify the main contributions by J. Sabater to this project:

- Refinements to the sample:
  - distances: Compilation of the distances to the sources with a velocity redshift of less than 1500 km s^{-1} (see § 2.2).
  - morphology: Compilation of the actual morphology of the nearby AMIGA galaxies and management of the stored data (see § 2.2).
  - isolation: Determination of the local density estimator that correspond to a determined tidal force and the comparison of the isolation parameters of visually identified interacting galaxies (see § 2.2).
- Multiwavelength study:
  - optical study: Determination of the 3D location of the CIG galaxies with respect to the main galactic structures known (see § 2.3).
  - FIR study: Contribution to the study of the colors of the sample and management of the stored data (see §).
  - Radio continuum study: co-manager (together with Dr. S. Leon) for the compilation of radio continuum data and analysis (see § 2.3).
  - Nuclear activity study: manager for the compilation of nuclear activity data and analysis. This study constitutes the bulk of the PhD work (from § 3 on).

2.1. CIG sample

AMIGA is trying to avoid two forms of "nurture": one-on-one interaction and galaxy environmental density. Our reference sample is drawn from the Catalog of Isolated Galaxies, which originally included N = 1050 nearby galaxies in the northern hemisphere, which corresponds to 3% of the galaxies included in the CGCG (Catalog of Galaxies and Clusters of Galaxies, Zwicky et al. 1961, 1963, 1965, 1966, 1968; Zwicky & Kowal 1968) with $m_{pg} < 15.7$ and $\delta > -3$ deg. The main properties and strengths of this sample are explained in detail in Verdes-Montenegro et al. (2005) and Sulentic et al. (2006). The number of individuals in the catalogue allows us to have a statistically useful sample of several hundred galaxies after refinement of the sample.

The CIG sample was assembled by Karachentseva (1973) with the requirement that no similar sized galaxies with angular diameter D_i between 1/4 and 4 times diameter D_P of the CIG galaxy lie within $20 \times D_i$:

$$R_{ip} \geq 20 \times D_i$$

$$\frac{1}{4} \times D_P \leq D_i \leq 4 \times D_P$$

where R_{ip} is the angular separation between the primary and the companion galaxy.

CIG is complemented by catalogs of galaxy pairs (CPG, Catalog of Paired Galaxies; Karachentsev 1972), triplets (Karachentseva et al. 1979) and compact groups (Hickson catalog of Compact Groups, HCG; Hickson 1982, largely quartets). All of these interacting comparison samples were visually compiled using an isolation criterion.

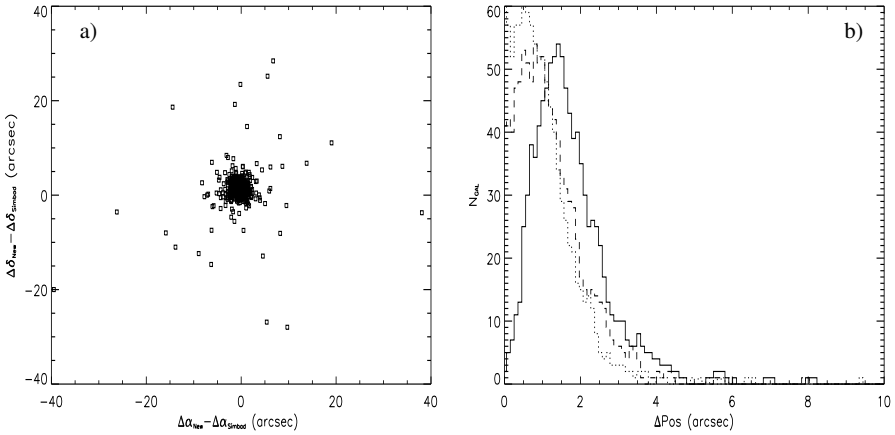

Figure 2.1: Shifts between the new positions and the positions retrieved from the SIMBAD database. The panel a) shows the differences in α and δ and the panel b) the histogram of these differendes. The dotted line is the difference in α, the dashed line the difference in δ and the solid line is the difference in the absolute distance between the new position and the SIMBAD one.

2.2. Refinement

We have performed several improvements to the CIG sample, being among the most relevants the reevaluation of the positions, redshifts and distances, morphologies and isolation degree.

Positions

Main paper: Leon & Verdes-Montenegro (2003)

A comparison between the CIG positions found in the SIMBAD database and in the Updated Zwicky Catalogue (UZC; Falco et al. 1999), Leon & Verdes-Montenegro (2003) found differences of up to several tens of arcsec. New positions were calculated by applying SExtractor to the Digitized Sky Survey CIG fields with a spatial resolution of 1.2″. The results were visually checked and for 118 galaxies it was necessary to recompute the assigned positions due to complex morphologies (e.g. distorted isophotes, undefined nuclei, knotty galaxies) or the presence of bright stars. There were found differences between older and newer positions of up to 38″ with a mean value of 2.96″ relative to SIMBAD and up to 38″ and 2.42″ respectively relative to UZC. Based on star positions from the APM catalog it was determined that the Digitized Sky Survey astrometry of five CIG fields has a mean offset in (α, δ) of (−0.90″, 0.93″) with a dispersion of 0.4″. These results were confirmed using the 2MASS All-Sky Catalog of Point Sources. The intrinsic errors of the method combined with the astrometric ones were of the order of 0.5″.

Redshifts and distances

Main paper: Verdes-Montenegro et al. (2005)

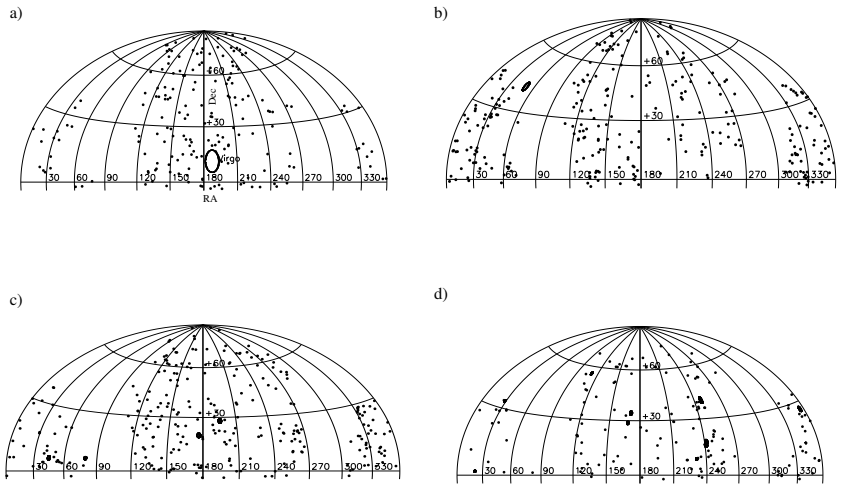

Figure 2.2: Aitoff projection in ecuatorial coordinates with the location of CIG galaxies divided in radial velocity ranges. The different subplots correspond to the following velocities: a) 0–3000 km s^{-1}; b) 3000–6000 km s^{-1}; c) 6000–9000 km s^{-1} and d) 9000–12000 km s^{-1}. The position of Virgo cluster is indicated with a circle ($\varnothing = 12^{\circ}$) in panel a), Abell clusters with a richness class of 1 or 2 are also plotted as circles proportional to their radii.

The archival and bibliographic search carried out by Verdes-Montenegro et al. (2005) reveals data for almost the entire sample, from NED (50% of the sample) and 41 other different sources. This includes 10 new redshifts obtained from HI observations performed by us. Redshift distances were derived there for all galaxies with V > 1000 km s^{-1} assuming H_0 = 75 km s^{-1} Mpc^{-1}. A total of 50% or more of the sample shows a quasi-homogeneous redshift distribution.

The redshift distribution for the CIG galaxies re-enforces the evidence for a bimodal structure seen earlier in smaller samples. The peaks at redshift near 1500 and 6000km/s correspond respectively to galaxies in the local supercluster and those in more distant large-scale components (particularly Perseus-Pisces). The two peaks in the redshift distribution are superimposed on 50% or more of the sample that is distributed in a much more homogeneous way. The CIG probably represents one of the most homogeneous local field example that has ever been compiled.

Morphologies

Main paper: Sulentic et al. (2006)

All morphological types are found in the CIG catalogue, and the CIG sample is large enough to permit discrimination on the basis of galaxy type. Compilation of the

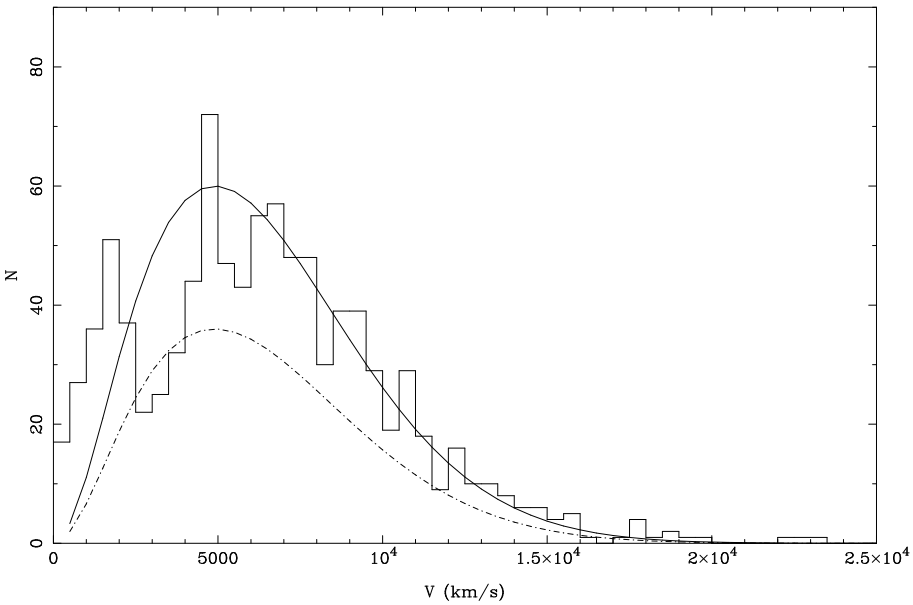

Figure 2.3: Distribution of recesion velocities of CIG galaxies. Histogram of the optical heliocentric recesion velocities. One galaxy (CIG 402) is out of the velocity range of the plot with a recesion velocity of 40 658 km s^{-1}. The solid line corresponds to a homogeneous redshift distribution of the same sample size, velocity distribution and Schechter function. The dashed line has been obtained by scaling down the previous distribution by a factor of 0.6.

types given by several databases was obtained (NED and LEDA), but in many cases contradictions were found. This motivated Sulentic et al. (2006) to revise the morphologies for the whole sample using the Palomar Observatory Sky Survey 2 (POSS2) images ($\simeq$ 80% of the sample) and new CCD images observed mainly at the 1.5m Observatorio de Sierra Nevada in Granada, Spain. These images improve the sensitivity achieved by Palomar Observatory Sky Survey I (POSS-I) images and allowed us to obtain more accurate morphological classifications.

The comparison with independent classifications made for an SDSS overlap sample of more than 200 galaxies confirmed the reliability of the early vs. late-type discrimination and the accuracy of spiral subtypes.

The results of the morphological reevaluation of the CIG galaxies with $V_R > 1000$ km s^{-1} (N = 1018) are listed in Table 2.1.

A considerable number of galaxies in the catalog (n = 193) are flagged for the presence of nearby companions or signs of distortion likely due to interaction. This most isolated sample of galaxies in the local Universe is dominated by two populations:

1. 82% are spirals (Sa-Sd) with the bulk being luminous systems with small bulges (63% between types Sb-Sc) and

2. a significant population of early-type E-S0 galaxies (14%).

Most of the types later than Sd are low luminosity galaxies concentrated in the local

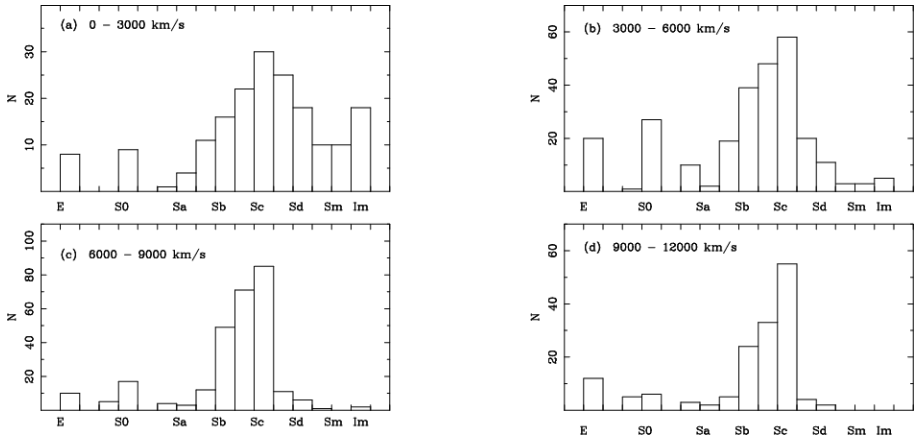

Figure 2.4: Distribution of morphologies of CIG galaxies depending on the radial velocity. The different subplots correspond to the following recession velocities: a) 0–3000 km s^{-1}; b) 3000–6000 km s^{-1}; c) 6000–9000 km s^{-1} and d) 9000–12000 km s^{-1}.

Table 2.1: Revised morphological classification of the CIG sample (Sulentic et al. 2006).

Type	T	N	$N/1018$
E	−5	58	0.057
E/S0	−3	14	0.014
S0	−2	67	0.066
S0/a	0	19	0.019
Sa	1	13	0.013
Sab	2	52	0.051
Sb	3	159	0.156
Sbc	4	200	0.196
Sc	5	278	0.273
Scd	6	61	0.060
Sd	7	41	0.040
Sdm	8	15	0.015
Sm	9	15	0.015
Im	10	26	0.026
E–S0		139	0.137
Sa–Sd		804	0.790
Sb–Sc		637	0.626

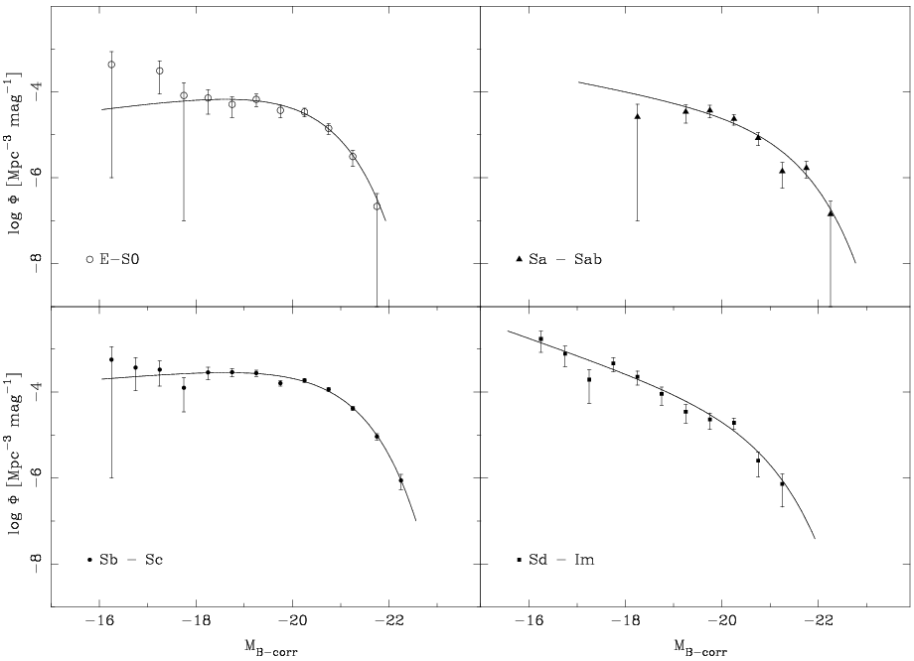

Figure 2.5: OLF for the different morphological types present in the CIG sample together with the corresponding Schechter fit shown as a solid line.

supercluster where isolation is difficult to evaluate. The late-type spiral majority of the sample spans a luminosity range $M_{\mathrm{B-corr}} = -18$ to -22 mag. Few of the E/S0 population are more luminous than -21.0 marking the absence of the often-sought super L^* merger (e.g. fossil elliptical) population. The rarity of high luminosity systems results in a fainter derived M^* for this population compared to the spiral optical luminosity function (OLF, see Figure 2.5). In other samples, which always involve galaxies in higher density environments, $M*_{\mathrm{E/S0}}$ is almost always 0.3-0.5 mag brighter than $M*_{\mathrm{S}}$, presumably reflecting a stronger correlation between M^* and environmental density for early-type galaxies.

Isolation

Main papers: Verley et al. (2007c,b)

After revision, Adams et al. (1980) and Karachentseva et al. (1986) assigned codes to the galaxies that were seen to violate these criteria: 902 galaxies remained as isolated (code=0), 85 as marginally isolated (code=1) and 64 were interacting galaxies (code=2).

One of the improvements of the AMIGA sample was the revision and quantification of the isolation criteria in a computerized way. Verley et al. (2007c) used digitised POSS-I images to perform this task. These images were analysed out to a minimum projected radius R $\geq$ 0.5 Mpc around 950 CIG galaxies (those within V_{r} = 1500 km s^{-1} were excluded). All galaxy candidates in each field brighter than B = 17.5 were identified with a high degree of confidence using the LMORPHO software (Odewahn

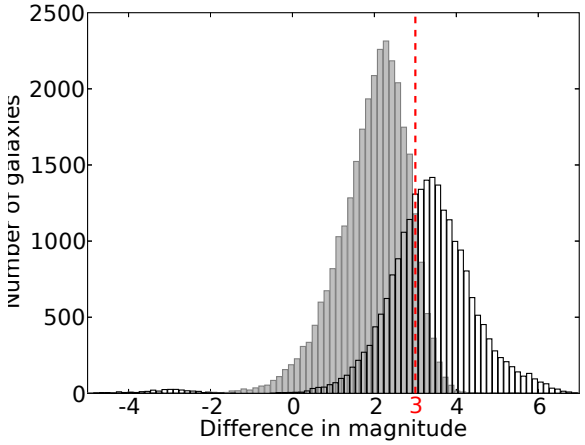

Figure 2.6: Comparison of the magnitude difference distributions for the neighbour galaxies considered by Karachentseva's criterion (factor 4 in size with respect to their associated CIG galaxy, grey histogram) and for the remaining neighbours (outside the factor 4 in size, unfilled histogram).

1995). It was generated a catalogue of approximately 54000 potential neighbours (redshifts exist for ~30% of this sample).

Six hundred sixty-six galaxies pass and two hundred eighty-four fail the original CIG isolation criterion. The available redshift data confirm that the catalogue of neighbours involves a largely background population rather than physically associated companions. We found that the exclusion of neighbours within a factor of four in size around each CIG galaxy, employed in the original isolation criterion, corresponds to $\Delta V_{\rm r} \approx 18000 km\ s^{-1}$ indicating that it was a conservative limit.

In Figure 2.6 is shown the comparison of the magnitude difference distributions for neighbour galaxies considered by Karachentseva's criterion and for the remaining neighbours. With this comparison is posible to test whether a criterion of isolation based in the difference in magnitudes between the candidate to isolated galaxy and its neighbours is equivalent or not to Karachentseva's criterion as claimed by Allam et al. (2005) and Xinfa et al. (2005). The overlap between the two distributions shows that a cut in magnitude at 3 is a rather good approximation because it loses only 10% of the neighbours selected by Karachentseva on the basis of the linear size of 4. But the contamination also shows that the hypothesis of flat surface brightness profile of galaxies is not always true: the cut in magnitude includes a large number of galaxies not considered by Karachentseva. Hence, the two definitions to seek for the neighbours are not fully equivalent.

We used two parameters to estimate the influence exerted by the neighbour galaxies on the CIG galaxy: the local number density of neighbour galaxies and the tidal strength affecting the CIG galaxy defined as:

k-density estimator from the distance to the k-th companion (neither the central galaxy nor the k-th companion are taken into account), we can obtain the fol-

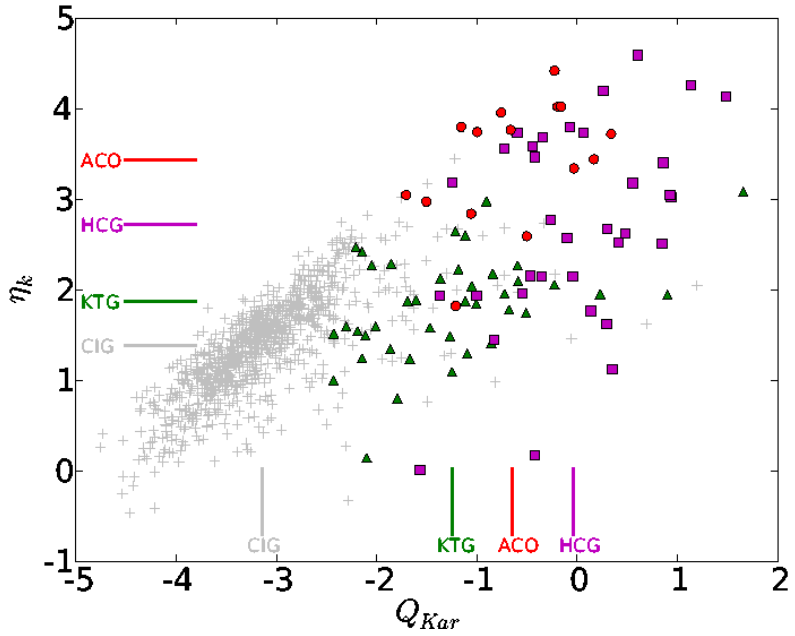

Figure 2.7: Isolation characterization of CIG galaxies. The y-axis represents the "k-density estimator" and the x-axis the "Tidal forces estimator". CIG galaxies are represented as grey crosses, green triangles are galaxies in triplets, red circles are galaxies of Abell clusters and magenta squares are galaxies in Hickson Compact Groups. The mean value for each sample is indicated as vertical and horizontal lines with the same colour code.

lowing parameter:

$$\rho_k = \frac{k-1}{V(r_k)}$$

with $V(r_k) = 4\pi r_{k^3}/3$, where r_k is the distance to the k-th nearest neighbour.

Tidal forces estimator the tidal force per unit mass produced by a companion, as explained in (Dahari 1984), is proportional to:

$$\frac{M_i}{r_{ip}^3}\alpha\frac{(D_iD_P)^{1.5}}{S^3} = Q$$

where M_i is the mass of the companion, r_{ip} is the distance from the primary galaxy to the companion and S the projected separation between the centers of the two galaxies. The parameter Q, defined by this equation, is a dimensionless estimation of the gravitational interaction strength.

We show that both parameters together provide a comprehensive picture of the environment. For comparison, those parameters have also been derived for galaxies in denser environments such as triplets, groups and clusters. In Figure 2.7 are shown

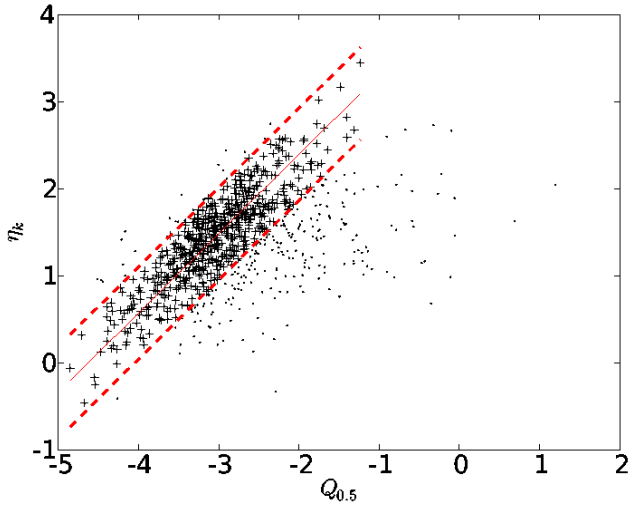

Figure 2.8: Local number density vs. tidal strength. The final bisector fit is shown by the plain red line. The dotted red lines represent the final 2σ dispersion: the CIG galaxies within these limits are depicted by pluses, the CIG rejected during the successive iterations are shown by points.

the two types of isolation parameters for CIG galaxies and the other samples of galaxies in denser environments. The mean tidal strenght estimator increases from CIG galaxies to triplets and compact groups samples. The separation is not so clear in the y-axis because triplets and compact groups are samples defined with the help of isolation requirements. The tidal strength and the local number density estimations are complementary parameters and it is important to use both in order to have an accurate picture of the repartition of galaxies surrounding a primary galaxy.

The CIG galaxies show a continuous spectrum of isolation, as quantified by the two parameters, from very isolated to interacting. The fraction of CIG galaxies whose properties are expected to be influenced by the environment is however low (159 out of 950 galaxies). The isolated parameters derived for the comparison samples gave higher values than for the CIG and we found clear differences for the average values of the 4 samples considered, proving the sensitivity of these parameters.

In Figure

2.3. ISM multiwavelength study

In order to study the properties of the different components of the ISM, the star formation and the nuclear activity in isolated galaxies, we have observed or compiled multiwavelength information for the CIG sample: optical, far-infrared, HI line and radio continuum data for the whole sample and Hα and CO line for a velocity limited sample. The data is publicly available in the web page of the project.

Table 2.2: Optical luminosity function parameters for the CIG sample.

Sample	Φ(Mpc^{-3} mag^{-1})	α	M*	Mag range for the fit
CIG N = 725	$6.3(\pm 0.7) \times 10^{-4}$	-1.27 ± 0.06	-20.31 ± 0.07	-16.3 to -22.3
CIG N = 666	$7.5(\pm 0.6) \times 10^{-4}$	-0.82 ± 0.09	-20.11 ± 0.07	-16.3 to -22.3

Optical characterization

Main paper: Verdes-Montenegro et al. (2005)

The optical luminosity is a tracer of the visible light and stellar content. We performed an analysis of the properties of the nearly redshift-complete CIG with emphasis on the Optical Luminosity Function (OLF) which we compared with other recent estimates of the OLF for a variety of environments. Our derivation of the CIG OLF was consistent with other studies of the OLF for lower density environments. This comparison via the Schechter parameter formalization (Schechter 1976) showed that: 1) M* increases with galaxy surface density on the sky and 2) α shows a weaker tendency to do the same. The OLF of the CIG sample as a function of the morphology is studied in Sulentic et al. (2006).

We corrected the apparent magnitudes due to systematic errors in the CGCG catalog, galactic dust extinction, internal extinction and K correction.

The optical luminosity function of our set of galaxies can be parametrized by means of a Schechter function model with the parameters M* and α:

$$\Phi(M) = \Phi_* 10^{0.4(\alpha+1)(M^*-M)} exp(-10^{0.4(M-M^*)})$$

Verdes-Montenegro et al. (2005) used N = 725 galaxies with known distance and magnitudes in the range 11-15 mag, once having excluded 9 galaxies with very high or low luminosity scattered in bins containing a low number of galaxies. We also computed the fit when galaxies with V_r <1500 km s^{-1} are excluded (N = 666). The parameters of the Schechter fit are shown in Table 2.2.

The CIG represents the largest and most complete foundation for studies of isolated galaxies and is likely as close as we can come to a field sample.

We also studied the completeness of the sample which is shown in § 3.1.

Hα

Main paper: Verley et al. (2007a)

Hα is a good tracer of recent star formation in places where the extinction is not high.

Verley et al. (2007a) have studied the properties of H_α in the same subsample than the one considered in the CO part of the AMIGA project (containing 205 CIG spiral galaxies with velocities between 1500 and 5000 km s^{-1}). A total of 96 % of the galaxies in the subsample have been observed at several 1-2 meter-class telescopes: OSN (Observatorio de Sierra Nevada - IAA), CAHA (Calar Alto Hispano Alemán - MPI,IAA) , EOCA (Estación de Observación de Calar Alto - OAN), JKT (Jakobus Kapteyn Telescope - ING) and SPM (San Pedro Mártir - UNAM). A total of 45 of the largest and less inclined galaxies were selected then to study their Hα morphology in comparison with r-gunn filter images, by using a numerical program developed by Dr.

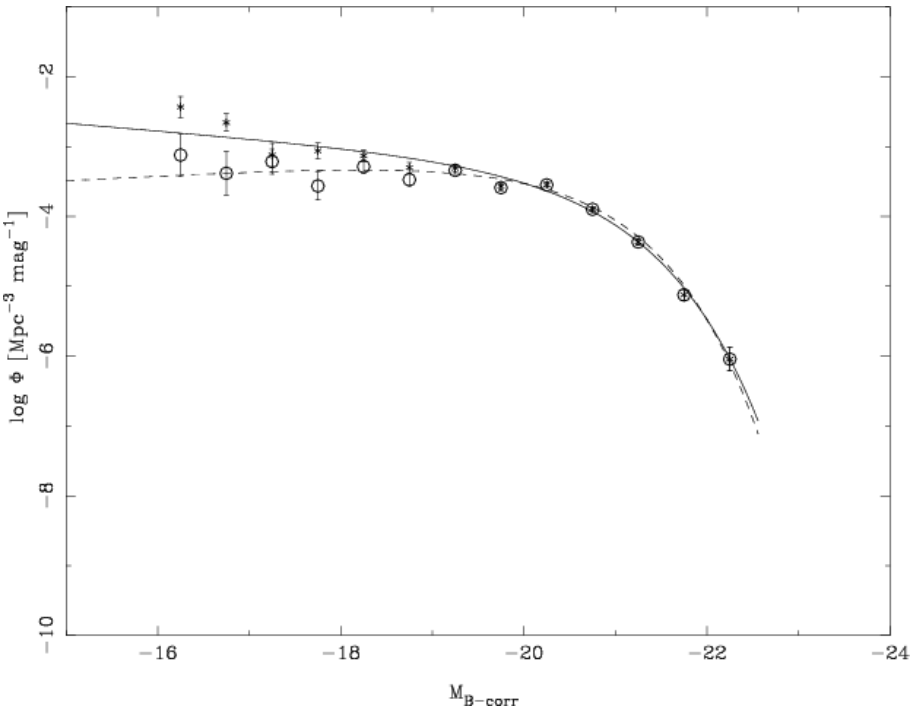

Figure 2.9: Optical luminosity function for CIG galaxies for which velocity information exists and with apparent magnitudes between 11 and 15 (n = 725). The Schechter fit to this sample is plotted as a solid line. The dashed line corresponds to a fit to the same sample when galaxies with Vr ¡ 1500 km s^{-1} are removed.

F. Combes, to study the potential, density and torques. The main result is the inference of an evolutive sequence, from galaxies in the first stage of the bar (presenting Hα emission all over the bar) to galaxies where the gas is gradually depopulated from the bar due to infall of material towards the center (thus possesing a strong central peak in the Hα emission). The latter is the most frequent phase in this subsample (N = 45 galaxies). Numerical simulations trying to model the Hα distribution suggest that the star formation law may differ from a simple Schmidt law.

Far infrared

Main paper: Lisenfeld et al. (2007)

The far-infrared emission (FIR) is mainly due to the emission produced by gas and dust grains warmed by ultraviolet radiation from newly formed massive stars ($M >$ 8M$_\odot$). Most of the studies about FIR emission are skewed toward bright galaxies, which are usually much brighter than isolated ones.

Lisenfeld et al. (2007) reprocessed IRAS MIR/FIR survey data using the ADDSCAN/SCANPI utility for 1030 out of 1050 galaxies from the Catalogue of Isolated Galaxies. We focus on diagnostics (FIR luminosity $L_{\rm FIR}$, R = log($L_{\rm FIR}/L_{\rm B}$), and IRAS colours) thought to be sensitive to effects of environment or interaction. The distribution of log($L_{\rm FIR}$)

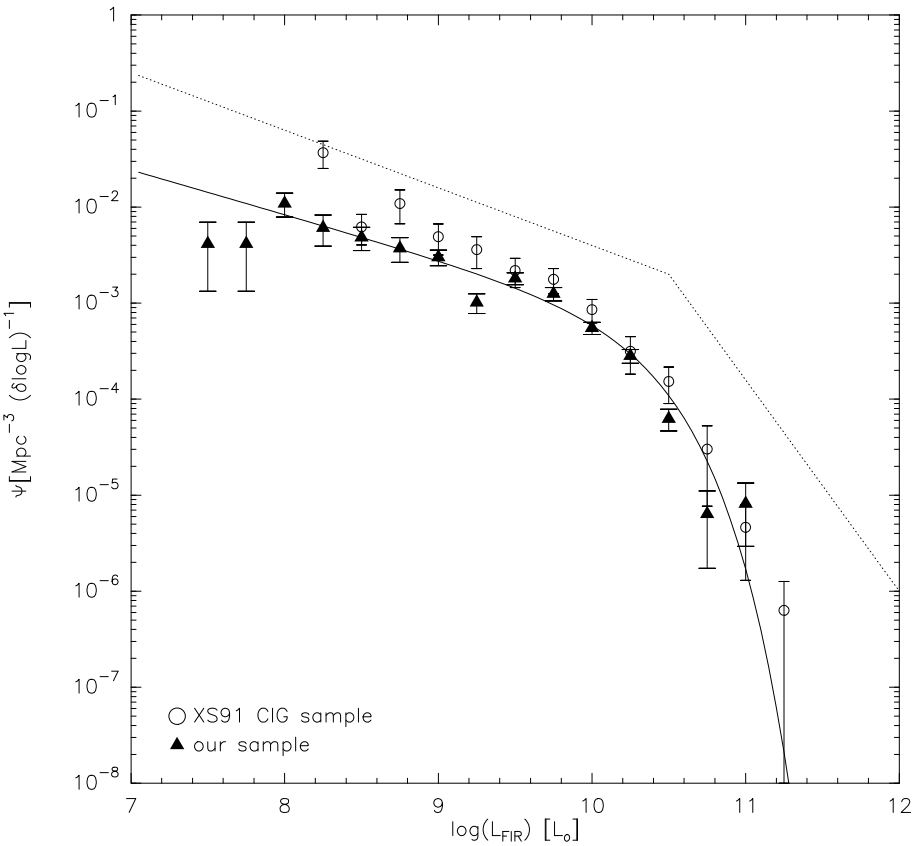

Figure 2.10: FIR Luminosity Function for the CIG galaxies (triangles) in comparison to that by Xu & Sulentic (1991, circles and stars). The solid line is the Schechter fit to our data and the dotted line is the fit with a double power law derived in Sanders et al. (2003) for the "IRAS Revised Bright Galaxy Sample".

sharply peaks from 9.0-10.5, with very few (<2%) galaxies above 10.5. Review of available optical images of the most FIR luminous galaxies found the majority likely to be interacting systems missed in our earlier morphological reevaluation. The optically normalised luminosity diagnostic R = $\log(L_{\rm FIR}/L_{\rm B})$ shows a sharply peaked distribution between 0.0 and −1.0. These results were compared to the magnitude limited sample of the Center for Astrophysics that was selected without environmental discrimination. This modestly (e.g., compared to cluster, binary galaxy, and compact group samples) environmentally affected sample shows a significantly higher mean $\log(L_{\rm FIR})$, and R, whereas the mean $\log(L_{\rm B})$ is the same. Our sample shows a strong $L_{\rm FIR}$ vs. $L_{\rm B}$ correlation, with a slope steeper than one ($L_{\rm FIR} \propto L_{\rm B}^{1.41}$). Interacting galaxies were found above this correlation, showing an enhancement in $L_{\rm FIR}$. With respect to the IRAS colours, we found higher F60/F100 values for ellipticals and late-type galaxies than for spirals, indicating a higher dust temperature. The mean value of F60/F100 was found to be lower than for interacting samples from the literature.

The results indicate that the FIR emission is a variable enhanced by interaction, and that our sample probably shows the lowest possible mean value. This attests to

the utility of our sample for defining a nurture-free zero point.

Atomic gas

Main papers: Espada (2009a); Espada et al. (2009); Espada (2009b)

The atomic gas is a fundamental ingredient of the ISM and is the most sensible tracer of interaction, due mainly to the fact that the extent of this component is usually much larger than any other component forming part of a galaxy. HI spectra have been obtained for the CIG galaxies from a compilation in the bibliography and from our observations at four radio-telescopes: Arecibo, GBT, Effelsberg and Nançay. In total 836 galaxies have HI data from the whole sample.

Currently we are preparing three papers about the atomic gas in the AMIGA sample: a) *HI content characterization*. To obtain the reference of HI content normalcy from HI single-dish data for 836 AMIGA galaxies, as a function of optical properties (luminosity, morphology, size). b) *HI Lopsidedness Characterization*. We use HI global velocity profiles with S/N ¿ 10 of a sample of isolated galaxies (N = 318). We restrict our study to N = 182 galaxies with accurate measures of the HI shape properties. We obtain a visual classification and a quantification of the asymmetry using a flux ratio asymmetry parameter. c) *Origin of asymmetries in HI disks: VLA observations*. In order to study the origin of asymmetries in the atomic gas of well isolated spiral galaxies, we have made use of the large statistical HI study of isolated galaxies performed in former papers to select a well defined subsample with lopsided HI profiles and with a minimized probability of contamination by companions. We have observed a total of 12 isolated galaxies at the VLA in D-array configuration in order to discriminate whether the lopsidedness is in the HI density distribution, the velocity field or is due to confusion with a HI-rich companion.

Molecular gas

Main paper: Lisenfeld et al. (2009)

The J=1-0 rotational transition of the CO molecule traces the molecular gas component, which is the raw material for star formation.

The search for CO data has been focused on a subsample containing the 273 CIG galaxies with velocities between 1500 and 5000 km s^{-1}. Data have been obtained from a compilation in the bibliography and from our observations with two single-dish radio-telescopes: FCRAO 14m (N = 102 galaxies) and IRAM 30m (N = 103) and Nobeyama 45m (N = 7). In the main paper we present the data the CO content of these 273 isolated galaxies, mostly obtained from our own observation and also from the literature. The molecular gas content is compared to the blue and the FIR luminosity and the content in the HI.

Radio continuum

Main paper: Leon et al. (2008)

Radio-continuum emission is an useful tracer of current SFR and nuclear activity which is not affected by extinction. There exist a close correlation between radio-continuum and FIR luminosities, although the nature of these two emissions are very

Table 2.3: Compiled data for the different radio continuum surveys.

Survey	Frequency (MHz)	Resol. (arcmin)	5-σ (mJy)	$N^1_{\rm CIG}$	$N^1_{\rm det}$
WENSS	325 & 352	$\sim$ 1	$\sim$ 18	405/278	49/37
NVSS	1420	$\sim$ 0.8	$\sim$ 2	1050/719	374/311
FIRST	1420	$\sim$ 0.08	$\sim$ 1	560/360	81/58
GB6	4850	$\sim$ 3.5	$\sim$ 18	1017/691	32/12

[1] Total number of galaxies with radio data ($N_{\rm CIG}$) and with radio detection ($N_{\rm det}$), followed by the number of galaxies belonging to the complete subsample of N = 719 galaxies (explained in 3.1).

different. Radio-continuum emission is produced by thermal radiation (mainly due to supernovae) and synchrotron radiation (non-thermal, due to relativistic electrons accelerated by magnetic fields) whose contribution is important if the galaxies possess nuclear activity. Candidates to host Active Galactic Nuclei can then be identified by looking for example to the outliers of such correlation as we will explain in the following chapters.

Leon et al. (2008) compiled radiocontinuum information for the CIG sample from four different sources:

- WENSS: Westerbork Northern Sky Survey at 325 and 352 MHz ($\sim$ 90 cm).
- NVSS: NRAO VLA Sky Survey at 1.4 GHz (20cm)
- FIRST: Faint Images of the Radio Sky at Twenty-centimeters at 1.4 GHz (20cm)
- GB6: Green Bank at 4.85 GHz (6cm).

These data have been reprocessed using SExtractor, obtaining in this way a higher detection rate. Comparison between the NVSS and FIRST detections indicates that the radio continuum is coming from disk-dominated emission in spiral galaxies, in contrast to the results found in high-density environments where nuclear activity is more frequent. The comparison of the radio continuum power with a comparable sample, which is however not selected with respect to its environment, the Condon et al. (2002) UGC-SF sample of starforming field galaxies, shows a lower mean value for the AMIGA sample. We have obtained radio-to-optical flux ratios (R) using the NVSS radio continuum flux. The distribution of R for the AMIGA galaxies is consistent with a sample dominated by radio emission from star formation and a small number of active galactic nuclei (AGN), with less than 3% of the sample with R ¿ 100. We derived the radio luminosity function (RLF) and total power density of the radio continuum emission for the AMIGA sample at 1.4 GHz, and compared them with results from other low-redshift studies. The Schechter fit of the RLF indicates a major weight of the low-luminosity galaxies.

The results indicate the very low level of radio continuum emission in our sample of isolated galaxies, which is dominated by mild disk SF. It confirms thus the AMIGA sample as a suitable template to effectively quantify the role of interactions in samples extracted from denser environments

2.4. Extension to submillimeter

The AMIGA project performed a scientific and technological extension to the millimeter and submillimeter range, with a special emphasis on submillimeter interferometry, expecting to contribute to an optimum "return" of the Spanish contribution to the Atacama Large Millimeter Array (ALMA). Our activity concentrate into three different topic:

- **Scientific**: to get insight into the star formation process by means of observations with the Plateau de Bure Interferometer and with the Submillimeter Array (SMA, the first interferometer in the world working at submm wavelengths), selecting the best objects to be studied with ALMA when it will become operative.

- **Scientific - technical**: The AMIGA project participate in calibration tasks for SMA, relevant for the development and comissioning of ALMA.

- **Technical**: AMIGA participate in the development of systems allowing the access and display of large radioastronomical databases. These systems follow standards allowing their integration into the Virtual Observatory.

Submm calibration techniques: Our group have performed phase transfer and fast switching tests in collaboration with SMA/ASIAA. Fast switching testing data agree well with simulations. Preliminar results using our phase transfer data have allowed us to identify a set of engineering variables that may be involved in the phase drifts/jumps that are usually observed.

2.5. Virtual Observatory

The great diversity of the current astrophysical instrumentation allows us to obtain information of the Universe in almost the whole electromagnetic range. This is stored in astronomical archives, but the nature and access methods to them is very heterogeneous. It is for the millimetric and submillimetric astronomy where the astronomical archives are less available, which adds difficulty for those non-radioastronomers when reducing and interpreting the data. Within the last three years the concept of Virtual Observatory (VO) has been created, aiming to solve the mentioned hetereogenity. The VO aims to offer an integrated system to access a number of archives which are very different among them, as well as a set of services that can interact both direct or remotely over them at different levels. In the frame of VO there is a considerable experience in optical, infrared and ultraviolet archives (e.g. MAST Kamp et al. 2004). There exist a great interest to extend this experience to the radioastronomy range and to build data archives integrated in VO both coming from single dish or synthesis radiotelescopes.

The International Virtual Observatory Alliance (`http://www.ivoa.net`) is world-level confederation and the reference for all the work done in VO (development of standards, workgroups coordination, etc.). Its analogue at a national level is the Spanish Virtual Observatory (SVO, `http://svo.laeff.esa.es`)

The AMIGA project has developed a VO compliant interface (conesearch service and unfolding of VOtables) for the access to the data that are periodically made public. Our group also developed for the VO:

- RADAMS: Development of RAdio DAta Model for Single-dish telescopes, only existing data model for radio archives based upon existing IVOA data models, now implemented by our group to the DSS-63 and IRAM-30m antennas archives. It has been presented to the IVOA within the Current Data Modelling Efforts.
- MOVOIR (MOdular Virtual Observatory Interface for Radio-astronomy) developed by J. Santander. It aims to combine existing VO open source packages in order to produce an easily embeddable modular interface for radio astronomy tools.
- SMA/CASA Converter: A Python based tool that allows exporting SMA interferometric data to FITS formatted data in order to be treated by the ALMA software reduction package CASA. CASA stands for Common Astronomy Software Applications and is a suite of applications developed by ALMA and intended to be the principal reduction package for ALMA data.

Part II

Radio continuum and far infrared emission

Chapter 3

Sample and data used for this study

3.1. Definition of the sample

The starting sample for the AMIGA project is based on the Catalogue of Isolated Galaxies (CIG; Karachentseva 1973) which is composed of 1050 galaxies. As explained in the previous chapter, in previous works we have: 1) revised all of the CIG positions (Leon & Verdes-Montenegro 2003); 2) optically characterised the sample (Verdes-Montenegro et al. 2005); 3) performed a revision of the morphologies (Sulentic et al. 2006); 4) derived mid-infrared (MIR) and FIR basic properties (Lisenfeld et al. 2007); 5) performed a careful reevaluation of the degree of isolation of the CIG (Verley et al. 2007c,b); and 6) derived the radio continuum properties (Leon et al. 2008).

Completeness of the sample

In order to reduce biases in our statistical study we have used the completeness test < V/Vm > (Schmidt 1968), as explained in Verdes-Montenegro et al. (2005) and Lisenfeld et al. (2007). We adopted $m_B = 15.0$ as the cutoff magnitude necessary to have a reasonably complete sample (see Figure 7.4 in Chapter 7).

We focus our statistical analysis on the complete AMIGA subsample described in (Verdes-Montenegro et al. 2005). We use in the present work the same selection as described in Sect. 4.1 of (Lisenfeld et al. 2007):

- The subsample contains galaxies with corrected Zwicky magnitudes in the range 11.0–15.0 for which we found $< V/V_m >= 0.43$, indicating 80–90% completeness.
- Morphological revision of the sample, described in (Sulentic et al. 2006), identified 32 galaxies that are probably not isolated in the sense that they might involve isolated interacting pairs and/or multiplets. These galaxies are excluded from the most isolated sample studied further here.
- We excluded two nearby dwarf ellipticals (CIG 663 ≡ Ursa Minor and CIG 802 ≡ Draco) for which we only have upper limits for the radio and FIR fluxes, and the inferred luminosities are very low.

This subsample contains 719 galaxies and in this study we will refer to it as the ”complete subsample”, while the 1050 galaxies will be referred to as the ”total sample”.

For studies that use IRAS satellite data, the total sample is reduced to 1030 galaxies while the complete subsample contains only 710 galaxies due to a number of galaxies falling in the region uncovered by IRAS known as the "IRAS gap" (see Lisenfeld et al. 2007). This difference in the number of galaxies does not affect the completeness of the subsample.

3.2. Presentation of the data

We performed our study using archive data that we reprocessed as well as data found in the literature.

Observed and reprocessed data

We obtained the FIR data for 1030 galaxies of the total sample by reprocessing the data of the IRAS satellite with the SCANPI tool (Lisenfeld et al. 2007). We obtained a better detection rate and an improved signal-to-noise level than in previous IRAS catalogues.

The radio continuum data have been obtained from two different sources: a) NRAO VLA Sky Survey (NVSS, 1.4 GHz; spatial resolution 45″) and b) Faint Images of the Radio Sky at Twenty-cm (FIRST, 1.4 GHz; spatial resolution 5″) as explained in detail in Leon et al. (2008). The radio continuum fluxes used in this paper were either taken from the NVSS survey catalogue or derived using the original survey data and extracting the flux with SExtractor (Bertin & Arnouts 1996) within a radius of 35″, obtaining in the latter case a higher detection rate. We use NVSS fluxes because of the high detection rate and sensitivity of this survey, which contains all galaxies belonging to our sample (n = 1050). In those cases where we found a radio enhancement (see Sect. 5.4), we complemented the NVSS data with the higher resolution images provided by FIRST when available. In this way, we improved the spatial location of the radio continuum emission to check whether this emission is due to a nuclear source or to a projected, unrelated source.

We used the distances given in Verdes-Montenegro et al. (2005) calculated with the Hubble constant $H_o = 75$ km s^{-1} Mpc^{-1}.

We have computed the radio continuum and FIR luminosities with the following relations:

$$\log L_{1.4\mathrm{GHz}}(\mathrm{W\ Hz^{-1}}) = 20.08 + 2\log D + \log S_{1.4\mathrm{GHz}}$$

$$\log L_{60\mu\mathrm{m}}(\mathrm{L_\odot}) = 6.014 + 2\log D + \log S_{60\mu\mathrm{m}}$$

where D is the distance of the galaxy in Mpc and $S_{1.4\mathrm{GHz}}$ and $S_{60\mu\mathrm{m}}$ are the flux densities in Jy (1 Jy = 10^{-26}W m^{-2} Hz^{-1}). The FIR luminosity (L_{FIR}; Helou et al. 1988) is related to $L_{60\mu\mathrm{m}}$ by this formula:

$$L_{\mathrm{FIR}}(\mathrm{L_\odot}) = \left(1 + \frac{S_{100\mu\mathrm{m}}}{2.58 S_{60\mu\mathrm{m}}}\right) L_{60\mu\mathrm{m}}$$

The distribution of the FIR luminosities for our sample peaks in $\log(L_{\mathrm{FIR}}/\mathrm{L_\odot})$ = 9.5–9.75 (see Lisenfeld et al. 2007) and practically all galaxies have FIR luminosities between $\log(L_{\mathrm{FIR}}/\mathrm{L_\odot})$ = 7.5 and $\log(L_{\mathrm{FIR}}/\mathrm{L_\odot})$ = 11.25. The bulk of the FIR luminosities (98%) lies below $\log(L_{\mathrm{FIR}}/\mathrm{L_\odot})$ = 10.5.

Data from the literature

We cross-correlated our sample with existing databases of active galaxies, in particular, the NASA Extragalactic Database (NED) [1] and the Véron-Cetty Catalogue of Quasars and Active Nuclei (Véron-Cetty & Véron 2006, 12th Edition).

The NED contains information on the type of nuclear activity for $n = 77$ galaxies of our sample. The different classifications found in the sample are: LINER, HII, Starburst, DANS (dwarf amorphous nuclear starburst), SBNG (small, bright nucleus galaxy), NLAGN (narrow line AGN) and Seyfert. In some cases, the information on the Seyfert type is also given. The NLAGN are a mixture of Seyfert 2's, LINERs, and starburst/AGN composites. HII and starburst are not taken into account in our analysis since they are not considered as AGN, but we list them in Table 3.1. A total of $n = 16$ galaxies from the AMIGA sample are classified as Seyferts, 1 as AGN and 5 as NLAGN in their catalogue.

The Véron-Cetty Catalogue of Quasars and Active Nuclei is a very complete compilation of active galaxies and quasars. It includes position and redshift as well as optical photometry (U, B, V bands) and 6 and 21 cm flux densities when available. We have found $n = 25$ of our galaxies in this catalogue. A total of $n = 18$ are classified as Seyfert galaxies, 3 as HII, 3 as LINER and one has no assigned class. The 3 HII galaxies are included in this catalogue because in a previous version they were classified as Seyfert galaxies.

The LINERs are also known as Sy3 (Seyfert 3) in these catalogues. Although recent studies suggest that some LINERs are low-luminosity AGN (Ho 1999; González-Martín et al. 2006) this topic is not clear yet. In our study we consider LINERs separately from other kinds of active galaxies.

In Table 3.1 we list those galaxies found in the literature to show nuclear emissions. The first column is the CIG number, the second column is the type of emission found in NED, and the third column the one in the Véron-Cetty catalogue. In the fourth column, we indicate the classification taken for our study. It is obtained discarding those cases where a disagreement is found between the NED and Véron-Cetty (V-C) classification.

Table 3.1: Galaxies from AMIGA sample listed as active in the literature.[1]

CIG	NED	V-C[2]	Classification choosed[3]
6	HII		HII
33	Sy? LINER	Sy?	
45	HII		HII
55	LINER HII		
56	Sbrst		Sbrst
57	Sy2	Sy2	Sy
72	Sy1.9	Sy1.9	Sy
103		?	
105	HII		HII
116	HII	Sy2	
138		Sy2	Sy
143	HII		HII
197	HII		HII

[1] http://nedwww.ipac.caltech.edu/

CIG	NED	V-C[2]	Classification choosed[3]
214	Sy1 Sbrst	Sy1.0	Sy
231	NLAGN		NLAGN
250	HII		HII
302	HII		HII
324	Sy1 LINER	Sy3	
339	Sbrst		Sbrst
347	HII		HII
349	Sy1.5 LINER	Sy1	Sy
356	DANS		DANS
359	Sy3	Sy3	LINER
383	HII Sbrst		
393	HII	HII	HII
401	NLAGN		NLAGN
428	HII		HII
435	HII		HII
438	HII		HII
442	HII		HII
444	HII		HII
447	LINER HII		
461	LINER		LINER
463	HII		HII
478		Sy2	Sy
495	Sy2		Sy
499	NLAGN		NLAGN
503	HII		HII
508	Sbrst	Sy1	
518	HII		HII
534	HII		HII
538	HII		HII
543	HII		HII
549	LINER		LINER
553	Sbrst		Sbrst
559	Sy2	Sy	Sy
575	SBNG		SBNG
592	NLAGN		NLAGN
604	AGN		AGN
619	Sbrst		Sbrst
624	HII		HII
627	HII		HII
634	LINER		LINER
671	Sy1	Sy1.5	Sy
692	Sy2	Sy2	Sy
710	HII		HII
712	LINER		LINER
719	Sy1	Sy1n	Sy
733	HII		HII
745	Sy1.5	Sy1.0	Sy
748	Sbrst		Sbrst

CIG	NED	V-C[2]	Classification choosed[3]
766	HII		HII
795	NLAGN		NLAGN
837	LINER HII		
866	LINER HII		
877		Sy2	Sy
936	HII		HII
940		Sy1.9	Sy
943	HII		HII
947	Sy LINER	Sy3	
974	Sbrst		Sbrst
976	HII		HII
985	HII		HII
993	Sy2 Sbrst	HII	
1004	Sy2 LINER	Sy1.9	Sy
1006	HII		HII
1008	Sy1.2	Sy1.2	Sy
1019	Sbrst		Sbrst
1023	Sy2	Sy2	Sy
1038	LINER		LINER
1039	HII		HII

[1] Columns: 1) CIG number; 2) NED classification; 3) Véron-Cetty Catalogue classification; 4) Classification adopted for our study.

[2] Sy = Seyfert; HII = nuclear HII region; Sbrst= Starburst; SBNG = small, bright nucleus galaxy; NLAGN = narrow line active galaxies (a mixture of Seyfert 2's, LINERs, and starburst/AGN composites); DANS = dwarf amorphous nuclei starburst galaxies

[3] Classification obtained discarding those cases where a disagreement was found between the NED and Véron-Cetty classification.

Chapter 4

Properties of the radio continuum emission

This chapter present part of the work developed by J. Sabater for the study of the properties of the radio emission of the AMIGA galaxies that was presented in Leon et al. (2008).

4.1. NVSS and FIRST data

We found 359 CIG sources in the NVSS catalog. Source extraction using SExtractor with a 5-σ threshold yielded 368 detections, where 9 are not in the NVSS catalog or were recalibrated in cases of extended or weak sources (CIG 324, 436, 442, 543, 559, 837, 869, 950, 988). CIG 199 was excluded from the catalog because of corrupted data.

We cross-correlated the FIRST catalog with our revised optical positions, yielding 81 source detections. The number of detections was low and the data could not be used for statistical purposes. They were however very useful for a comparison with NVSS data which allowed us to infer the relative strengths of disk vs. nuclear emission in many galaxies. Mean positional differences are small ($-0\farcs22, -0\farcs07$) with a dispersion of $1\farcs6$ and $2\farcs0$, respectively. We found 8 galaxies that were detected in FIRST but not in the NVSS (CIG 236, 238, 258, 364, 544, 618, 678 and 749). Normally we expect the NVSS flux to be stronger than the FIRST values because FIRST is only sensitive to compact (high spatial frequency) radio emission. These sources showed fluxes near the NVSS/FIRST detection limits and were not further considered in our analysis.

4.2. Detection rate

Figure 4.1 shows the NVSS radio detection fraction as a function of morphological type (see Sulentic et al. 2006) for a description of the morphological types). It peaks in the Sb–Sc range (type T = 3–5) which is the core of the AMIGA sample, comprising fully two thirds of our sample (Verdes-Montenegro et al. 2005, see). Assuming that the radio continuum emission is driven by star formation this is not surprising because these galaxies show the highest average star formation rates (Kennicutt et al. 1987). This is partially offset by the higher molecular/neutral gas fraction found in earlier types (Young & Knezek 1989) which may explain why the detection fraction drops so

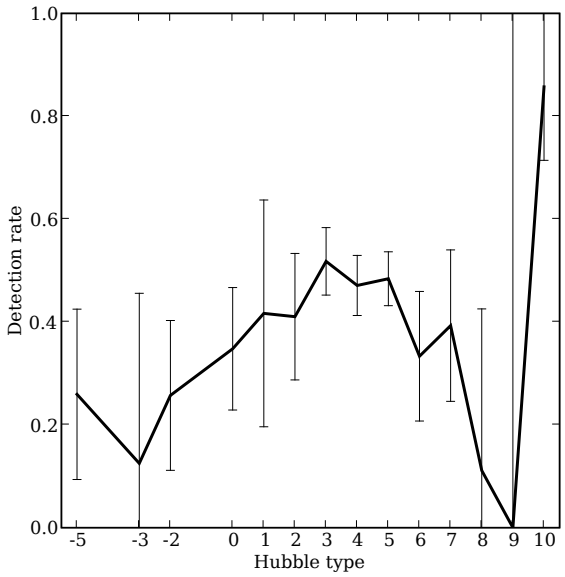

Figure 4.1: Detection rate at 1.4 GHz with NVSS as a function of Hubble type.

slowly towards types earlier than $T = 3$ (Sb). This can be contrasted to the much more rapid drop in the FIR detection fraction found in Lisenfeld et al. (2007). Alternative explanations for the relatively high detection fraction of earlier types include: 1) Sb–c spirals misclassied as Sa-ab ($T = 1$–2) due to low resolution imagery; 2) spirals misclassified as E/S0 ($T = -5$ to -2); and 3) the growing influence of radio emission unrelated to star formation in *bona fide* early types. The large fluctuation among the very late types likely involves small sample statistics.

4.3. Luminosities

Fig. 4.2 shows the distribution of radio luminosities as a function of type for all detections. In addition, we plot mean values including upper limits which were derived using the Kaplan-Meier survival analysis and calculated with our own software (see Appendix A) derived from the ASURV package (Lavalley et al. 1992). Since the radio detection fraction is less than 50% for all types the mean values lie quite low relative to the detections. Note that the mean of $\log(L)$ can be lower than the median of $\log(L)$. The weakest known classical radio loud quasars (FRIIs: Sulentic et al. 2003) show radio luminosities near $\log L_{1.4\mathrm{GHz}} = 23.5$ and the strongest sources in this sample are 0.5 dex below, with the majority of detected sources 1.5–2 dex below. With the exception of a few of the strongest sources all luminosities are consistent with nonthermal emission related to star formation. Figure 4.2 can be compared with the equivalent for FIR emission (Figure 5 in Lisenfeld et al. 2007).

The radio power distribution for the NVSS is shown in Figure 4.3. The vertical dotted line indicates the radio power corresponding to a completeness higher than 80% (i.e., more than 80% of the galaxies are detected at the corresponding radio frequency).

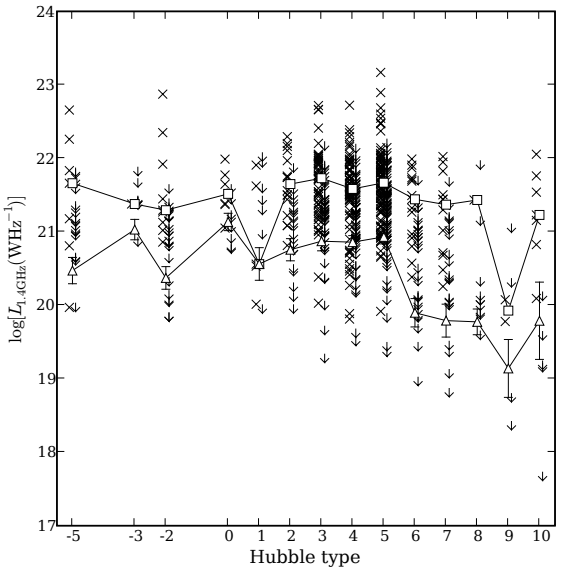

Figure 4.2: Distribution of radio luminosity at 1.4 GHz as a function of Hubble type. Only detections are shown. The open triangles give the mean value of $\log(L_{1.4\mathrm{GHz}})$ for each Hubble type, calculated with ASURV and taking the upper limits into account. The open squares are the median values for the detections only.

This line is calculated based on the sensitivity of NVSS survey, combined with a recession velocity lower than 9300 km s^{-1} for 80% of the CIG galaxies. We point out that the peak of the distribution for the NVSS data is above the level of radio completeness, leading to a better confidence in the radio properties at that frequency. Table 4.1 shows the mean value of the radio power using the Kaplan-Meier survival analysis, and the median value taking only detections into account. The big difference between the median and mean values reflects the large number of upper limits in the sample. The number of galaxies per frequency band in the AMIGA sample is indicated in the column N_{gal}, and the number of detections by N_{det}.

We compare the radio power distribution of the CIG sample with the one of the star-forming galaxies selected from the UGC sample (UGC-SF) in Condon et al. (2002). They studied the radio and star formation properties of the entire Uppsala Galaxy Catalog (UGC). They distinguished between star-forming galaxies and AGN in their study, finding that the star-forming galaxy population may be evolving even at moderately low redshift. The AGN have been discarded of the control sample, following their classification. We recomputed the radio continuum power and the distances of the sample by using the same Hubble constant that for the CIG sample. The UGC-SF and the CIG samples are located in a very similar local volume.

To compute the mean value of the radio continuum power for the UGC-SF, we used our version of ASURV, as for the CIG sample, by including the detections and the upper limits. The corrected *B* magnitude, retrieved from the HYPERLEDA database, was used for the UGC-SF sample. This photographic corrected magnitude is very sim-

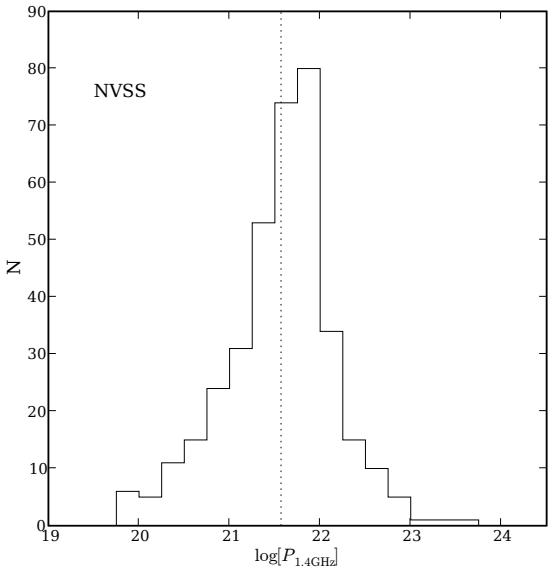

Figure 4.3: Distribution of the 1.4 GHz radio power for the CIG sample. The dotted line indicates the completeness for a velocity of 9300 km s^{-1} (80% of the sample). The x-axis indicates the logarithm of the power in W Hz^{-1}.

Table 4.1: Average properties of the radio power, log(P), for galaxies in the complete subsample and for the 1.4 GHz radiocontinuum emission of the UGC-SF sample (Condon et al. 2002).

Frequency	Mean log(P) (W Hz^{-1})	Median log(P) (W Hz^{-1})	$N_{\rm gal}$	$N_{\rm det}$
CIG/1.4 GHz	20.11±0.10	21.59	719	311
UGC-SF/1.4 GHz	21.61±0.62	21.65	3136	2815

ilar to the m_{B-corr} magnitude of the CIG sample (see Figure 4.7). To be consistent with the CIG sample, we applied a magnitude cut-off at $m_B = 15$ (see Verdes-Montenegro et al. 2005). Using owr own version of the survival analysis package ASURV (see Appendix A), the mean of log(P) = 21.61 appears significantly higher than for the CIG sample (20.11), as shown in Table 4.1. The median values are computed using the detections. The difference comes mainly from the upper-limits which are a much larger fraction in the CIG sample than in the UGC-SF sample (see Table 4.1) with a detection rate of 43% and 90% resp. for the CIG and UGC-SF samples. Moreover the Fig. 4.4, showing the log(P) distribution for both samples, indicates that the UGC-SF sample has a larger population with high radio continuum power (log(P) > 22).

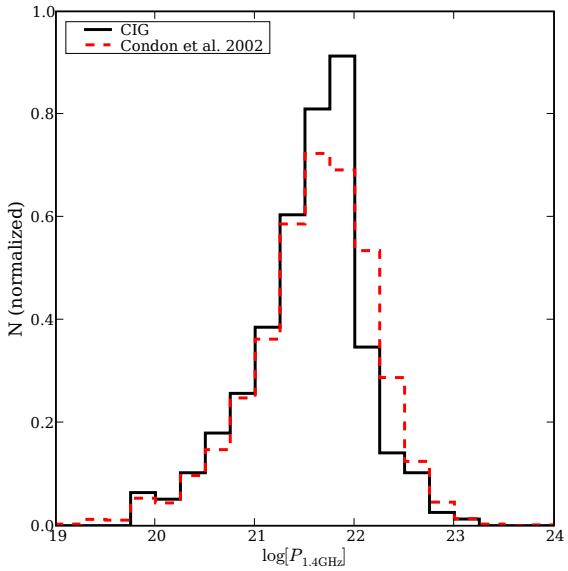

Figure 4.4: Frequency distribution of the 1.4 GHz radio power for the CIG sample (solid line) compared with the frequency distribution of the UGC-SF sample (dashed line) of Condon et al. (2002).

4.4. Radio vs. optical properties

Since our sample involves many of the most isolated galaxies (see Verley et al. 2007c,b) in the local Universe and, if radio emission is enhanced by interactions, then we expect it to show very passive radio continuum properties relative to almost any other local galaxy sample. Figure 4.5 compares the radio/optical flux density ratio R defined as:

$$R = S_{1.4\mathrm{GHz}} \times 10^{0.4(m_B - 14.2)}$$

where m_B is the apparent B magnitude of the galaxy and $S_{1.4\mathrm{GHz}}$ the flux density (in Jy) at 1.4 GHz. The definition is similar to the one used by (Condon 1980) (the optical magnitude was normalized to 15.0 in that study).

Comparison with KISS

We chose the value $m_B = 14.2$ for a better comparison with a sample of emission line galaxies (Van Duyne et al. 2004) which involved 207 emission-line galaxy candidates from the KPNO International Spectroscopic Survey (KISS) with NVSS or FIRST detections. Figure 4.6 shows the distribution of R values for detections in our sample, with E/S0 and spiral galaxies indicated separately. R shows a median value of 4.48 which is likely overestimated due to the bias introduced by the $\sim$ 2 mJy flux limit of the NVSS survey (as shown in Figure 4.5 by the dashed line).

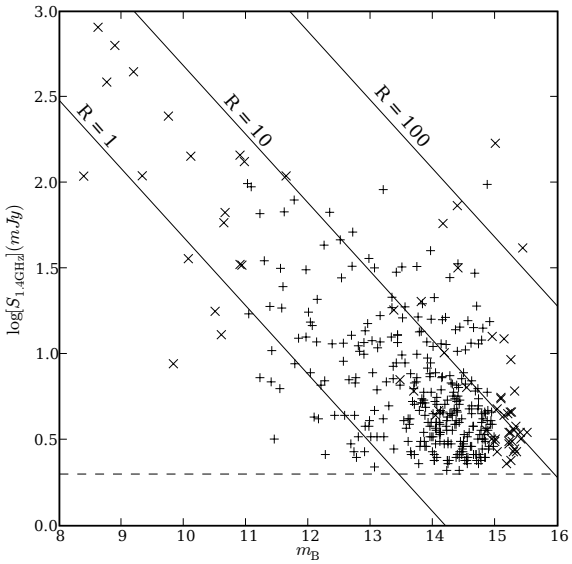

Figure 4.5: Radio flux density at 1.4 GHz (mJy) vs. apparent B magnitude. The lines represent constant radio-to-optical ratio R. The dashed line shows the value of R corresponding to the NVSS sensitivity level (2 mJy). In order not to overload the figure, we show only detections. The radio continuum upper limits were however taken into account in the calculation of the mean values. The plus signs denote galaxies within the complete AMIGA subsample and the crosses indicate galaxies outside this subsample.

As expected, we find the galaxies in our sample to be very radio quiet relative to their optical luminosities. Generally, high values of R ($R > 100$, e.g. Van Duyne et al. 2004) indicate the presence of a radio quasar while values between 10 and 100 can arise from a mix of Seyfert, LINER and starburst activity. Dusty galaxies with above average internal extinction can also boost some normal galaxies into this range. The dominance of low-R galaxies ($R < 10$) in our sample indicates that the radio emission from star formation is responsible for the majority of the detections. The KISS sample (Van Duyne et al. 2004) represents a good counterpoint with most of the galaxies showing $R > 10$. Only three galaxies in our sample show $R > 100$ (CIG 187, 349 and 836). CIG 187 radio continuum emission comes from an underlying background source (see Section 5.5) while CIG 349 is classified as Seyfert 1, is almost certainly an interacting/merger system and do not belong to the complete sample. CIG 836 is a relatively high redshift E galaxy ($V_R = 14\,900$ km s^{-1}) and is outside our complete sample. 17% of the Van Duyne et al. (2004) sample show $R > 100$.

Comparison with UGC-SF

We compare the R distribution of the CIG with the one of the UGC-SF sample of Condon et al. (2002). Figure 4.6 shows little differences between the two samples: the

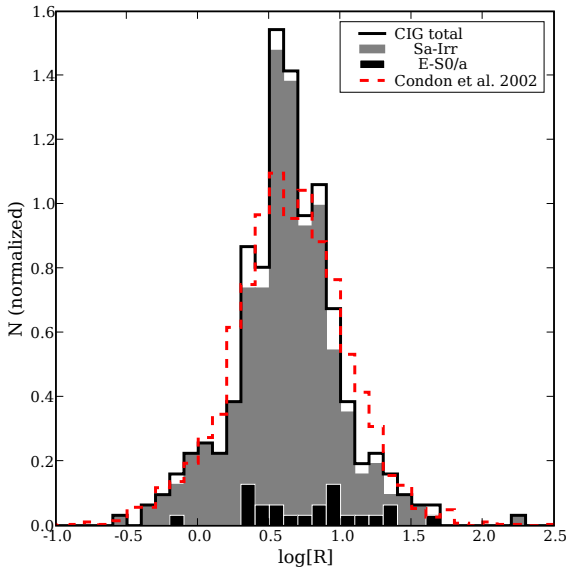

Figure 4.6: Distribution of the radio-to-optical ratio R (logarithmic scale) for the CIG sample (solid line). The elliptical and spiral galaxy distribution are represented respectively by black and grey shaded areas.The dashed line shows the R distribution for the UGC-SF sample (Condon et al. 2002).

R distribution of the CIG is sharper than the one of the UGC-SF sample. This later has more important wings, especially an excess for the large R ($\log(R) > 0.8$). The median value of 4.38 for R of the UGC-SF sample is just slightly larger than the one of the CIG sample (4.19). Figure 4.7 shows the optical luminosity L_B distribution for the CIG and the UGC-SF sample where it appears that the UGC-SF sample is slightly brighter in the B band than the CIG sample. The similar value of R between both samples is consistent with the higher radiocontinuum and L_B for the UGC-SF than for the CIG. The difference for the star formation activity is minimal between both samples, nevertheless the UGC-SF sample has a larger fraction of galaxies with more intense star formation per optical luminosity unit.

4.5. Comparison between NVSS and FIRST fluxes

The NVSS and FIRST surveys were obtained with different VLA configurations, resulting in different effective resolutions and, more importantly, in diminished spatial frequency sensitivity (scales larger than $\sim 30''$) for FIRST. Comparing NVSS and FIRST observations of the same source provides insights about the spatial distribution of emission in a galaxy. FIRST will largely sample only compact (likely nuclear) emission while NVSS will detect both nuclear and disk emission from galaxies in our sample. If low level star formation dominates the radio emission from most of our galaxies, then we expect NVSS fluxes to be larger than corresponding FIRST fluxes for our sample. A strong FIRST detection might indicate an active nucleus; these

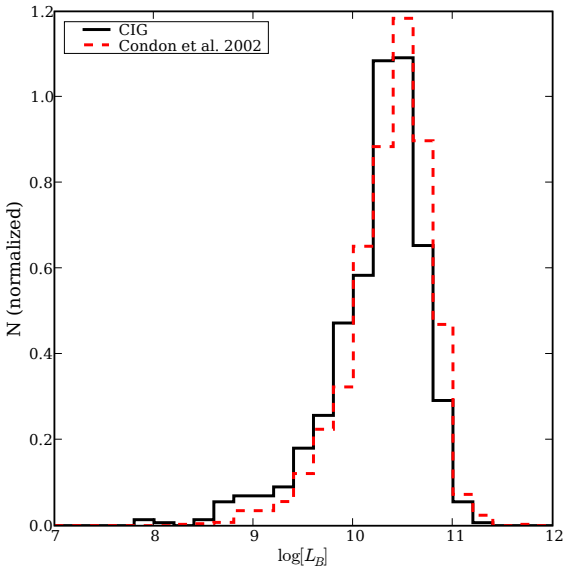

Figure 4.7: Optical luminosity distribution in *B* for the CIG (solid line) and the UGC-SF (dashed line) sample.

sources are expected to be rare in an isolated sample like AMIGA.

The much smaller FIRST detection fraction (14% vs. 35% for NVSS) immediately tells us what to expect – a sample dominated by disk star formation. FIRST fluxes are smaller than NVSS values in almost all sources. Most galaxies with a FIRST detection are Sb–Sc spirals, which represent 2/3 of the entire isolated population. This detection fraction suggests that more than half of our NVSS detected galaxies have disk-dominated radio continuum emission at 1.4 GHz because they are fully attenuated by FIRST. Figure 4.8 shows the FIRST/NVSS flux ratio distribution for our sample. About 40% of the galaxies detected by FIRST show core-dominated emission at 1.4 GHz, which implies ~ 20% of core-dominated galaxies in our sample. The radio continuum emission in core-dominated galaxies may originate either from nuclear SF or from an active nucleus. That question is addressed in the following chapters.

We note that Menon (1995), using VLA B- and C- configurations at 1.4 GHz, found that 46/56 radio detected members of compact galaxy groups showed compact core radio emission. Figure 4.9 compares the cumulative distribution function of FIRST/NVSS flux ratios for AMIGA and the Menon (1995) compact group sample – a striking comparison of nature vs. nurture in the radio domain. The CDF comparison shows that only 13% of compact groups have a ratio lower than 0.5, while 36% are found for the CIGs. This shows that isolated galaxies have a more disk-dominated radio emission than galaxies in groups where extreme interaction effects are expected.

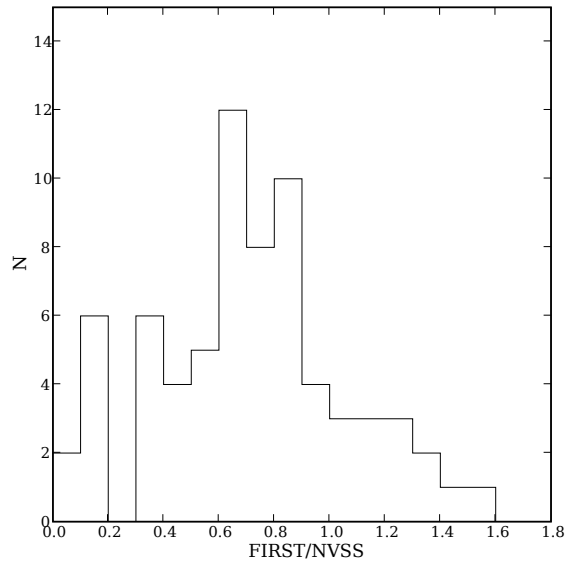

Figure 4.8: Histogram of the flux ratio between the FIRST and NVSS detections for the CIGs.

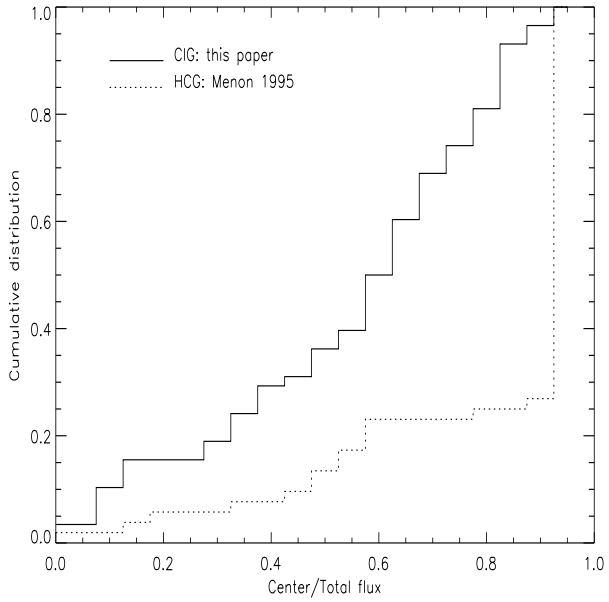

Figure 4.9: Cumulative distribution of the FIRST/NVSS flux ratio for the CIG (solid line) and the center/total flux ratio (dotted line) from Menon (1995).

Chapter 5

Radio continuum to far-infrared correlation

5.1. Introduction

The correlation between the FIR and the radio continuum emission in galaxies is very tight and is attributed to star formation (Helou et al. 1985; Condon et al. 1991). Massive stars ($M \gtrsim 8\mathrm{M}_{\odot}$) heat the dust which re-emits in the FIR. On the other hand, the supernovae produced at the end of the lives of these short-lived stars are ultimately responsible for the radio synchrotron emission from cosmic ray electrons accelerated in their shocks. Deviation from this correlation may be produced by nuclear activity (Sopp & Alexander 1991; Niklas 1997; Yun et al. 2001; Drake et al. 2003), since those AGN with compact (200 pc) radio cores, i.e., some radio-quiet AGN and all radio-loud AGN (e.g., Impey & Gregorini 1993; Roy et al. 1998) exhibit a radio excess.

Radio-loud active galaxies account to approximately 10% of the optically-identified galaxies with an AGN (Kellermann et al. 1989; Hooper et al. 1995). In radio-loud AGN, the radio emission from the nucleus is added to the emission produced by star formation. If this additional emission is strong enough, an excess of radio emission will be found with respect to the radio-FIR correlation. We use the radio-FIR correlation to identify radio AGN candidates.

5.2. Luminosity correlation

Since 468 galaxies in our complete subsample have at least one upper limit (radio or FIR) we have used survival analysis to compute the correlation to exploit the information carried in the upper limits. The Schmitt method (Schmitt 1985; Isobe et al. 1986) allows us to compute a correlation when upper limits exist in both the dependent and the independent variables. We use the complete subsample to calculate the correlation. We computed two regression lines to compare with other regressions of different samples and authors, one for $\log L_{1.4\mathrm{GHz}}(\mathrm{W\ Hz^{-1}})$ versus $\log L_{60\mu\mathrm{m}}(\mathrm{L}_{\odot})$ and the other for $\log L_{1.4\mathrm{GHz}}(\mathrm{W\ Hz^{-1}})$ versus $\log L_{\mathrm{FIR}}(\mathrm{L}_{\odot})$. The regression lines are:

$$\log L_{1.4\mathrm{GHz}}(\mathrm{W\ Hz^{-1}}) = [1.02 \pm 0.03] \log(L_{\mathrm{FIR}}/\mathrm{L}_{\odot}) + [11.4 \pm 0.3]$$

$$\log L_{1.4\mathrm{GHz}}(\mathrm{W\ Hz^{-1}}) = [1.025 \pm 0.023] \log(L_{60\mu\mathrm{m}}/\mathrm{L}_{\odot}) + [11.75 \pm 0.21].$$

In both cases, the slope is close to one. These regression lines have been computed adopting $\log L_{1.4\mathrm{GHz}}$ as the independent variable and minimising the residuals in the

y-axis. This is the usual way of computing the radio-FIR correlation in the literature, which enables us to carry out comparisons. Since we are interested in the physical relation between the two variables we prefer to use a symmetric method, the bisector best-fit (Isobe et al. 1990). In this case the regression lines are:

$$\log L_{1.4\mathrm{GHz}}(\mathrm{W\ Hz^{-1}}) = [1.06 \pm 0.03] \log(L_{\mathrm{FIR}}/\mathrm{L_\odot}) + [11.1 \pm 0.3]$$

$$\log L_{1.4\mathrm{GHz}}(\mathrm{W\ Hz^{-1}}) = [1.07 \pm 0.03] \log(L_{60\mu\mathrm{m}}/\mathrm{L_\odot}) + [11.31 \pm 0.23],$$

hence deviating slightly from linearity.

Radio-excess galaxies

Radio-excess galaxies are defined, according to Yun et al. (2001), as those whose radio luminosity is larger than 5 times the value predicted by the radio-FIR correlation. In Fig. 5.1, we show the galaxies of our complete subsample with the regression fit plotted as a solid line. The dashed lines denote a deviation by a factor 5. Galaxies above the upper-dashed line are selected as radio-excess galaxies. There are 6 radio-excess galaxies in the complete subsample (n = 710) and 2 more in the total sample. Other studies (Niklas et al. 1995; Condon et al. 2002; Mauch & Sadler 2007) use a cutoff factor of 3 for the radio excess, hence this cutoff will be also used to allow comparison with these samples. Using this value for our sample, we find 16 radio-excess galaxies in the complete subsample and 4 more in the total sample. In Table 5.1, we list the galaxies with a radio-excess (of a factor 3) for the total sample and, in Table 5.2, we detail separately the number of radio-excess galaxies and percentages for the complete subsample and for the early and late-type galaxies. The percentages are normalised to the number of galaxies that can be classified using this method. We can classify galaxies with detections in both bands, galaxies detected in radio continuum with an upper limit in FIR above the selection line and galaxies detected in FIR with an upper limit in radio continuum below the selection line.

5.3. Q parameter

The q-parameter (Helou et al. 1985) is a good estimator of the deviation from the radio-FIR correlation. It has been found to be independent of the starburst strength (Lisenfeld et al. 1996) and distance (Yun et al. 2001). It is defined as:

$$q \equiv \log\left[\frac{\mathrm{FIR}}{3.75 \cdot 10^{12}\mathrm{Wm^{-2}}}\right] - \log\left[\frac{S_{1.4\mathrm{GHz}}}{\mathrm{Wm^{-2}Hz^{-1}}}\right]$$

where $S_{1.4\mathrm{GHz}}$ is the flux density at 1.4 GHz in units of $\mathrm{Wm^{-2}Hz^{-1}}$ and FIR is the FIR flux calculated as:

$$\mathrm{FIR} \equiv 1.26 \cdot 10^{-14}\left(2.58 S_{60\mu\mathrm{m}} + S_{100\mu\mathrm{m}}\right)\mathrm{Wm^{-2}}$$

where $S_{60\mu\mathrm{m}}$ and $S_{100\mu\mathrm{m}}$ are IRAS 60μm and 100μm band flux densities in Jy.

We have computed the q-parameter using only the galaxies detected both in FIR and in radio continuum (n = 248) because non-detections will result in upper and lower limits of the q-parameter and, as far as we know, there is no statistical method to take both of them into account simultaneously. In Fig. 5.2, a histogram of the q-parameter is shown. The mean value is 2.36 with a dispersion of σ = 0.24. We define radio-excess galaxies in the same way as before by a deviation of more than a factor

Table 5.1: Radio-excess galaxies found using the radio-FIR correlation.

CIG	log $L_{\rm FIR}$ [1]	Code[2]	log $L_{1.4\rm GHz}$ [3]	T[4]	Excess factor[5]
Galaxies belonging to the complete subsample.					
41	9.67	0	22.07	Sc	5.7
72	9.72	1	21.91	Sbc	3.6
97	10.19	0	22.47	Sc	4.3
156	9.41	0	21.74	SBab	5.0
187	9.83	0	23.17	Sc	50.2
248	10.40	0	22.60	Sc:	3.5
287	9.97	0	22.39	SBbc	6.0
480	9.48	0	21.65	S0a	3.4
488	10.50	1	22.72	Sb	3.7
571	8.93	0	21.39	Sc	6.9
591	9.46	1	21.39	Sbc	4.1
692	10.33	0	22.67	Sb	4.9
734	8.79	1	21.05	S0a	4.4
877	10.40	0	22.66	E:	4.0
893	10.69	1	22.87	E/S0	3.4
1045	8.78	1	21.92	S0	19.7
Galaxies not belonging to the complete subsample.					
57	10.23	1	22.73	Sb	5.6
510	9.42	1	21.61	Sc	3.6
836	10.17	1	23.29	E/S0	29.7
999	9.90	0	22.09	Sa	3.5

[1] log $L_{\rm FIR}$ from Lisenfeld et al. (2007) in $L_\odot$ units.

[2] Detection code for log $L_{\rm FIR}$: 0 for detections and 1 for upper limits.

[3] log $L_{1.4\rm GHz}$ from Leon et al. (2008) in W Hz^{-1} units.

[4] Morphological type from Sulentic et al. (2006), except for CIG 999 (Karachentseva 1973, NED).

[5] Radio luminosity excess above the radio-FIR correlation.

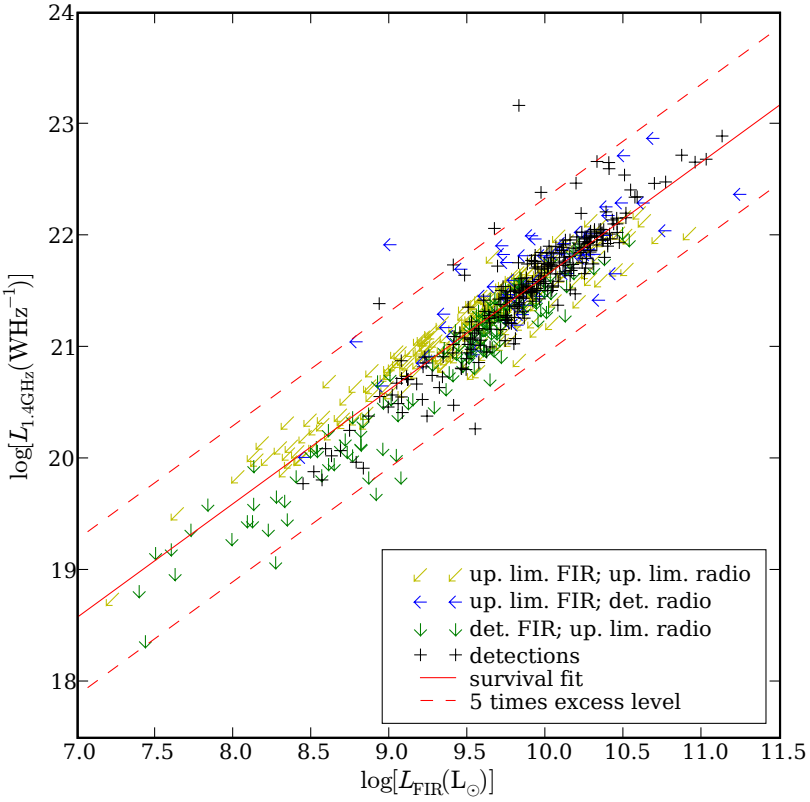

Figure 5.1: Radio versus FIR luminosity for the complete subsample (n = 710). We show the correlation as a solid line and the 5 times radio-excess and FIR-excess levels as dashed lines. The galaxies above the upper-dashed line are the radio-excess galaxies.

5, which translates into $q < 1.66$. This condition is fullfilled for 4 out of 248 galaxies (CIG 41, 187, 287 and 571), corresponding to 1.6% of the studied galaxies. This rate is slightly higher than the one derived from the luminosity correlation ($\approx$ 1%), but we have to take into account that the errors are very high (small numbers) and that radio-excess galaxies probably have a higher chance of being detected in both radio continuum and FIR. So this fraction could be considered as an upper limit for the fraction of radio-excess galaxies.

5.4. Background sources

Since the spatial resolution of the NVSS is not very high with respect to the size of the galaxies in our sample (97% of them are smaller than 4′, cf. Lisenfeld et al. 2007) there is a chance that the radio excess found using the NVSS data is in fact due to a background/foreground source projected in the line of sight of the galaxy. We

Table 5.2: Radio-excess ratios for the complete subsample.[1]

Morphology[3]	Radio-excess galaxies				FIRST revised [2]			
	Factor 5		Factor 3		Factor 5		Factor 3	
	N	%	N	%	N	%	N	%
All T (n = 397)	6	1.5	16	4.0	3	0.8	12	3.0
E-S0a (n = 21)	1	4.8	4	19.1	1	4.8	4	19.1
Sa-Irr (n = 376)	5	1.3	12	3.2	2	0.5	8	2.1

[1] All percentages for the fraction of radio-excess galaxies are upper limits as explained in Sect. 5.4.

[2] In Sect. 5.4 we explain how we revise these numbers using the FIRST survey.

[3] Morphological subsamples. The percentages are computed over the number of galaxies for each subsample.

computed this probability with two methods. In the first method, we estimated the density of radio sources expected in the NVSS dividing the number of sources in the catalogue by the covered area, and obtained a value of 159825.4 sources/sr. Since we have searched for a NVSS source within a radius of 35″ of each CIG galaxy, we determine that we could expect $n \approx 15$ unrelated sources in our total sample. In order to refine the previous value with a more local estimation of the probability, we estimated the average density of NVSS radio sources within a radius of 5° of each CIG galaxy. The mean value found for the density is similar to the previous one within 10% (172561.7 sources/sr), hence implying $n \approx 16$ unrelated sources in our complete sample. The radio flux of a source projected in the field of a CIG galaxy would add to its normal emission and take it above the radio-FIR correlation. Since the expected number of unrelated sources is of the same order as the number of radio-excess galaxies, we expect an even lower ratio of galaxies above the radio-FIR correlation.

In the second method, we have made use of the higher spatial resolution of the FIRST survey to check whether the radio emission of the radio-excess galaxies is associated with the nucleus of the galaxy. Three among the 6 galaxies in the complete subsample with a radio excess larger than a factor 5 are covered by FIRST and all of them turn out to be sources unrelated to the nuclei. Seven of the 16 galaxies with a radio excess larger than a factor 3 in the same sample are covered by FIRST, and 4 of them are also unrelated sources. One of the 4 galaxies showing a radio excess not belonging to the complete subsample is covered by FIRST and we find its radio emission also to be separated from the nucleus. In Table 5.3, we list for all these sources the NVSS and FIRST fluxes and the distance between the nucleus and the closest FIRST source. NVSS and FIRST data were taken on different dates, but the fluxes in both surveys are very similar so that we can discount the possibility that the extranuclear emission is produced by a supernova. With these results, we have revised the percentages of radio-excess galaxies and give them in Table 5.2.

Since 5 out of the 8 galaxies revised with FIRST have proven to be projected sources and given the number of unrelated sources that we have estimated, there is a high probability that many of the remaining radio-excess galaxies are also unrelated sources. We computed the revised fractions of radio-excess galaxies considering

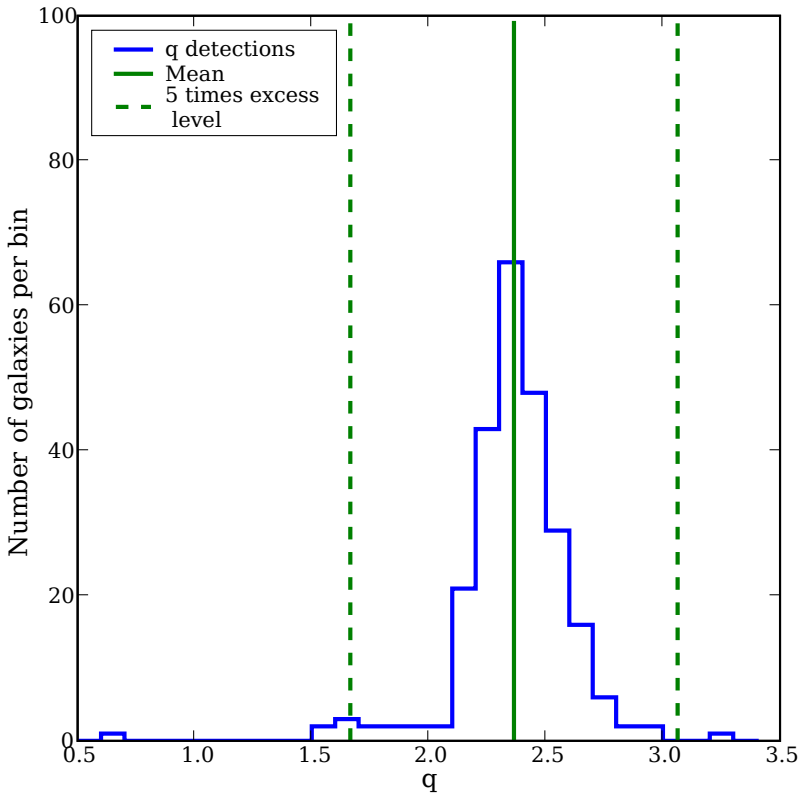

Figure 5.2: Histogram of the q-parameter showing the galaxies of the complete subsample detected both in radio and infrared ($n = 248$). We also show the mean with a solid line and the 5 times radio-excess and FIR-excess limits with a dashed line. Radio-excess galaxies are located in the left tail of the histogram with lower q values.

all the galaxies without FIRST data as genuine detections, consequently the derived fractions (Table 5.2) should be considered as upper limits.

5.5. High resolution imaging of radio-excess galaxies

We have observed the sample of radio-excess galaxies whit the Very Large Array (VLA) radio-interferometer in Socorro (NM, USA), in order to confirm the actual origin of the nuclear radio emission. Our aim was to distingish between genuine nuclear radio emission and emission from unrelated back-foreground sources. In the cases where the emission comes from the nucleus we study the properties of the nuclear source. We also observed a control sample, selected among the non radio-excess candidates, with similar galactic properties as the radio-excess sample.

We observed the galaxies with the configuration B of the VLA. The baselines for

Table 5.3: Radio-excess galaxies in FIRST.

CIG	NVSS flux (mJy)	FIRST flux[1] (mJy)	Distance[2] (″)
187	97.9	90.30	18.3
248	14.3	10.24	0.5
287	15.7	11.42	30.3
480	6.1	5.56	0.3
510	4.6	2.61	16.5
571	16.3	13.88	36.9
591	5.1	6.54	0.6
734	3.3	2.11	26.8

[1] Sum of FIRST fluxes within the NVSS search radius if more than one source is present.

[2] Distance from the CIG galaxy centre to the FIRST source. Distance to the nearest FIRST source if more than one source is present.

this configuration ranges from 0.21 km to 11.4 km. [1] Galaxies were observed in the X band (3.6 cm) in continuum mode. With the combination of B configuration and X band frequency we can reach a resolution of 0.7″. The bandwidth was of 50.0 MHz in each polarization. The obtained data was calibrated with AIPS. There is more information on the scheduling, calibration and additional information in the Apendix C.

In Table 5.4 we show the properties of the sources, nearby to the CIG observed galaxies, that we could identify in our data. The target column is the name of the galaxy observed plus a letter that identify the observing session when we observed more than once the source. The cutoff chosed for the signal to noise ratio was 10. We also add the information of two sources near the detection limit for CIG 287 and CIG 510 that visually seems to be genuine detections. We detected a source above the signal to noise limit for almost all the galaxies observed. In the case of CIG 33 and CIG 963 we did not observed any source near the galaxy. The emission of the NVSS looks to be extended and diffuse. It probably points out to an soft but intense star formation origin for the radio emission in these two galaxies.

We use the information obtained from this observations to check wether we have a genuine nuclear radio detection or an unrelated source of radio emission. In Table 5.5 it is shown the information about the confirmation for each galaxy. The columns are the following: 1) Name of the galaxy; 2) Type of galaxy: 1 for the radio-excess sample and 0 for the control sample; 3) Code indicating the subsample: 1 for the complete subsample and 0 for tha galaxies not belonging to the complete subsample, discarded in the statistical studies; 4) Level of radio-excess presented by the galaxy; 5) Distance from the observed source and the nucleus of the CIG galaxy; 6) Detection code: DET.- Nuclear source, OUT.- Background foreground source, NO.- Source not detected; 7) Comments.

[1] http://www.vla.nrao.edu/astro/guides/vlas/current/node9.html

Table 5.4: VLA sources

		Source position				
Target	Source	RA (J2000)	Dec (J2000)	RMS (μJy)	I (μJy)	Ext.
CIG33	-	-	-	28	-	
CIG41	a	00:58:24.20	36:43:17.4	39	852	
CIG57	a	01:37:48.25	02:17:27.6	44	2736	
CIG69	a	01:53:42.28	29:55:60.0	33	1243	
CIG72	a	01:55:22.03	06:36:42.4	51	5476	
CIG97	a	02:21:06.35	23:36:02.6	40	1207	
CIG129	a	03:32:38.44	01:22:57.2	41	1108	
CIG156	a	05:10:44.78	00:24:55.2	42	1616	
CIG156	b	05:10:44.50	00:24:49.2	42	600	
CIG187	a	07:23:31.99	41:26:17.4	66	34896	
CIG187	b	07:23:31.79	41:26:17.2	66	2003	
CIG204	a	07:45:07.25	46:04:22.6	32	391	
CIG248	a	08:24:14.31	17:19:55.1	31	1447	
CIG287	a	08:50:24.13	25:56:46.9	32	229	Low S/N
CIG287	b	08:50:27.32	25:59:36.1	32	727	
CIG480	a	11:26:55.08	18:49:57.2	32	1036	
CIG488	a	11:35:41.87	73:27:06.6	64	2086	
CIG510	a	11:54:50.12	02:57:31.0	34	321	Low S/N
CIG571	a	13:05:19.92	56:19:12.0	33	336	
CIG591	a	13:32:04.81	17:02:56.3	36	1518	
CIG692	a	-	-	67	-	
CIG692	b	15:35:46.99	73:27:01.1	67	1996	
CIG692	c	15:35:48.44	73:27:03.7	67	1053	
CIG692B	a	15:35:47.69	73:27:02.5	48	812	
CIG692B	b	15:35:46.94	73:27:01.3	48	3164	
CIG692B	c	15:35:48.39	73:27:03.9	48	1744	
CIG692C	a	15:35:48.05	73:27:04.8	55	359	
CIG692C	b	15:35:48.50	73:27:04.2	55	627	
CIG692C	c	15:35:47.02	73:27:01.5	55	946	
CIG734	a	16:17:15.89	61:56:26.2	32	716	
CIG771	a	16:46:49.17	22:54:18.5	43	1381	
CIG771B	a	16:46:49.16	22:54:18.4	32	1511	
CIG836	a	17:50:41.13	39:56:59.2	76	24149	
CIG893	a	20:55:36.50	−00:38:11.7	40	3508	
CIG963	-	-	-	136	-	
CIG999	a	22:55:56.92	06:23:18.2	34	627	
CIG999B	a	22:55:56.92	06:23:18.2	115	588	
CIG1004	a	23:04:56.63	12:19:24.6	35	2422	
CIG1004	b	23:04:58.50	12:19:19.2	35	553	
CIG1045	a	23:55:13.86	05:55:00.9	36	385	
CIG1045B	a	23:55:13.86	05:55:01.0	29	443	

Table 5.5: VLA confimation of sources

Galaxy	Type	Complete	Radio-excess	dist	Det	Notes
CIG 187	1	1	50.2	18.1	OUT	
CIG 836	1	0	29.7	1.3	DET	
CIG 1045	1	1	19.7	83.4	OUT	
CIG 571	1	1	6.9	41.5	OUT	
CIG 287	1	1	6.0	28.1	OUT	
CIG 41	1	1	5.7	34.1	OUT	
CIG 57	1	0	5.6	0.6	DET	
CIG 156	1	1	5.0	29.5	OUT	
CIG 692	1	1	4.9	1.0	DET	pos
CIG 734	1	1	4.4	26.7	OUT	
CIG 97	1	1	4.3	1.0	DET	
CIG 591	1	1	4.1	0.7	DET	
CIG 877	1	1	4.0	-	-	Not observed
CIG 488	1	1	3.7	2.3	DET	pos
CIG 510	1	0	3.6	16.3	OUT	
CIG 72	1	1	3.6	4.8	DET	pos!
CIG 999	1	0	3.5	49.7	OUT	
CIG 248	1	1	3.5	0.1	DET	
CIG 893	1	1	3.4	4.7	OUT	pos!
CIG 480	1	1	3.4	0.3	DET	
CIG 33	0	1	1.4	-	NO	
CIG 1004	0	1	1.0	4.0	DET	pos!
CIG 69	0	1	2.1	1.2	DET	
CIG 129	0	1	2.8	15.2	OUT	
CIG 204	0	1	2.5	3.0	DET	pos
CIG 771	0	0	2.4	0.7	DET	
CIG 963	0	0	2.4	-	NO	
CIG 80	0	0	1.1	-	-	Lost obs.
CIG 116	0	1	0.9	-	-	Lost obs.
CIG 312	0	1	1.1	-	-	Lost obs.
CIG 309	0	0	0.5	-	-	Lost obs.
CIG 359	0	1	1.3	-	-	Lost obs.

Table 5.6: Final radio-excess ratios for the complete subsample.[1]

Sample	Number of galaxies	N radio-excess galaxies	% radio-excess galaxies
Factor 5 complete	390	0	0.0%
Factor 3 complete	393	8	2.0%

5.6. Final rate of radio-excess galaxies

Combining the data of the radio-excess sample of § 5.2 and the high resolution data from the VLA observations we can obtain improved statistics of the rate of radio excess galaxies in our sample of isolated galaxies.

All the galaxies with a factor 5 radio excess belonging to the complete subsample are identified as unrelated sources. There are 7 genuine nuclear sources with factor 3 radio-excess and one source not confirmed (CIG 877) that we will consider for the statistics as a genuine source. In Table 5.6 are shown the final rates of radio excess galaxies.

The rate of radio-excess galaxies with a factor 3 is 2.0%. There are no radio-excess galaxies with a factor 5 of radio excess in the AMIGA sample of isolated galaxies.

Chapter 6

Far infrared colour

6.1. Introduction

In the work of de Grijp et al. (1985) a method to identify AGN candidates using FIR properties was presented. Galaxies hosting an AGN have, in general, a flatter spectrum in FIR. This is due to the warmer temperatures of the dust heated by the central engine. The advantage of the method is that it can identify obscured AGN that cannot be found with other wavelengths or methods. The success rate of this method is about 70% (de Grijp et al. 1985, 1992).

The original selection criterion of de Grijp et al. (1985) was to select IRAS objects with $-1.25 < \alpha_{25\mu m,60\mu m} < -0.5$ where $\alpha_{25\mu m,60\mu m}$ is the spectral index between $S_{25\mu m}$ and $S_{60\mu m}$. [1] The upper limit to $\alpha_{25\mu m,60\mu m}$ in the de Grijp et al. (1985) criterion is thought to reject stars and other galactic objects like planetary nebulae if the objects of the sample are not known to be only galaxies. All the objects of our sample are galaxies so we did not apply a upper limit to $\alpha_{25\mu m,60\mu m}$. The lower limit in the selection criterion changes from author to author. In Table 6.1 are shown the different selection criterion for different authors.

For our analysis, we select those galaxies with $S_{25\mu m}/S_{60\mu m} \geq 0.18$ (which is equivalent to $\alpha_{25\mu m,60\mu m} > -1.958$) as AGN-candidates, following the studies by Yun et al. (2001) and Reddy & Yun (2004).

6.2. Statistics

In Fig. 6.1, we plot $\log S_{25\mu m}$ versus $\log S_{60\mu m}$ for the total sample. The $S_{25\mu m}/S_{60\mu m}$ ratio of 0.18 is plotted as a solid line. The triangles and squares denote detections and the arrows upper limits. A total of 197 galaxies of the total sample or 162 of the complete subsample can be classified using this method (Table 6.2) since they are: a) detections in both bands; b) detections at $S_{60\mu m}$ and upper limits at $S_{25\mu m}$ with flux ratios below the $S_{25\mu m}/S_{60\mu m} = 0.18$ line; or c) detections at $S_{25\mu m}$ and upper limits at $S_{60\mu m}$ with flux ratios above the $S_{25\mu m}/S_{60\mu m} = 0.18$ line. Fifty-eight galaxies in the total sample and 46 in the complete subsample are AGN-candidates. Hence 28.4%

[1] The spectral index (α) is defined as the slope of the flux at a given frequency: $S_\nu \propto \nu^{-\alpha}$ where α is the spectral index, S is the flux density and ν is the frequency. Some authors deffined the spectral index with the oposite sign. The spectral index between two frequencies is calculated as the slope of the flux between these two frequencies if this should follow a power law: $\alpha_{1,2} = \dfrac{\log \frac{S_1}{S_2}}{\log \frac{\nu_1}{\nu_2}}$.

Table 6.1: Spectral index selection criterion in the FIR for different authors.

Authors	Year	$\alpha_{25\mu m,60\mu m}$
de Grijp et al.	1985	-1.25
de Grijp et al.	1987	-1.5
Keel et al.	1988	-1.5
Low et al.	1988	-1.58
Sanders et al.	1988	-1.84
Xu et al.	1998	-1.5
Xu et al.	2001	-1.84
Yun et al.	2001	-1.958
Reddy & Yun	2004	-1.958

Table 6.2: Classified galaxies using the IRAS colour method.

CIG	$S_{25\mu m}$ (Jy)[1]	Code[1,2]	$S_{60\mu m}$ (Jy)[1]	Code[1,2]	Classification[3]
Galaxies belonging to the complete subsample.					
4	0.61	0	5.19	0	normal
41	0.19	0	0.39	0	AGN
55	0.36	0	2.30	0	normal
56	0.23	1	1.60	0	normal
66	0.21	0	1.23	0	normal
...	...	...	...	...	...
Galaxies not belonging to the complete subsample.					
26	0.48	0	0.22	0	AGN
62	0.25	0	2.07	0	normal
80	0.92	0	6.84	0	normal
105	0.66	0	7.60	0	normal
121	0.60	0	6.22	0	normal
...	...	...	...	...	...

[1] Data from Lisenfeld et al. (2007).

[2] Detection code: 0 for detections and 1 for upper limits.

[3] Normal for $S_{25\mu m}/S_{60\mu m} < 0.18$ and AGN for $S_{25\mu m}/S_{60\mu m} \geq 0.18$.

of the galaxies for which a classification could be assigned are AGN-candidates. We obtained a lower limit to the total fraction of AGN-candidates of 6.5% by normalising to the complete subsample ($n = 710$). This is a lower limit because it assumes that the unclassified galaxies do not host an AGN.

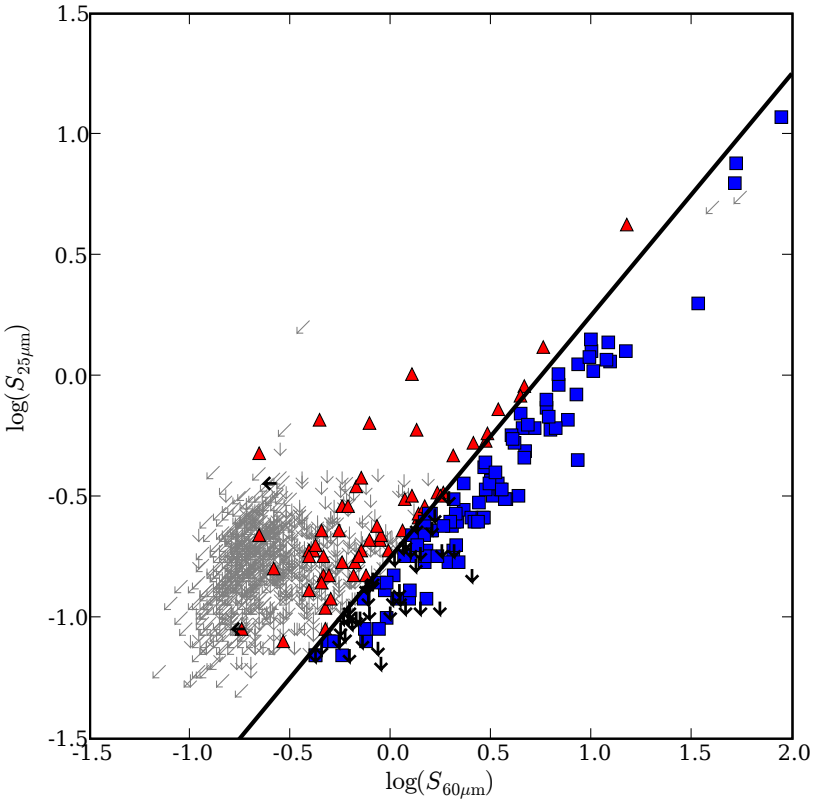

Figure 6.1: Plot of $\log S_{25\mu\mathrm{m}}$ versus $\log S_{60\mu\mathrm{m}}$ for the total sample (n = 1030). The solid line corresponds to $S_{25\mu\mathrm{m}}/S_{60\mu\mathrm{m}} = 0.18$. Galaxies classified as AGN-candidates lie above this line and are plotted as triangles and black left-arrows. Galaxies classified as non AGN-candidates are below the line, plotted with squares and black down-arrows. The remaining galaxies can not be classified due to upper limit in the fluxes (grey arrows).

Part III

Optical spectra

Chapter 7

Sloan Digital Sky Survey spectra

7.1. Introduction

The Sloan Digital Sky Survey (SDSS; York et al. 2000; Adelman-McCarthy et al. 2008) is a large optical survey that provides images and spectra for almost a quarter of the sky. They use a dedicated 2.5 metres telescope with 3 degree field of view located at the Apache Point Observatory in New Mexico (USA). The imaging survey is performed by a mosaic CCD camera. The filters used are u, g, r, i and z that cover all the optical bands, from the atmospheric cutoff in the blue to the sensitivity limit of the CCDs in the red. Spectra are obtained with two multifiber spectrographs. The diameter of the fibers of the spectrographs is $3''$.

The imaging is done in a drift-scan mode and the total integration time for each image in each filter is 54.1 seconds. The image data are processed by automatic pipelines which perform several measurements on the detected objects. The spectra covers the range from 3800 to 9200Å over 4098 pixels. Each spectroscopic snapshot is done with a mask plate which can hold up to 640 fibers. The minimum separation between fibers is $55''$. The spectral resolution ranges between 1850 and 2200 ($\lambda/\Delta\lambda$) and the accuracy of the spectrophotometry is up to about 20%.

The targets for the spectral observations are selected uniformly from the imaging data. The algorithm to select the main sample of galaxies is described in Strauss et al. (2002) and the one to select QSOs is described in Richards et al. (2002). Galaxies are separated from stars by their morphology and QSOs are selected by their non-stellar colours and by the matching with FIRST radio sources. Although none of our galaxies is a QSO, some of them could have fallen in the a priori selection by Richards et al. (2002).

The data are reduced with automatic pipelines and are made public periodically in data releases. Each new data release improves the sky coverage and the quality of the data reduction. At present the last data release available is Data Release 7[1] but we used the Data Release 6[2] that was the one available when we started the study.

7.2. SDSS data

We looked for the galaxies of the AMIGA sample that are covered by the SDSS survey region and we took the data from the Data Release 6 (DR6) of the SDSS

[1] http://www.sdss.org/dr7/
[2] http://www.sdss.org/dr6/

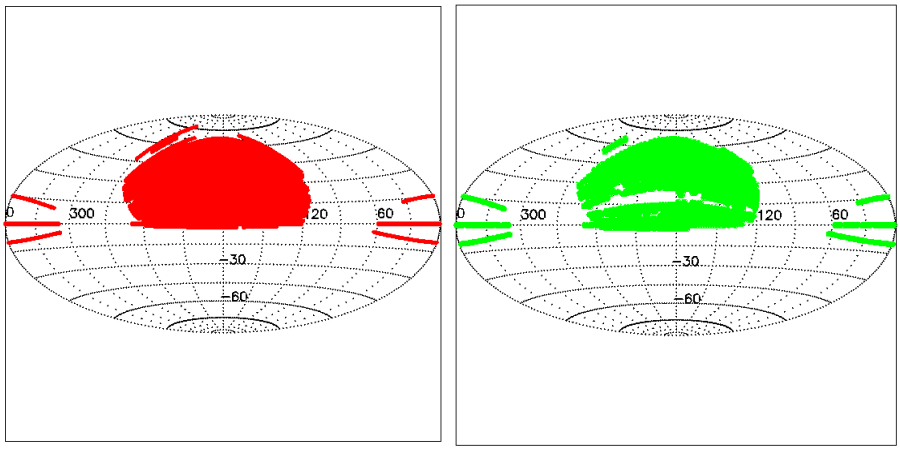

(a) Coverage of the imaging survey (b) Coverage of the spectral survey

Figure 7.1: SDSS DR6 sky coverage. Aitoff projection of Equatorial coordinates for the imaging and spectral survey. Source: SDSS

(Adelman-McCarthy et al. 2008). There are 549 AMIGA galaxies covered by the DR6. In DR7 there are 83 new AMIGA galaxies covered by the survey.

The SDSS images are indexed by the parameters: *run*, *rerun*, *camCol*, *field* and *filter*. The spectra are indexed by: *plate*, *mjd* and *fiberid*. There is also a unique *ObjID* and *SpecID* number for imaging objects and spectra respectively. These parameters are necessary to take the data from the data server. Hence, the first step was to find these parameters for the images and spectra of our galaxies.

We entered our list of coordinates in the interface available in the SDSS webpage[3] in order to cross-correlate the coordinates with the SDSS photometric objects, selecting the option "All nearby primary objects", a search radius of 0.5′, and using the following SQL query:

```
1  SELECT
2      p.objID, p.ra, p.dec, p.run,
3      p.rerun, p.camCol, p.FIELD,
4      "ugriz" AS filter,
5      dbo.fPhotoTypeN(p.type) AS type,
6      p.modelMag_u, p.modelMag_g,
7      p.modelMag_r, p.modelMag_i, p.modelMag_z,
8      ISNULL(s.z,-9999), ISNULL(s.specobjID,0),
9      ISNULL(s.plate,0), ISNULL(s.mjd,0),
10     ISNULL(s.fiberid,0)
11 FROM #x x, #upload u, PhotoTag p
12 LEFT OUTER JOIN SpecObj s ON s.bestobjid=p.objid
13 WHERE u.up_id = x.up_id AND x.objID=p.objID
14 ORDER BY x.up_id
```

[3] http://cas.sdss.org/astrodr6/en/tools/crossid/upload.asp

This query gave us a list of photometric objects, catalogued by the SDSS pipeline, near the estimated center of our galaxy, and the corresponding SDSS spectral object if available. Selecting "primary objects" we reject the duplicated objects in the overlapping zones for different strips of the survey and we took only the best detection for each object. We tried searches within different radii and we decided to use a value of $0.5'$, which provides us with the better relation between the number of detected galaxies and a reasonable number of objects to check within each radius.

To choose the correct photometric and spectral objects among the detections within the selected search radius we used a semi-automatic selection algorithm. The algorithm chose the object with more flux in the z band and later we visually inspected the images and the selected objects as a cross-check for the accuracy of the selection. The selection usually worked well but $\sim 8\%$ of the photometric objects were misclassified. The usual source of confusion was a nearby star and the correct object was usually ranked as the second in flux intensity. We changed manually the selection in order to choose the correct object. In 5 cases the correct photometry for the galaxy was assigned to an object whose estimated position was distant from the centre of the galaxy where the spectrum was taken. In these cases we manually chose the correct photometric object and the correct spectrum but we also recorded in our database the photometric object associated to the spectrum. Only in one case (CIG 936) the selection of the spectrum and the photometric object was done totally in a manual way.

In some cases the spectra were taken in positions shifted with respect to the centre of the galaxies. They were recorded for future studies but discarded for the study of the nuclear activity. These two kinds of spectra are marked in our database. Usually, the distinction was automatically done but we visually inspected all the selected spectra. In one case, CIG 262, we found that the spectrum of was centred in a nearby star or stellar cluster but not in the centre so we excluded this as a nuclear spectrum (see Fig. 7.2a).

We inspected in more detail some special cases. CIG 402 is completely dazzled by the light of a nearby star (see Fig. 7.2b), hence, the photometry and the selected spectrum were flagged off as invalid. Two diffuse galaxies of our sample are actually Milky Way satellites, CIG 802 (Draco dwarf) and CIG 388 (Sextans B). They had non-accurate photometry because their stars are resolved, and their spectra do not correspond to any nucleus (see Fig. 7.2c and Fig. 7.2d). These two galaxies were also marked as invalid.

Finally, we have obtained the photometry for 545 of the 549 AMIGA galaxies covered by the DR6. The photometric parameters were stored in the database with the index number of the corresponding SDSS photometric object for each galaxy. This index number can be used to extend the number of photometric parameters from the SDSS database in the future. At this stage we had found a nuclear spectra for 362 of our galaxies.

The next step was the downloading of the spectral data. The data was downloaded with the *SDSS Data Archive Server: DR6*[4]. A parameter file has to be entered and the system returns a list with the urls of the FITS files. We prepared a *csv* file with the appropriate parameters for our spectra and downloaded the actual spectra FITS files with *wget*.

The spectral FITS files of the SDSS are composed by 6 Header and Data Units (HDU) which are the basic components of FITS files, consisting of header keyword records followed by optional associated data records. The first HDU has associated an

[4] http://das.sdss.org/DR6-cgi-bin/DAS

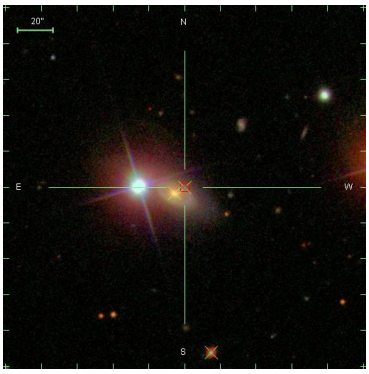

(a) CIG 262. Spectrum outside the centre.

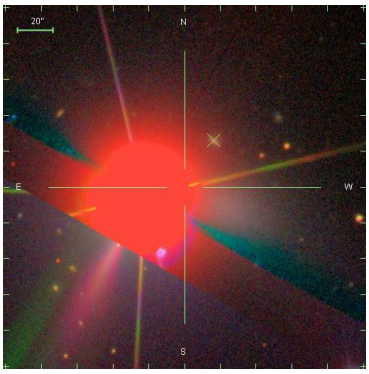

(b) CIG 402. Galaxy dazzled by a nearby star.

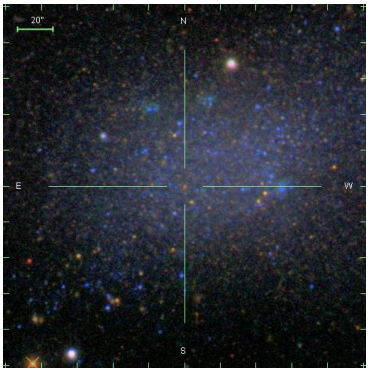

(c) CIG 388. Diffuse nearby galaxy, Sextans B, with bad photometry.

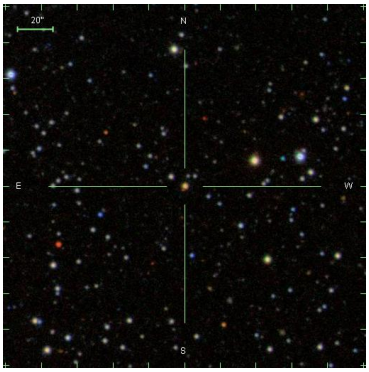

(d) CIG 802. Diffuse nearby galaxy, Draco dwarf, with bad photometry.

Figure 7.2: SDSS-DR6 special photometric and spectral cases.

array of spectral data and the following 5 HDUs are arrays with additional data like, e.g. line detections and measurements. The format of the FITS file and the HDUs is described in `http://www.sdss.org/dr6/dm/flatFiles/spSpec.html`. From the spectral array we compile the data for the flux, the error in the flux and the error mask.

The first HDU contains some important headers that we entered in our database (they are listed in Appendix B.1). The wavelengths of the spectral data are not directly available as an array and they have to be derived from the keywords `COEFF0` and `COEFF1`. The first is the central wavelength of the first pixel of the array given in units of decimal logarithm of the wavelength in Ångstroms. The second is the "dispersion per pixel" in the same units. Thus, the wavelength array has to be computed in this way:

$$\lambda = 10^{(\texttt{COEFF0}+\texttt{COEFF1}*i)}$$

where i is the pixel index number, starting by 0 for the first pixel. One important disadvantage of giving the wavelength units in such manner is the possible propagation of the computational error when calculating the wavelength array. This error could depend on the numerical precision of the used computational system and on the method

Table 7.1: Nuclear spectra rejected due to bad data in zones of lines.

CIG	Zone(s)
190	Hβ
328	Hα, [O I] and [S II]
330	[S II]
347	All the spectrum
479	Hα
499	[S II]
636	Hα and [S II]
658	Hα and [S II]
702	Hα and [S II]

used to reconstruct the wavelength array.

We visually checked all the spectra and found that some of them had zones with bad data. In some of the cases the bad zones do not affect the zones used to measure the lines but in other cases they were located on the top of the lines to be measured. In one case, CIG 347, all the spectral data were lost. In table 7.1 we show galaxies with bad zones. These galaxies were not taken into account for our study in order to avoid inhomogeneities in the processing of the data. It should not lead to any bias due to the random distribution of the probability of having a bad zone in the spectrum.

After flagging galaxies with bad zones we have a final number of 353 galaxies for our study of nuclear spectra of the AMIGA isolated galaxies.

Princeton data

There is an alternative reduction of the SDSS data (it is called re-reduction), done at Princeton University and publically released at `http://spectro.princeton.edu/`. The description taken from the web page is the following: "Note that these reductions are not identical to the "official SDSS data release", but have several improvements and include our redshift fits, spectral classifications, velocity dispersions for galaxies, and emission line fits." These data really improve the measurement of the velocity dispersion and the redshift. The velocity dispersion is determined for 42.4% of the galaxies in the standard data and for 97.5% of the galaxies in the Princeton data. The differences in the redshifts between them are negligible; there are only 3 galaxies with a difference of more than 100 km/s (see Fig. 7.3). This spectral reduction pipeline is also known as *specBS* and determines the parameters of the spectrum via a comparison with carefully selected templates of stars, galaxies and quasars from the SDSS and the ELODIE survey (Moultaka et al. 2004) as explained in `http://www.sdss.org/dr6/algorithms/redshift_type.html`.

We proceeded to obtain the FITS files for our galaxies from the Princeton archive. We took the data from the FITS HDUs and entered them in our database. The two parameters that we will use from this database are the velocity dispersion and the redshift. This pipeline produces measurements of the emission lines by fitting of a Gaussian there where a line is expected. We entered these data for future comparison with our own fitting of the emission lines.

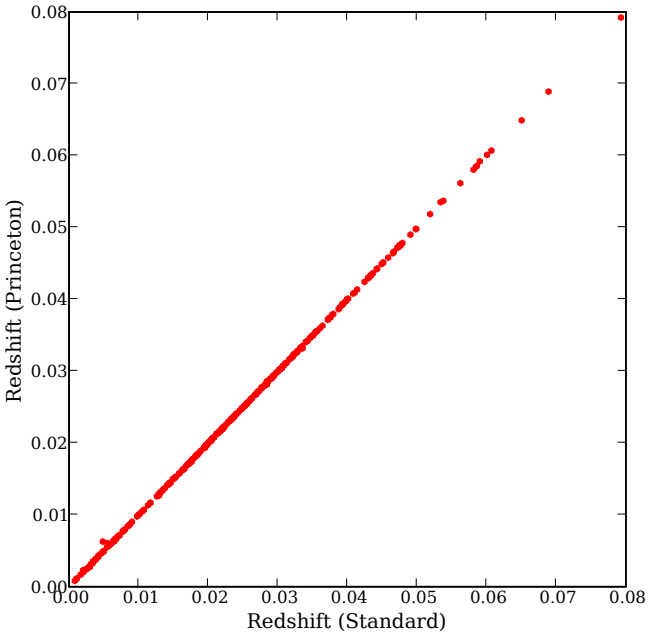

Figure 7.3: Comparison between the redshifts measured with the standard pipeline and the specBS pipeline (Princeton).

7.3. SDSS sample

The SDSS-DR6 subsample for our nuclear activity study is composed of 353 galaxies. From now, we will call this sample *the SDSS subsample*.

We estimated the completeness of the SDSS subsample using the $\langle V/V_m \rangle$ test (explained in Section 3.1). In Figure 7.4 the completness for the AMIGA samples and for the AMIGA SDSS subsample are shown. The SDSS subsample is even more complete than the total AMIGA sample taking a limiting magnitude of 15.0. The galaxies that are both in the SDSS subsample and in the complete subsample form *the SDSS complete subsample*.

We compared the optical luminosities, the distances and the morphologies of the galaxies of the SDSS complete subsample with the ones of its parent sample (the AMIGA complete subsample). The SDSS complete subsample will be the reference sample used in our statistical studies and it is important to test whether any bias exists in its selection. We consider the optical luminosity and the morphology parameters as two of the most representative of the properties of AMIGA galaxies which were selected using optical wavelengths. The distribution of distances is an indicator of the possible observational effects that could affect our subsample. E.g. the signal to noise level of the measured lines depends on the distance to the galaxy. We will only consider the SDSS subsample representative of the AMIGA sample if there are no bias in its selection.

To test if the two samples, the parent sample and the SDSS sample, are signifi-

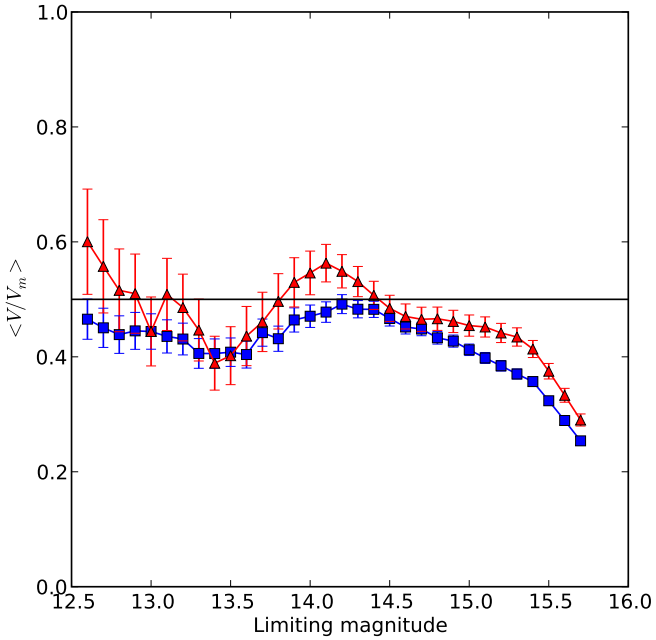

Figure 7.4: The $\langle V/V_m \rangle$ test for the SDSS subsample ($n = 353$) and the CIG total sample ($n = 1051$) excluding galaxies brighter than 11 mag. The red triangles indicate the SDSS subsample and the blue squares indicate the total sample.

cantly different. We used the Kolmogorov-Smirnov test (Kolmogorov 1933; Smirnov 1936) to estimate at what significance level we cannot reject the null hypothesis that the SDSS subsample is derived from the parent sample. As the parent samples are not continuum distributions and this is required by the Kolmogorov-Smirnov test, we interpolated the values of the cumulative distribution to obtain the reference distribution. Due to the large number of galaxies in the complete subsample, we obtained a smooth parent distribution. We could only apply this test to the luminosity and to the distance distribution. In Table 7.2 we show the statistical parameters computed for the Kolmogorov-Smirnov tests. D* is the Kolmogorov-Smirnov statistic, defined as the the largest value of the maximum positive or the maximum negative differences between the parent cumulative distribution and the observed cumulative distribution, P* is the probability to reject the null hypothesis at this level and α is the probability to not reject the null hypothesis (1-P*). A widely used significance level limit to reject the null hypothesis is $\alpha \leq 0.05$. Looking at this test, the luminosity distribution is clearly derived from the parent sample but this is not so clear in the case of the distance distribution.

If we change the null hypothesis to check if the two samples come from the same (undefined) parent sample the statistics slightly changes. This test is more appropriate in the cases where the two distributions are discrete. In Table 7.2 in the "Kolmogorov-Smirnov two-sample test" section we show the new statistics. K* is the scaled version of D* defined as $\sqrt{n}D^*$, but in the case of the two sample test it is: $K^* = \sqrt{\frac{n_1 n_2}{n_1+n_2}}D^*$.

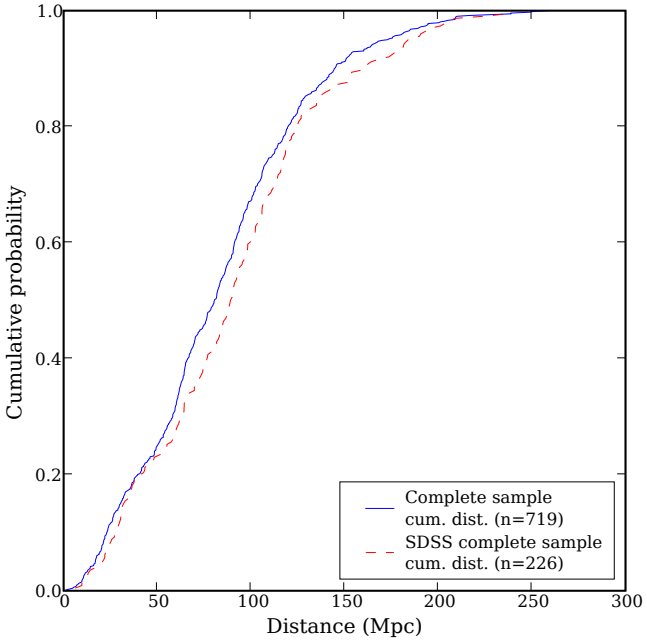

(a) Cumulative distribution of the distance

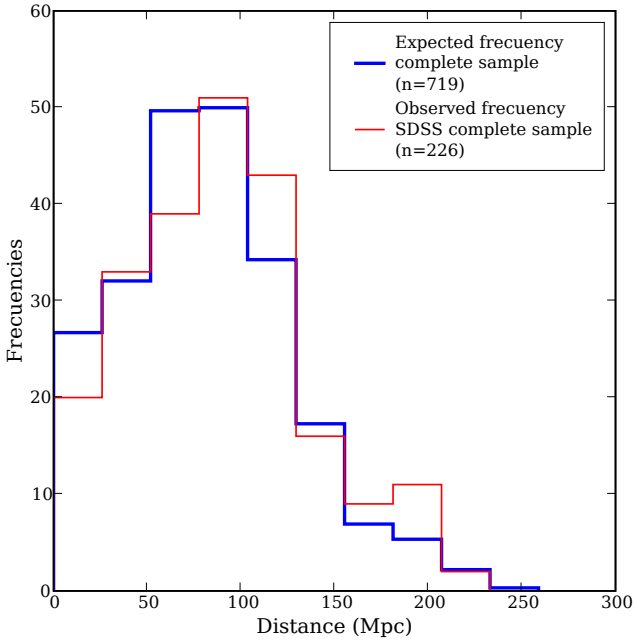

(b) Observed and expected binned distributions of the distance

Figure 7.5: Comparison between the statistical distribution of the distance for the complete subsample and the SDSS complete subsample. Subplot (a) shows the cumulative distribution for the SDSS complete subsample as a dashed line and the one for the complete subsample as a solid line. The cumulative distribution is used to perform the Kolmogorv-Smirnov test. The binned distribution plot shows the observed and the estimated frequencies (derived from the complete subsample). These frequencies are used to perform a χ^2 test.

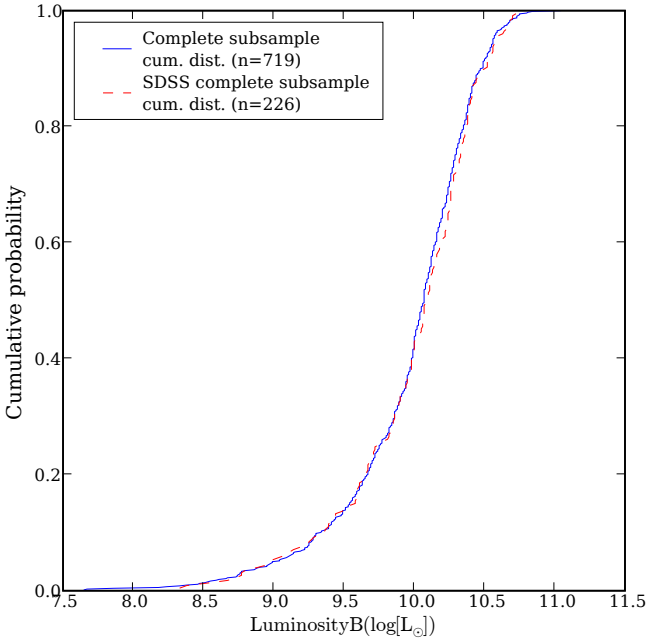

(a) Cumulative distribution of the optical luminosity

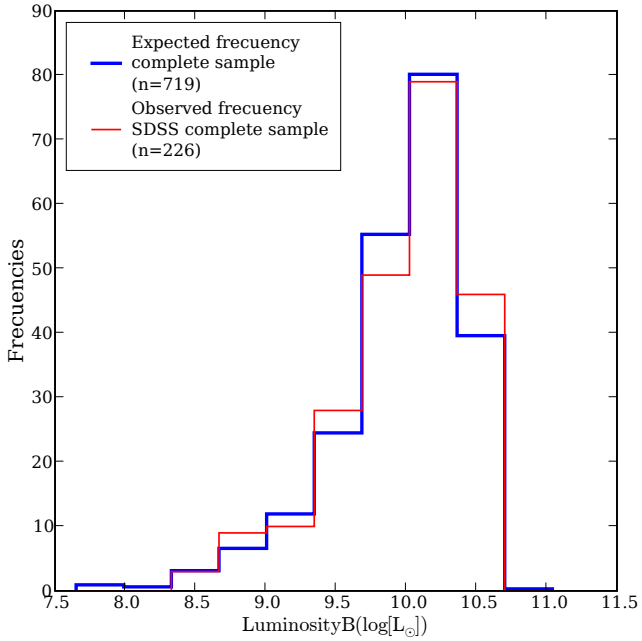

(b) Observed and expected binned distributions of the optical luminosity

Figure 7.6: Comparison between the statistical distributions of the optical luminosity for the complete subsample and the SDSS complete subsample. Subplot (a) shows the cumulative distribution for the SDSS complete subsample as a dashed line and the one for the complete subsample as a solid line. The cumulative distribution is used to perform the Kolmogorv-Smirnov test. The binned distribution plot shows the observed and the estimated frequencies (derived from the complete subsample). These frequencies are used to perform a χ^2 test.

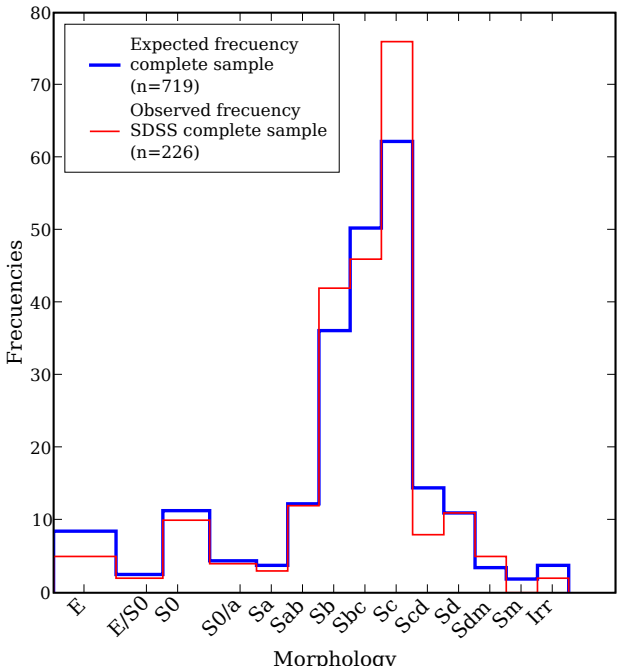

Figure 7.7: Observed and expected binned distributions of the morphology.

In this case the α level of the Kolmogorov-Smirnov test for the distance distributions is big enough to not to reject that the two samples come from the same parent sample at a 10% significance level.

In Fig. 7.5a and Fig. 7.6a the cumulative distributions of the distance and the luminosity respectively are plotted. The distribution for the complete subsample is plotted as a continuum blue line and the distribution for the SDSS complete subsample as a red dashed line. It is clear from the figures than the two distributions of the luminosity are very similar. There are slight differences between the two distributions of the distance. Depending on the Kolmogorov-Smirnov method used these differences are significant or not.

We applied the χ^2 test to the distributions. This test is very suitable for the study of the morphology distribution due to its discrete nature. First, we divided the luminosity and the distance distributions in 10 bins. The morphology has 14 bins corresponding each one to a morphological type. The observed values (O_i) for each bin correspond to the galaxies counted in this bin for the SDSS subsample. The expected values (e_i) are the values expected if they should follow the same distribution of the complete subsample. χ^2 is computed as:

$$\chi^2 = \sum_i \frac{(O_i - e_i)^2}{e_i}$$

To calculate the significance level we have to take into account the degrees of freedom. In this case the degrees of freedom are one less than the number of bins. The statistical parameters computed for the χ^2 test are shown in Table 7.2. The significance level is

Table 7.2: Parameters of the statistical tests.

Kolmogorov-Smirnov test			
Parameter	Distance	L_B	Morphology
D*	0.0872	0.0542	-
P*	0.9698	0.7441	-
α	0.0302	0.2559	-
Kolmogorov-Smirnov two-sample test			
Parameter	Distance	L_B	Morphology
K*	1.1436	0.7108	-
P*	0.8538	0.3069	-
α	0.1462	0.6931	-
χ^2 test			
Parameter	Distance	L_B	Morphology
df	9	9	13
χ^2	13.7393	5.5900	12.5401
α	0.1852	0.8484	0.4839

in all cases larger than 0.10. Thus we can say that the SDSS sample follows the same distribution as the parent sample with a significance level of (at least) 10%. The higher the α the more similar the distributions.

In Fig. 7.5b, Fig. 7.6b and Fig. 7.7 we show the binned distributions of the distance, the optical luminosity and the morphological classification respectively. The blue thick lines represent the expected values of the SDSS complete subsample distribution if it follows the same distribution of the complete subsample. The red thin lines are the actual distribution of the SDSS subsample. As we can see in the figures the distributions are very similar in all the cases. Applying the χ^2 test they can be considered as similar.

We can derive from the statistical tests that there are no clear bias in the SDSS complete subsample in comparison with the complete subsample. This is especially clear in the case of the optical luminosity and the morphology. Hence, we will consider the SDSS complete subsample as representative of the AMIGA complete subsample of galaxies.

Fiber size

We estimated the size of the fiber of the spectrographs with respect to the size of the galaxy. The amount of measured light in the spectrum can depend on the relation between the area covered by the fiber and the total area of the galaxy. This dependence directly affects absolute quantities like the luminosities of the lines. It would also affect to the measurement of the equivalent widths although we will not use this quantity for our study. The relation between the diameter of the fiber and the diameter of the galaxy could affect to the observed velocity dispersion, e.g. in spiral galaxies the velocity dispersion could depend on the zone of the rotation curve that is covered by the fiber.

We took the size of the AMIGA galaxies from Hyperleda[5] catalogue. Hyperleda

[5] http://leda.univ-lyon1.fr/

presents the compilation of apparent diameters of galaxies collected from the literature and from different surveys of galaxies. They are not corrected for Galactic extinction or for any other effect. The compiled data are: a) the homogenised *logd25*, diameter standardised at the isophotal level B = 25 mag/arcsec^2 and its error and b) the axis ratio logR25=log(D/d) (log of the ratio major axis to minor axis). From these data we derive the size of the major axis, the minor axis, the area of the ellipse defined by these axis and their respective errors. We suppose this area as the area subtended by the galaxy.

The distribution of the fraction of the fiber diameter over the major axis of the galaxy is shown in Fig. 7.8a. The mean of the fraction is 0.06 ± 0.03 with a maximum of 0.148 and a minimum of 0.002. The distribution of the fraction of the fiber area over the galactic area is shown in Fig. 7.8b. The mean of the fraction is 0.008 ± 0.005 with a maximum of 0.028 and a minimum of $4.5 \cdot 10^{-6}$.

7.4. Determination of the stellar populations

The spectrum of a galaxy is composed by: a) a contribution of the interstellar medium and the possible AGN and b) a contribution of stellar origin, the stellar population emission. For a proper study of the AGN and the ISM we need to distinguish between the two contributions.

The stellar component of a typical galaxy spectrum is very rich in absorption lines. Weak emission lines could be easily diluted by this contribution. Hence, it has to be extracted to perform a reliable fitting of the emission lines (Ho et al. 1997a). Depending on the method used it is also possible to extract the information about the underlying stellar populations like age, reddening and metallicity. Almost all methods are based in stellar absorption-line spectra templates which are used as the base of the stellar component. The library of templates has to be complete to allow the fitting of the stellar template in a wide range of galatic properties like metallicities, ages and velocity dispersions. These libraries are usually composed of stellar spectra generated from population synthesis codes (Kauffmann et al. 2003b; Cid Fernandes et al. 2005, e.g.), actual spectra of absorption-line galaxies (Ho et al. 1997a, e.g.), spectra of stars (Engelbracht et al. 1998, e.g.), eigenvector of a principal component analysis of a combination of these spectra (Hao et al. 2005, e.g.), etc.

Some of these methods are also capable of determining accurately the properties of the underlying populations. It would give us extra information about the physical properties of the studied object like the reddening or the metallicity, velocity dispersion and ages of the underlying stellar populations. This ability plus the public availability, the ease-of-use, the precise documentation and the accuracy in the calculation made us to choose Starlight.

Starlight code

Starlight is a program designed to fit an observed spectrum with a model (Cid Fernandes et al. 2005; Mateus et al. 2006; Asari et al. 2007). The model is composed of spectral components from a pre-defined set of base spectra. The spectral base can be made up of observed template spectra, evolutionary synthesis models (Cid Fernandes et al. 2004, 2005), individual stars, etc. The spectral range for the fitting is restricted to the 3500–9000 Å range.

The Starlight source code is not yet distributed, though this is planed to be done in the future, but there are precompiled binary versions availabe at `http://www.`

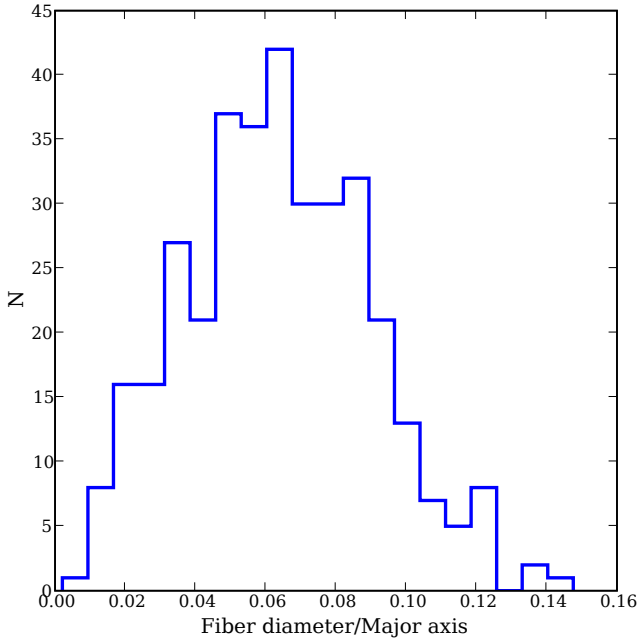

(a) Fiber diameter over the major axis length

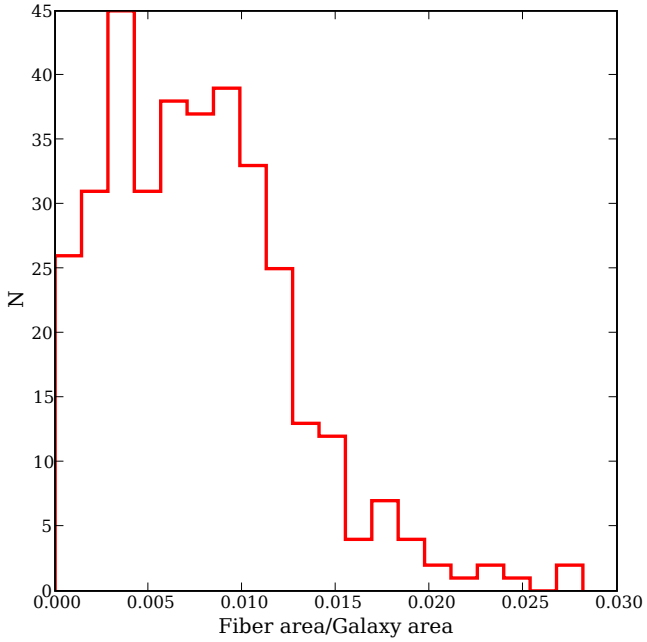

(b) Fiber area over the galactic area

Figure 7.8: Distribution of the fiber size with respect to the galaxy size for the galaxies in the SDSS subsample. The first subplot show the distribution of the fiber diameter with respect to the length of the major axis of the galaxy. The second subplot shows the distribution of the area covered by the fiber with respect to the area of the galaxy.

starlight.ufsc.br/. We installed the Starlight binaries in different computers. Some of them were able to manage batch queues and parallelise the jobs and others did it in a serial way. Depending on the hardware platform of each computer we installed the 32-bit version or the two 64-bit binaries, one compiled with the `Intel ifort` compiler and the other compiled with `GNU gcc`. We used the statically linked versions of the binaries to avoid problems with library dependences.

The program takes as input parameters: a) an array with the wavelength, flux, error in the flux and error mask, b) the selected set of spectral bases, c) the initial values for the velocity shift and dispersion and d) a set of advanced options. The input of the array is done in a file. The wavelength has to be uniformly sampled and the flux must be calibrated. The error is an estimation of the flux error and the error mask signals if the corresponding value is good or has to be flagged as incorrect. We used as the spectral base 45 synthetic spectra, with 3 metallicities and 15 different ages, of Bruzual & Charlot (2003). The 3 metallicities are: 0.004 (0.2 $Z_{\odot}$); 0.02 ($Z_{\odot}$) and 0.05 (2.5 $Z_{\odot}$) and the 15 ages are: 1.0 Myr; 3.16 Myr; 5.01 Myr; 10.0 Myr; 25.12 Myr; 40.0 Myr; 101.52 Myr; 286.12 Myr; 640.54 Myr; 904.79 Myr; 1.434 Gyr; 2.5 Gyr; 5.0 Gyr; 11.0 Gyr and 13 Gyr. These base spectra were distributed with Starlight and are reliable to fit the stellar populations of our galaxies (Cid Fernandes et al. 2005).

We made some programs to adapt the original SDSS spectra to the input of Starlight. The programs performed these steps:

- The first task was to uniformly resample the spectra. We used a spline interpolation with a very large sampling rate (small differences in wavelength) to avoid loosing flux and then resampled the spectrum with a spectral resolution of 1 Å.
- SDSS wavelengths are given in vacuum wavelengths instead of the normally used air wavelengths. Air wavelengths were calculated from vacuum wavelengths based on IAU standards (Morton 1991).
- The spectra are affected by reddening due to the gas and dust of the Milky Way. We performed a dereddening of the flux and of the error in the flux based on the dust emission maps of Schlegel et al. (1998). The extinction curve used was the one of O'Donnell (1994) which is an improvement in the optical and the near infrared of the extinction curve of Cardelli et al. (1989).
- We shifted the spectra to the rest-frame with the redshifts taken from the Princeton re-reduction of the SDSS data.
- We also took the velocity dispersion from the Princeton re-reduction as the initial value because it was usually more accurate that the one obtained from the SDSS default pipeline.

After some tests we found out that there were differences between the results obtained with different binaries. Sometimes one of the binaries did not find a fitting to the stellar population for a galaxy while the others did. There were also differences depending on the mask array that we chose to enter to the program. We used two different types of masks for each galaxy:

- The first type flagged all the errors marked in the original SDSS FITS file, i.e. where the error flag was not set to 0.[6] Some of these errors were actually minor

[6]The error mask is an array of the same length of the flux data. It contains the error code assigned

errors, e.g. a low signal to noise ratio in some pixel. But they can significantly affect the number of points to be fitted in the spectra.

- The second type flagged only errors that we considered major error, i.e. where the error flag in the SDSS FITS file was set to a number above or equal to 16777216 (0x1000000) and below 67108864 (0x4000000) which correspond to the errors: *"No data available in combine B-spline"* and *"Rejected in combine B-spline"*respectively.

In some cases the first type of mask gave better results while in other cases the second type was the best. As we wanted the best fit independently of the mask and the binary used, we performed a fit with each binary (32-bit, 64-bit ifort and 64-bit gcc) and each kind of mask (with all the errors and with only major errors) for each galaxy. After doing the six different fits we compared among them to find the best result for each galaxy.

To compare among the different fits we used the χ^2 parameter. Starlight estimates this parameter, the exact output parameter is χ^2 divided by the total number of spectral points that could be fitted by the program. Thus, the parameter takes into account not only the goodness of the fitted zone but also the width of spectral range that was correctly fitted. Although this parameter is a good estimator for the accuracy of the fit we empirically found that a new parameter: $\chi^2/(N_{\rm fit})^2$ is even better to discriminate the best fit. In Figure 7.9 and Figure 7.10 are plotted the different fits for two galaxies, CIG 366 and CIG 437. For CIG 437 the better spectral fit using $\chi^2/(N_{\rm fit})$ is the one obtained using the 64-bit *gcc* compiled version of Starlight with the mask including all the errors. But is clear from the image that this is not the best fit. This is due to the small number of fitted points. On the other hand the better fit with $\chi^2/(N_{\rm fit})^2$ is the one of the *ifort* version with only the major errors masked. As we said, $\chi^2/(N_{\rm fit})^2$ works better than $\chi^2/(N_{\rm fit})$ to choose the best fit. In the case of CIG 366 the *gcc* compiled version of Starlight could not find a fit when we used the mask with all the errors.

for each spectral point (what we call error flag) denoted with an hexadecimal code. The error codes are explained in detail in: `http://www.sdss.org/dr6/dm/flatFiles/spSpec.html` and are reproduced for reference in Appendix B.1

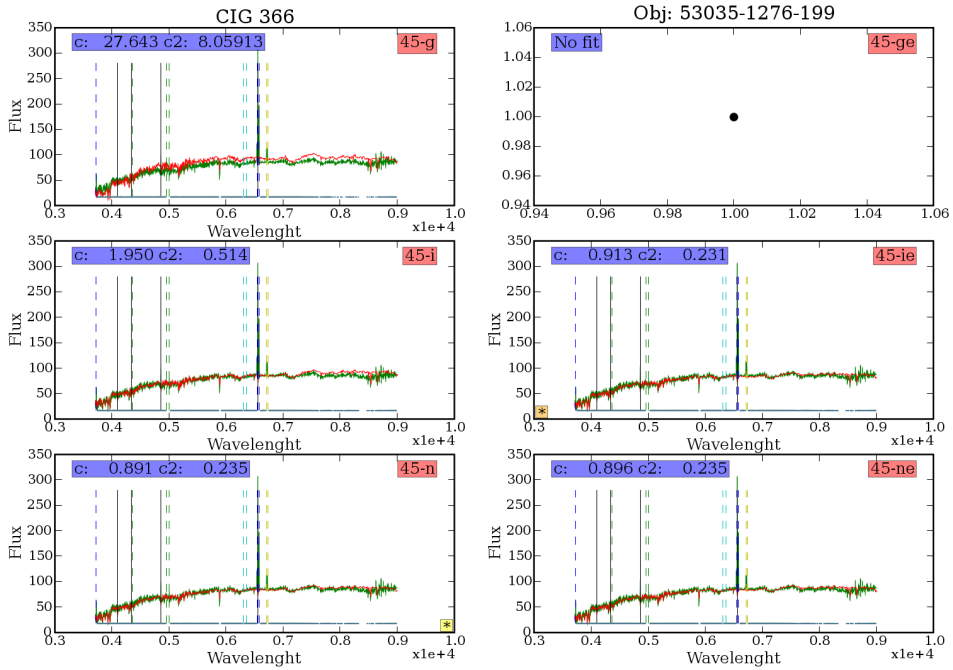

Figure 7.9: Example of a Starlight fit. There are six different fits for this galaxy. The red labels indicate the used compiler and error mask: g - 64-bit gcc, major errors masked; ge - 64-bit gcc, all the errors masked; i - 64-bit ifort, major errors masked; ie - 64-bit ifort, all the errors masked; n - 32-bit, major errors masked; ne - 32-bit, all the errors masked. The blue label contains the parameters $\chi^2/(N_{\rm fit})$ marked as "c" and $\chi^2/(N_{\rm fit})$ marked as "c2". The best fit with "c" is indicated by a yellow label with a cross in the lower-right corner and the best fit with "c2" by a orange label with a cross in the lower-left corner. The black dot in the figure indicate that no fit was found.

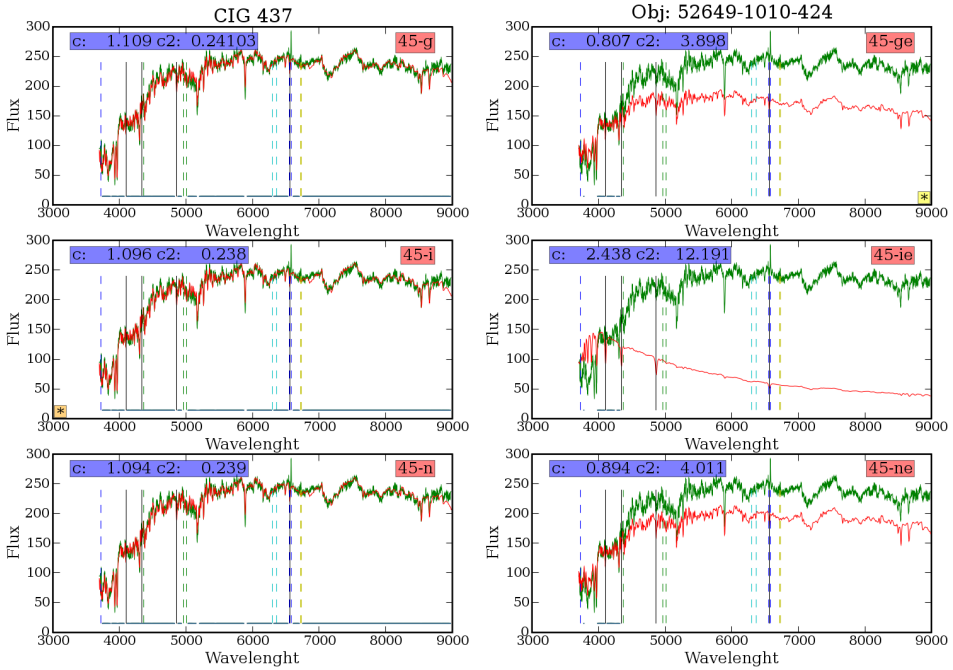

Figure 7.10: Example of a Starlight fit. There are six different fits for this galaxy. The red labels indicate the used compiler and error mask: g - 64-bit gcc, major errors masked; ge - 64-bit gcc, all the errors masked; i - 64-bit ifort, major errors masked; ie - 64-bit ifort, all the errors masked; n - 32-bit, major errors masked; ne - 32-bit, all the errors masked. The blue label contains the parameters $\chi^2/(N_{\rm fit})$ marked as "c" and $\chi^2/(N_{\rm fit})$ marked as "c2". The best fit with "c" is indicated by a yellow label with a cross in the lower-right corner and the best fit with "c2" by a orange label with a cross in the lower-left corner. This fit is one of the most difficoult cases, the different fits diverge due to the low number of points where to perform the adjustment.

Finally, we stored all the stellar population data as well as the fitting data in our database. These data will be made publicly avaliable in the AMIGA webpage under a VO interface.

7.5. Measurement of the spectral lines

Using the stellar populations derived from the execution of the Starlight program we could estimate the contribution of the component composed by the ISM emission and the AGN emission (in those cases where there was an AGN). This component is usually composed of emission lines although in some cases there is also a continuum contribution.

We fitted the neccesary lines to provide a diagnostic on the presence of an AGN, as will be explained in the next section. These lines are: [O III] at 5007Å, [O I] at 6364Å, [N II] at 6583Å, [S II] at 6716Å and 6730Å, Hα (6563Å) and Hβ (4861Å) (see the wavelengths in Table 7.7). We also fitted [N II] at 6548Å for testing purposes since the emission of [N II] at 6583Å should be 3.06 times higher than the emission of [N II] at 6548Å (Osterbrock & Ferland 2006).

Fitting regions and zones

To perform the fitting we took 5 different regions into account: a) the Hβ region, b) the [O III] region, c) the [O I] region, d) the Hα and [N II] region and e) the [S II] region. The first two regions slightly overlap but this does not affect the fitting.

Each region is somewhat affected by the presence of some residual continuum emission remaining from the subtraction of the underlying stellar populations. We calculated a linear continuum baseline for each region and subtracted it before performing the fit. We chose two flanking regions, one after the line and one before the line, in relatively line-free zones and measured the mean remaining continuum level and the noise in each of these zones. We subtract a baseline computed from these two means. We consider the mean of the two measured noise as the mean noise in the region. It will be used to estimate the error in the measurement of the lines.

We used decimal logarithms of the wavelengths to define the limiting points of the different regions and zones. The difference of logarithms of the wavelengths is directly related to the velocity dispersion of a line by Doppler shifting by this relationship:

$$v_{disp} = \mathrm{c}\left(1 - 10^{\Delta[\log_{10}(\lambda)]}\right)$$

where c is the speed of light and $\Delta[\log_{10}(\lambda)]$ is the difference of the wavelengths in decimal logarithm. Using this method, fixed $\Delta[\log_{10}(\lambda)]$ correspond to a fixed v_{disp}, independently of the location of the spectral zone.

The baseline zones are located at ±0.0015 of the nearest line in $\Delta[\log_{10}(\lambda)]$ units which corresponds to a velocity of $\sim$ 1000 km/s. The width of these zones is 0.0040 in $\Delta[\log_{10}(\lambda)]$ units. Following this scheme the lines have a region of $\sim$ 2000 km/s around them in order to perform the fit without a significant blending. In these cases where the lines are closer to this limit the possible blending is taken into account in the fitting method.

We will fit each line with a Gaussian. The fitting regions are the spectral zones where we perform the fitting of the Gaussians. In the cases where nearby lines exist (less than 0.0030 in $\Delta[\log_{10}(\lambda)]$ units) we take a single fitting region for all the nearby lines. These regions are the one for [N II] and Hα and the one for [S II].

The regions, the flanking zones to calculate the baseline and the noise, and the fitting regions, are detailed in Table 7.3. The beginning of the first flanking zone is denoted as "zone 1a" and the end as "zone 1b", for the second flanking zone the names are "zone 2a" and "zone 2b" respectively.

Fitting process

After defining the different zones we started the fitting process. We fitted one, two or three Gaussians depending on the region, to minimise the differences between the actual spectrum and the spectrum model given by the Gaussians in the fitting zone defined for each region. The minimisation was performed using the function `fmin` contained in the module `optimize` of the `scipy` Python module (`http://www.scipy.org/`). This function iterates, changing in each iteration the fitting parameters to minimise the residuals, until reaching a minimum of the sum of the residuals or a given iteration limit. The value of the residuals can be weighted with a given weight distribution to modify the behaviour of the minimising function. The free parameters entered to fit the Gaussians are the height, position and width of the Gaussians. It is possible to join two or more free parameters to minimise the degrees of freedom of the fitting, this can help for the fitting of low signal to noise lines in exchange for a loose in the quantity of obtained information.

Initial fitting process

First, we apply the fitting in the Hα and [N II] region. The first step was to estimate the initial conditions to input to the minimising function. The initial position of the lines is estimated from the theoretical position and the shift in velocity computed by Starlight. The height is estimated finding the maximum of the spectrum around the computed position of the line. The initial positions of the lines are shifted to the maximum level of the Hα line, which is usually the stronger line. The weight is estimated finding the distance between the points where the height of the spectrum is half of the maximum estimated height for a line, one point towards the left and the other towards the right of the point of the maximum.

We applied the minimising function to find the first set of estimated parameters for the lines. These parameters are used as input parameters for a second minimisation. In the second minimisation we weight the residuals with an `arctan` function, the shape of the function used is an arctan shifted in the x-axis 3σ and adding $\pi/2$ to the y-axis:

$$\text{weight} = \text{atan}(x - 3\sigma) + \pi/2$$

. With this weight function we give a nearly null weight to the points of the spectrum dominated by the noise (below 3σ) and a nearly full weight to the points dominated by the actual emission of the lines (above 3σ). The process is repeated again with a third minimisation without an input weight and a fourth one with the `arctan` weight. The output parameters of this fourth minimisation were used to derive the initial parameters for the other regions, where the lines usually had worse signal to noise ratios.

The free parameters estimated in this zone are:

- Height of the Hα line.
- Width of the Hα line.
- Position shift of the Hα line.

Table 7.3: Selection regions for the measurement of the emission lines.

Point or line	log(λ) in air [log(Å)]	λ in air [Å]	fit	comment
		Hβ region		
zone 1a	3.6814	4801.76		
zone 1b	3.6854	4846.19	begin	−1000 km/s limit
Hβ line	3.6869	4862.95	*	
zone 2a	3.6884	4879.78	end	+1000 km/s limit
zone 2b	3.6924	4924.93		
		[O III] region		
zone 1a	3.6900	4897.79		
zone 1b	3.6940	4943.11		−1000 km/s limit
[O III] 4959 line	3.6955	4960.21		
v limit	3.6970	4977.37		+1000 km/s limit
Middle point	3.6971	4978.52		between lines
v limit	3.6982	4991.14	begin	−1000 km/s limit
[O III] 5007 line	3.6997	5008.41	*	
zone 2a	3.7012	5025.74	end	+1000 km/s limit
zone 2b	3.7052	5072.24		
		[O I] region		
zone 1a	3.7940	6223.00		
zone 1b	3.7980	6280.58	begin	−1000 km/s limit
[O I] 6300 line	3.7995	6302.31	*	
v limit	3.8010	6324.12	end	+1000 km/s limit
Middle point	3.80165	6333.59		between lines
v limit	3.8023	6343.08		−1000 km/s limit
[O I] 6363 line	3.8038	6365.02		
zone 2a	3.8053	6387.05		+1000 km/s limit
zone 2b	3.8093	6446.14		
		[N II] and Hα region		
zone 1a	3.8107	6466.96		
zone 1b	3.8147	6526.80	begin	−1000 km/s limit
[N II] 6548 line	3.8162	6549.38	*	
Middle point	3.8167	6556.92	*	between lines
Hα line	3.8172	6564.48	*	
Middle point	3.8179	6575.06	*	between lines
[N II] 6583 line	3.8186	6585.67	*	
zone 2a	3.8201	6608.46	end	+1000 km/s limit
zone 2b	3.8241	6669.60		
		[S II] region		
zone 1a	3.8218	6634.37		
zone 1b	3.8258	6695.76	begin	−1000 km/s limit
[S II] 6716 line	3.8273	6718.93	*	
Middle point	3.82775	6725.89	*	between lines
[S II] 6730 line	3.8282	6732.87	*	
zone 2a	3.8297	6756.16	end	+1000 km/s limit
zone 2b	3.8337	6818.68		

- Height of the [N II] at 6548Å line.
- Height of the [N II] at 6583Å line.
- Width of the [N II] lines. The width of the two lines are linked, they are considered to be the same.
- Position shift of the [N II] lines. The position shifts of the two lines are linked, the lines are considered to be separated 35.4Å.

The position shift and width of the Hα line are used as the initial position shift and width of the Hβ. And the position shift and width of the [N II] lines are used as the initial position shift and width of the [O III], [O I] and [S II] lines. If the position shift of any of the lines is larger than 15Å we reset its value to 0. We use the same minimisation method for the Hβ, [O III], [O I] and [S II] lines. In the case of the [O I] we fixed the position shift and the line with to the one of the [N II] lines. Although we lost some information we really improve the accuracy in the fitting of this line which is usually diluted by the noise. The separations between the [S II] lines and their widths are also fixed.

The free parameters estimated in these zones are:

- Height of the Hβ line.
- Width of the Hβ line.
- Position shift of the Hβ line.
- Height of the [O III] line.
- Width of the [O III] line.
- Position shift of the [O III] line.
- Height of the [O I] line. The position shift and width are considered to be the same as the ones of the [N II] lines.
- Height of the [S II] at 6716Å line.
- Height of the [S II] at 6730Å line.
- Width of the [S II] lines. The width of the two lines are linked, they are considered to be the same.
- Position shift of the [S II] lines. The position shifts of the two lines are linked, the lines are considered to be separated 14.38Å.

After following these steps we visually inspected the accuracy of the fitted parameters. With this method we obtained accurate measurements of the parameters of the lines for 272 galaxies. In almost all the other cases the fit of one or more lines was not correct, i.e. the fitted Gaussian did not follow the shape of the line ($n = 66$). There were some cases where the fit process failed and the program crashed ($n = 5$). The presence of wide components in the Hα or Hβ lines ($n = 8$) or an error in the entered velocity shift ($n = 2$) are other issues that prevented us to perform the fitting. In Table 7.4 we show the number of galaxies for each case and the numerical code that we assigned to it in the database. In these cases we examined the origin of the problem in a one-to-one basis.

Table 7.4: Errors or features detected in the fitting process.

Database code	Error or feature	number of galaxies
0	Program crash	5
1	Ok	272
2	Bad fit of Hβ	17
3	Bad fit of [O III]	7
4	Bad fit of [S II]	4
5	Bad fit of Hβ and [O III]	4
6	Bad fit of Hβ and [S II]	1
7	Bad fit of [O III] and [S II]	1
8	Bad fit of forbiden lines	8
10	Bad fit in general	24
11	Presence of wide lines	8
20	Bad velocity shift input	2

Improved fitting process

Before identifying the source of the error in the fitting, we developed alternative schemas to perform the fitting. Usually it was only neccesary to fix one or more of the free parameters of the minimisation method.

In the cases where one or more lines could not be fitted we fixed the position shift of the problematic line instead of taking it as a free parameter. With this change we were able to fit all the galaxies with an error in the fit of one or two lines (codes 2 to 7 in Table 7.4).

In the cases where there were errors in the fit of the forbidden lines (code 8 in Table 7.4) the origin of the problem was usually an error in the determination of the position shift of the [N II] lines. The initial estimation of the position shift for these lines was used as an input parameter for the fit of the other forbidden lines. If this input parameter was wrong the error was propagated. In three cases it was enough to fix the position of the lines in the Hα and [N II] regions.

For the remaining 5 cases of errors in the fit of the forbidden lines, for the cases where the fits of the lines was wrong in general and for the cases where the program crashed, we used a different approximation. First we estimate the position, width and height of the Hα and [N II] lines measuring them directly over the spectrum. These parameters are taken directly as the final parameters for this region and are used, in the same way than before, as the initial parameters for the fit of the other lines. For the other lines we fixed some parameters: a) the position shift, the position shift of the Hβ line is the one of the Hα line and the position shift of the forbidden lines is the one of the [N II] lines and b) the width of the [S II] lines is fixed to the one of the [N II] lines. And performed the minimisation of the residuals to obtain the final parameters. Using this method we could find the fitting parameters of the lines for 31 of the remaining galaxies without fit.

The two cases where the velocity shift was wrong (CIG 569 and CIG 383) were fitted with the original method but reseting the velocity shifts to 0. In these two cases it is possible that the spectrum is not centred in the nucleus of the galaxy hence, a small shift in the velocity may appear depending on the recession velocity of the zone

Table 7.5: Final method chose for the fitting of the lines.

Method	Explanation
0	No final fit
1	Initial method
2	Position shift fixed for the line with problems
3	Position shift fixed for the lines in the Hα region
4	Position shift fixed for all the lines
5	Position shift fixed for all the lines
6	Velocity shift reseted to 0
7	Manual fit of CIG 536
8	Manual fit of CIG 486
9	Manual fit of CIG 396

of the pointing with respect to the nuclear zone of the galaxy.

The remaining three cases (CIG 396, CIG 486 and CIG 536) were fitted manually using the same fitting functions but entering the initial parameters by hand.

The final method used for each galaxy was recorded in the database for future reference. The codes used in the database are explained in Table 7.5.

We stored in the database all the parameters measured for the lines and the regions.

Measurement of the lines

Using the final measurements of the width and height of each line we could estimate the flux of the line. We consider that a line is detected when the height of the line is more than 3 times the noise level. In the cases where the line is not detected we assign to the line a value of 3σ as its upper limit. There is one case (CIG 581) where one of the [S II]lines has a height below -3σ, in other cases it would correspond to an absorption line but in this case it is clear that the absorption feature is due to an error in the spectrum and not due to a genuine line.

There are some cases ($n = 29$) where the computed width of the line is of the order of thousands of Å, in these cases the Gaussian looks like a flat line. It usually happends in the fit of the Hβ line. In these cases we assign to the line the width of the Hα line. CIG 517 had a very noisy spectrum and the width of all the lines where fitted to a value of 0. We manually assigned an arbitrary value of 10Å to the width of the lines. The height of the [S II] line at 6176 Å of CIG 189 and the height of the [S II] line at 6730 Å line of CIG 517 were manually fixed. All the cases where a line measure was changed were indicated and explained in the database.

To calculate the flux of the line we calculate the corresponding area of the fitted Gaussian: $\sqrt{2\pi}\,(\texttt{height}\,\texttt{width})$. The error assigned for the flux of the line is proportional to the noise in the region and is calculated as: $\sqrt{2\pi}\,(\sigma\,\texttt{width})$. In the cases where the height of the line is below the 3σ level (non-detections, upper limits) the upper limit of the flux is: $\sqrt{2\pi}\,(3\sigma\,\texttt{width})$.

Database

The output units of the flux measured for each line are 10^{-17} erg/s/cm^2 or 10^{-20} W/m^2. The data of the lines measurement is stored in our database. These data will

Table 7.6: Galaxies classified as Seyfert 1.

CIG	Comment
204	
214	Sy 1.0 in the literature.
336	Weak wide line.
349	To be updated from Sy2 to Sy1 in the catalogue.[1]
719	Sy 1.0 in the literature.
747	
749	
893	Very weak wide line.
1008	Sy 1.2 in the literature.

[1] See Section 9.3.

be made publicly available in AMIGA web page under a VO interface.

Broad lines

Some galaxies of the SDSS subsample have broad emission lines. All these galaxies are Seyfert 1 galaxies or any of the subtypes found in the literature (Seyfert 1.2, 1.5, 1.8, 1.9 or 1n). We have selected these galaxies looking for a wide component at the Hα, [N II] region. Since the Seyfert 1/Seyfert 2 separation was not the main objetive of the work, we did a first visual inspection to classify the Seyfert type of the galaxies. We looked for a broad component in the Hα, [N II] region (see Figure 7.11). We found 8 Seyfert 1 galaxies (see Table 7.6) from which 6 clearly exhibit the broad component of the Hα line. CIG 336 and 893 showed a faint wide Hα component but the large width of the [N II] lines made us to classify them as Seyfert 1. For the completion of this work we will use a parametric classification scheme like the one of Hao et al. (2005) and Martínez et al. (2008).

7.6. Diagnostics

Baldwin et al. (1981) proposed an empirical diagnostic method using emission lines rates. The aim was to classify the different types of excitation mechanisms that produced the emission. This method was later refined by Veilleux & Osterbrock (1987). They focused on galaxies with pure narrow emission lines excluding all types of Seyfert 1 and looked for the best suitable lines to do a reliable classification using their ratios. They imposed five criteria:

- The lines involved should be strong, with a good signal to noise ratio in a typical spectrum.
- The lines should not be blended with other lines in order to avoid confusion.
- The distance between the two lines of the ratio should be as small as possible to avoid the effects of reddening and the errors coming from the flux calibration.

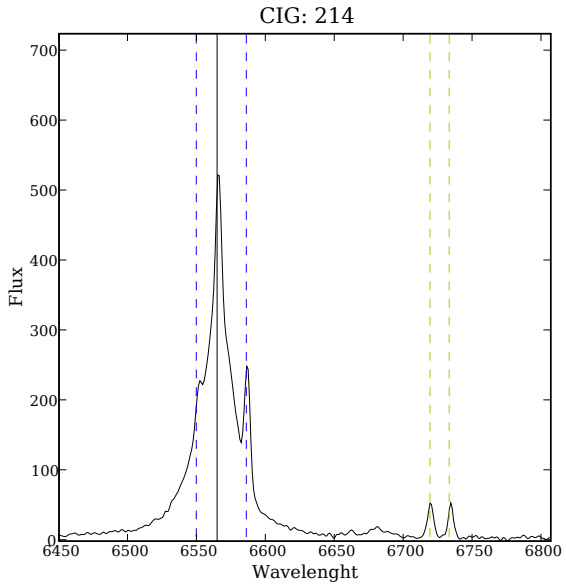

(a) CIG 214 shows a clear strong wide component in Hα.

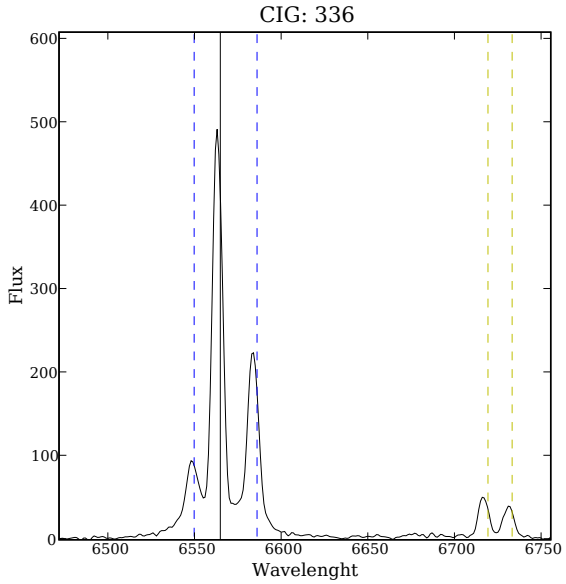

(b) CIG 336 has a weak wide component in Hα

Figure 7.11: Examples of the spectra of galaxies classified as Seyfert 1. The wavelength units are Å and the flux units are 10^{-20} W/m^2. The stellar component has been already subtracted from the spectra. The theoretical location of the Hα line is marked with a solid black line, the locations of [N II] and [S II] lines are marked as blue dashed lines and as yellow dashed lines respectively.

Table 7.7: Wavelengths of the emission lines.

Line	Wavelength in vacuum (Å)	Wavelength in air (Å)
Hβ (4861)	4861.3	4862.72
[O III] 5007	5006.9	5008.24
[O I] 6364	6363.8	6365.54
[N II] 6548	6548.0	6549.86
Hα (6563)	6562.8	6564.61
[N II] 6583	6583.4	6585.27
[S II] 6716	6716.5	6718.29
[S II] 6730	6730.8	6732.68

- The line ratios should be between an Hydrogen line of the Balmer series and a forbidden line, less sensitive to abundances.
- The lines should be easily accessible by the instrumentation, hence they choose optical lines and rejected UV ones.

The chosen forbidden lines were [O III] at 5007Å, [O I] at 6364Å, [N II] at 6583Å, [S II] at 6716Å and 6730Å and the Balmer series lines of Hydrogen Hα and Hβ (see Table 7.7). Based on these lines they proposed 4 line ratios: a) log([O III]/Hβ); b) log([N II]/Hα); c) log([S II]/Hα) and d) log([O I]/Hα). The [O III]/Hβ ratio is mainly an indicator of the mean level of ionization and temperature, the [S II]/Hα and [O I]/Hα ratios are indicators of the relative importance of a large partially ionized zone produced by high-energy photoionization. The significance of the ratio [S II]/Hα is not immediately obvious but provides a good separation between star forming nuclei and AGN (Osterbrock & Ferland 2006).

Finally, these ratios were grouped to form the 3 following diagnostic diagrams:

- log([O III]/Hβ) - log([N II]/Hα)
- log([O III]/Hβ) - log([S II]/Hα)
- log([O III]/Hβ) - log([O I]/Hα)

Veilleux & Osterbrock (1987) proposed several boundaries separating the theoretical starburst region from objects of other types of excitation like an AGN in the diagnostic diagrams. These boundary lines are semi-empirical. Ho et al. (1997a) proposed different empirical selection lines for these three diagrams that also take into account the difference between Seyfert and LINERs. Kewley et al. (2001) proposed a theoretical line to divide the regions. They used PEGASE v2.0 (Fioc & Rocca-Volmerange 1997) and STARBURST99 (Leitherer et al. 1999) codes to generate the spectral energy distribution of the star forming galaxies and used their code MAPPINGS III (Dopita et al. 2000) to compute the photoionization models for these galaxies. E.g. in the figure 4 of Kewley et al. (2001) (Figures 7.12a and 7.12b here) are plotted, with a grid, the different locations of a theoretical starburst with different metallicities (z) and ionization parameters (q), over this grid they plot the location of a sample of infrared starburst galaxies. The location for some galaxies can be explained directly by a starburst but for some galaxies it is clear that there is a systematic separation from the pure starburst models. To explain the location of these galaxies it is needed to take

into account an additional ionization source like an AGN. Kauffmann et al. (2003a) provided an empirical separation line between pure star forming galaxies and galaxies that they assumed powered by an AGN. This study made use of a sample of 122 808 galaxies from the SDSS, one of the larger if not the largest sample used until that moment. The separation line is below the one of Kewley et al. because it takes into account the empirical shape of the distribution of galaxies, which is well below the theoretical "extreme starburst" line of Kewley et al.. Stasińska et al. (2006) provided a new line of separation used their own photoionization code (see Figure 7.13a). This theoretical line was even below the one of Kauffmann et al..

Some authors use different lines from the above mentioned to perform their own classification Decarli et al. (2007); Miller et al. (2003). The difference in the definitions must be taken into account to compare between different samples.

Stasińska et al. (2008) studied the possibility that some of the galaxies in the region of AGN could actually be galaxies powered by stellar processes. The photoionization of some of these galaxies could be produced by hot post-asymptotic giant branch stars and withe dwarfs (Binette et al. 1994). In Figure 7.13b are shown the new grids and extension of the photoionization models of Stasińska et al. (2008) in the diagnostic diagram.

LINERs were defined as an own class of galactic nuclei by Heckman (1980). The classification was based on the relative strengths of [O I], [O II] and [O III] emission. [O II] at 3727Å has to be at least as strong as [O III] at 5007Å and [O I] at 6300Å has to be at least as strong as one third of [O III] at 5007Å. As Ho et al. (1997a) explain in their paper, although a criterion using the log([O III]/Hβ) - log([O I]/Hα) diagnostic diagram is different from the original criterion of Heckman (1980), in practice the two sets of classification criteria identify the same objects (Ho et al. 1997a). This comes from the inverse correlation between [O III]/Hβ and [O II]/[O III] for conditions of ow excitation. Kewley et al. (2006) gave an empirical classification scheme to separate Seyferts and LINERs. It is based in the empirical separation of Seyferts and LINERs in two clearly separated branches in the diagnostic diagrams.

Classification criteria

The lines of separation between different types of galactic nuclei are usually clearly and unambiguously defined in the literature. This is not the case for the final classification of a nucleus. The first source of ambiguity occurs when a condition for the classification of a galaxy is not hold simultaneously in the three different diagnostic diagrams. In some cases the weight of the classification accuracy is assigned depending on the diagnostic diagram. Some diagrams are considered as more reliables than others. E.g. Ho et al. (1997a) consider the log([O III]/Hβ) - log([O I]/Hα) diagnostic diagram as the most sensitive to the shape of the ionizing spectrum, hence, a higher weight is given to the classification of this diagram. In other cases galaxies classified as different types are directly considered as "ambiguous galaxies" (Kewley et al. 2006).

Another source of confussion appears when a line is not measured due a low signal to noise ratio. This means that one or two of the ratios involved in a diagnostic diagram is an upper or lower limit or is even not defined when the two lines involved are non-detections. These cases are usually discarded from the classification or are studied in a case by case basis.

Some studies only use one diagnostic diagram or even one line ratio to classify the galaxies. The usual diagnostic diagram used is log([O III]/Hβ) - log([N II]/Hα) and

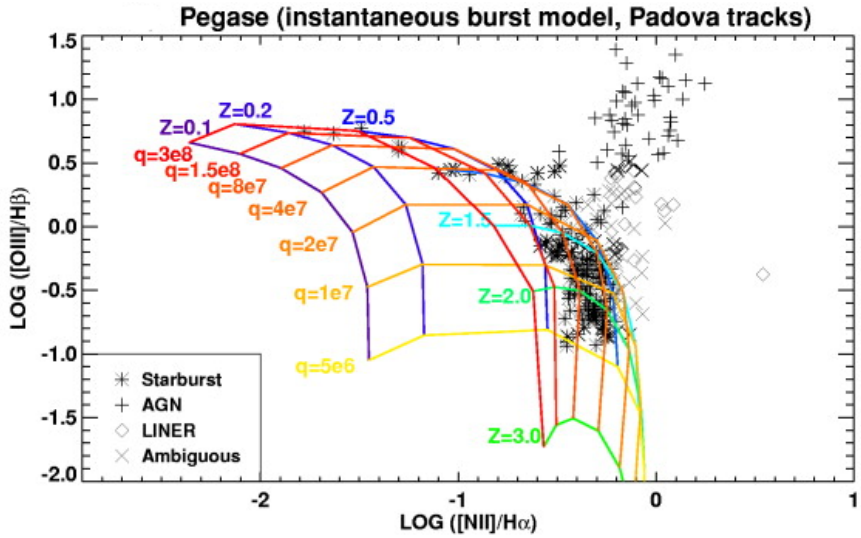

(a) Starburst models of Kewley et al. (2001) computed with PEGASE

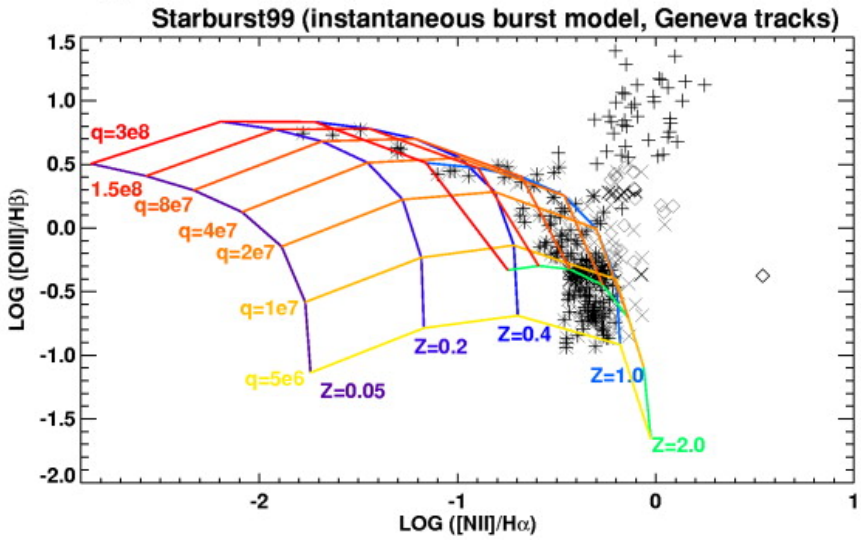

(b) Starburst models of Kewley et al. (2001) computed with STARBURST99

Figure 7.12: Theoretical models in the diagnostic plot of log([O III]/Hβ) and log([N II]/Hα). In both the subplots the grid corresponds to the theoretical model for different metallicities (z) and ionization parameters (q) from Kewley et al. (2001). A sample of infrared starburst galaxies is plotted over the theoretical models. Source: Kewley et al. (2001).

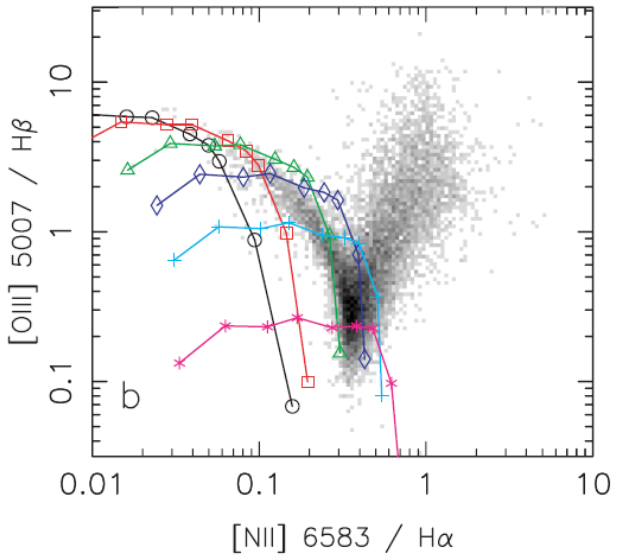

(a) Starburst models of Stasińska et al. (2006)

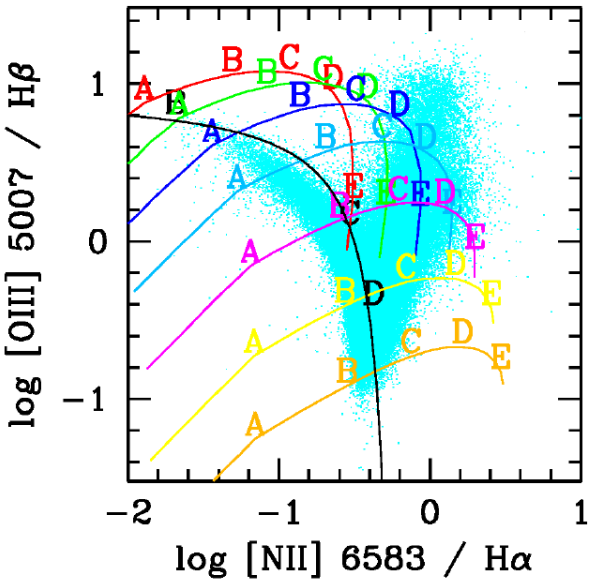

(b) Models of Stasińska et al. (2008)

Figure 7.13: Theoretical models in the diagnostic plot of log([O III]/Hβ) and log([N II]/Hα). In both the subplots different colours stand for different ionization parameters and the letters stand for different metalicities. A sample of galaxies from the SDSS are plotted in the same axis. Sources: Stasińska et al. (2006) and Stasińska et al. (2008).

the usual line ratio used is log([N II]/Hα). They are used because usually involves the lines with a higher signal to noise ratio and allow a higher number of galaxies classified. The classification assigned using this ratios is usually "narrow line AGN" or "AGN" because of the difficulty in distinguishing between Seyferts and LINERs.

We will classify the galaxies in each of the diagnostics diagrams taking into account the upper limits in the lines. Later we will combine the classification obtained in the three diagrams to estimate a final classification.

[N II] diagram

We divided the diagnostic plot in different zones in order to classify the galaxies. The zones are defined depending on the presence of upper limits in the line ratios and using separation lines from the bibliography. We used as separation lines the lines of Kewley et al. (2001) and Kauffmann et al. (2003a) and, we also separated galaxies based in fixed values of their individual line ratios. One separation line is log([O III]/Hβ) = 0.8 and the other is log([N II]/Hα) = 0.0. Usually we consider AGN galaxies the ones with values above these lines. Each zone is associated with a type of galaxy that correspond to this locus in the diagnostic diagram, e.g., galaxies in the zone below the Kauffmann et al. (2003a) are associated with star forming galaxies. Using this diagram we classified galaxies as narrow line AGN, star forming nuclei and transition objects. [7]

The zones for classifying the galaxies (see Figure 7.14) are:

- Zone 10.- All the lines are upper limits, hence, the galaxy cannot be located in the diagnostic diagram.
- Zone 9.- If both [N II]and Hα are upper limits and at least one of [O III]or Hβ is detected. The position of the galaxy in the x-axis cannot be located but it is possible to locate it in the y-axis. If the galaxy has log([O III]/Hβ) $\leq$ 0.8 it is located in this zone. Zone of star forming galaxies.
- Zone 8.- It is the same than zone 9 but with log([O III]/Hβ) $>$ 0.8. Zone of NLAGN.
- Zone 7.- In this case both [O III]and Hβ are upper limits and one of [N II]or Hα are detected and log([N II]/Hα) $>$ 0.0. Zone of NLAGN.
- Zone 6.- The same that zone 7 but with log([N II]/Hα) $\leq$ 0.0. Zone of star forming galaxies.
- Zone 5.- At least one line for each ratio of the diagnostic diagram is detected. The galaxy has log([N II]/Hα) $>$ 0.0. Zone of NLAGN.

[7] The acronyms are the following:

AGN	Active galactic nucleus
SFN	Star forming nucleus
TO	Transition object (composite of AGN and SFN)
LINER	Low ionization nuclear emitting region
Sy	Seyfert nucleus
Sy1	Seyfert nucleus with broad lines
Sy2	Seyfert nucleus with narrow lines
NLAGN	Narrow line AGN (Sy2 or LINER)

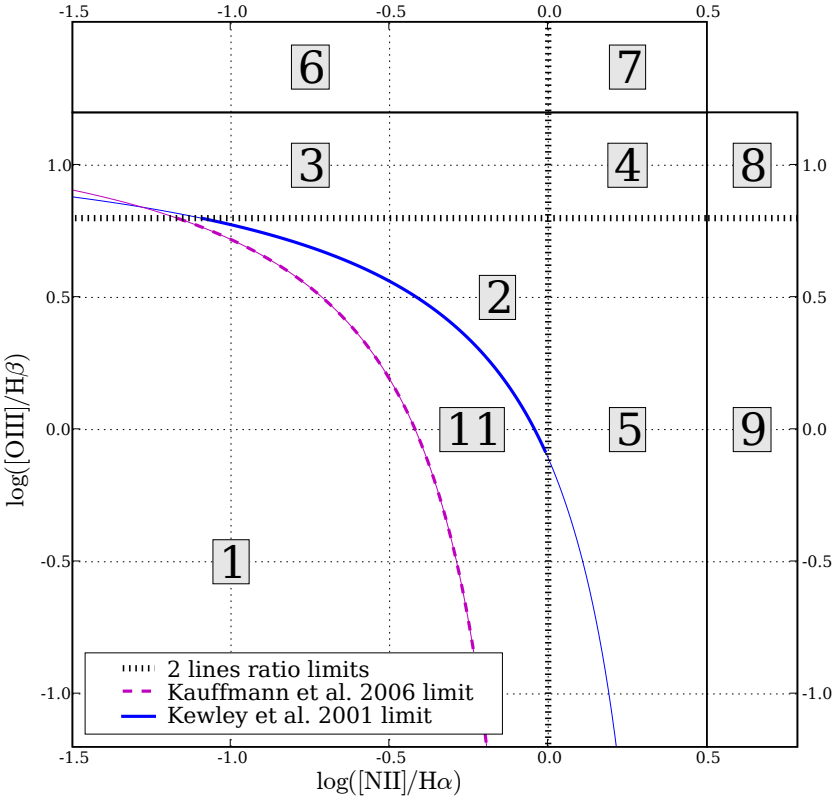

Figure 7.14: Zones for log([O III]/Hβ) - log([N II]/Hα).

- Zone 4.- At least one line for each ratio of the diagnostic diagram is detected. The galaxy has log([N II]/Hα) > 0.0 and log([O III]/Hβ) > 0.8. Zone of NLAGN.

- Zone 3.- At least one line for each ratio of the diagnostic diagram is detected. The galaxy has log([O III]/Hβ) > 0.8. Zone of NLAGN.

- Zone 2.- At least one line for each ratio of the diagnostic diagram is detected, log([N II]/Hα) $\leq$ 0.0 and log([O III]/Hβ) $\leq$ 0.8. The galaxy is above the Kewley et al. (2001) separation line. Zone of NLAGN.

- Zone 1.- At least one line for each ratio of the diagnostic diagram is detected, log([N II]/Hα) $\leq$ 0.0 and log([O III]/Hβ) $\leq$ 0.8. The galaxy is below the Kauffmann et al. (2003a) separation line. Zone of star forming galaxies.

- Zone 11.- At least one line for each ratio of the diagnostic diagram is detected, log([N II]/Hα) $\leq$ 0.0 and log([O III]/Hβ) $\leq$ 0.8. The galaxy is above the Kauffmann et al. (2003a) separation line and below the Kewley et al. (2001) separation line. Zone of transition objects.

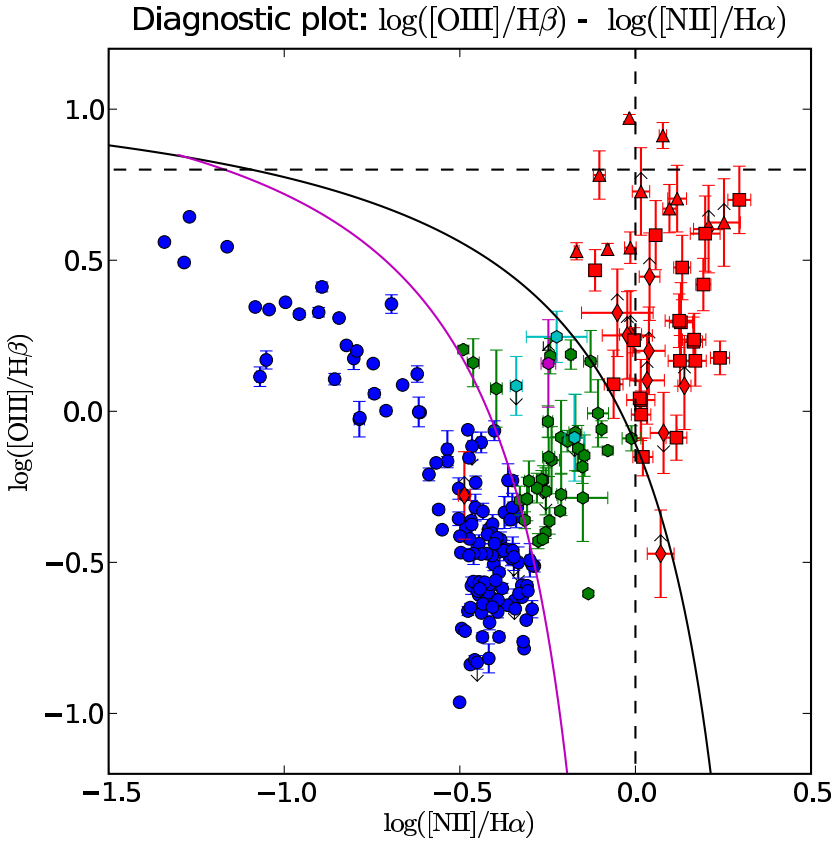

Figure 7.15: Diagnostic plot of log([O III]/Hβ) and log([N II]/Hα). We plot only galaxies belonging to the SDSS complete subsample (n = 221). AGN galaxies are indicated by red markers, star forming galaxies as blue markers, transition objects as green markers. Non classified galaxies that can be transition objects or star forming galaxies are denoted with cyan markers. CIG 325 can be a transition object or an AGN and is marked with a magenta hexagon. AGN galaxies (red) that are classified as Seyfert 2 are plotted with triangles, the ones that are classified as LINER are plotted with squares and the ones that cannot be classified in any of these subtypes (NLAGN) are plotted as diamonds.

When a galaxy is located in one of the zones we assign it a classification depending on the presence of a detection or an upper limit in each emission line. In the cases where all the lines of a galaxy are detected the classification is straightforward. In the case where there is one or more upper limits it has to be taken into account the direction of the limits, e.g., zone 1 correspond to star forming galaxies, if one galaxy is located in the zone 1 but have an upper limit in log([N II]/Hα) it is clear that the galaxy is located in zone 1 independently of the actual value of [N II], hence, it would be classified as an star forming galaxy.

In Figure 7.15 it is shown the diagnostic diagram for the SDSS complete subsam-

ple of galaxies although we apply the classification criteria to all the galaxies of the SDSS subsample. For the total SDSS subsample of galaxies (353 galaxies) 30 cannot be classified in the diagnostic diagram due to the presence of one or more upper limits. These galaxies are related to galaxies known in the bibliography as non-emission galaxies. Eleven of them are in the zone of the transition objects but cannot be unambiguously classified. There are 71 NLAGN, 49 transition objects and 184 star forming nucleus. The colour of each galaxy corresponds to the final classification, explained in the next section. There is a galaxy classified as an AGN in the zone of the star forming galaxies (with a lower limit in the log([O III]/Hβ) ratio), this galaxy (CIG 428) is clearly classified as an AGN in the other diagnostics diagrams.

[S II] and [O I] diagrams

We use a similar separation into zones in the log([O III]/Hβ) - log([S II]/Hα) and the log([O III]/Hβ) - log([O I]/Hα) diagrams. We will not use the zones where one of the ratios is undefined. Y-axis is in common in all the diagrams therefore, we would not obtain any additional information from the classification in the two zones associated to this axis. And there are not galaxies that can be classified in the two zones associated to the x-axis in any of these two diagrams. Thus, we do not deffined these kind of zones for these two diagrams. The defined zones are shown in Figure 7.16.

The zones for classifying the galaxies are:

- Zone 10.- All the lines are upper limits and the galaxy cannot be located in the diagnostic diagram.
- Zone 4.- Both [O III]and Hβ are upper limits and at least one of the other lines are detected.
- Zone 3.- Galaxies above the Kewley et al. (2001) separation line and below the Kewley et al. (2006) separation line. Zone of LINERs.
- Zone 2.- Galaxies above the Kewley et al. (2001) separation line and above the Kewley et al. (2006) separation line. Zone of Seyferts 2.
- Zone 1.- Galaxies below the Kewley et al. (2001) separation line. Zone of the star forming nuclei.

The presence and direction of the upper limits in the diagram will be taken into account with the zone to estimate the classification of the galaxy as in the previous diagnostic diagram.

In Figure 7.17 the two diagnostic diagrams are shown. There is a small overlap in the boundaries between regions. The transition objects are widely spread in both the NLAGN and star forming regions as is usually found in the literature.

Final classification

Finally, we took into account the classification with each of the former diagnostic diagrams to choose a final classification for each galaxy. The classification obtained with the log([O III]/Hβ) - log([N II]/Hα) diagram was chose to prevail over the classification in the other diagrams but usually they agree. If an object is not classified with this diagram then the classification of the other two is taken if they are the same. In the cases where a transition object is classified as an AGN or SF nucleus in the [S II]and [O I]diagrams then we chose this classification.

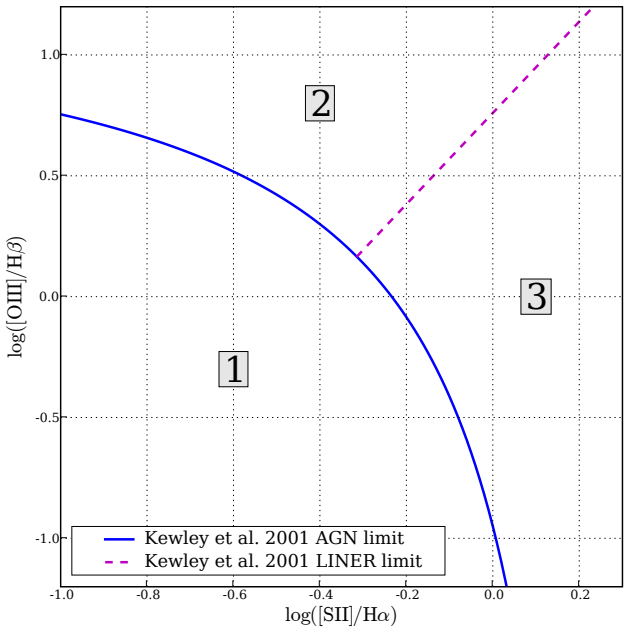

(a) Zones for log([O III]/Hβ) - log([S II]/Hα)

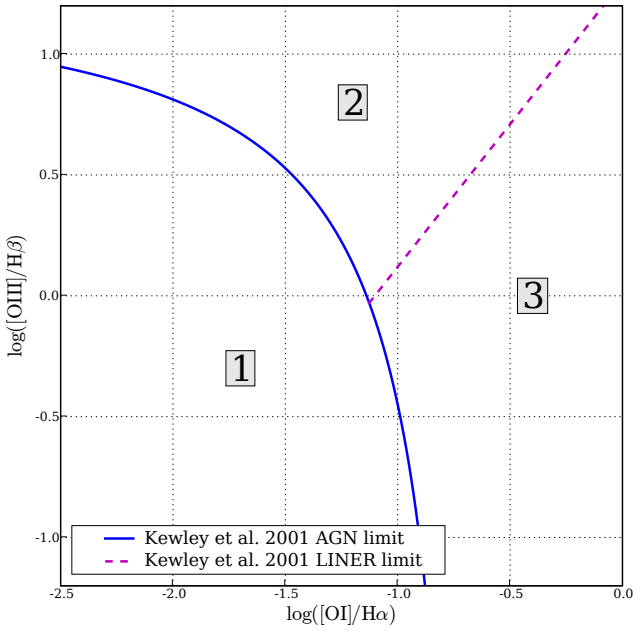

(b) Zones for log([O III]/Hβ) - log([O I]/Hα)

Figure 7.16: Zones for log([O III]/Hβ) - log([S II]/Hα) and log([O III]/Hβ) - log([O I]/Hα).

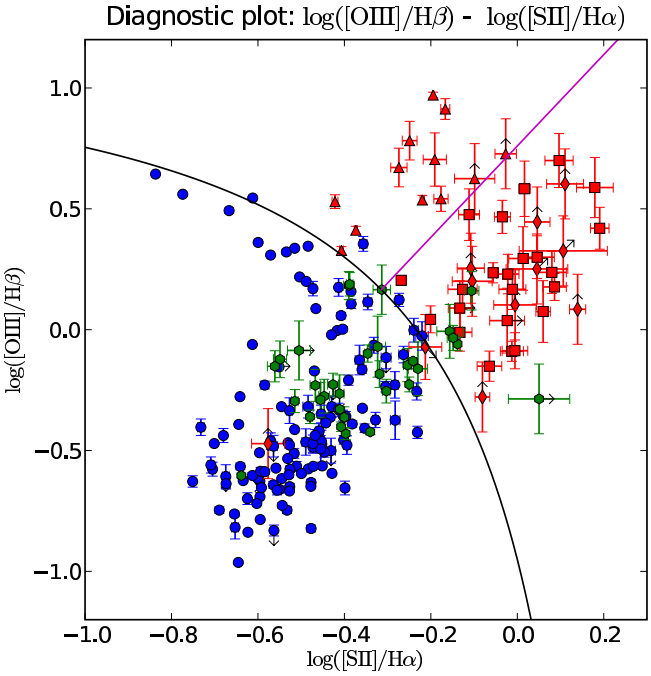

(a) Diagnostic diagram log([O III]/Hβ) - log([S II]/Hα)

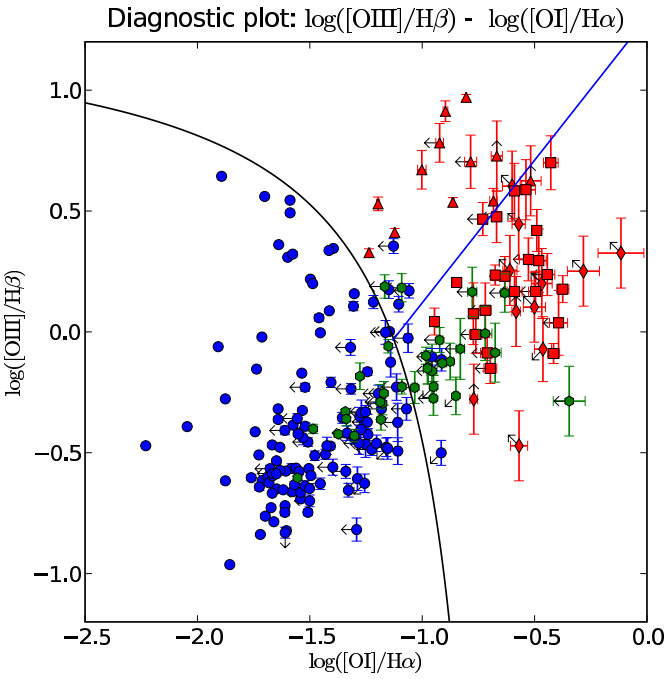

(b) log([O III]/Hβ) - log([O I]/Hα)

Figure 7.17: Diagnostic plots for the SDSS complete subsample. The symbols are the same as in fig. 7.15.

Finally, we assigned an arbitrary classification code to each galaxy:

- **-5** - *TO or NLAGN* - Galaxy located in the TO zone but cannot be unambiguously classified as TO, it can be a TO or an AGN.
- **-4** - *TO or SFN* - Galaxy located in the TO zone but cannot be unambiguously classified as TO, it can be a TO or an SFN.
- **-3** - *Unclassified - Non emission* - Galaxy without detected emission lines.
- **-2** - *Unclassified - One ratio* - Galaxy with one line ratio undefined and that cannot be classified.
- **-1** - *Unclassified* - Galaxy that cannot be unambiguously located in the diagnostic diagram due to the upper limits.
- **1** - *SFN* - Galaxy classified as an SFN.
- **2** - *Sy2* - Galaxy classified as a Sy2.
- **3** - *LINER* - Galaxy classified as a LINER.
- **4** - *TO* - Galaxy classified as a TO.
- **5** - *NLAGN* - Galaxy classified as a NLAGN (LINER or Sy2).
- **10** - *Sy1* - Galaxy classified as a Sy1.

7.7. Statistics

After applying our classification criteria we are able to study the sample statistically dividing it into types of galaxies. We added to the study the broad line galaxies previously identified. The figures obtained are shown in Table 7.8. Although we show the figures for the total SDSS subsample we only consider the figures for the SDSS complete subsample as statistically meaningfull.

We can classify a high percentage of galaxies (92.9%), this maybe caused by the following reasons: a) the high signal to noise in the measurement of our lines because of the subtraction of the stellar populations and because our galaxies are nearby in comparison with other samples that do not reach our percentage of classifications. b) the high relative number of late type galaxies in our sample which are supposed to have a relatively high star forming rate in comparison with early type galaxies. c) The classification method that used the information carried by upper limits.

In Section 10.4 we compare this figures with the ones found in other samples.

7.8. Study

We studied the properties of the different types of nuclear activity found with respect to the complete sample. All this study will take into account only the galaxies belonging to the SDSS complete subsample to ensure the statistical significance.

In Figure 7.18 is shown the comparison of optical luminosities of galaxies classified as AGN and TO with respect to the luminosities of the whole SDSS complete subsample. In 7.18b it is shown the histogram of the distribution of optical luminosities of the SDSS complete subsample and the histograms of galaxies classified as

Table 7.8: SDSS statistics.

Classification (code)	Total sample	Complete subsample	Percentage
Unclassified (negative code):	32	16	7.1%
Without emission lines (code -3)	8	3	1.3%
With emission line/s (codes -2 and -1)	18	9	4.0%
TO or NLAGN (code -5)	2	1	0.4%
TO or SFN (code -4)	4	3	1.3%
Classified (positive code):	321	210	92.9%
SFN (code 1)	184	126	55.8%
TO (code 4)	54	35	15.5%
AGN (codes 2; 3; 5 and 10):	83	49	21.7%
NLAGN total (codes 2; 3 and 5):	75	44	19.5%
LINER (code 3)	32	20	8.9%
Sy2 (code 2)	12	10	4.4%
NLAGN (code 5)	31	14	6.2%
Sy1 (code 10)	8	5	2.2%
TO + AGN (codes 2; 3; 4; 5 and 10):	137	84	37.2%
Total:	353	226	100.0%

AGN and the sum of galaxies classified as AGN and TOs. In 7.18a it is shown the fraction of galaxies classified as AGN with respect with the whole SDSS complete subsample as a red line and the fraction of galaxies classified as AGN and TOs as a green line. From this figure it is clear a very steep increase of the rate of nuclear activity as a function of the optical luminosity.

In Figure 7.19 we show the relationship of the activity rate with respect to the morphology. Figure 7.19a shows the histograms for the complete sample, the galaxies with an AGN and the galaxies with an AGN or a TO nucleus. The fraction of galaxies with AGN or AGN plus TOs with respect to the complete subsample is shown in Figure 7.19a. There are not AGN nor TOs from Scd to Irregular galaxies. Starting from Sc types and decreasing the morphological code toward earlier types there is an increase of the fraction of galaxies with an AGN until Sab types. The zone of galaxies from E types to Sa looks more noisy probably due to the lower number of galaxies, but the fraction of AGN could be considered constant around a value of ≈ 0.30 within the error from E types to Sab types. If we group the galaxies with morphoogical types between E and Sa in one bin the value obtained is 0.29 ± 0.9, very similar to the value found for Sab types (0.29 ± 0.7).

The distribution of morphology and luminosity of the galaxies in the SDSS complete subsample is shown on Figure 7.20. The different types of activity are represented as different colours and shapes. The mean and the standard deviation are represented as crosses. There is a clear trend of AGN galaxies toward higher luminosities and earlier types. This trend is clearly vissible in the possition of the different means for the different samples. Star forming nuclei are located toward latest types and lower luminosities than the mean of the whole sample, the mean for transition objects are located between the one for AGN and the one for the whole sample. In this plot can be seen the relationship between morphology, luminosity and activity.

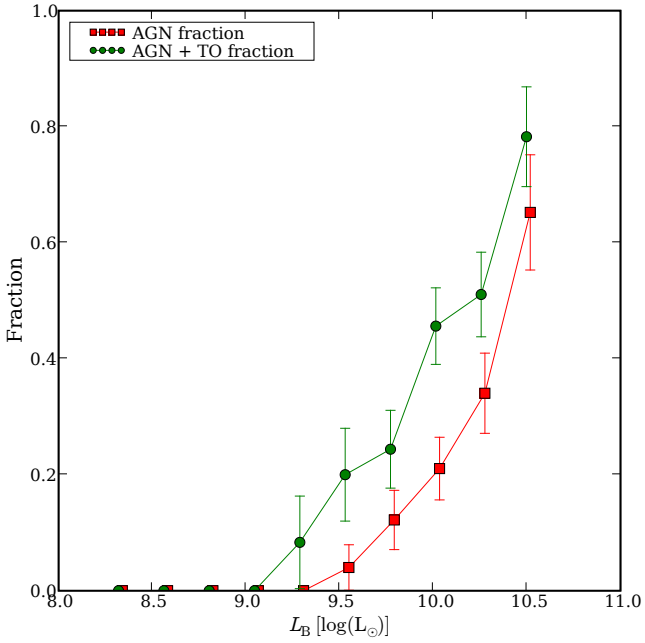

(a) Fraction

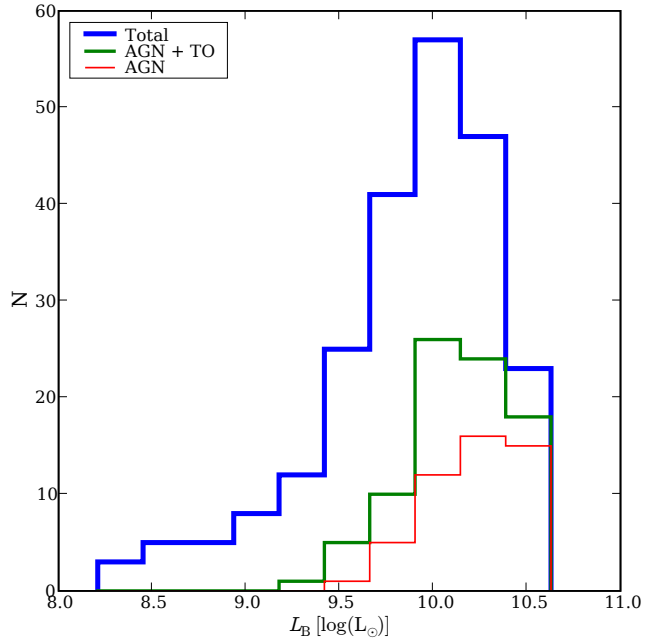

(b) Histogram

Figure 7.18: Relationship between the AGN fraction and the optical luminosity for the SDSS complete subsample. In Figure 7.18a it is shown the fraction for each luminosity bin taking into account only the AGN galaxies (red line) and the AGN plus the transition objects (green line). Figure 7.18b shows the distribution of the optical luminosities for the same samples in comparison with the total sample, the y-axis shows the total amount of galaxies in each bin.

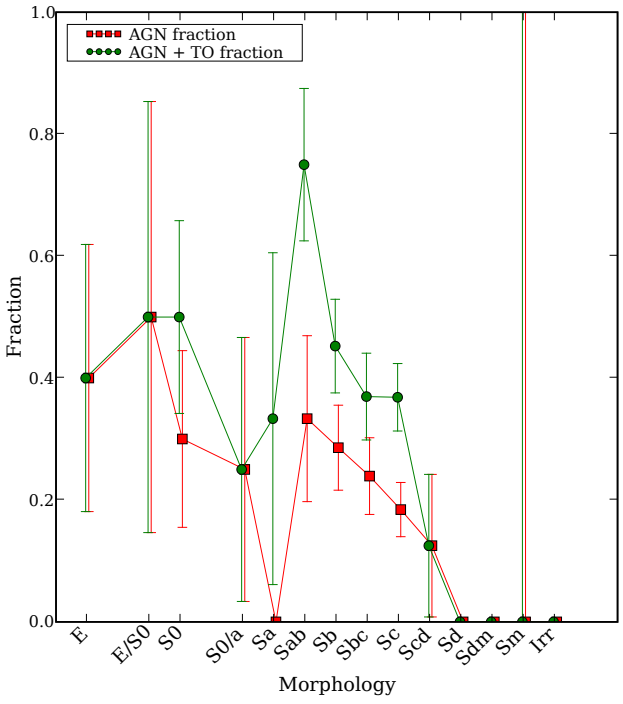

(a) Fraction

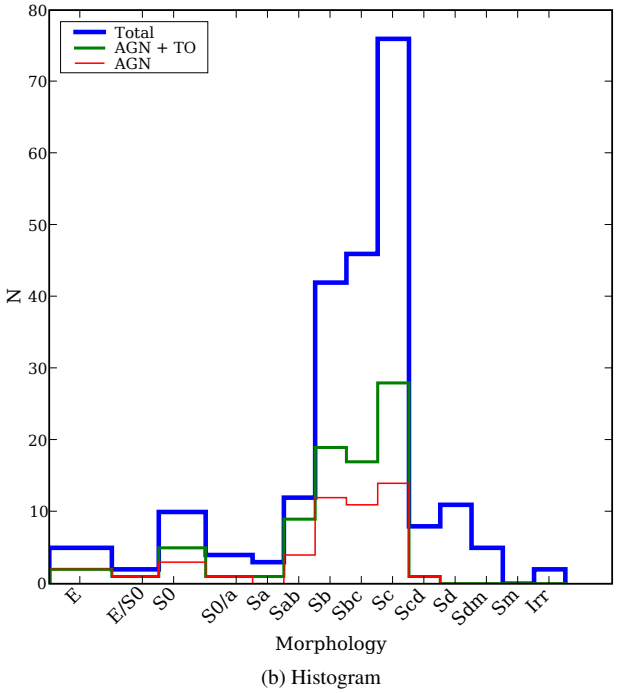

(b) Histogram

Figure 7.19: Relationship between the AGN fraction and the morphology for the SDSS complete subsample. In Figure 7.19a it is shown the fraction for each morphological type taking into account only the AGN galaxies (red line) and the AGN plus the transition objects (green line). Figure 7.19b shows the distribution of the morphologies for the same samples in comparison with the total sample, the y-axis shows the total amount of galaxies in each bin.

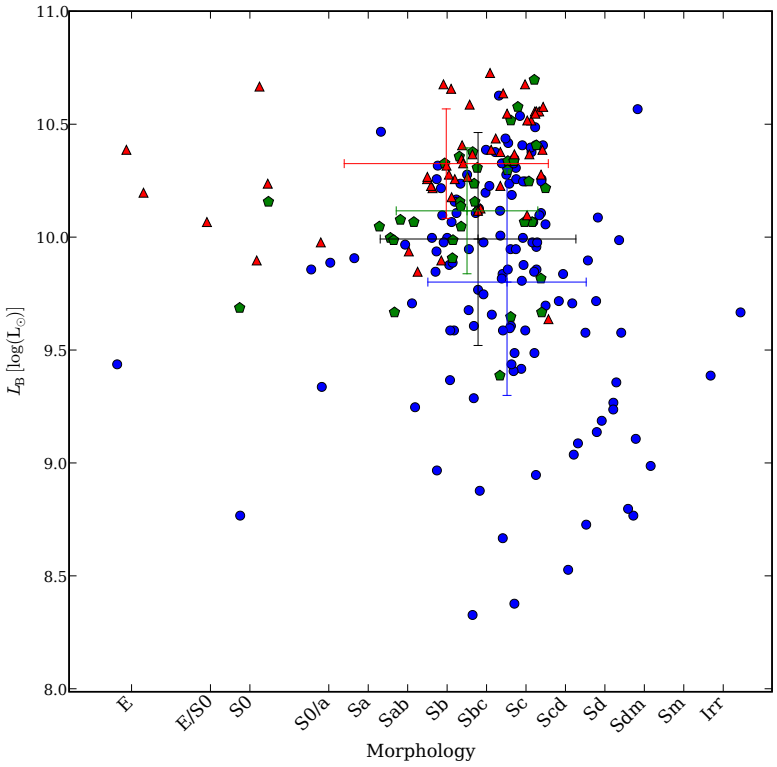

Figure 7.20: Relationship of the activity with the morphology-luminosity distribution for the SDSS complete subsample. Red triangles are galaxies classified as AGN, green pentagons are transition objects and blue circles are star forming galaxies. The mean and standard deviation for the total sample is plotted as a big black cross. The means and standard deviations for the star forming, transition objects and AGN samples are plotted as big blue, green and red crosses respectively.

Part IV

Global study

Chapter 8

AGN candidates catalogue

We have compiled the results obtained from the methods explained in the former chapters as well as the data from the literature to produce a single catalogue of AGN-candidate galaxies for the total sample (Table 8.1). In the catalogue, we also indicate the galaxies composing the complete subsample. Since our confindence level on the presence of an AGN varies depending on the selection method and its properties, as explained in the previous chapters, we have included information on the used method.

The final catalogue is composed of:

- *Active galaxies found in the NED and the Véron-Cetty catalogue (see Sect. 3.2).* We have selected the 29 galaxies classified as Seyfert, LINER, NLAGN, or AGN as listed in column 4 of Table 3.1.
- *Radio-excess candidates galaxies selected with the radio-FIR correlation (see Sect. 5.2 and Sect. 5.4).* We have included the 15 galaxies with at least a factor 3 radio excess using the $\log L_{1.4\mathrm{GHz}}(\mathrm{W\ Hz^{-1}})$ versus $\log L_{\mathrm{FIR}}(\mathrm{L_\odot})$ correlation, taking into account the FIRST and the VLA revision (Table 5.1).
- *AGN-candidates selected with the IRAS colour criterion (see Sect. 6.2).* We have added the 58 AGN-candidates selected using this method to the catalogue (Table 6.2).
- *Optical AGN selected from the SDSS spectra (see Sect. 7.7).* We have added the 83 AGN selected using this method to the catalogue (Table 7.8).

Finally, there are 155 galaxies in the cataloge of AGN candidates in isolated galaxies amog the 1050 AMIGA galaxies.

Table 8.1: Catalogue of AGN-candidates for the total sample.[1]

CIG	α (J2000)	δ (J2000)	Literature	FIR colour	Radio-excess Factor 3	Radio-excess Factor 5	SDSS-DR6 subsample	SDSS-DR6 type	Complete subsample
19	00:24:16.21	+14:14:12.0	-	-	0	0	1	5	0
26	00:31:52.85	+37:40:43.2	-	AGN	0	0	0	0	0
41	00:58:23.36	+36:43:50.2	-	-	1	1	0	0	1
57	01:37:48.25	+02:17:27.3	Sy2	-	1	1	0	0	0
69	01:53:42.23	+29:56:01.5	-	AGN	0	0	0	0	1
...	...	...	...	...	...	...	...	...	...

[1] Columns:
(1) CIG number.
(2) α (J2000).
(3) δ (J2000).
(4) Classification in the literature as listed in column 4 of Table 3.1.
(5) AGN candidates using the FIR colour criterion.
(6) 1 if is a radio-excess candidate galaxy using a factor 3 cutoff, 0 if not.
(7) 1 if is a radio-excess candidate galaxy using a factor 5 cutoff, 0 if not.
(8) 1 if the galaxy belongs to the SDSS subsample, 0 if not.
(9) Classification code as explained in Section 7.6.
(10) 1 if the galaxy belongs to the complete subsample, 0 if not.

Chapter 9

Comparison between different methods

We compared the activity classification obtained using the different methods for the galaxies of the AMIGA sample. As the classification of the galaxies was taken from the literature and obtained from the study of the radio-FIR correlation, the FIR colour and the SDSS spectra, we were able to perform six different comparisons that will be presented in the following sections.

9.1. Radio-excess galaxies

None of the galaxies show a radio-excess with respect to the radio-FIR correlation by a factor 5 or more. Hence, we study the classification of the 8 galaxies in the complete subsample that show radio excess above a factor 3.

FIR colour and radio-excess galaxies

Three of the radio-excess candidate galaxies can be also classified with the IRAS colour method and all of them (CIG 248, CIG 692 and CIG 877) are found to be AGN candidates. These galaxies have very warm IRAS colours with $S_{25\mu\mathrm{m}}/S_{60\mu\mathrm{m}}$ being higher than 0.45 in all cases.

Data from the literature and radio-excess galaxies

Three of the radio-excess galaxies were also classificated in the literature and their classification was as Seyfert galaxies: CIG 72, 692 and 877. CIG 72 has an upper limit in FIR and, according to J. Lim (priv. comm.), shows a tidal tail in HI linking it to a small companion. CIG 692 has been observed with the VLA in its A configuration at 8.3 GHz by Schmitt et al. (2001) finding a symmetric triple source with a total extent of 3 kpc. CIG 877 is an elliptical galaxy studied by Marcum et al. (2004). They suggest that the IRAS emission assigned to this galaxy might be produced by two nearby stars. If this is true the radio excess would be even higher.

SDSS spectra and radio-excess galaxies

There are 158 galaxies for which we could study both their SDSS spectra and their radio properties, i.e., possible radio-excess. Among the 8 galaxies with radio excess

above a factor 3 only one could be studied with the SDSS. CIG 248 is classified as a Seyfert 2 galaxy.

9.2. Far infrared colour

There are 197 galaxies classified with the FIR colour method, 162 of them belong to the complete subsample.

Data from the literature and FIR colour

Since for a number of CIG galaxies a detailed classification of their nuclear emission has been found in the literature (Sect. 3.2), we investigate specifically their location in the IRAS colour plot. This has allowed us to test the accuracy of the classification method. In Fig. 9.1, we plot the 197 galaxies that we were able to classify based on their IRAS colour and flag those galaxies classified as AGN, HII, LINER or starburst in the literature. A large fraction of the AGN galaxies are located above the selection cut ($7/12 \approx 60\%$), and almost all the HII and starburst galaxies ($23/25$) are below the line. This confirms our expectation that dust in AGN is usually warmer, hence, showing a higher $S_{25\mu m}$ to $S_{60\mu m}$ ratio while galaxies classified as HII should have lower values for that ratio. This result has no statistical significance, but shows the good agreement between the classification of their nuclear emission and their location in the $S_{25\mu m}$ versus $S_{60\mu m}$ plot.

SDSS spectra and FIR colour

We compared the optical classification of the SDSS subsample with the FIR colour classification. There are 51 galaxies classified with both methods and 40 of them belong to the complete subsample.

We take as a reference the SDSS classification to test the goodness of the FIR colour classification. Transition objects are excluded and we only consider galaxies classified as AGN or SF. For the total sample of galaxies we have 45 galaxies. In table 9.1 it is shown the rate of correct classifications for each type of galaxy and for all the galaxies, both for the total sample and for the complete subsample. The rate is very constant for different types ranging from 71,4% to 75,0%. This result confirms the expected accuracy for the FIR colour method.

9.3. SDSS spectra and data from the literature

The number of galaxies with data about activity from the literature studied with SDSS spectra is 29. Twenty ofive of them were unambigously classified in the literature. Twenty one ($\approx 84\%$) of the final classifications for our galaxies fully agree with the classification obtained from the SDSS data and the classification for 4 of them disagrees. In Table 9.2 we show these 4 cases. Four galaxies has an ambigous classification in the NED database: a) CIG 349 is classified as “Sy1.5 LINER” in NED, as “Sy1” in the V-C catalogue and our classification is Seyfert 2; b) CIG 383 is classified in NED as “HII Sbrst” and we classify it as a star forming nuclei which is compatible with the former classification; c) CIG 447 appears in NED as “LINER HII” and our classification is as a star forming nuclei and d) CIG 508 is classified in NED as “Sbrst Sy1” and we classify it as a star forming nuclei and did not found any evidence of

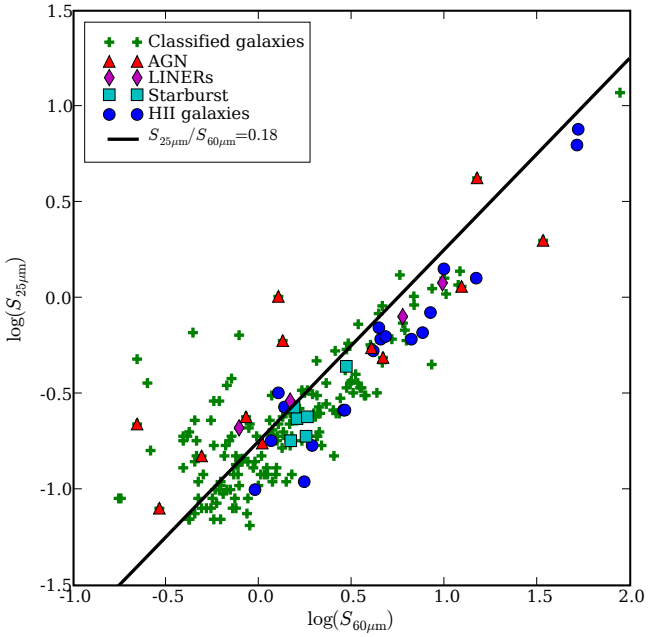

Figure 9.1: Plot of $\log S_{25\mu m}$ versus $\log S_{60\mu m}$ for the CIG sample with available data about nuclear emission from the literature. The solid line corresponds to $S_{25\mu m}/S_{60\mu m} = 0.18$. Galaxies that can be classified using this method are plotted as crosses ($n = 197$). AGN galaxies from the literature (triangles) are usually above the line. LINERs are plotted as diamonds. Most of the galaxies classified as HII and starburst in the literature (circles and squares respectively) are below the selection line.

Table 9.1: Goodness of the FIR colour method compared with the SDSS classification for the total sample and the complete subsample.

SDSS classification		FIR classification		Percentages	
type	n	n AGN	n normal (SF)	well-classified	badly classified
Total sample					
SF	31	8	23	23/31 - 74,2%	8/31 - 25,8%
AGN	14	10	4	10/14 - 71,4%	4/14 - 28,6%
Total	45	18	27	33/45 - **73,3%**	12/45 - **26,7%**
Complete subsample					
SF	28	8	20	20/28 - 71,4%	8/28 - 28,6%
AGN	8	6	2	6/8 - 75,0%	2/8 - 25,0%
Total	36	14	22	26/36 - **72,2%**	10/36 - **27,8%**

Table 9.2: Galaxies classified in the literature whose classification disagrees with the one that we obtained from SDSS data.

CIG	Literature classification	SDSS classification
250	HII	TO
428	HII	NLAGN
553	Sbrst	TO
634	LINER	TO

wide lines. Please notice that the concept of NLAGN used in NED includes also the transition objects and we consider transion objects separately.

CIG 349 has a faint but clear wide Hα line that we did not detect in our first visual inspection due to the high ratio between the narrow and the wide component of the Hα line. This high ratio allowed us to obtain a good fit to the narrow components without finding any hint about the presence of the broad line. This case shows the difficulty in the detection of the wide components for some galaxies and suggests that it is possible that some of our galaxies could have very faint wide lines that we missed. As explained in Section 7.5 in the future work we will use a parametric selection scheme to detect the presence of a wide component.

Chapter 10

Comparison with different environments

10.1. Radio-excess galaxies

Studies of the radio power and FIR emission of galaxies have been performed mostly for two kinds of samples: those referred to as field galaxies in the literature (e.g., Condon & Broderick 1991; Yun et al. 2001; Miller & Owen 2001; Corbett et al. 2002; Condon et al. 2002; Drake et al. 2003) where usually no environmental selection criterion has been applied, and cluster samples (e.g., Niklas et al. 1995; Andersen & Owen 1995; Miller & Owen 2001; Reddy & Yun 2004; Omar & Dwarakanath 2005). We summarise the main results of these papers in Table 10.1 and 10.2.

Table 10.1: Rate of radio-excess galaxies in the literature.

Sample	Environment	Rate of Radio-excess galaxies[1]									Notes
		Total			E-S0a			Sa-Irr			
		N[2]	F5[3]	F3[3]	N[2]	F5[3]	F3[3]	N[2]	F5[3]	F3[3]	
AMIGA[4]	Isolated	397	0.8	4.0	21	4.7	19.1	376	0.5	2.1	$m_B < 15$
Condon 1991	-	122	32.0	33.6	11	90.9	90.9	71	9.9	12.7	$S_{60\mu m} > 0.2$Jy and $S_{4.85GHz} > 25$mJy
Yun 2001	-	1809	1.3	-	-	-	-	-	-	-	$S_{60\mu m} > 2$Jy
Corbett 2002	-	82	2.4	4.9	-	-	-	-	-	-	$S_{60\mu m} > 4$Jy
Condon 2002	-	1897	8.2	10.8	287	42.2	51.6	1498	2.1	3.4	$S_{1.4GHz} > 2.5$mJy and $m_P < 14.5$
Drake 2003	-	178	55.1	60.7	-	-	-	-	-	-	$S_{4.8GHz} \gtrsim 16$mJy and $S_{60\mu m} \gtrsim 0.1$Jy
Omar 2005	Eridanus group	72	2.8	2.8	20	5.0	5.0	46	2.2	2.2	
Niklas 1995	Virgo cluster	37	-	16.2	2	-	0.0	35	-	17.1	radio@4.8 GHz
Andersen 1995	Cluster & group (poor)	23	8.7	21.7	-	-	-	-	-	-	
	Cluster & group (rich)	20	15.0	25.0	-	-	-	-	-	-	
Miller 2001	Clusters $0 < r < 1$ Mpc	120	28.3	37.5	54	46.3	53.7	53	3.8	17.0	$S_{1.4GHz} > 10$mJy
	Clusters $1 < r < 2$ Mpc	96	21.9	29.2	23	60.9	73.9	50	6.0	10.0	$S_{1.4GHz} > 10$mJy
	Clusters $2 < r < 3$ Mpc	94	6.4	12.8	19	26.3	31.6	47	0.0	4.3	$S_{1.4GHz} > 10$mJy
Reddy 2004	X-ray clusters	114	13.2	19.3	33	30.3	45.5	81	6.2	8.6	$L_{60\mu m} > 8.92 L_\odot$
	X-ray clusters core	33	24.2	39.4	15	40.0	66.7	18	11.1	16.7	$L_{60\mu m} > 8.92 L_\odot$
	X-ray clusters ring	81	8.6	11.1	18	22.2	27.8	63	4.8	6.3	$L_{60\mu m} > 8.92 L_\odot$

[1] The percentages are computed over the number of galaxies for each morphological subsample.
[2] Number of galaxies in the total samples or the morphological subsamples.
[3] F3: factor 3 radio excess; F5: factor 5 radio excess. Figures given in percentages.
[4] All percentages for the fraction of radio-excess galaxies are upper limits as explained in Sect. 5.4.

Table 10.2: Rate of AGN candidates in the literature from FIR colour.

		Rate of AGN-candidates[1]	
Sample	Environment	Total	2 Jy cutoff
AMIGA	Isolated	28.4	14.3
Condon 1991	-	21.8	12.4
Yun 2001	-	15.9	15.9
Condon 2002	-	13.3	-
Drake 2003	-	45.0	22.6
Andersen 1995	Cluster & group (poor)	56.5	-
	Cluster & group (rich)	75.0	-
Reddy 2004	X-ray clusters	59.0	20.0

[1] Figures given in percentages.

We notice that a detailed comparison of these papers is difficult for a number of reasons that we list below. The selection criteria of the samples differ significantly, introducing different biases depending on whether the selection was performed at optical wavelengths or with a FIR or radio cut selection criterion. Normalisation of the percentages is also a delicate issue since, in some cases, the values are divided by the total number of galaxies with available data, but in others only detections are used. In the cases where AGN selection was performed using the radio-FIR correlation, the wavelength of the radio-emission is usually 1.4 GHz but in some cases it is 4.8 GHz. The radio excess cutoff varies for different papers, the most used factors are 3 times or 5 times above the radio-FIR correlation. Finally, the used radio-FIR correlation is, in some cases, the one obtained for the sample analysed in the paper, but in others the one for a different reference sample is used, e.g., Omar & Dwarakanath (2005) used Yun et al. (2001) correlation.

We have obtained the figures given in Table 10.1 by reanalysing the data given in the papers (e.g. most of them had not performed an analysis by morphological type) or provided by the authors, in an attempt to homogenise the statistics. We have defined the radio excess in two ways: a factor 3 or a factor 5 above the radio-FIR correlation for our sample of isolated galaxies, corresponding to $q < 1.88$ or $q < 1.66$, respectively. The percentages are calculated with respect to the total number of galaxies that can be classified as explained in Sect. 5.2. The rates for different morphological types are not calculated with respect to the total number of galaxies but normalised for the corresponding subsamples of early and late-type galaxies. Comparison of the AGN candidate rate based on the FIR colour selection was possible for some of the references given above (Condon & Broderick 1991; Yun et al. 2001; Drake et al. 2003; Andersen & Owen 1995; Reddy & Yun 2004). In these studies, $S_{25\mu m}$ and $S_{60\mu m}$ fluxes or $\alpha_{25,60}$ (spectral index between $S_{25\mu m}$ and $S_{60\mu m}$) were given, and we selected as AGN candidates those with $S_{25\mu m}/S_{60\mu m} \geq 0.18$ (see Sect. 6.2) equivalent to $\alpha_{25,60} < 1.958$. We have to be careful when comparing these numbers, since, e.g., the sample of Yun et al. (2001) has been selected to have $S_{60\mu m} \geq 2$ Jy. This will bias the result since the AGN candidate rate depends directly on this variable. However, we think that this cut has a significant advantage since much of the AGN candidates have low IRAS fluxes (Fig. 6.1) near the detection limit. Therefore, the error is very high in comparison to the measurements, hence confidence in the selection of AGN

candidates gets lower. For this reason, we have both provided the statistics using the original data in each paper and applying the $S_{60\mu m} \geq 2$ Jy cut to all samples when it was possible, including ours (see Table 10.2).

"Field" environments

As indicated above some studies of radio-excess galaxies were performed for samples usually referred to as "field" in the sense that they were not selected in any particular way with respect to their environment. However, it is found that, for instance, many cD galaxies belong to these "field" samples. We comment below on these studies.

Condon & Broderick (1991) studied a sample of IRAS sources applying a high radio flux cutoff at 4.75 GHz and with no definition of the environment (e.g., several pairs are included in their sample). They also apply a FIR cutoff but not as strict as the radio one. Using their data in Table 2 we have calculated the ratios of radio-excess listed in our Table 10.1 and that of AGN candidates based on $\alpha_{25,60}$ as given in Table 10.2. When the 2 Jy cut is applied to their sample the percentage of galaxies with $\alpha_{25,60} < 1.958$ decreases, as expected. The radio flux cut leads also to a bias since it will increase the ratio of radio-excess galaxies with respect to other samples listed in Table 10.1, selected without such a cutoff or using a higher FIR cutoff, the latter obviously producing the opposite bias.

Yun et al. (2001) studied in detail an IR flux-limited complete sample with no selection concerning the environment. Their fit to the radio-FIR correlation is identical to ours within the errors since both samples are dominated by star formation activity, with very few galaxies deviating from the correlation, hence leading to very similar q-parameters, 2.34 in their sample versus 2.36 in ours. Their ratio of radio-excess galaxies being very low, is still a factor 3 larger than ours. Two main differences are found between both samples. While our sample is optically selected, Yun et al. selected their sample in the FIR. Applying the same FIR flux cutoff to our complete subsample leads to a decrease of the ratio of radio-excess galaxies to 0%. On the other hand, galaxies in their sample lie in higher density environments than ours: among the 23 radio excess galaxies in their sample 2 are giant E/S0 in clusters and 16 galaxies are interacting in pairs or higher ranked environments. Furthermore, a comparison of the $\log L_{60\mu m}(L_\odot)$ distribution for both samples (Fig. 10.1) shows a higher ratio of galaxies at the low luminosity end for the AMIGA sample, with a difference in the mean of 0.31. Since the FIR luminosity is a variable widely known to be driven by interaction this supports further the higher density of the environment traced by the sample in Yun et al. (2001). They kindly provided the $S_{25\mu m}$ and $S_{60\mu m}$ fluxes and we used them to derive the statistics of AGN candidates based on IRAS colours for their sample (Table 10.2).

Corbett et al. (2002) studied a sample of objects with IRAS data to perform a comparison of the multiwavelength properties of a sample of AGN with and without compact radio cores and a matched sample of galaxies without an AGN. They imposed a FIR flux limit higher than Yun et al. (2001). As a consequence, the Corbett et al. selected galaxies have FIR luminosities greater than $10^{10.5}$ $L_\odot$ which, as they indicate, results in an enhanced fraction of interacting galaxies in the sample. They estimate that 40% of their sample is obviously involved in either tidal interactions or are major mergers, and 20% are apparently non-interacting. Using the data in Table 2 of Corbett et al. (2002), we obtained their ratio of radio-excess galaxies. We found a slightly higher value of radio-excess galaxies than for the sample of Yun et al. (2001); the

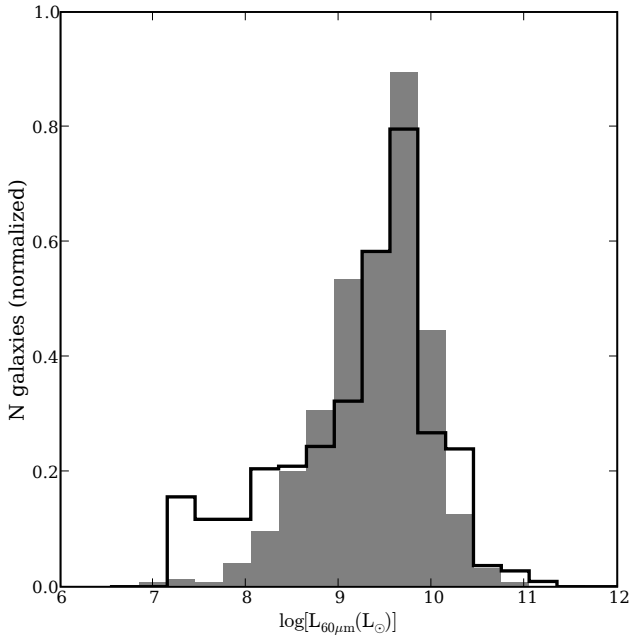

Figure 10.1: Histogram of $L_{60\mu m}$ luminosity for our complete subsample (n = 710; black line) and the Yun et al. (2001) sample (n = 1248; grey bars).

Corbett et al. (2002) data yielded 3 times our value, but is still only a few percent. This low value is, as they indicate, most likely due to their high FIR cutoff, artificially lowering the rate of radio-excess galaxies.

Condon et al. (2002) studied an Uppsala General Catalogue of Galaxies (UGC) sample composed of sources detected in the NVSS and covered by the IRAS survey, using a radio-flux cutoff and no selection in terms of the environment. Using the data in their Table 1, we have calculated their rate of radio-excess galaxies as well as the percentage of AGN candidates with $\alpha_{25,60} < 1.958$. We could not apply a cut at $S_{60\mu m} \geq 2$ Jy since $S_{60\mu m}$ was not available. We note that the radio cutoff for this sample is lower than in Condon & Broderick (1991), and the ratio of radio-excess galaxies is also lower.

Drake et al. (2003) used a sample selected by cross-correlating the IRAS Faint Source Catalogue with the 5 GHz Parkes-MIT-NRAO catalogue. We derived the ratio of AGN candidates with $S_{25\mu m}/S_{60\mu m} \geq 0.18$ using the data in their Table 1 and list the value with and without the 2 Jy cut in Table 10.2. They find a radio-excess rate of $\approx 55\%$, using a factor 5 cutoff at 4.8 GHz with respect to the mean of the u parameter in Condon et al. (1995) ($u \equiv \log(S_{60\mu m}/S_{4.8\ GHz})$; $< u >= 2.5$). They sample lower IRAS flux densities than previous authors and thus find a larger fraction of objects with intermediate radio fluxes. In a later paper (Drake et al. 2004) the host galaxies of radio-excess sources are studied, finding that only 23% of them are isolated and with no evidence of disturbance.

Dense environments

Niklas et al. (1995) analysed the radio-FIR correlation for Virgo cluster galaxies at 4.8 and 10 GHz. Inspection of their Fig. 4 indicates that they used a cutoff of a factor 3 to select radio-excess galaxies with respect to their radio-FIR correlation. We have used the data in their paper to obtain the remaining values given in Table 10.1.

Andersen & Owen (1995) compared the FIR-radio correlation for spirals in rich and poor cluster and group environments. Using the data in their Table 4 and 5 we calculated the radio-excess ratio in their subsample.

Miller & Owen (2001) considered a sample of nearby Abell clusters galaxies. They kindly provided the data used in their paper which we have used to estimate the ratio of radio-excess galaxies in their sample for different distances from the cluster centre, as we list in Table 10.1. They considered 3 subsamples: one including galaxies in the inner Mpc of clusters, one in the 1 - 2 Mpc range and the last one at the periphery of clusters, between 2 and 3 Mpc from the cluster core in projection. The last subsample is likely to be very similar to field-like environments. They find a considerable gradient in the ratio of radio-excess galaxies from the outer parts to the centre of the cluster (see Table 10.1). They suggest that this is probably a result of the presence of centrally concentrated radio-luminous elliptical galaxies as we will discuss in Section 10.2.

Reddy & Yun (2004) studied a sample of cluster galaxies located in the seven nearest clusters with prominent X-ray emission using a cut in the FIR luminosities. They use $q < 1.64$ as cutoff for radio-excess galaxies, very similar to our value (1.66) but for coherence we recalculated the ratios referred to our value. We also estimated the ratios for early and late-type galaxies using the data in their Table 2. Their ratios are similar to the values in other clusters, except for those cases where a radio flux cutoff was applied, in which case the radio-excess ratios are higher due to selection effects. We provide also the ratios for galaxies with projected cluster-centric distances lower than 0.5 Mpc and between 0.5 and 1.5 Mpc, defined by them as core and ring respectively. These data are not given in their paper and were kindly provided by the authors. This result cannot be directly compared with Miller & Owen (2001) since the area defined as ring by Reddy & Yun (2004) is still in the inner area of the Miller & Owen sample. We used the $S_{25\mu m}$ and $S_{60\mu m}$ fluxes provided by them to derive the statistics of AGN candidates based on IRAS colours for their sample (Table 10.2).

Omar & Dwarakanath (2005) studied the radio-FIR correlation for the Eridanus group, which is not dynamically relaxed. They consider the 72 galaxies detected in the IRAS survey. Using the data in their Fig. 3 and Table 2 we have calculated the radio excess for the total sample.

Radio-excess, environment and density-morphology relation

A comparison with the above discussed samples from the literature shows that the AMIGA sample has the lowest ratio of radio-excess galaxies (Table 10.1). Higher ratios of radio excess galaxies are found in denser but still poor environments as the outer parts of clusters with prominent X-ray emission (Reddy & Yun 2004), outer parts of Abell clusters (Miller & Owen 2001), poor cluster and group environment (Andersen & Owen 1995), Virgo cluster (Niklas et al. 1995) and Eridanus group (Omar & Dwarakanath 2005). The values in the outermost, field-like sample of Miller & Owen are similar to the ones in Condon et al. (2002), suggesting that the outer parts of clusters are as efficient as the "field" environment to trigger radio emission in active

galaxies. For the densest environments an even higher ratio of radio-excess is found, as in the core sample of Reddy & Yun, the inner area of Abell clusters (Miller & Owen 2001) or rich environments (Andersen & Owen 1995). It is interesting to note that the Drake et al. sample is dominated by one-to-one interactions, i.e., higher local density, and its radio-excess rate is the highest among all. Although the radio-flux cutoff used in their sample is high, hence producing an artificial increase in radio-excess galaxies, the result might also reflect that one-to-one interactions are more efficient in inducing radio activity in galaxies than the larger scale environment. This could be explained by the fuelling of gas towards the centre of galaxies in interacting pairs, feeding the AGN and leading to the radio-excess regime.

The same result is found using FIR colours, independently whether the 2 Jy cut is applied or not: we find that the rate of AGN candidates based on IRAS colours increases from the most isolated environments to the densest ones. We notice that when the 2 Jy cut is applied, although the trend is kept the gradient is significantly reduced, confirming the limited reliability of the method.

Finally, we have studied several subsets of the AMIGA sample, taking into account the refinement of the CIG with respect to the environment that our group carried out. In our reevaluation of the optical morphologies of the CIG galaxies we identified 32 objects candidates to be suffering interactions based on evidence for asymmetries/distortions that might be of tidal origin (Sulentic et al. 2006). None of these galaxies show a radio excess above a cutoff of 3. A further revision of the sample showed that 150 additional galaxies lie in environments that could affect their evolution based on the value of their local number density of neighbours and the tidal forces at play (Verley et al. 2007b). These galaxies are uniformly distributed with respect to the radio-FIR correlation suggesting that weak interactions in a low density environment do not significantly affect the radio activity of galaxies.

10.2. Improved study of the morphology, luminosity and environment relation with the radio-excess

In this section we will take into account the possible effect of the luminosity as well as the morphology on the rate of radio-excess galaxies. Best et al. (2005a) showed the probability for a given galaxy to host a radio AGN rises very rapidly with the mass of the host galaxy. The masses were computed from SDSS optical fluxes (Kauffmann et al. 2003a) and correlate, with some dispersion, with the optical luminosities. The rate of radio-excess galaxies could be affected by the density-morphology relation. Radio galaxies are suposed to be hosted by earlier morphological types, thus, a lower rate of radio-excess galaxies is expected in isolated galaxies if they have less early types than galaxies in denser environments, as predicted by the density-morphology relation. Hence, a comparison of both optical luminosities and morphologies between AMIGA galaxies and the galaxies of the comparison samples is needed. With this comparison we will be able to discard that our low rate of radio-excess galaxies arises due to the difference in luminosity ranges or morphologies of our sample with respect to the comparison samples.

Our sample is selected in the visible, hence, we will use the optical B band absolute magnitudes of the galaxies to compare with other samples. To perform the comparison we compiled the absolute magnitudes and morphologies of all galaxies from HYPERLEDA in order to guarantee the homogeneity of the data. In some cases it is clear that the HYPERLEDA morphology classification is not accurate, as e.g.,

in Figures 10.6c and 10.7f some Irregular or Sm galaxies are classified according to HYPERLEDA as radio AGN, which is very improbable. This seems to come from a missclassification on the HYPERLEDA database or due to an error in the determination of the HYPERLEDA counterpart of the source that appeared in the paper.

The search of HYPERLEDA data for galaxies belonging to the comparison samples was done looking for a matching of the catalogue name when possible. In some cases it was not possible to find an adequate match in HYPERLEDA and a manual search in NED was done allowing us to find the HYPERLEDA catalogue number (PGC number). But there were still some cases where it was not possible to find a catalogue match. In these cases the search was done using the coordinates of the sources. For the galaxies of Andersen & Owen (1995) it was imposible to find an accurate matching and we had to discard this sample from our study.

In Figures 10.2, 10.3 and 10.4 the optical luminosities of the galaxies of the comparison samples are compared with the ones of the AMIGA complete sample. The distribution of optical luminosities for the subsamples with radio-excess emission, normalized to the size of the sample, as well as the relative fraction of radio-excess galaxies for each luminosity bin are also plotted.

There is an increase of the fraction of radio-excess galaxies with the luminosity. This trend was previously found in the samples of galaxies of Carter et al. (2001) and Kauffmann et al. (2003a). The exceptions to this trend are usually bins with a low number of galaxies and hence with a worse statistic. In the samples with the lower number of galaxies like Niklas et al. (1995), Omar & Dwarakanath (2005) and Corbett et al. (2002) (less than 100 galaxies each one) this trend is not so clear but this maybe produced by the low count of galaxies. The sample of Drake et al. (2003) does not show this clear trend. This sample is dominated by one-to-one interactions and mergers, hence this can produce a bias in the trend if these mechanisms are relatively more efficient in inducing radio activity in galaxies than the effect of the luminosity.

We used the morphological classification in order to study the effect of the morphological type in the rate of radio-excess galaxies. The data separated into morphological types is presented in Table 10.1. For the sample of Condon & Broderick (1991) the separation of the data by morphological types clearly shows a higher rate of radio excess for early-type galaxies. We calculated the rate of radio-excess galaxies for the samples of Condon et al. (2002) and Omar & Dwarakanath (2005) separated by morphological types as listed in Table 10.1. In Condon et al. (2002) sample as in Condon & Broderick (1991) a higher rate of radio excess is found for early-type galaxies. Elliptical galaxies in Drake et al. (2003) sample show a large range of radio excess, while the disk systems all have only a moderate radio excess. For the low density parts of Abell clusters (Miller & Owen 2001) we find a very low ratio of spirals with radio-excess and a much higher one for early types. For the inner 2 Mpc the ratio of radio-excess galaxies increases by a factor 2-3 both for early and late-type galaxies. The sample of Reddy & Yun (2004), when divided Reddy & Yun (2004) into early and late-type galaxies, both early and late types show a significant increase in the ratio of radio-excess for smaller radii. A comparison with the above discussed samples from the literature shows that the AMIGA sample has the lowest ratio of radio-excess galaxies, both globally and separated into early and late types (Table 10.1).

The morphological properties of the galaxies of the comparison samples are shown in Figures 10.5, 10.6 and 10.7. The distribution of morphologies of galaxies with radio-excess for the same samples (normalized to the size of the sample) and the relative fraction of radio-excess galaxies for each morphology bin are plotted. These distributions confirms the increase of the fraction of radio-excess galaxies toward ear-

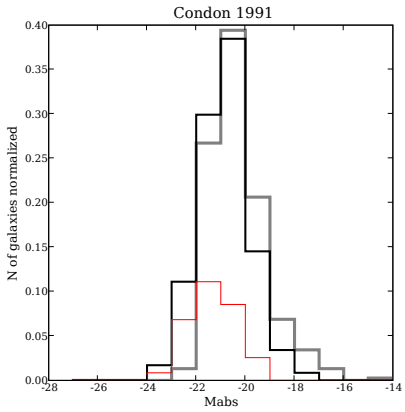

(a) Histogram of optical luminosity.

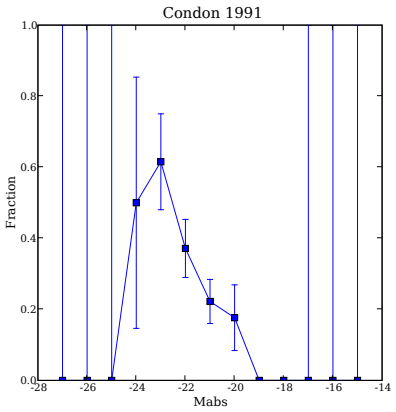

(b) Relative fraction of radio-excess galaxies.

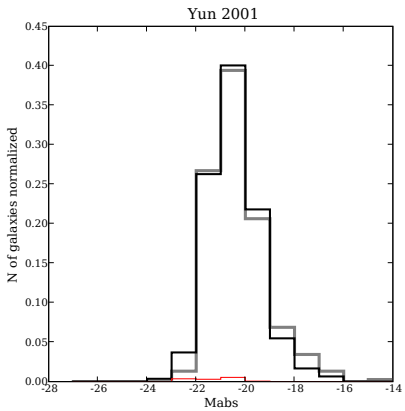

(c) Histogram of optical luminosity.

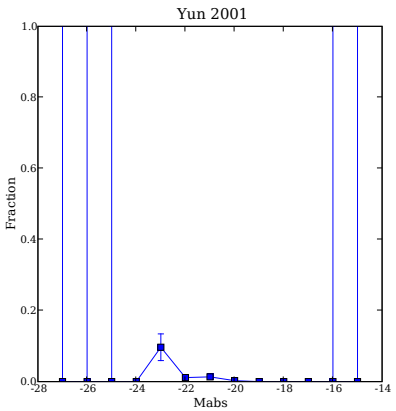

(d) Relative fraction of radio-excess galaxies.

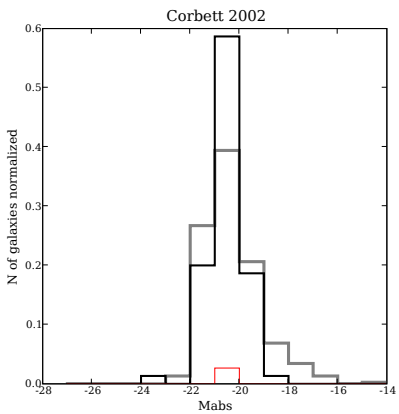

(e) Histogram of optical luminosity.

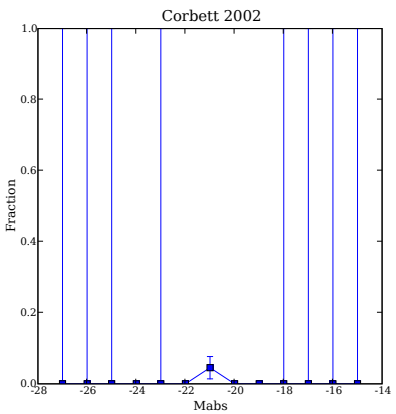

(f) Relative fraction of radio-excess galaxies.

Figure 10.2: Histograms and relative fractions of radio-excess galaxies with respect to the optical absolute magnitude for the comparison samples.

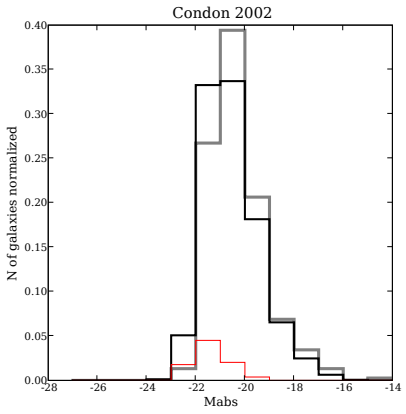

(a) Histogram of optical luminosity.

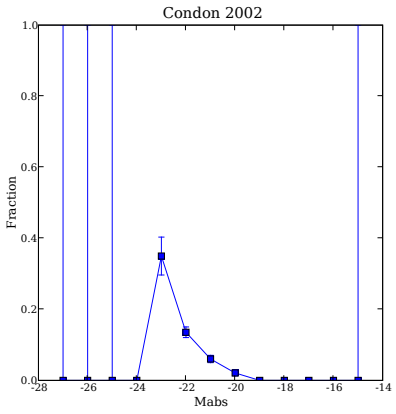

(b) Relative fraction of radio-excess galaxies.

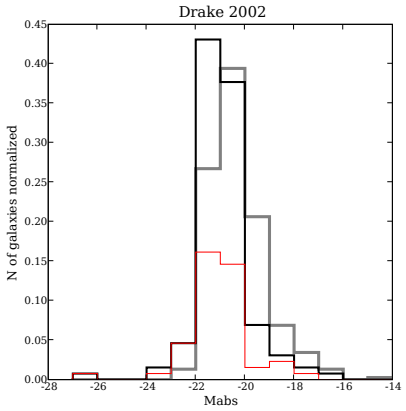

(c) Histogram of optical luminosity.

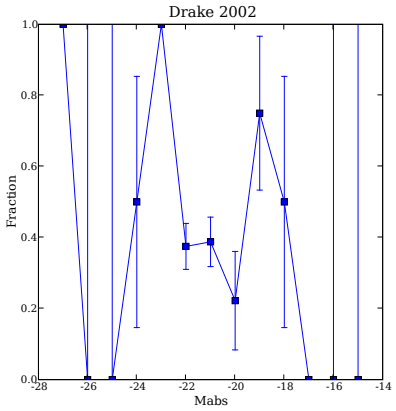

(d) Relative fraction of radio-excess galaxies.

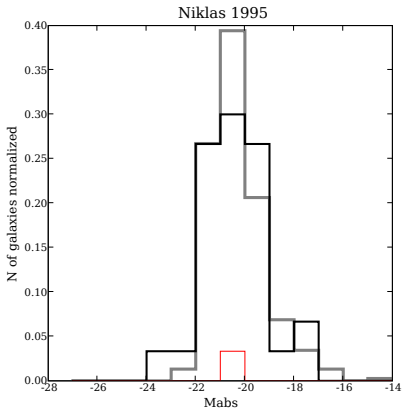

(e) Histogram of optical luminosity.

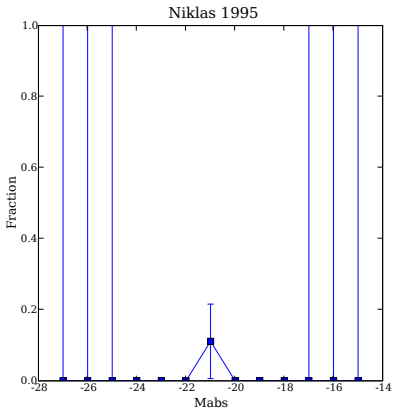

(f) Relative fraction of radio-excess galaxies.

Figure 10.3: Histograms and relative fractions of radio-excess galaxies with respect to the optical absolute magnitude for the comparison samples.

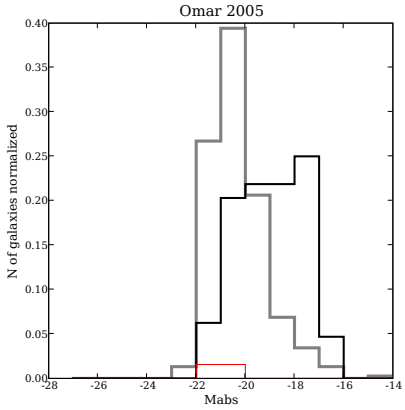

(a) Histogram of optical luminosity.

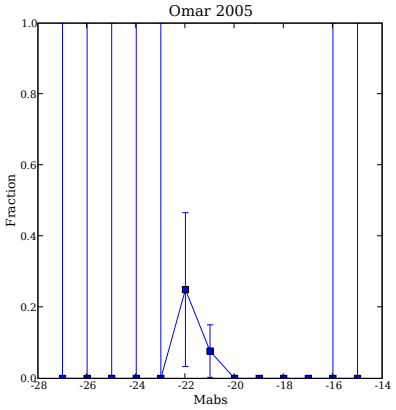

(b) Relative fraction of radio-excess galaxies.

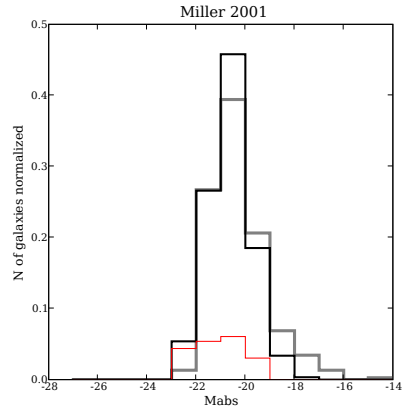

(c) Histogram of optical luminosity.

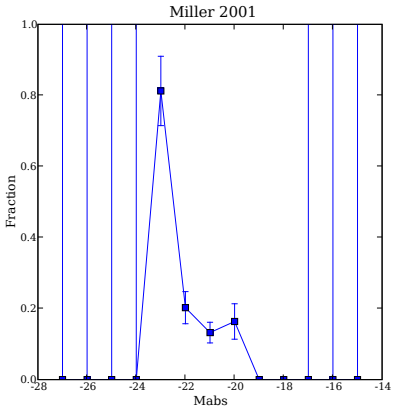

(d) Relative fraction of radio-excess galaxies.

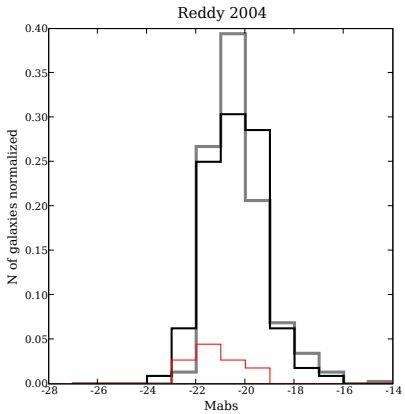

(e) Histogram of optical luminosity.

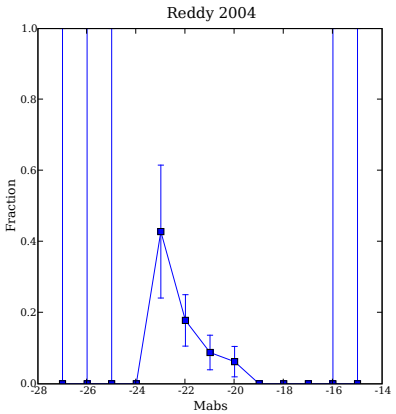

(f) Relative fraction of radio-excess galaxies.

Figure 10.4: Histograms and relative fractions of radio-excess galaxies with respect to the optical absolute magnitude for the comparison samples.

lier types but not restricted just to E galaxies.

The distribution of morphological types and the absolute magnitudes for the comparison samples are plotted in Figure 10.8 and Figure 10.9). In these figures we also plot the distribution of AMIGA galaxies in order to compare with. There is a clear trend of the radio-excess galaxies toward higher luminosities and earlier morphological types. This trend is clear when comparing the mean for the whole sample (marked as a black cross) and the mean for the radio-excess galaxies (marked with a red cross). The mean for the radio-excess galaxies is sistematically shifted to higher absolute magnitudes and earlier types for all samples, except in the case of Corbett et al. (2002) sample where the two means are very similar. In this case there are only two galaxies that present radio excess.

Many of the AMIGA galaxies have morphologies and absolute magnitudes located in zones where the fraction of radio-excess galaxies is very high for other comparison samples. This suggest that the low rate of radio-excess for isolated galaxies is not just linked to the morphology-density or the fraction of AGN-luminosity relations.

We compared the effect of the optical luminosity and morphology for the different samples (see Figure 10.10). We divided the optical absolute magnitude in three bins: a) $M_{\rm abs} < -21.0$ (high luminosities); b) $-21.0 < M_{\rm abs} < -20.0$ (medium luminosities) and c) $M_{\rm abs} > -20.0$ (low luminosities). We also divided the morphological types in three bins: a) E-S0/a; b) Sa-Sb and c) Sbc-Sm. The luminosity and morphology bins where defined in order to sample them uniformly.

In all bins the fraction of radio-excess galaxies is null for AMIGA galaxies. The rate of radio-excess galaxies increases toward earlier types and higher luminosities in the samples of cluster and interacting galaxies (Miller & Owen 2001; Reddy & Yun 2004; Drake et al. 2003) and in the samples of UGC galaxies (Condon et al. 1991, 2002) and bright IRAS galaxies (Yun et al. 2001). The sample of Corbett et al. (2002) only presents 2 radio-excess galaxies in the central bin ($-21.0 < M_{\rm abs} < -20.0$ and Sa-Sb).

The higher ratio of radio-excess galaxies in denser environments has often been explained as due to the density-morphology relation. In all the samples studied in this paper, a larger ratio of radio-excess galaxies is found for early types, which is not surprising since usually the typical host galaxies of an AGN with powerful radio continuum emission are massive ellipticals. The higher abundance of early-type galaxies in denser environments could by itself justify the higher ratio of radio active galaxies. We think however that although it might explain in part the results, the environment also has to play a prominent role in triggering the radio activity. On one hand the ratio of early-type galaxies with radio-excess in our sample, higher than for late-type galaxies, is still much lower than for all other environments (only 4.8% of the early-type galaxies have a radio excess above a factor 5 cutoff). This result might be explained by the low luminosities of the AMIGA early-type population relative to the AMIGA spiral population and to early-type populations found in most surveys (Sulentic et al. 2006). This shows that the low ratio of radio-excess galaxies in our sample can not be only due to the small percentage of early-type galaxies (12% in the complete subsample, see Table 5.2), as expected for a low-density environment. On the other hand, we find evidence that spiral galaxies also increase their rate of radio activity with environment. The ratios for the spirals in our sample of isolated galaxies are clearly lower than for samples in denser environments.

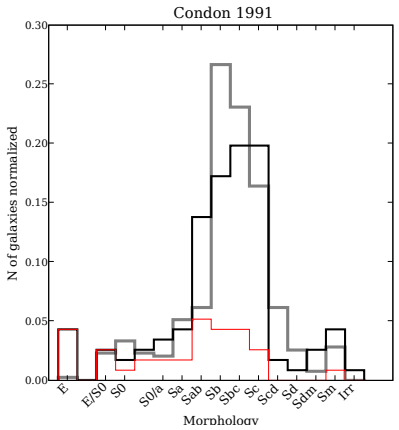

(a) Histogram of morphologies.

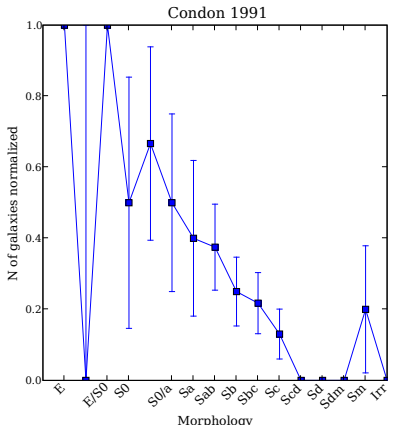

(b) Relative fraction of radio-excess galaxies.

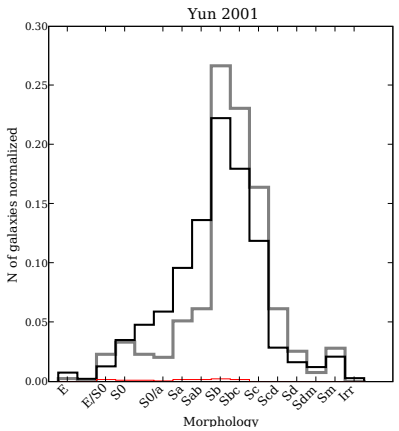

(c) Histogram of morphologies.

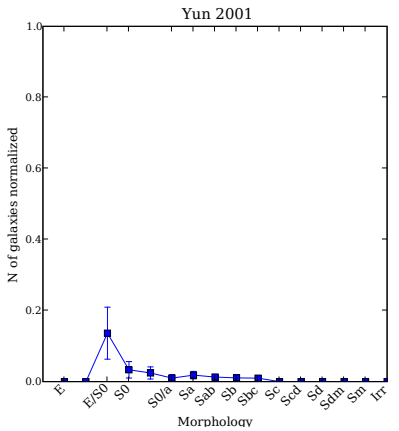

(d) Relative fraction of radio-excess galaxies.

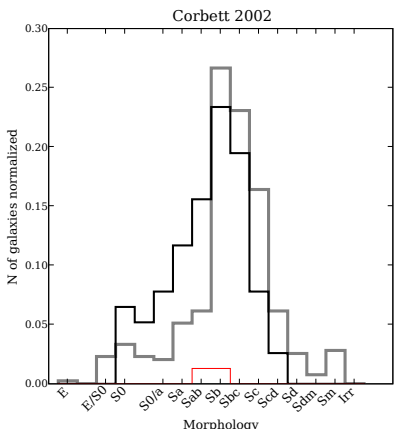

(e) Histogram of morphologies.

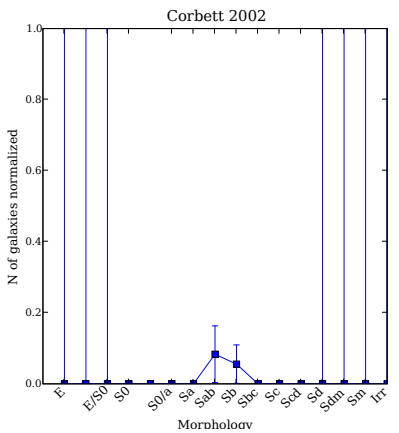

(f) Relative fraction of radio-excess galaxies.

Figure 10.5: Histograms and relative fractions of radio-excess galaxies with respect to the morphology for the comparison samples.

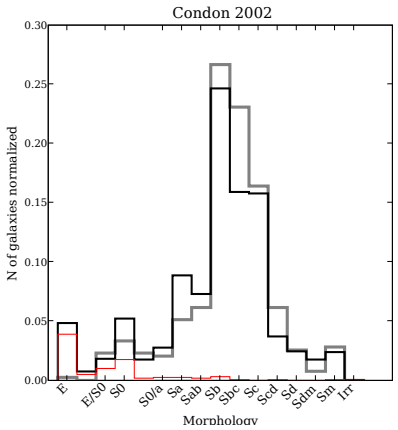

(a) Histogram of morphologies.

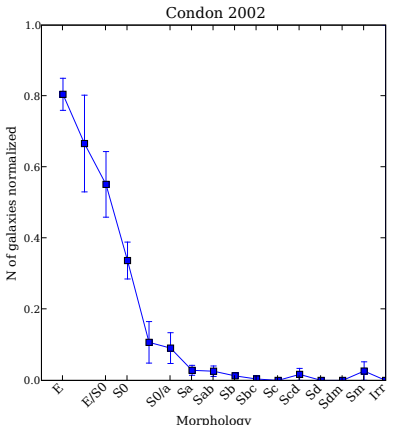

(b) Relative fraction of radio-excess galaxies.

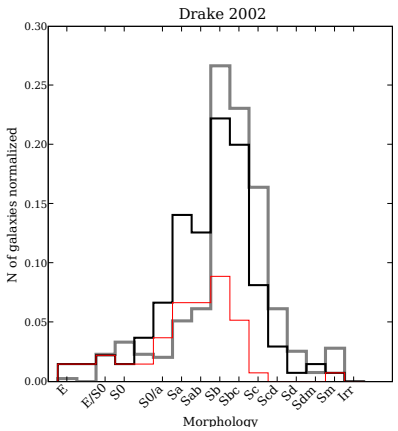

(c) Histogram of morphologies.

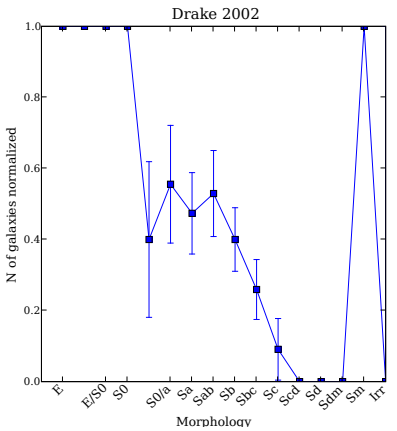

(d) Relative fraction of radio-excess galaxies.

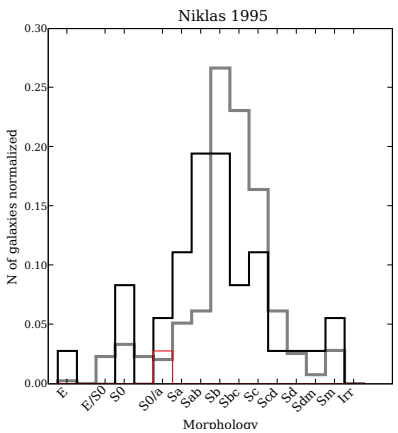

(e) Histogram of morphologies.

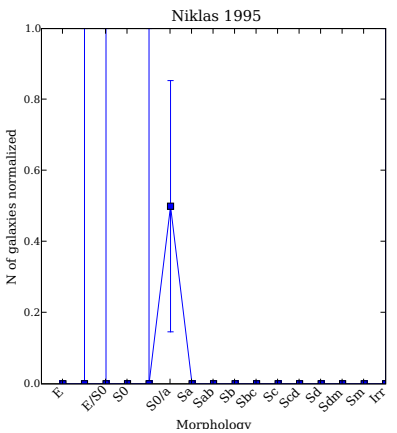

(f) Relative fraction of radio-excess galaxies.

Figure 10.6: Histograms and relative fractions of radio-excess galaxies with respect to the morphology for the comparison samples.

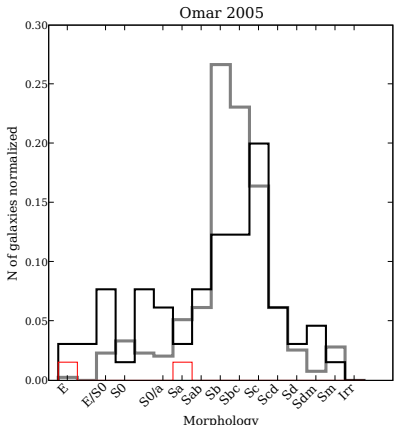

(a) Histogram of morphologies.

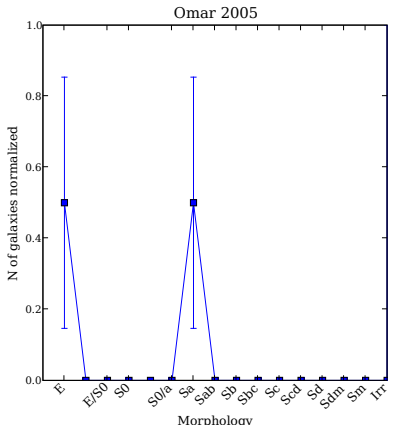

(b) Relative fraction of radio-excess galaxies.

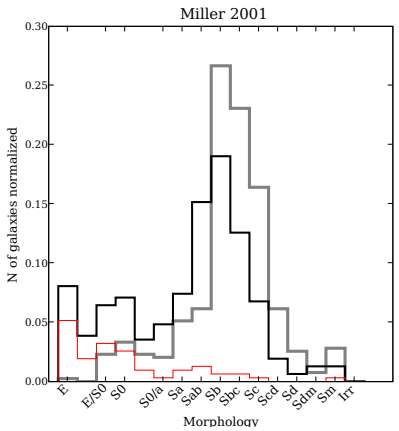

(c) Histogram of morphologies.

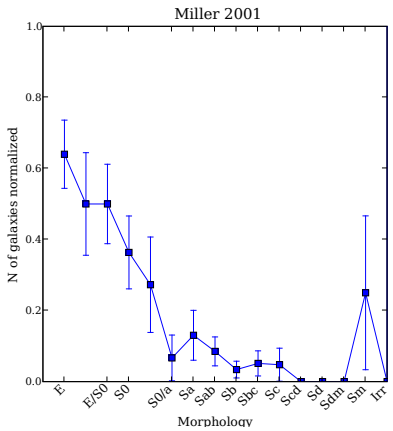

(d) Relative fraction of radio-excess galaxies.

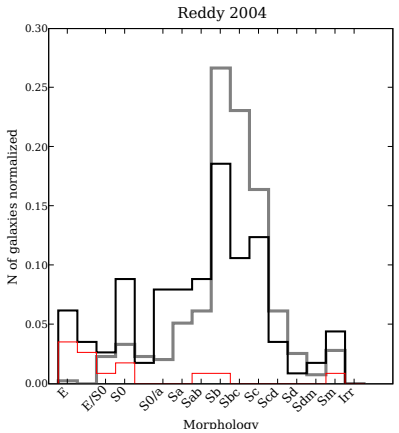

(e) Histogram of morphologies.

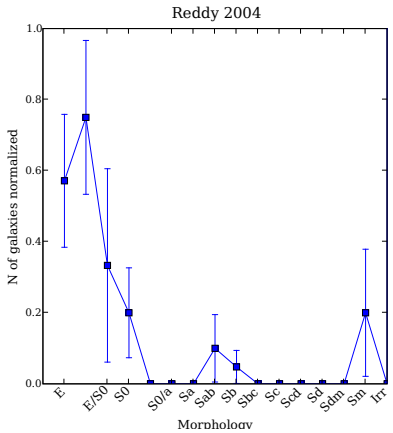

(f) Relative fraction of radio-excess galaxies.

Figure 10.7: Histograms and relative fractions of radio-excess galaxies with respect to the morphology for the comparison samples.

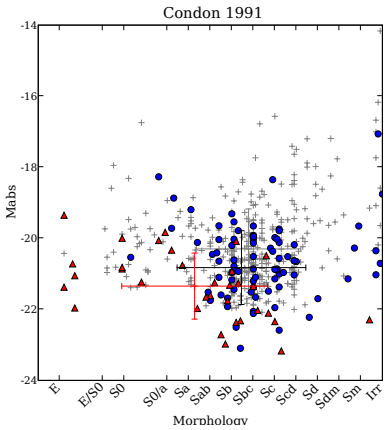

(a) Morphology - luminosity distribution.

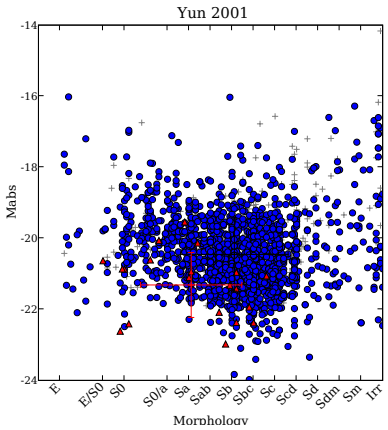

(b) Morphology - luminosity distribution.

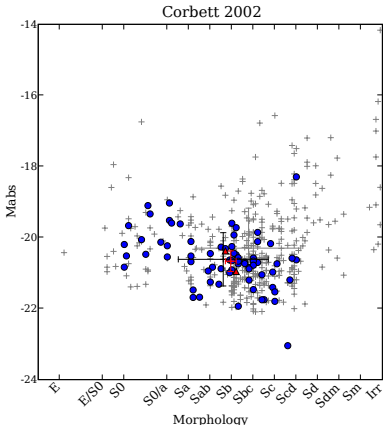

(c) Morphology - luminosity distribution.

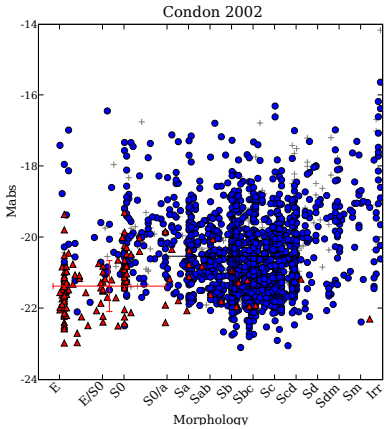

(d) Morphology - luminosity distribution.

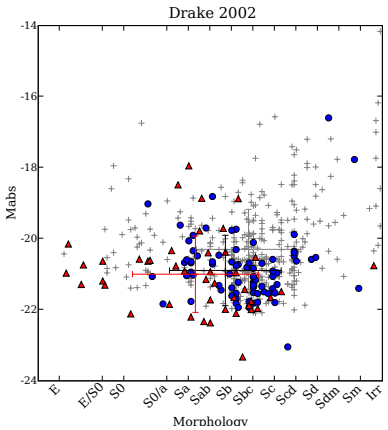

(e) Morphology - luminosity distribution.

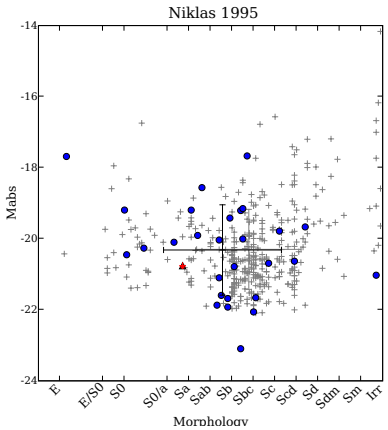

(f) Morphology - luminosity distribution.

Figure 10.8: Distribution of optical abspolute magnitudes and morphology for the comparison samples. Radio-excess galaxies are plotted in red and the remaining galaxies in blue. The distribution of the AMIGA sample is ploted with grey crosses. The mean and standard deviation are marked with a big black cross for the whole sample and with a big red cross for the radio-excess galaxies of the sample.

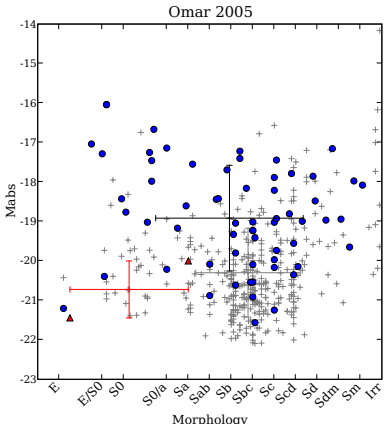

(a) Morphology - luminosity distribution.

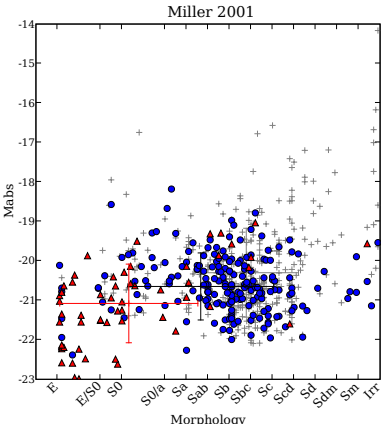

(b) Morphology - luminosity distribution.

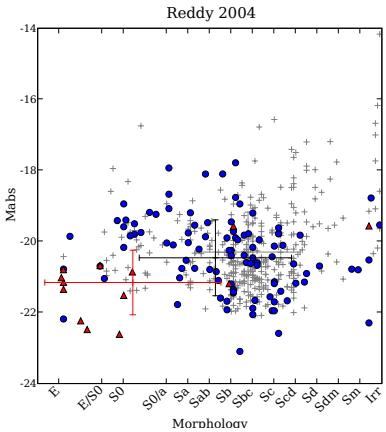

(c) Morphology - luminosity distribution.

Figure 10.9: Distribution of optical abspolute magnitudes and morphology for the comparison samples. Radio-excess galaxies are plotted in red and the remaining galaxies in blue. The distribution of the AMIGA sample is ploted with grey crosses. The mean and standard deviation are marked with a big black cross for the whole sample and with a big red cross for the radio-excess galaxies of the sample.

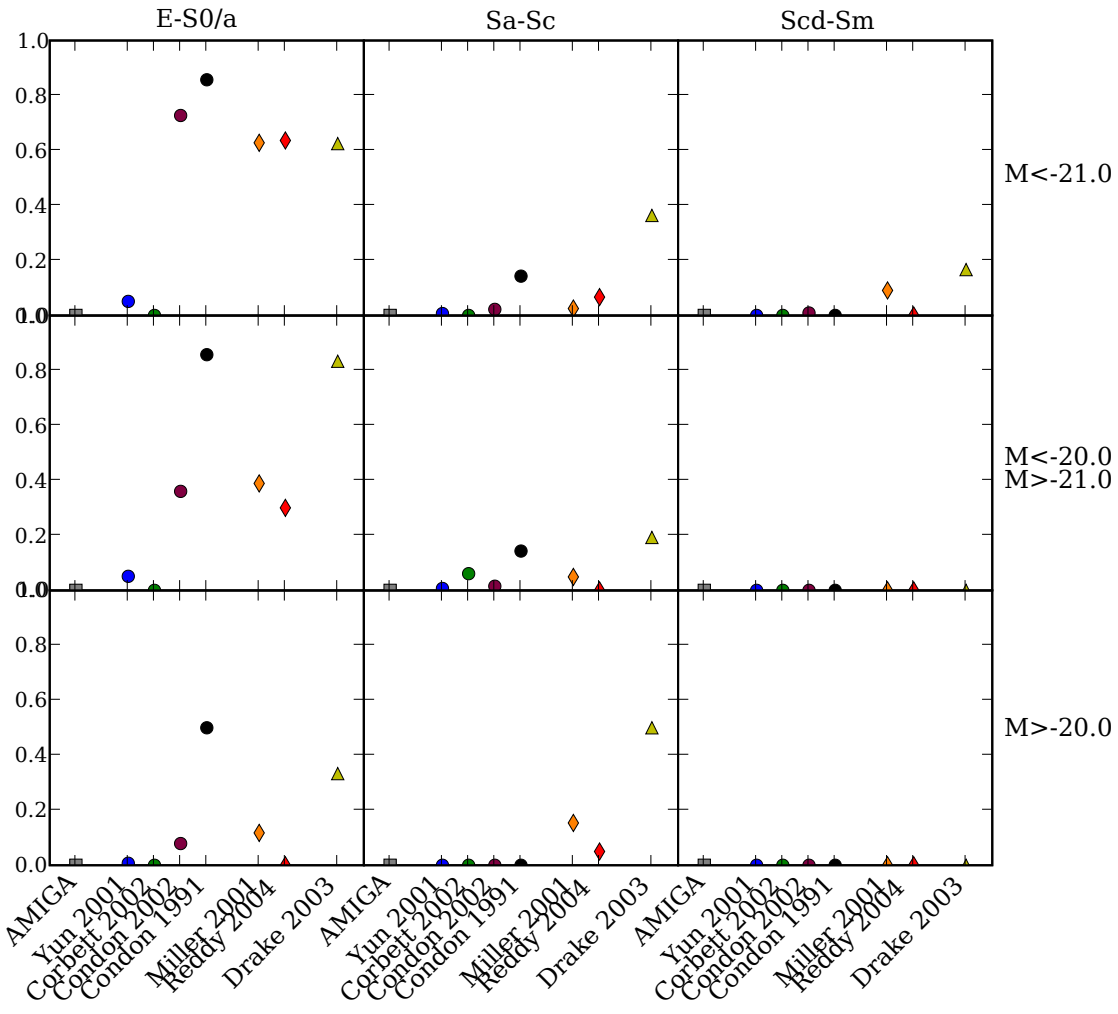

Figure 10.10: Fraction of radio-excess galaxies in different samples. The fraction is presented for 9 different ranges of morphologies and absolute magnitudes.

10.3. SDSS radio-loud AGN

In this section we will study if isolated galaxies have less radio-loud galaxies (as defined by Best et al. (2005b)) than the expected value. Best et al. (2005b) studied a sample of 2712 radio-luminous galaxies derived from the SDSS using NVSS and FIRST data. They compare the radio luminosity per unit stellar mass with the 4000Å break strength to distingish between AGN and star formation finding 2215 *radio-loud AGN* galaxies brighter than 5 mJy at 1.4 GHz. Best et al. (2005a) studied the properties of the hosting galaxies, among them, they studied the fraction of galaxies that host radio-loud AGN with $L_{1.4\mathrm{GHz}} > 10^{23}\mathrm{W\ Hz^{-1}}$ as a function of the stellar mass, finding that there is a strong dependence of this fraction rising from nearly zero below a stellar mass of $10^{10}\mathrm{M_\odot}$ to more than 30% at masses of $5 \times 10^{11}\mathrm{M_\odot}$.

The sample of Best et al. (2005a) is derived from the sample of Best et al. (2005b) and it is not selected using an environmental criterion. In order to estimate how many galaxies would be expected to be radio-loud in AMIGA sample for its mass distribution when compared with Best et al. (2005a), we have compared the distribution of masses for the galaxies of their sample with the distribution of masses of AMIGA galaxies.

Kauffmann et al. (2003b) and Gallazzi et al. (2005) derived the stellar masses for galaxies of the second and fifth SDSS data releases respectively. Here we have obtained the data derived with a similar method applied to the SDSS photometric data for the seventh data release from `http://www.mpa-garching.mpg.de/SDSS/DR7/Data/stellarmass.html`,[1]. Although the methods for the estimation of the stellar masses used in Best et al. (2005a) and in `http://www.mpa-garching.mpg.de/SDSS/DR7/Data/stellarmass.html` are slightly different it is claimed that this difference is not significant (see the comparison of mass estimates at: `http://www.mpa-garching.mpg.de/SDSS/DR7/mass_comp.html`. We selected from these data the mass estimates for the SDSS subsample of AMIGA galaxies. Arranging our galaxies in the same bins of luminosity as the ones of the Best et al. (2005a) study, and using their rates of radio-loud galaxies, we estimated the number of radio-loud AGN (with $L_{1.4\mathrm{GHz}} > 10^{23}\mathrm{W\ Hz^{-1}}$) expected for AMIGA galaxies.

In Figure 10.11 we show the mass distribution of the SDSS complete subsample of AMIGA galaxies and the corresponding number of radio-loud AGN galaxies with $L_{1.4\mathrm{GHz}} > 10^{23}\mathrm{W\ Hz^{-1}}$. We also show the total number of expected galaxies for this sample. We could expect 1.8 galaxies for this subsample and, if we suppose that the complete AMIGA subsample is uniformly sampled by the SDSS complete subsample (see Chapter 7.3), we estimate a number of 5.2 galaxies for the complete AMIGA subsample ($n = 719$).

We apply a χ^2 to test whether this difference is statistically significant. Using 7 bins, i.e., 6 degrees of freedom for the SDSS complete subsample, the value of χ^2 is 1.82 which corresponds to a value of α of 0.93. If we consider that the whole complete sample is well represented by the SDSS subsample as explained in Section 7.3 and that there are not radio-excess galaxies in the complete sample, the value of α is 0.52. Although lower it is still larger than 0.05 which is the typical value used to discard the null hypothesis that the two samples follow the same distribution. We find that we cannot discard the possibility that our sample follow the same distribution of radio-loud AGN that the one of Best et al. (2005a).

[1]Data released at: `http://www.mpa-garching.mpg.de/SDSS/`

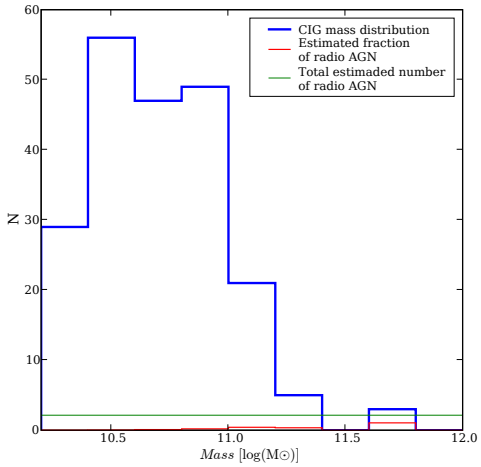

Figure 10.11: Mass distribution of the CIG galaxies (blue line) and the corresponding number of radio AGN with $L_{1.4\mathrm{GHz}} \geq 10_{23}$ W Hz^{-1} for the masses of CIG galaxies with the probabilities of Best et al. (2005a) (red line). The total number of radio-AGN galaxies estimated for the SDSS complete subsample is 1.8 ± 1.4 and is marked as a green line.

10.4. SDSS active galaxies

We compared the rates of diferent types of activity derived from SDSS data for AMIGA galaxies with the ones found for galaxies in denser environments. In § 10.4 we compare the rate of nuclear activity found in other samples and its relation with the environment and in § 10.4 we compare the ratio of broad line AGN over narrow line AGN in different samples.

Rate of activity

The effect of the environment on the rate of AGN is not clear yet. While the studies of Carter et al. (2001) and Miller et al. (2003) claim that this rate is constant, Dressler et al. (1985); Kauffmann et al. (2004) detect a decrease of this rate towards higher local densities while Reviglio & Helfand (2006) detect an increase of the fractional abundance of AGN with increasing density if passive galaxies with AGN activity (radio AGN) are taken into account. Constantin & Vogeley (2006) and Montero-Dorta et al. (2009) found that Seyfert galaxies are less clustered and LINERs are more clustered in comparison to normal galaxies in the local universe. Alonso et al. (2007) found a slight increase (≈ 10%) in the rate of AGN in pairs of galaxies in comparison with field galaxies. These studies used optical spectra to determine the presence of an AGN (with the exception of Reviglio & Helfand 2006, which also used radio data) but their samples are defined in different ways and the selection criteria and definition for an "AGN" are usually different from one study to another. Sorrentino et al. (2006) require the detection of all the lines used in the three diagnostics diagrams (see Section 7.6) to classify a galaxy. Dressler et al. (1985); Huchra & Burg (1992); Ho et al. (1997a); Ivezić et al. (2002); Maia et al. (2004) and Hao et al. (2005) also require this

while Carter et al. (2001); Miller et al. (2003) and Martinez (2008) allow the use of only the log([O III]/Hβ) - log([N II]/Hα) diagram or even a ratio between [O III] and Hβ or [N II] and Hα, which is very similar to our criteria. The fraction of AGN in the studies that require all lines to be detected will decrease with respect with the fraction found in the other studies because [S II] and [O I] lines are usually weaker than the other involved lines. The subtraction or not of the underlying stellar population would also affect to the fraction of AGN galaxies. With the subtraction of the stellar population is possible to detect a higher number or weak lines which are usually present in AGN galaxies, hence, an increase in the fraction of galaxies classified as AGN is expected in studies where the stellar populations are subtracted from the spectra. Some differeces could also arise from the different signal to noise ratio required by different studies for a line to be considered as a detection, e.g., Carter et al. (2001) and Miller et al. (2003) used a 2σ limit. It is important to know which of the selection lines was used to consider a galaxy as an AGN beacuse it could change the fraction of AGN, e.g., Miller et al. (2003) use a line 1σ below the line of Kewley et al. (2001) (althought they do not explain it in the main text of the paper, it appears in the caption of their Figure 3 and, this limit has been confirmed using their data). Finally the selection criteria used to select the different samples could affect the final fraction of AGN, e.g., a higher cut in absolute magnitudes could enhance the fraction of AGN.

The fraction of AGN galaxies found in Sorrentino et al. (2006) is $\sim$ 2%. This values are comparable to the ones found by Dressler et al. (1985, 5% in the field and 1% in clusters), Huchra & Burg (1992, 1.3%), Ivezić et al. (2002, 5% using SDSS data) and Maia et al. (2004, 3-4%) and it lower that the fraction found by Carter et al. (2001, $\sim$ 17% using data from the 15R-North galaxy redshift survey), Miller et al. (2003, 20-40% using SDSS data) and Martinez (2008, 44-46% for compact groups).

We compared the rates obtained by Martinez (2008) with our rates. They obtained the relative fractions for the different types of nuclear activity in a sample of HCG galaxies and in a sample of compact groups from the Updated Zwicky Catalogue (Focardi & Kelm 2002, UZC-CG). The compact groups samples are defined with the help of isolation requirements and are small systems of several galaxies in a compact configuration. Galaxies of the group are affected by strong galaxy interactions which is confirmed by their high value of the "Tidal forces estimator" (see Section 2.2), hence, compact groups are perfect to test the effects of galaxy interaction, being isolated systems just in the opposite extreme to isolated galaxies in terms of tidal force strength. In Table 10.3 and Table 10.4 we show the different number and rates for the different types of galaxies in the AMIGA complete subsample and the two samples studied by Martinez (2008).

Table 10.3: Fraction of the different types of AMIGA galaxies and compact groups galaxies from Martinez (2008). Fractions given with respect to the total number of galaxies.

Sample	AMIGA		HCG		UZC-CG[1]	
	N[2]	frac[3]	N[2]	frac[3]	N[2]	frac[3]
Total:	226	100.0	269	100.0	397	100.0
Unclassified or non-emission:	16	7.1	101	37.5	123	31.0
Classified or emission[4]:	210	92.9	168	62.5	274	69.0
SFN	126	55.8	54	20.1	83	20.9
TO	35	15.5	36	13.4	50	12.6
AGN:	49	21.7	78	29.0	141	35.5
NLAGN total:	44	19.5	76	28.3	133	33.5
LINER	20	8.9	35	13.0	11	2.8
Sy2	10	4.4	24	8.9	43	10.8
unclassified NLAGN (LLAGN)	14	6.2	17	6.3	79	19.9
Sy1	5	2.2	2	0.7	8	2.0
TO + AGN:	84	37.2	114	42.4	191	48.1

[1] UZC-CG subsample with spectra from FAST and the SDSS.

[2] Number of galaxies.

[3] Figures given in percentages.

[4] Classified galaxies in the AMIGA sample and galaxies with emission in the compact groups sample.

Table 10.4: Fraction of the different types of galaxies for isolated galaxies and galaxies in compact groups from Martinez (2008). Fractions given with respect to the total number of classified galaxies (AMIGA sample) or emission line galaxies.

Sample	AMIGA		HCG		UZC-CG[1]	
	N[2]	frac[3]	N[2]	frac[3]	N[2]	frac[3]
Classified or emission[4]:	210	100.0	168	100.0	274	100.0
SFN	126	60.0	54	32.1	83	30.3
TO	35	16.7	36	21.4	50	18.2
AGN:	49	23.3	78	46.4	141	51.5
NLAGN total:	44	21.0	76	45.2	133	48.5
LINER	20	9.5	35	20.8	11	4.0
Sy2	10	4.8	24	14.3	43	15.7
unclassified NLAGN (LLAGN)	14	6.7	17	10.1	79	28.8
Sy1	5	2.4	2	1.2	8	2.9
TO + AGN:	84	40.0	114	67.9	191	69.7

[1] UZC-CG subsample with spectra from FAST and the SDSS.

[2] Number of galaxies.

[3] Figures given in percentages.

[4] Classified galaxies in the AMIGA sample and galaxies with emission in the compact groups sample.

Table 10.5: Rate of BLAGN over NLAGN in different samples.

Sample	BLAGN/NLAGN[1]	Sy1/Sy2[1]
Martínez et al. (2008) - HGC	2.6%	8.3%
Martínez et al. (2008) - UZC-CG	5.7%	18.6%
AMIGA	**11.4%**	**50.0%**
Ho et al. (1997b)	22.2%	60.8%
Hao et al. (2005)	42.8%	54.3%
Sorrentino et al. (2006)	65.7%	-

[1] Figures given in percentages.

Rate of broad versus narrow line components

The ratio of broad line AGN (BLAGN) and narrow line AGN[2] seems to be very low in highly interacting systems like Hickson Compact Groups (HCG) of galaxies (Martínez et al. 2008) in comparison with other samples. In particular, Martínez et al. (2008) compared the ratio of BLAGN over NLAGN in a sample of HCG galaxies and in a sample of UZC-CG with the ratios found in Hao et al. (2005), Sorrentino et al. (2006) and Ho et al. (1997b) for the Ho et al. (1997a) sample. If we consider the AMIGA sample as a reference of interaction-free galaxies we could estimate the effect of the interaction by comparing the values found by Martínez et al. (2008) and the values found for the AMIGA sample.

We found a value of 11.4% for the ratio of BLAGN over NLAGN. If we consider only Seyfert galaxies the ratio of Seyferts of type 1 over Seyferts of type 2 is 50.0%. In Table 10.5 we show the values obtained by Martínez et al. (2008) compared with the values found for the AMIGA SDSS complete subsample. Hence, we confirm the clear deficiency of BLAGN found in compact groups by Martínez et al. (2008).

[2]We consider TOs separately from NLAGN composed of Seferts 2, LINERs and NLAGN that cannot be clasiffied as Seyferts 2 or LINER which are called in some studies Low Luminosity AGN (LLAGN).

Part V

Conclusions

Chapter 11

Conclusions

This thesis aimed to study the impact of the environment on the galaxy evolution, in particular on the nuclear activity and the ISM For such purpose we have studied the rate of AGN candidates in a well-defined complete sample of isolated galaxies as part of the AMIGA project. We have focused on three methods that make use of the radio (NVSS), FIR (IRAS) and optical (SDSS) data for our galaxy sample, and complemented them with additional data found in the literature.

Our main results for the AMIGA sample are:

- Our sample is mostly radio quiet, with most galaxies (98.6%) having radio powers lower than 10^{23} W Hz^{-1}, consistent with the high ratio of late-type galaxies in our sample.

- We have selected radio-excess candidate galaxies above the radio-FIR correlation for our complete subsample, and revised the results using FIRST and VLA data to exclude back/foreground sources. We find 0% radio-excess galaxies with an excess of a factor 5 and 2.0% for a lower excess of a factor 3.

- Using the IRAS flux ratio $S_{25\mu\mathrm{m}}/S_{60\mu\mathrm{m}}$ to select AGN candidates we find a frequency of AGN candidates of $\backsim$ 28% (number of AGN candidates over the number of classified galaxies) with a lower limit of $\backsim$ 7% (number of AGN candidates over the number of galaxies studied using this method).

- From NED and the Véron-Cetty catalogues, we found $n = 29$ AGN candidates (including LINERs and NLAGN).

- We have studied the SDSS spectra of AMIGA galaxies. We were able to classify more than 92% of the galaxies. In the complete AMIGA subsample 55.8% of the galaxies are classified as SF nuclei, 15.5% as TO, 21.7% as AGN and 7.1% cannot be classified, usually (75% of them) due to the lack of emission lines.

- The rate of AGN showing broad line emission (Seyfert 1) with respect to the total number of AGN is 10.2%.

- With the SDSS spectra we could confirm the success rate of the IRAS flux ratio selection method. The success rate of the method is estimated to be $\approx$ 70%.

- The final catalogue contains a total of 155 AGN candidates among the 1050 AMIGA galaxies. This catalogue is available in electronic form at the AMIGA web page[1].

We have compared our results with those found in the literature and interpreted them, taking into account that our sample was selected using optical criteria and that we used a well-defined criterion of isolation. We conclude that:

- The AMIGA sample has the lowest rate of radio AGN candidates, both globally, as well as considering early-type and late-type galaxies separately and considering different optical luminosity ranges separately.
- Field galaxies as well as galaxies in poor cluster and group environments (e.g., outer parts of clusters) show intermediate values, although the numbers are only illustrative as numerous selection effects affect the conclusions. The outer parts of clusters seem as efficient as field/poor environments to trigger radio emission in AGN.
- The highest rates of radio AGN candidates are found in the central parts of clusters, but also in pair/merger dominated samples.
- For all environments, a higher ratio of radio excess is found for early-type galaxies, as can be expected since massive elliptical galaxies are the usual hosts for powerful radio jets.
- Both elliptical and spiral galaxies increase their radio excess activity for denser environments. This increment supports that the density-morphology relation is not the only explanation for the enhancement in AGN frequency in denser environments, i.e., nuclear activity is not only associated with dense environments due to its higher content in ellipticals, but is directly triggered by it.
- The number of optical AGN found in the AMIGA sample is relatively high in comparison with the number of radio AGN candidates. A detailed study of the rate of optical AGN in terms of environment, morphology and luminosity will be the subject of a further study.

Hence, the environment seems to play a crucial role in the development of radio nuclear activity both at large scales and in strong one-to-one interactions.

Finally, we notice that the AMIGA sample appears to represent the most nurture-free population of luminous galaxies, including early-types, as confirmed by their lack of radio excess above the FIR-radio correlation. The catalogue presented in that work can be used as a baseline for forthcoming studies about the relation between environment and nuclear activity.

[1] http://www.iaa.csic.es/AMIGA.html

Chapter 12

Conclusiones

El objetivo de esta tesis es el estudio del impacto del entorno en la evolución galáctica, en particular en la actividad nuclear y en el medio interestelar. Con este propósito hemos estudiado la tasa de incidencia de actividad nuclear (nucleos activos de galaxias o AGN) en un muestra bien definida de galaxias aisladas como parte del proyecto AMIGA. Hemos usado tres métodos que hacen usos de datos en radiocontinuo (NVSS), infrarrojo lejano (IRAS) y visible (SDSS) para nuestra muestra de galaxias y los hemos complementado con datos de la bibliografía.

Nuestros principales resultados para la muestra AMIGA son:

- Nuestra muestra tiene baja emisión en radiocontinuo, con la mayoria de galaxias (98,6 %) con una potencia por debajo de 10^{23} W Hz^{-1}, resultado consistente con la alta tasa de galaxias espirales en nuestra muestra.

- Hemos seleccionado las galaxias candidatas a tener exceso de radio, por encima de la correlación entre infrarrojo lejano y radiocontinuo, en nuestra muestra completa. Hemos revisado los resultados usando datos de FIRST y del VLA para excluir fuentes de fondo no relacionadas con nuestra galaxia. Encontramos una tasa de galaxias con exceso de radio del 0 % con un exceso de factor 5 y un 2.0 % con un factor 3.

- Usando el cociente $S_{25\mu\mathrm{m}}/S_{60\mu\mathrm{m}}$ entre flujos IRAS para seleccionar candidatos a AGN hemos encontrado una frecuencia de candidatos a AGN de $\backsim$ 28 % (número de candidatos a AGN sobre el número de galaxias clasificadas) con un límite inferior de $\backsim$ 7 % (número de candidatos a AGN sobre el número de galaxias a las que se les aplicó este método).

- Hemos encontrado $n = 29$ candidatos a AGN (incluyendo LINERs y AGN de lineas estrechas) en los catálogos de la NED y de Véron-Cetty.

- Hemos estudiado los espectros del SDSS de las galaxias de la muestra AMIGA. Pudimos clasificar el 92 % de las galaxias. En la muestra completa AMIGA el 55.8 % son clasificadas como núcleos de formación estelar, el 15.5 % como objetos de transición, el 21.7 % como AGN y el 7.1 % no pueden ser clasificadas, en general (75 % de ellas) debido a la ausencia de líneas de emisión.

- La tasa de AGN que muestran líneas de emisión anchas (Seyfert 1), con respecto al total de AGN, alcanza el 10.2 %.

- Con los espectros del SDSS hemos podido confirmar la tasa de acierto del método de selección con flujos de IRAS situándola en $\approx 70\,\%$.
- El catálogo final contiene un total de 155 candidatos a AGN entre las 1050 galaxias de la muestra AMIGA. Este catálogo está disponible en forma electrónica en la página web de AMIGA[1].

Hemos comparado nuestros resultados con los encontrados en la literatura y los hemos interpretado teniendo en cuenta que nuestra muestra fue elegida siguiendo criterios de selección en el visible y que usamos un criterio bueno de aislamiento. Concluimos que:

- La muestra AMIGA tiene la tasa más baja de candidatos a AGN tipo radio, tanto globalmente, como considerando las galaxias de tipo temprano y tardío de forma separada y también considerando distintos rangos de luminosidades por separado.
- Tanto las galaxias "de campo" como las que pertenecen a cúmulos pobres y a grupos (por ejemplo, en la parte exterior de los cúmulos) muestran valores intermedios en la tasa de candidatos a AGN tipo radio. Hay que tener en cuenta que estos valores son orientativos pues las conclusiones pueden verse afectadas por varios efectos de selección. Las partes externas de los cúmulos son igual de eficientes en producir AGN radio como los entornos de campo o de grupos.
- Las tasas más altas de candidatos a AGN tipo radio se da en las partes centrales de los cúmulos y en las muestras dominadas por pares o galaxias en interacción fuerte.
- En todos los entornos se encuentra una tasa mayor en las galaxias de tipo temprano tal y como cabría esperar ya que las galaxias masivas elípticas son los huéspedes habituales de chorros potentes de radio.
- Tanto las galaxias elípticas como las espirales incrementan su tas de actividad cuando nos acercamos a entornos más densos. Este incremento apoya que la relación densidad-morfología no es la única explicación para este aumento. Esto indica que la actividad nuclear tipo radio en entornos densos, no solo viene producida por la alta tasa de galaxias elípticas que se encuentran en estos entornos, sino por el entorno en si mismo.
- El número de AGN seleccionados en el visible que se encuentran para la muestra AMIGA es relativamente alto en comparación con el número que se encuentra de AGN de tipo radio. En el futuro se realizará un estudio detallado de la fracción de AGN en óptico en función del entorno, morfología y luminosidad.

Por lo tanto, el entorno juega un papel fundamental para que una galaxia desarrolle un AGN tipo radio, tanto el entorno a gran escala como las interacciones fuertes entre galaxias individuales.

La muestra AMIGA contiene la población más numerosa de galaxias luminosas, incluso de tipo temprano, libres de interacción como viene confirmado por la ausencia de ninguna de estas galaxias por encima de la correlación infrarrojo lejano-radiocontinuo presentando exceso de radio. El catálogo que presentamos en este trabajo puede ser usado como una linea de base para futuros estudios sobre la relación entre el entorno y la actividad nuclear.

[1] http://www.iaa.csic.es/AMIGA.html

Acknowledgements

We would like to warmly thank everybody who provided data for this study.

José Sabater was partially supported by DGI Grants AYA 2002-03338; AYA 2005-07516-C02-01; Junta de Andalucía (Spain) and by a fellowship from the Secretaría de Estado de Educación y Universidades.

This research has made use of the NASA/IPAC Extragalactic Database (NED) which is operated by the Jet Propulsion Laboratory, California Institute of Technology, under contract with the National Aeronautics and Space Administration.

Funding for the SDSS and SDSS-II has been provided by the Alfred P. Sloan Foundation, the Participating Institutions, the National Science Foundation, the U.S. Department of Energy, the National Aeronautics and Space Administration, the Japanese Monbukagakusho, the Max Planck Society, and the Higher Education Funding Council for England. The SDSS Web Site is http://www.sdss.org/.

The SDSS is managed by the Astrophysical Research Consortium for the Participating Institutions. The Participating Institutions are the American Museum of Natural History, Astrophysical Institute Potsdam, University of Basel, University of Cambridge, Case Western Reserve University, University of Chicago, Drexel University, Fermilab, the Institute for Advanced Study, the Japan Participation Group, Johns Hopkins University, the Joint Institute for Nuclear Astrophysics, the Kavli Institute for Particle Astrophysics and Cosmology, the Korean Scientist Group, the Chinese Academy of Sciences (LAMOST), Los Alamos National Laboratory, the Max-Planck-Institute for Astronomy (MPIA), the Max-Planck-Institute for Astrophysics (MPA), New Mexico State University, Ohio State University, University of Pittsburgh, University of Portsmouth, Princeton University, the United States Naval Observatory, and the University of Washington.

We acknowledge the usage of the HyperLeda database (http://leda.univ-lyon1.fr)

Part VI

Appendices

Appendix A

Survival and bivariate analysis

A.1. Survival analysis

Survival analysis is a branch of statistics which deals with the survival probability for biological organisms. It has been usually used in medical studies to obtain information from statistical studies where the modelling of time events (like death) is fundamental. Survival studies usually have to deal with *censored data* (when the value of an observation is only partially known). E.g., if some individual disenrolled from a study about the effect of a medicament in survival probability it is only possible to know that this indivudual survived at least until the time he/she disenrrolled the study. In this case the information that we can obtain is a lower limit of the studied variable. It is possible to apply the techniques of survival analysis to astronomical data in the case where there are only upper limits to the measurement of a flux or luminosity.

Feigelson & Nelson (1985) present the univariate nonparametric survival analysis estimators and their application to astrophysics. A widely used distribution is the Kaplan-Meier. The Kaplan-Meier is an statistical distribution that can take into account censored data in the form of lower limits.

The Kaplan-Meier statistics for a typical study of survival probabilities is the following. In a sample of N individuals in a population, $S(t)$ is the probability for an element of a given population of surviving more time than t. Let the times until death of one or several individuals from the sample be

$$t_1 \leq t_2 \leq t_3 \leq \cdots \leq t_M.$$

. M is equal or lower than N if some individuals die at the same time. We define n_i as the number of individuals "at risk" before each time t_i and d_i is defined as the number of deaths at t_i. We have to take into account that some of the individuals can be "lost" (censored data), e.g., if any of the individuals retires itself from the study. The Kaplan-Meier estimator is the nonparametric maximum likelihood estimate of $S(t)$ defined as:

$$\hat{S}(t) = \prod_{t_i<t} \frac{n_i - d_i}{n_i}$$

When there is no censoring, n_i is just the number of survivors just prior to time t_i. With censoring, n_i is the number of survivors less the number of losses (censored cases). [1] For astronomical studies the distribution can be modified to take into account upper limits as explained in Feigelson & Nelson (1985).

[1] More references at: http://en.wikipedia.org/wiki/Kaplan-Meier_estimator

A.2. Bivariate analysis

Here we disscuss the use of different types of regression fits to bivariate data. Different linear regression methods can lead to different fits to the same dataset. Isobe et al. (1990) studied the different types of regressions and their use in astronomy. In the case of a linear regression different results can arise from the consideration of different ways to measure the distance to minimize between the data and the fit. The selection of the best type of regression depends on the nature of the variables and the purpose of the linear regression. Isobe et al. (1990) studied five kind of fits:

- OLS(Y|X): Ordinary least squares regresion of Y on X. Minimazation of the y-axis distances.
- OLS(X|Y): Ordinary least squares regresion of X on Y. Minimazation of the x-axis distances.
- OLS(bisector): Line that bisects OLS(Y|X) line and OLS(X|Y) line.
- Orthogonal regression: line minimizing the perpendicular distance between the fitting line and the data points.
- "Reduced major-axis" regression: geometric mean of the slopes of OLS(Y|X) and OLS(X|Y).

The regression type must be chosen depending on the scientific question that has to be answered. If we want to use the regression to predict values the existence of a independent and a dependent variable is not a problem but if we want to model a physical law the regression should treat both variables simetrically. In the last case we should choose between an OLS(bisector), an Orthogonal regression or a "Reduced major-axis" regression. In the first case OLS(Y|X) is appropriate if we want to give a prediction of Y given a value of X. In the literature it is usual to find OLS(Y|X) as the standard way to derive regression fits but it is also possible to find OLS(bisector). Isobe et al. (1990) recomend the use of OLS(bisector) when the goal of the study is to determine the underlying functional relation between the two variables.

These regressions are appropriate for problems where the intrinsic scater of the data dominates any error in the measurement of the data points. Feigelson & Babu (1992) studied the methods to take into account the errors in the measurements of the data points. Akritas & Bershady (1996) proposed two regression methods to take into account both the scater and the measurement error of the data. Kelly (2007) developed a Bayesian method to account for measurement errors in linear regression of astronomical data. This method is generalized to incorporate multiple independent variables, nondetections, and selection effects (e.g., Malmquist bias).

We used OLS(bisector) in this thesis to determine the regressions but we also obtained OLS(Y|X) regressions in order to compare with data in the literature that uses this regresssion.

A.3. Survival bivariate analysis

The use of survival analysis methods is needed to take into account the information carried by censored data (upper or lower limits). Isobe et al. (1986) presented statistical techniques to deal with censored bivariate data. Three methods to test the correlation between two variables were studied: the Cox hazars model, generalized

Kendall's tau and Spearsman's rho. Three linear regressions to estimate the fundamental relations between varaibles were also presented: the estimation-maximization method, the Buckley-James method and the Schmitt's binning method. Akritas & Siebert (1996) developed a test for partial correlation in the presence of censored data.

The Schmitt's binning method was presented by Schmitt (1985). It is a method to perform a linear regression to a bivariate dataset that could have censored data in any of the variables. The censored data can be both upper and/or lower limits mixed. This method is based in the fit of the data to a grid to apply a two-variable Kaplan-Meier distribution. The data is ordered in a two-dimension grid, them the determined and censored data are used to compute a probability based on the Kaplan-Meier estimator for each of the grid cells. This probability is related to the probability that has a data point of being in one cell. With the two-dimensional distribution of probability it is possible to fit a line to the grid which minimizes the Y-distance between the line and each cell weighted by the probability distribution for each cell. This line is the final computed regression. The errors of the line parametres are computed using a bootstrapping process. A number of datasets, e.g 100, with the same number of points than the original data is constructed. A random array of indexes is constructed for each of these datasets and the Schmitt method is applyed to the dataset defined taking the corresponding indexed data from the original dataset. The new regressions are used to determine the standard deviation for each of the parameters of the regression line.

One important issue for the aplication of the former methods to astronomical data is the following: "The Kaplan-Meier estimator works with any underlying distribution (*e.g*. Gaussian, power law, bimodal), but only if the censoring is *random*. That is, the probability that the measurement of an object is censored can not depend on the value of the censored variable."[2] Hence, it is very important to determine the randomness on the presence of the censored data. For example, the study of the apparent magnitude is not possible because the location of the censored data is determined by a limit in the studied variable thus not being randomly distributed. We took this into account whether we used survival analysis methods.

ASURV is a software package (Lavalley et al. 1992) writen in FORTRAN that implements the statistical survival analysis techniques presented in Feigelson & Nelson (1985), Isobe et al. (1986) and Schmitt (1985). ASURV was written between 1987 and 1992 and can be obtained at `http://astrostatistics.psu.edu/statcodes/asurv`

Although the implementation by ASURV of these methods is pioneering the use of the program is not straightfordward. Some versions of the program are buggy. The program must run in interactive mode, the data input have to be entered in a file (whose name must have less than eight characters), the random number generator needed for the Schmitt's binning method is not implemented in some versions of the program thus making this method unusable, etc. Due to these problems we developed a version of the Schmitt's binning method based in the ASURV routines but rewrited in `FORTRAN` and `python`.

The main routines that distribute the data into the grid, computed the probability and the regression line, were implemented in `FORTRAN`. We developed `python` wrappers to the routines using `f2py`.[3] The bootstrapping process and the computing of the errors were implemented in `python`. The final function is:

[2] ASURV documentation

[3] `http://www.scipy.org/F2py`

`twokm(x,y,z,binx,biny,iteraciones=100,tipo=0)`
were `x` and `y` are the variables; `z` is an indicator of the censoring; `binx` and `biny` are the number of bins in x and y respectively; `iteraciones` is the number of iterations for the bootstrapping and `tipo` is the type of regression, 0 for a OLS(bisector) and 1 for OLS(Y|X). The docstring of the functions is the following:

```
"""
Function to compute the linear regression with the
    Schmitt
method.
Return:
  a,b,sa,sb.- origin intersection, slope,
    origin intersection error, slope error.
Usage:
  twokm(x,y,z,binx,biny,iteraciones=100,tipo=0)
    x.- x values.
    y.- y values.
    z.- censoring value:
       0 - detection (+).
       1 - y is lower limit (a8).
       2 - x is lower limit (a6).
       3 - x and y are lower limits (a9).
       4 - y is lower limit and x is upper limit (a7).
      -1 - y is upper limit (a2).
      -2 - x is upper limit (a4).
      -3 - both are upper limits (a1).
      -4 - y is upper limit and x is lower limit (a3).
    binx.- number of bins in the x axis.
    biny.- number of bins in the y axis.
    iteraciones.- number of iterations for the
      bootstrapping. The number by default is 100.
    tipo.- Regression type:
      0 - slope bisector (default)
      1 - y distance minimization (usually used).
      2 - x distance minimization.
"""
```

We also developed a wraper to the asurv Kaplan-Meier computing methods to run it automately from python overriding the interactive interface. To perform this task we use the module `pexpect`.[4] Eventually we adapted the method and used it from python.

[4] http://pexpect.sourceforge.net/pexpect.html

Appendix B

Additional information

B.1. SDSS

FITS HDU codes

Some of the FITS HDU codes for a SDSS spectrum.

```
SN_G    = 8.04687000000000E+00 / Median S/N ration ig g'
MAG_G   = 1.95412000000000E+01 / Synthetic magnitude in g'
SN_R    = 1.08943000000000E+01 / Median S/N ratio in r'
MAG_R   = 1.92726000000000E+01 / Synthetic magnitude in r'
SN_I    = 8.89338000000000E+00 / Median S/N ratio in i'
MAG_I   = 1.91939000000000E+01 / Synthetic magnitude in i'
MAG     = ' 19.9526 19.4762 19.3762 19.1735 19.2537' / fiber Mags
COEFF0  = 3.57920000000000E+00 / Center wavelength (log10) of first pi
COEFF1  = 1.00000000000000E-04 / Log10 dispersion per pixel
VEL_DIS = -9.9990000000000E+03 / Velocity dispersion (km/s)
VEL_DISE= -9.9990000000000E+03 / Error on Velocity Dispersion (km/s)
Z       = -3.7987600000000E-05 / Final redshift
Z_ERR   = 3.97400000000000E-04 / Redshift error
Z_CONF  = 5.68167000000000E-01 / Redshift confidence
```

Error codes for the error mask

Error codes for the error mask contained in the FITS files of the SDSS spectra.

```
SP_MASK_OK           =  0x000,
SP_MASK_NOPLUG       =  0x001,      /*  Fiber not listed in plugmap file                    */
SP_MASK_BADTRACE     =  0x002,      /*  Bad trace from routine TRACE320CRUDE                */
SP_MASK_BADFLAT      =  0x004,      /*  Low counts in fiberflat                             */
SP_MASK_BADARC       =  0x008,      /*  Bad arc solution                                    */
SP_MASK_MANYBADCOL   =  0x010,      /*  More than 10% pixels are bad columns                */
SP_MASK_MANYREJECT   =  0x020,      /*  More than 10% pixels are rejected in extraction     */
SP_MASK_LARGESHIFT   =  0x040,      /*  Large spatial shift between flat and object position */
SP_MASK_NEARBADPIX   =  0x10000,    /*  Bad pixel within 3 pixels of trace                  */
SP_MASK_LOWFLAT      =  0x20000,    /*  Flat field less than 0.5                            */
SP_MASK_FULLREJECT   =  0x40000,    /*  Pixel fully rejected in extraction                  */
SP_MASK_PARTIALREJ   =  0x80000,    /*  Some pixels rejected in extraction                  */
SP_MASK_SCATLIGHT    =  0x100000,   /*  Scattered light significant                         */
SP_MASK_CROSSTALK    =  0x200000,   /*  Cross-talk significant                              */
SP_MASK_NOSKY        =  0x400000,   /*  Sky level unknown at this wavelength                */
SP_MASK_BRIGHTSKY    =  0x800000,   /*  Sky level > flux + 10*(flux error)                  */
SP_MASK_NODATA       =  0x1000000,  /*  No data available in combine B-spline               */
SP_MASK_COMBINEREJ   =  0x2000000,  /*  Rejected in combine B-spline                        */
SP_MASK_BADFLUXFACTOR=  0x4000000,  /*  Low flux-calibration or flux-correction factor      */
SP_MASK_BADSKYCHI    =  0x8000000,  /*  Chi^2 > 4 in sky residuals at this wavelength       */
SP_MASK_REDMONSTER   =  0x10000000, /*  Contiguous region of bad chi^2 in sky residuals     */
SP_MASK_EMLINE       =  0x40000000  /*  Emission line detected here                        */
```

Appendix C

VLA data

Appendix with data and extended information of the VLA observations.

C.1. VLA observing sessions

The data were observed in three different periods. The first correspond to the observing proposal AL649 (Tables C.1,C.2,C.3,C.4,C.5,C.6,C.7,C.8 and C.9), the second to the observing proposal AM869 (Table C.10) and the third to the proposal AS919 (Table C.11). With the first proposal we observed the bulk of the sample of radio-excess and control galaxies. With the second and third proposal we observed 4 more galaxies that could not be observed in the previus one. The only radio-excess galaxy that we could not observe was CIG 877.

The data of one session was lost due to a failure of the crosscorrelator. Fortunately all the galaxies of this session belonged to the control sample.

Table C.1: Observing session AL649 - 60176; 28/03/2005 and 29/03/2005

Source	Type	Comment
0137+331	Flux calib.	
0111+391	Phase calib.	
CIG41	Target	
0111+391	Phase calib.	
0149+059	Phase calib.	
CIG57	Target	
0149+059	Phase calib.	
CIG72	Target	
0149+059	Phase calib.	
0237+288	Phase calib.	
CIG97	Target	
0237+288	Phase calib.	
0339-017	Phase calib.	
CIG129	Target	
0339-017	Phase calib.	
0503+020	Phase calib.	
CIG156	Target	
0503+020	Phase calib.	
0713+438	Phase calib.	
CIG187	Target	
0713+438	Phase calib.	

Table C.2: Observing session AL649 - 60178 - 31/03/2005

Source	Type	Comment
1719+177	Phase calib.	Not obs.
CIG771	Target	One phase calib.
1719+177	Phase calib.	
2123+055	Phase calib.	
CIG893	Target	
2123+055	Phase calib.	
2241+098	Phase calib.	
CIG999	Target	
2241+098	Phase calib.	
0022+061	Phase calib.	
CIG1045	Target	
0022+061	Phase calib.	
0137+331	Flux calib.	
1642+689	Phase calib.	
CIG692	Target	One phase calib.
1642+689	Phase calib.	Not obs.

Table C.3: Observing session AL649 - 60179 - 01/04/2005

Source	Type	Comment
0137+331	Flux calib.	
0842+185	Phase calib.	
CIG248	Target	
0842+185	Phase calib.	
CIG287	Target	
0842+185	Phase calib.	
1122+180	Phase calib.	
CIG480	Target	
1122+180	Phase calib.	
1150-003	Phase calib.	
CIG510	Target	
1150-003	Phase calib.	
1642+689	Phase calib.	
CIG692	Target	
1642+689	Phase calib.	

Table C.4: Observing session AL649 - 60214 - 05/05/2005

Source	Type	Comment
0137+331	Flux calib.	
2212+239	Phase calib.	
CIG963	Target	
2212+239	Phase calib.	
2241+098	Phase calib.	
CIG999	Target	
2241+098	Phase calib.	

Table C.5: Observing session AL649 - 60221 - 13/05/2005

Source	Type	Comment
0137+331	Flux calib.	
1719+177	Phase calib.	
CIG771	Target	
1719+177	Phase calib.	
1624+576	Phase calib.	
CIG734	Target	
1624+576	Phase calib.	

Table C.6: Observing session AL649 - 60229 - 20/05/2005

Source	Type	Comment
0137+331	Flux calib.	
2253+331	Phase calib.	
CIG1004	Target	
2253+331	Phase calib.	
0022+061	Phase calib.	
CIG1045	Target	
0022+061	Phase calib.	

Table C.7: Observing session AL649 - 60232 - 23/05/2005

Source	Type	Comment
0137+331	Flux calib.	
0151+277	Phase calib.	
CIG69	Target	
0151+277	Phase calib.	
0750+482	Phase calib.	
CIG204	Target	
0750+482	Phase calib.	

Table C.8: Observing session AL649 - 60237 - 28/05/2005

Source	Type	Comment
0137+331	Flux calib.	
0152+221	Phase calib.	
CIG80	Target	
0152+221	Phase calib.	
0237+288	Phase calib.	
CIG116	Target	
0237+288	Phase calib.	
0854+201	Phase calib.	
CIG312	Target	
0854+201	Phase calib.	
0909+103	Phase calib.	
CIG309	Target	
0909+103	Phase calib.	
CIG359	Target	
0909+103	Phase calib.	

Table C.9: Observing session AL649 - 60239 - 30/05/2005

Source	Type	Comment
0137+331	Flux calib.	
0040+017	Phase calib.	
CIG33	Target	
0040+017	Phase calib.	
1642+689	Phase calib.	
CIG692	Target	
1642+689	Phase calib.	

Table C.10: Observing session AM869 - 17/07/2006

Source	Type	Comment
1048+717	Phase calib.	Not obs.
CIG488	Target	
1048+717	Phase calib.	
1335+587	Phase calib.	
CIG571	Target	
1335+587	Phase calib.	
1331+205	Flux calib.	

Table C.11: Observing session AS919 – /11/2007

Source	Type	Comment
0137+331	Flux calib.	
1327+221	Phase calib.	
CIG591	Target	
1327+221	Phase calib.	
1800+388	Phase calib.	
CIG836	Target	
1800+388	Phase calib.	

C.2. VLA data

CIG 33

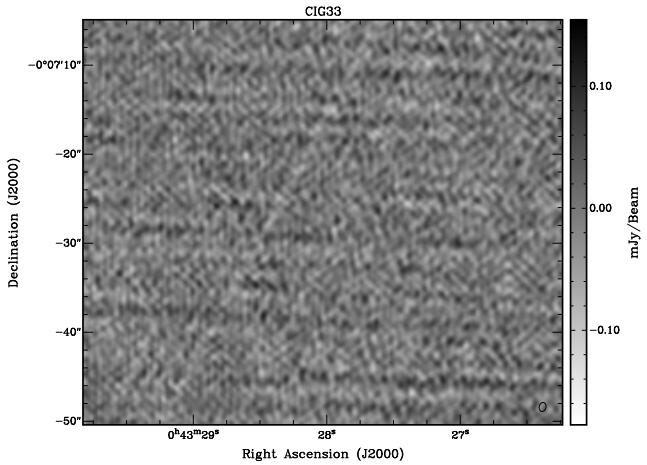

Galaxy name:		CIG 33
α (2000):	hh:mm:ss	00:43:27.81
δ (2000):	dd:mm:ss	−00:07:26.9
Type		Control
Complete		Yes
Radio-excess		1.4

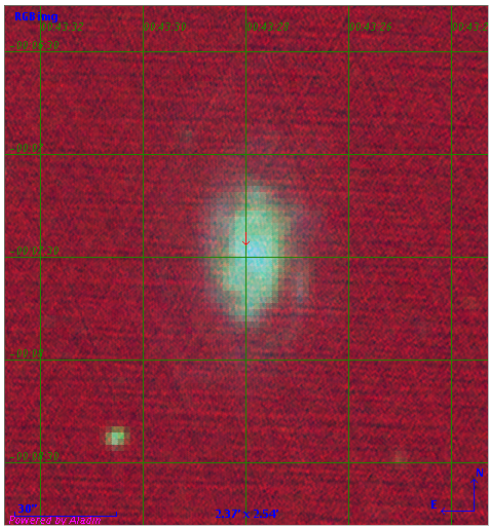

Source name:		-
α (2000):	hh:mm:ss	-
δ (2000):	dd:mm:ss	-
Distance	($''$)	-
RMS	(μJy)	28
Intensity	(μJy)	-

Determination: **NO**
Comments: Source not detected

CIG 41

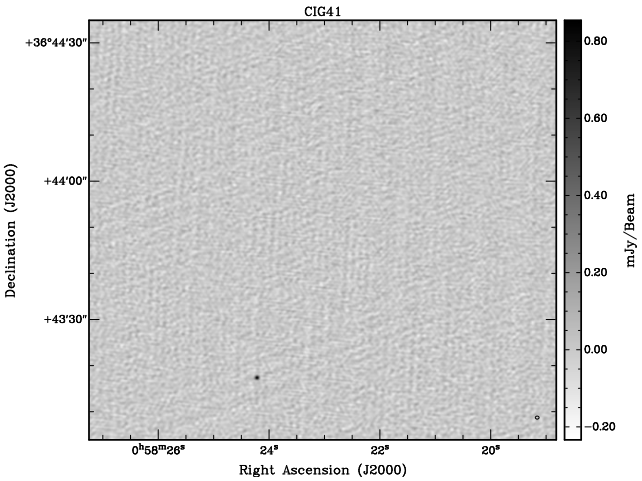

Galaxy name:		CIG 41
α (2000):	hh:mm:ss	00:58:23.36
δ (2000):	dd:mm:ss	36:43:50.2
Type		Factor 5
Complete		Yes
Radio-excess		5.7

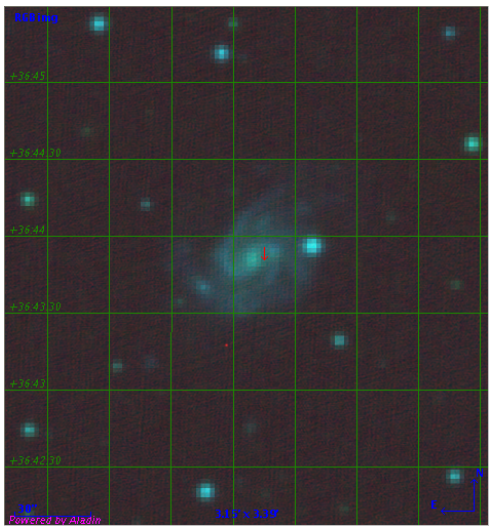

Source name:		a
α (2000):	hh:mm:ss	00:58:24.20
δ (2000):	dd:mm:ss	36:43:17.4
Distance	($''$)	34.1
RMS	(μJy)	39
Intensity	(μJy)	852

Determination: **OUT**
Comments: -

CIG 57

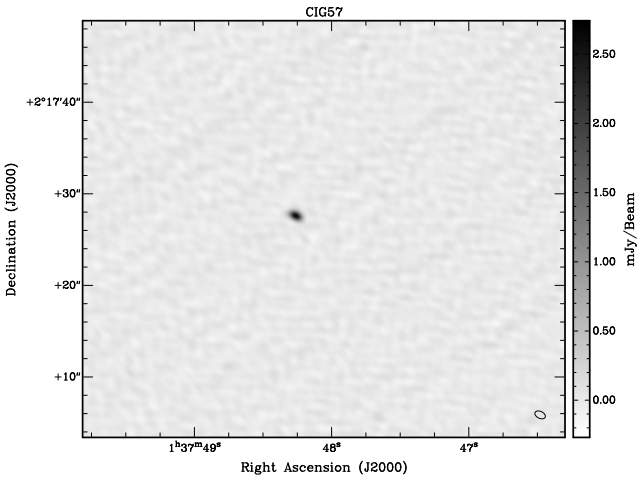

Galaxy name:		CIG 57
α (2000):	hh:mm:ss	01:37:48.25
δ (2000):	dd:mm:ss	02:17:27.3
Type		Factor 5
Complete		No
Radio-excess		5.6

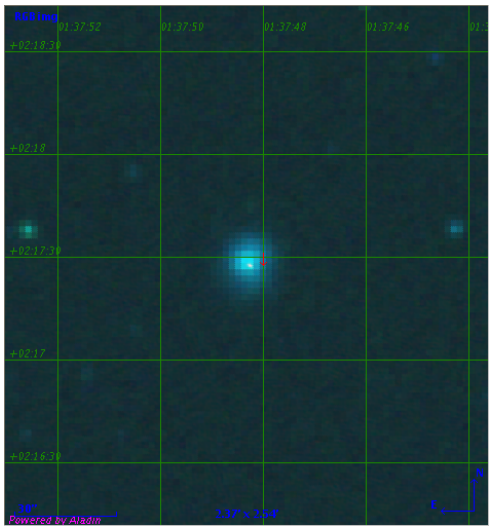

Source name:		a
α (2000):	hh:mm:ss	01:37:48.25
δ (2000):	dd:mm:ss	02:17:27.6
Distance	($''$)	0.6
RMS	(μJy)	44
Intensity	(μJy)	2736

Determination: **DET**
Comments: -

CIG 69

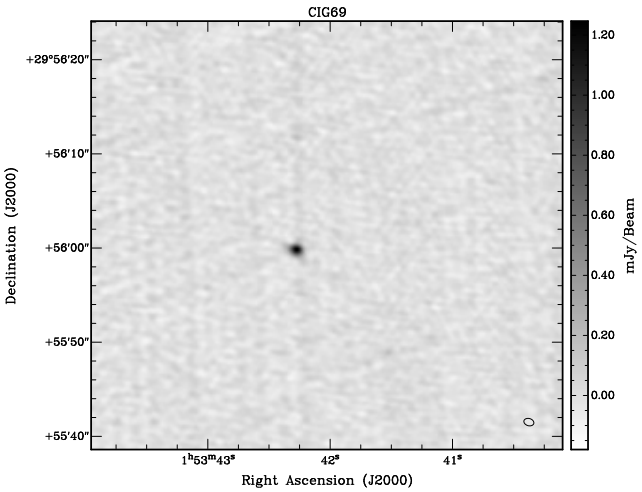

Galaxy name:		CIG 69
α (2000):	hh:mm:ss	01:53:42.23
δ (2000):	dd:mm:ss	29:56:01.5
Type		Control
Complete		Yes
Radio-excess		2.1

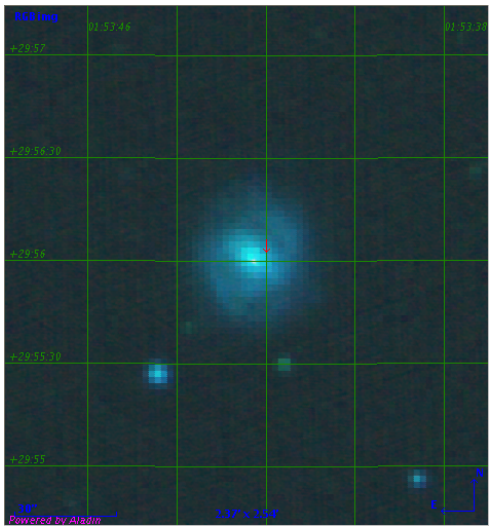

Source name:		a
α (2000):	hh:mm:ss	01:53:42.28
δ (2000):	dd:mm:ss	29:55:60.0
Distance	($''$)	1.2
RMS	(μJy)	33
Intensity	(μJy)	1243

Determination: **DET**
Comments: -

CIG 72

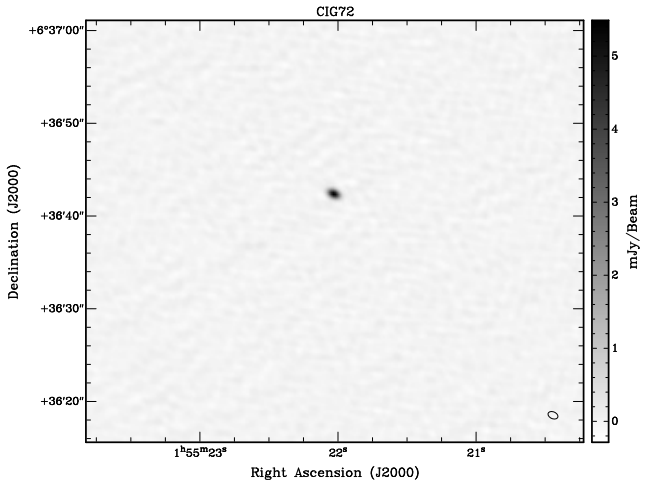

Galaxy name:		CIG 72
α (2000):	hh:mm:ss	01:55:21.91
δ (2000):	dd:mm:ss	06:36:38.7
Type		Factor 3
Complete		Yes
Radio-excess		3.6

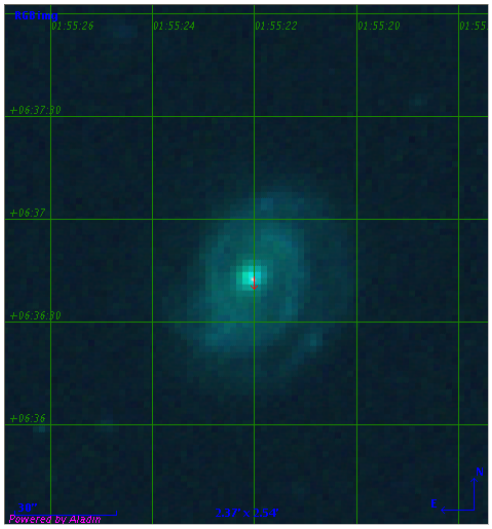

Source name:		a
α (2000):	hh:mm:ss	01:55:22.03
δ (2000):	dd:mm:ss	06:36:42.4
Distance	($''$)	4.8
RMS	(μJy)	51
Intensity	(μJy)	5476

Determination: **DET**
Comments: Possible error in the position of the galaxy. The coordinates of the source look accurate and in the center of the galaxy.

CIG 97

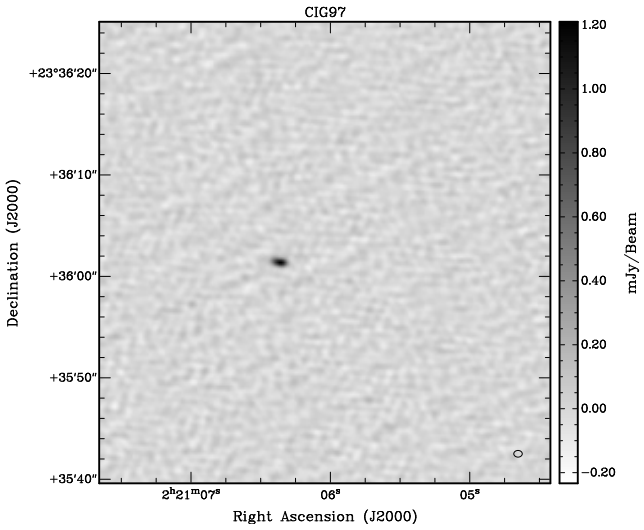

Galaxy name:		CIG 97
α (2000):	hh:mm:ss	02:21:06.41
δ (2000):	dd:mm:ss	23:36:02.7
Type		Factor 3
Complete		Yes
Radio-excess		4.3

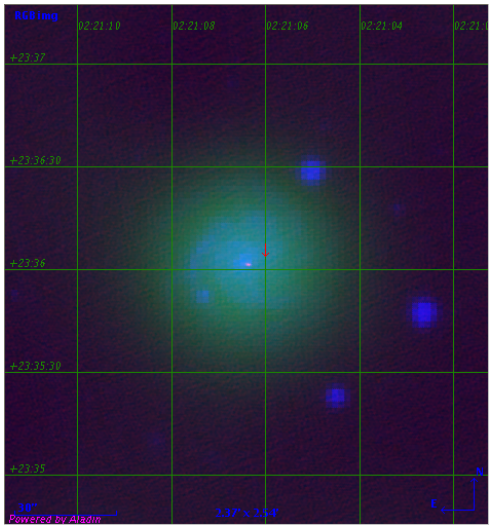

Source name:		a
α (2000):	hh:mm:ss	02:21:06.35
δ (2000):	dd:mm:ss	23:36:02.6
Distance	($''$)	1.0
RMS	(μJy)	40
Intensity	(μJy)	1207

Determination: **DET**
Comments: -

CIG 129

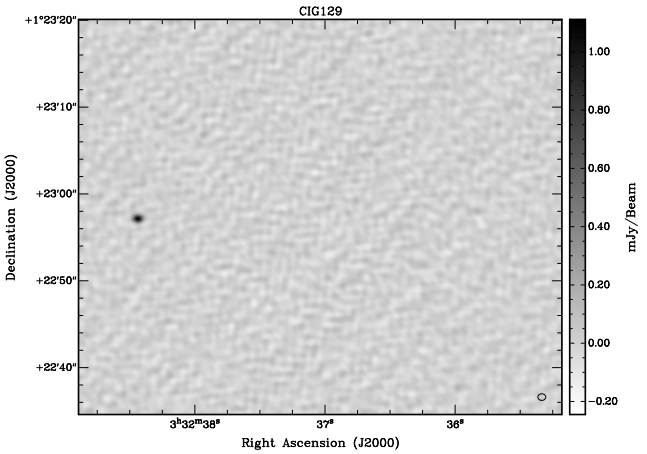

Galaxy name:		CIG 129
α (2000):	hh:mm:ss	03:32:37.43
δ (2000):	dd:mm:ss	01:22:57.8
Type		Control
Complete		Yes
Radio-excess		2.8

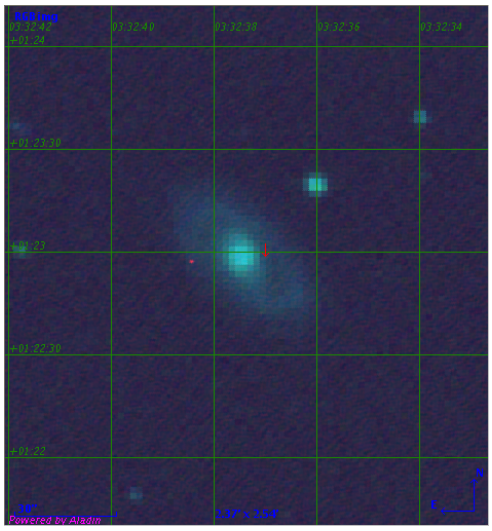

Source name:		a
α (2000):	hh:mm:ss	03:32:38.44
δ (2000):	dd:mm:ss	01:22:57.2
Distance	($''$)	15.2
RMS	(μJy)	41
Intensity	(μJy)	1108

Determination: **OUT**
Comments: -

CIG 156

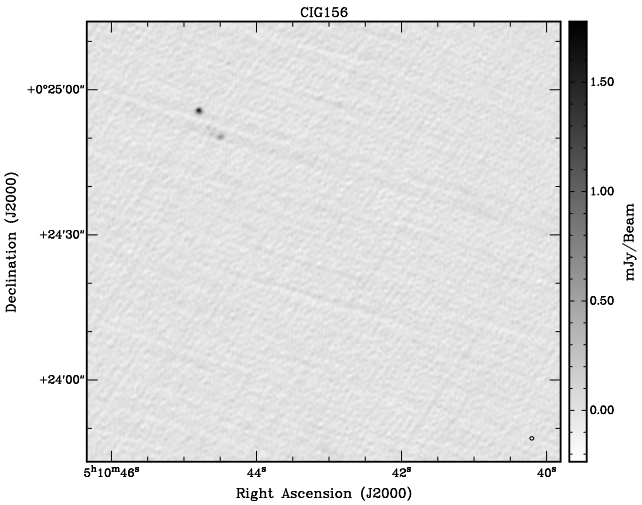

Galaxy name:		CIG 156
α (2000):	hh:mm:ss	05:10:43.01
δ (2000):	dd:mm:ss	00:24:30.1
Type		Factor 5
Complete		Yes
Radio-excess		5.0

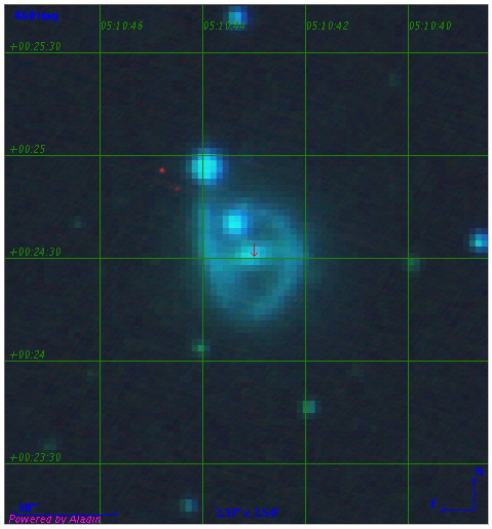

Source name:		a
α (2000):	hh:mm:ss	05:10:44.78
δ (2000):	dd:mm:ss	00:24:55.2
Distance	($''$)	29.5
RMS	(μJy)	42
Intensity	(μJy)	1616
Source name:		b
α (2000):	hh:mm:ss	05:10:44.50
δ (2000):	dd:mm:ss	00:24:49.2
Distance	($''$)	-
RMS	(μJy)	42
Intensity	(μJy)	600

Determination: **OUT**
Comments: -

CIG 187

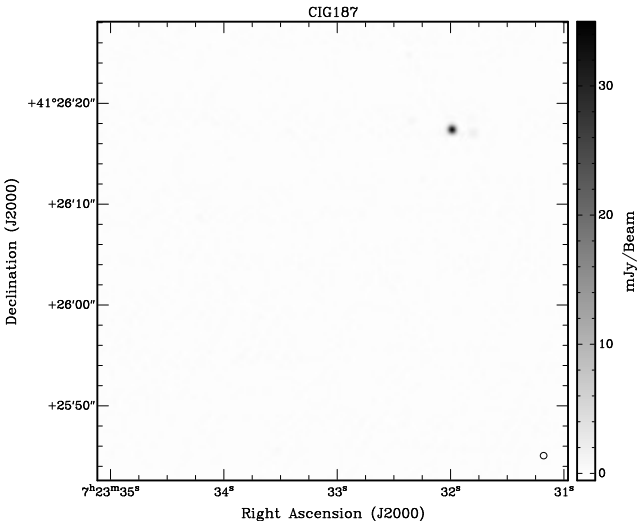

Galaxy name:		CIG 187
α (2000):	hh:mm:ss	07:23:33.16
δ (2000):	dd:mm:ss	41:26:05.6
Type		Factor 5
Complete		Yes
Radio-excess		50.2

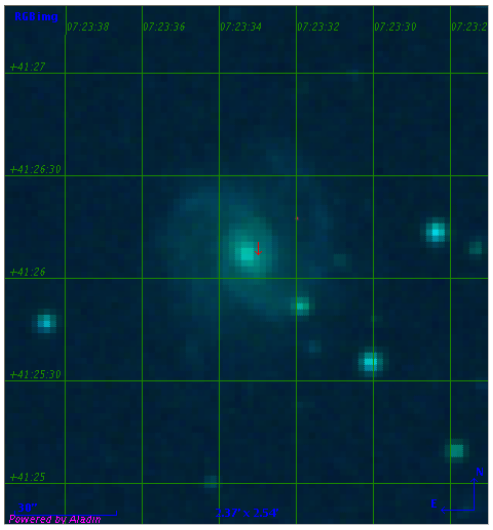

Source name:		a
α (2000):	hh:mm:ss	07:23:31.99
δ (2000):	dd:mm:ss	41:26:17.4
Distance	($''$)	18.1
RMS	(μJy)	66
Intensity	(μJy)	34896
Source name:		b
α (2000):	hh:mm:ss	07:23:31.79
δ (2000):	dd:mm:ss	41:26:17.2
Distance	($''$)	-
RMS	(μJy)	66
Intensity	(μJy)	2003

Determination: **OUT**
Comments: -

CIG 204

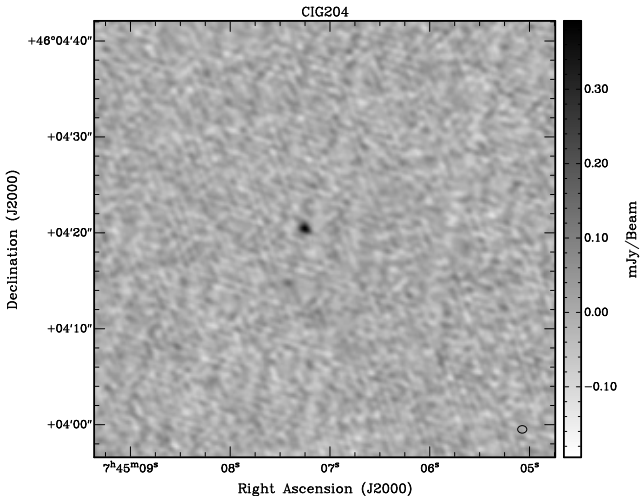

Galaxy name:		CIG 204
α (2000):	hh:mm:ss	07:45:07.10
δ (2000):	dd:mm:ss	46:04:20.1
Type		Control
Complete		Yes
Radio-excess		2.5

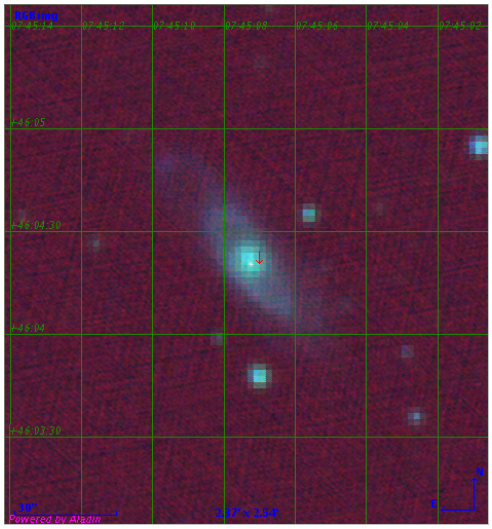

Source name:		a
α (2000):	hh:mm:ss	07:45:07.25
δ (2000):	dd:mm:ss	46:04:22.6
Distance	($''$)	3.0
RMS	(μJy)	32
Intensity	(μJy)	391

Determination: **DET**
Comments: Possible slight error in the position of the galaxy. The coordinates of the source look accurate and in the center of the galaxy.

CIG 248

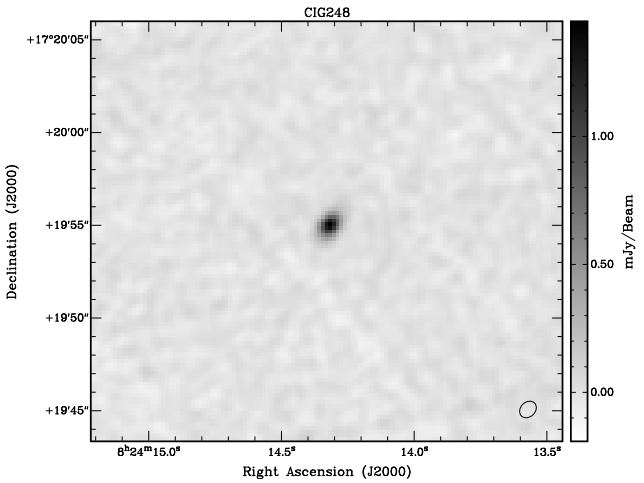

Galaxy name:		CIG 248
α (2000):	hh:mm:ss	08:24:14.31
δ (2000):	dd:mm:ss	17:19:55.5
Type		Factor 3
Complete		Yes
Radio-excess		3.5

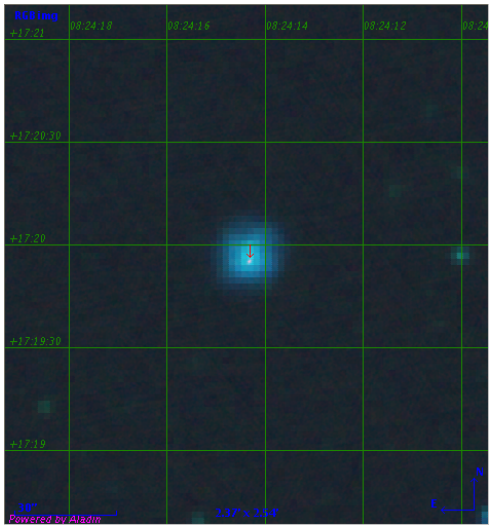

Source name:		
α (2000):	hh:mm:ss	08:24:14.31
δ (2000):	dd:mm:ss	17:19:55.1
Distance	($''$)	0.1
RMS	(μJy)	31
Intensity	(μJy)	1447

Determination: **DET**
Comments: -

CIG 287

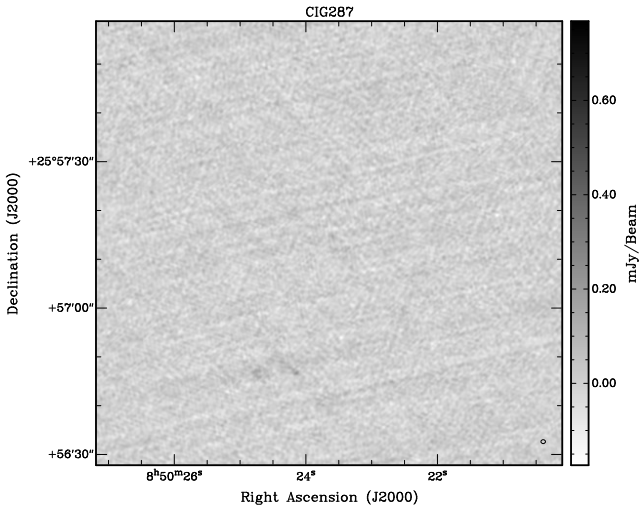

Galaxy name:		CIG 287
α (2000):	hh:mm:ss	08:50:23.58
δ (2000):	dd:mm:ss	25:57:14.5
Type		Factor 5
Complete		Yes
Radio-excess		6.0

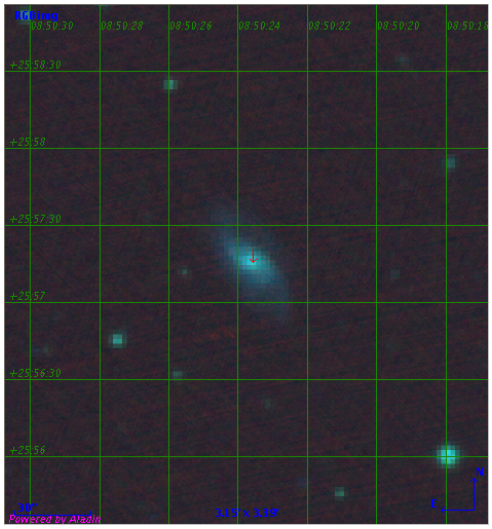

Source name:		a
α (2000):	hh:mm:ss	08:50:24.13
δ (2000):	dd:mm:ss	25:56:46.9
Distance	($''$)	28.1
RMS	(μJy)	32
Intensity	(μJy)	229
Source name:		b
α (2000):	hh:mm:ss	08:50:27.32
δ (2000):	dd:mm:ss	25:59:36.1
Distance	($''$)	-
RMS	(μJy)	32
Intensity	(μJy)	727

Determination: **OUT**
Comments: Low S/N in source a.

CIG 480

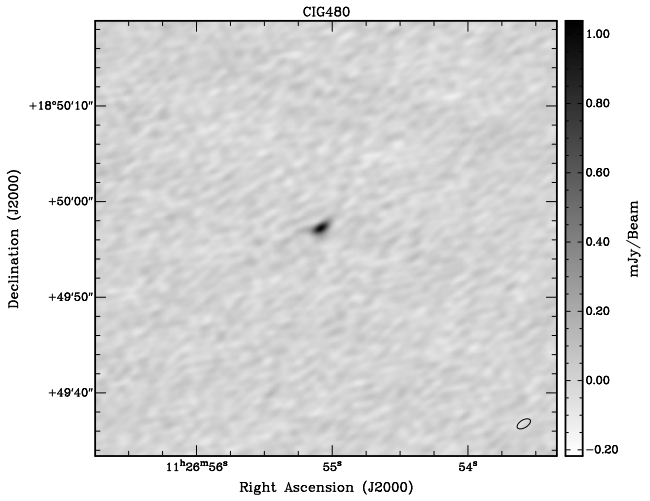

Galaxy name:		CIG 480
α (2000):	hh:mm:ss	11:26:55.09
δ (2000):	dd:mm:ss	18:49:57.0
Type		Factor 3
Complete		Yes
Radio-excess		3.4

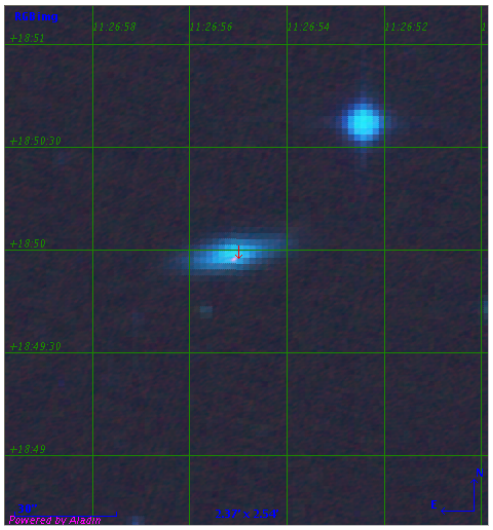

Source name:		a
α (2000):	hh:mm:ss	11:26:55.08
δ (2000):	dd:mm:ss	18:49:57.2
Distance	($''$)	0.3
RMS	(μJy)	32
Intensity	(μJy)	1036

Determination: **DET**
Comments: -

CIG 488

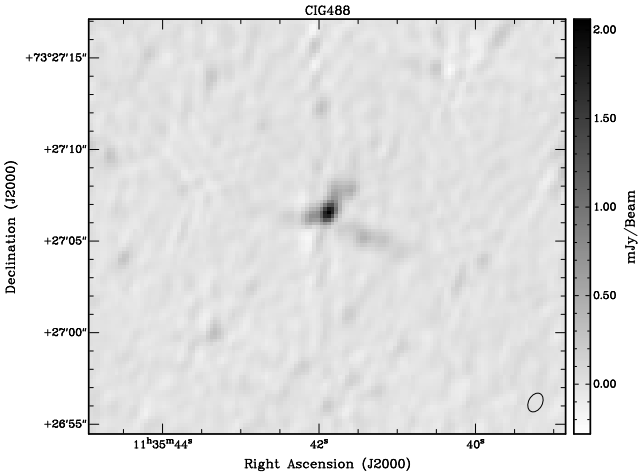

Galaxy name:		CIG 488
α (2000):	hh:mm:ss	11:35:41.36
δ (2000):	dd:mm:ss	73:27:06.7
Type		Factor 3
Complete		Yes
Radio-excess		3.7

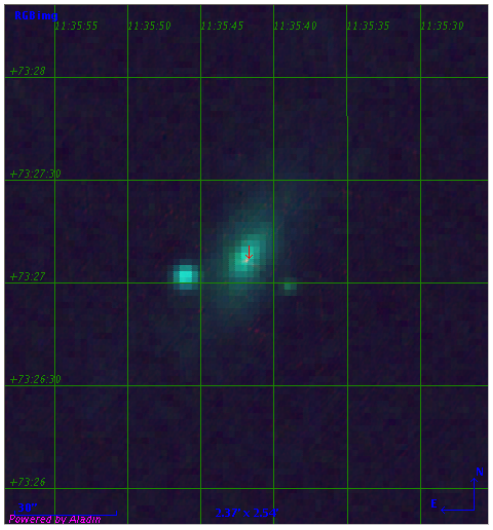

Source name:		a
α (2000):	hh:mm:ss	11:35:41.87
δ (2000):	dd:mm:ss	73:27:06.6
Distance	($''$)	2.3
RMS	(μJy)	64
Intensity	(μJy)	2086

Determination: **DET**
Comments: Possible slight error in the position of the galaxy. The coordinates of the source look accurate and in the center of the galaxy.

CIG 510

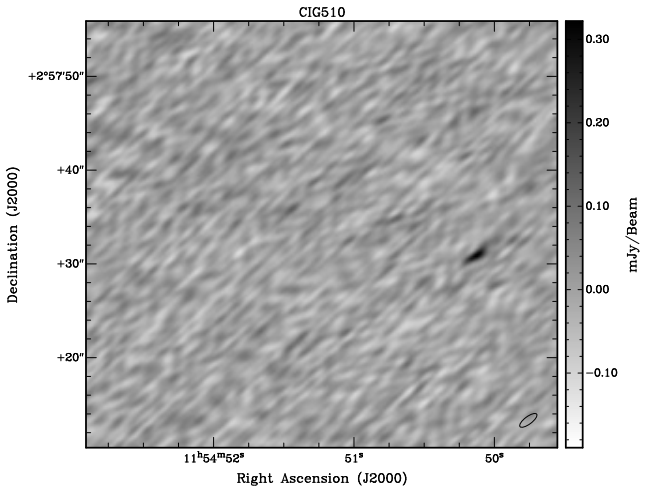

Galaxy name:		CIG 510
α (2000):	hh:mm:ss	11:54:51.20
δ (2000):	dd:mm:ss	02:57:33.8
Type		Factor 3
Complete		No
Radio-excess		3.6

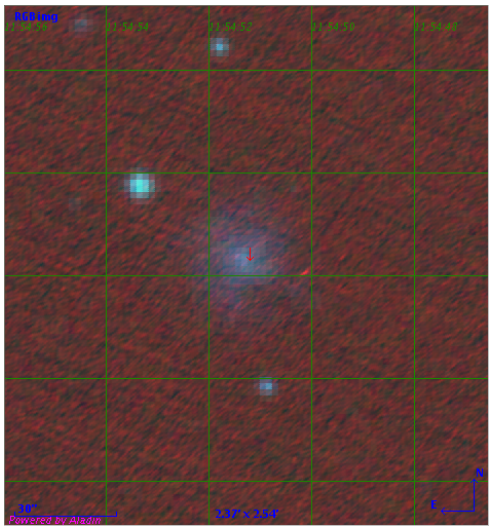

Source name:		a
α (2000):	hh:mm:ss	11:54:50.12
δ (2000):	dd:mm:ss	02:57:31.0
Distance	($''$)	16.3
RMS	(μJy)	34
Intensity	(μJy)	321

Determination: **OUT**
Comments: Low S/N in source a.

CIG 571

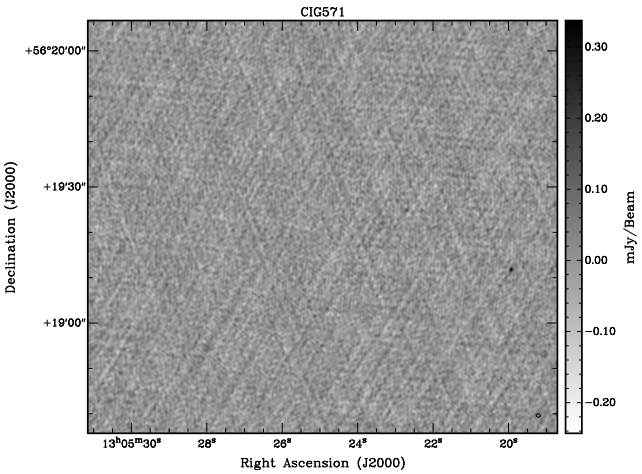

Galaxy name:		CIG 571
α (2000):	hh:mm:ss	13:05:24.69
δ (2000):	dd:mm:ss	56:19:24.7
Type		factor 5
Complete		Yes
Radio-excess		6.9

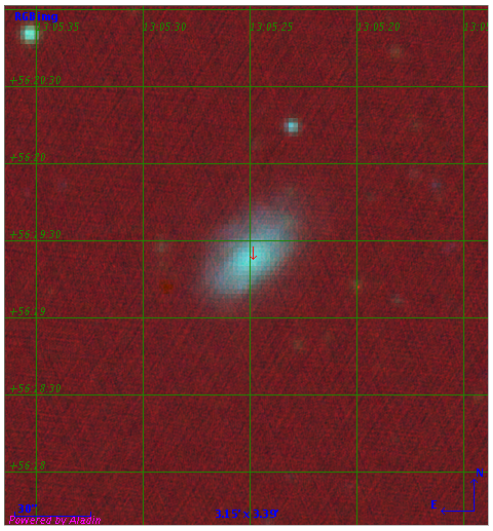

Source name:		a
α (2000):	hh:mm:ss	13:05:19.92
δ (2000):	dd:mm:ss	56:19:12.0
Distance	($''$)	41.5
RMS	(μJy)	33
Intensity	(μJy)	336

Determination: **OUT**
Comments: -

CIG 591

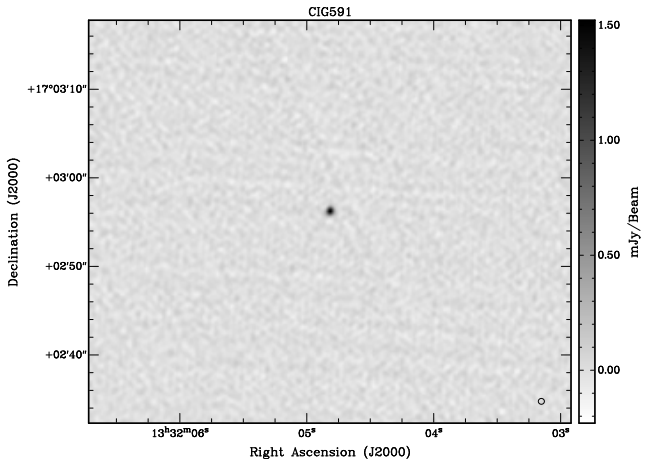

Galaxy name:		CIG 591
α (2000):	hh:mm:ss	13:32:04.78
δ (2000):	dd:mm:ss	17:02:55.7
Type		Factor 3
Complete		Yes
Radio-excess		4.1

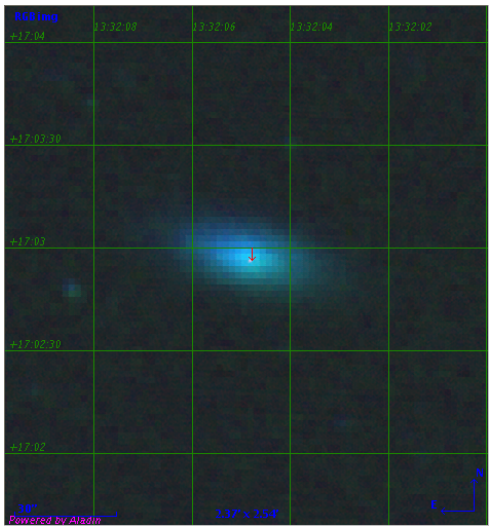

Source name:		a
α (2000):	hh:mm:ss	13:32:04.81
δ (2000):	dd:mm:ss	17:02:56.3
Distance	($''$)	0.7
RMS	(μJy)	36
Intensity	(μJy)	1518

Determination: **DET**
Comments: -

CIG 692

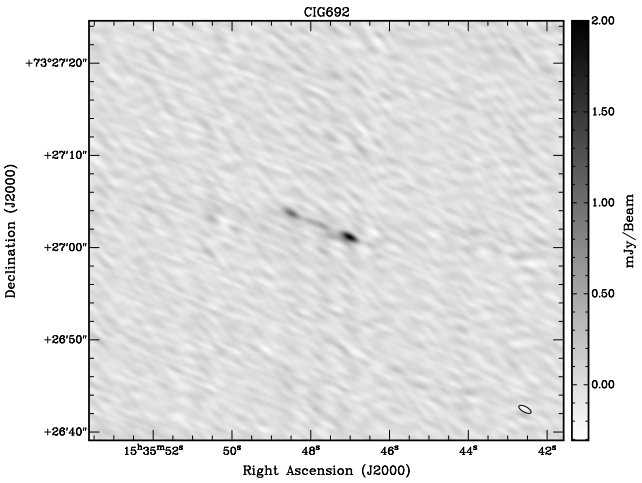

Galaxy name:		CIG 692
α (2000):	hh:mm:ss	15:35:47.50
δ (2000):	dd:mm:ss	73:27:02.5
Type		Factor
Complete		Yes
Radio-excess		4.9

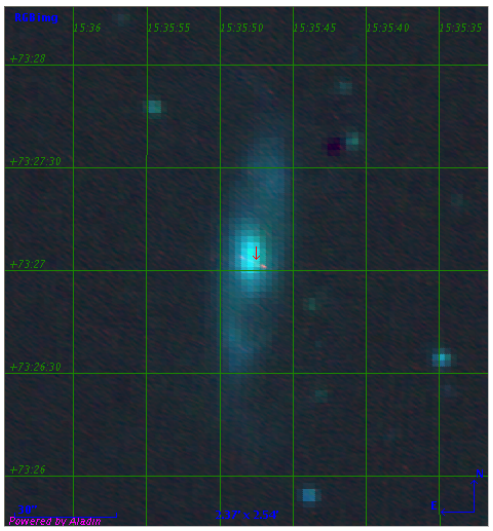

Source name:		a
α (2000):	hh:mm:ss	-
δ (2000):	dd:mm:ss	-
Distance	($''$)	-
RMS	(μJy)	67
Intensity	(μJy)	-
Source name:		b
α (2000):	hh:mm:ss	15:35:46.99
δ (2000):	dd:mm:ss	73:27:01.1
Distance	($''$)	
RMS	(μJy)	67
Intensity	(μJy)	1996
Source name:		c
α (2000):	hh:mm:ss	15:35:48.44
δ (2000):	dd:mm:ss	73:27:03.7
Distance	($''$)	
RMS	(μJy)	67
Intensity	(μJy)	1053

Determination: **DET**
Comments: Two-lobed source.

CIG 692B

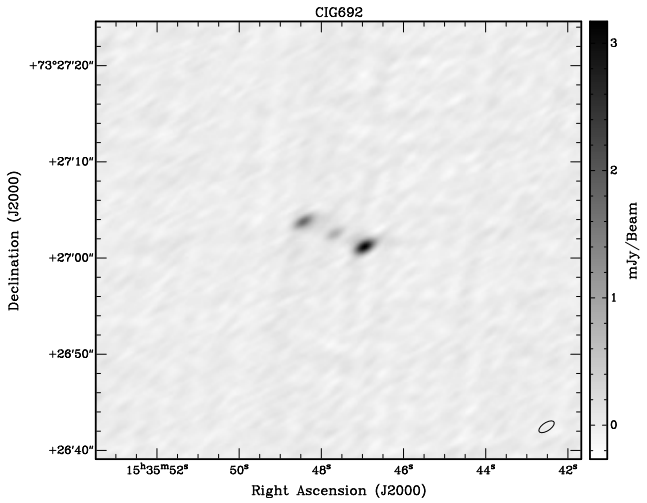

Galaxy name:		CIG 692B
α (2000):	hh:mm:ss	15:35:47.50
δ (2000):	dd:mm:ss	73:27:02.5
Type		Factor
Complete		Yes
Radio-excess		4.9

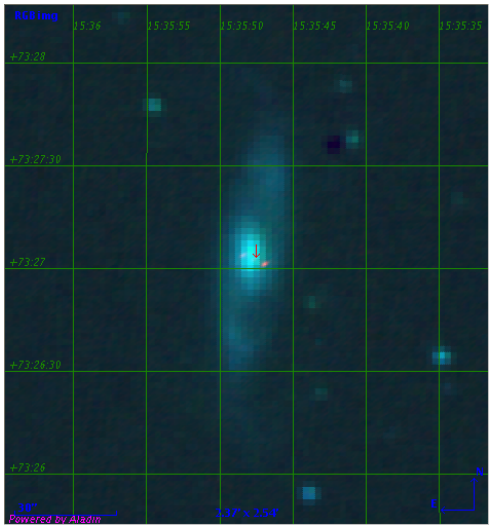

Source name:		a
α (2000):	hh:mm:ss	15:35:47.69
δ (2000):	dd:mm:ss	73:27:02.5
Distance	($''$)	1.0
RMS	(μJy)	48
Intensity	(μJy)	812
Source name:		b
α (2000):	hh:mm:ss	15:35:46.94
δ (2000):	dd:mm:ss	73:27:01.3
Distance	($''$)	-
RMS	(μJy)	48
Intensity	(μJy)	3164
Source name:		c
α (2000):	hh:mm:ss	15:35:48.39
δ (2000):	dd:mm:ss	73:27:03.9
Distance	($''$)	-
RMS	(μJy)	48
Intensity	(μJy)	1744

Determination: **DET**
Comments: Two-lobed source.

CIG 692C

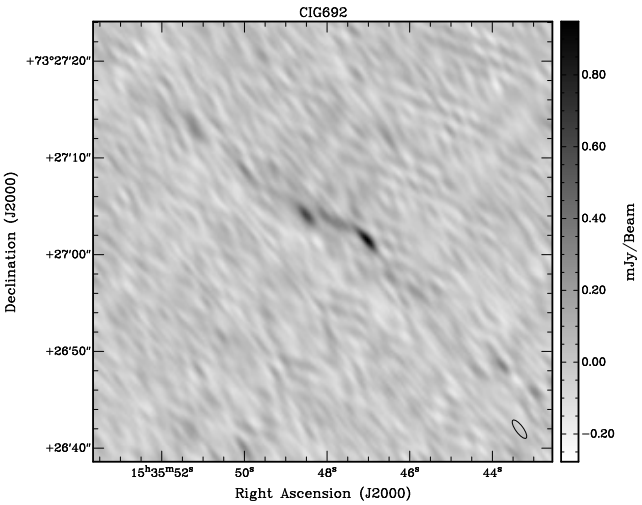

Galaxy name:		CIG 692C
α (2000):	hh:mm:ss	15:35:47.50
δ (2000):	dd:mm:ss	73:27:02.5
Type		Factor
Complete		Yes
Radio-excess		4.9

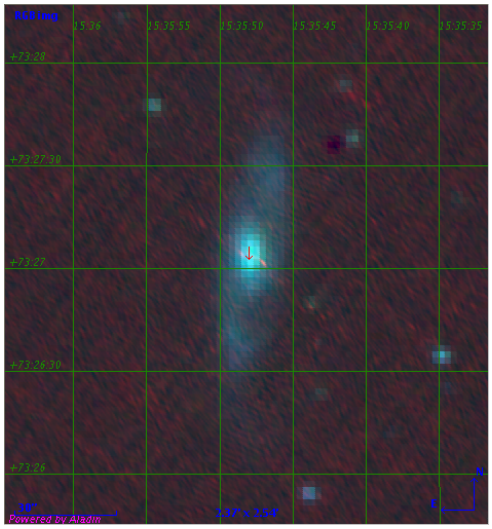

Source name:		a
α (2000):	hh:mm:ss	15:35:48.05
δ (2000):	dd:mm:ss	73:27:04.8
Distance	($''$)	1.0
RMS	(μJy)	55
Intensity	(μJy)	359
Source name:		b
α (2000):	hh:mm:ss	15:35:48.50
δ (2000):	dd:mm:ss	73:27:04.2
Distance	($''$)	-
RMS	(μJy)	55
Intensity	(μJy)	627
Source name:		c
α (2000):	hh:mm:ss	15:35:47.02
δ (2000):	dd:mm:ss	73:27:01.5
Distance	($''$)	-
RMS	(μJy)	55
Intensity	(μJy)	946

Determination: **DET**
Comments: Two-lobed source.

CIG 734

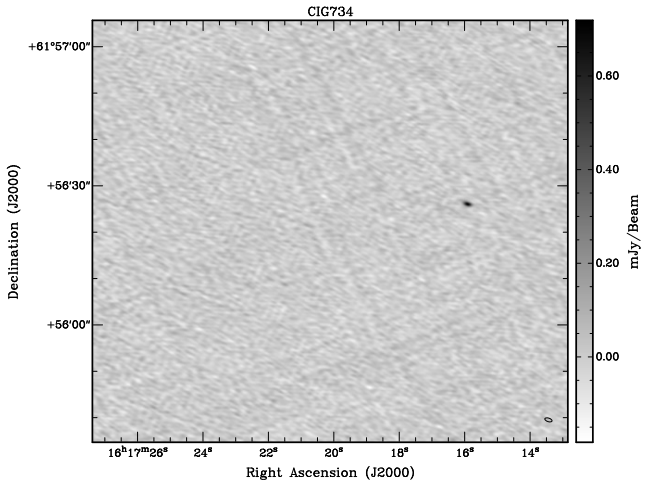

Galaxy name:		CIG 734
α (2000):	hh:mm:ss	16:17:19.61
δ (2000):	dd:mm:ss	61:56:21.1
Type		Factor 3
Complete		Yes
Radio-excess		4.4

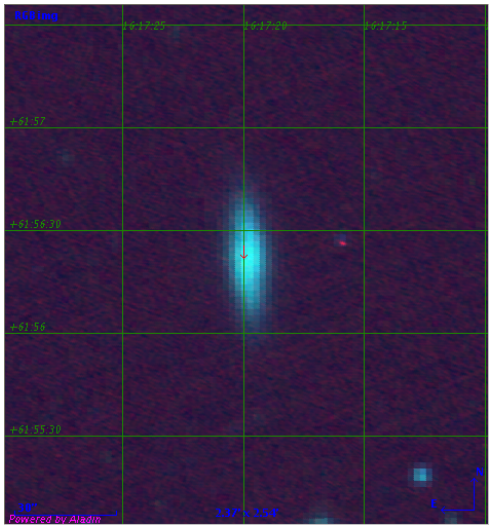

Source name:		a
α (2000):	hh:mm:ss	16:17:15.89
δ (2000):	dd:mm:ss	61:56:26.2
Distance	($''$)	26.7
RMS	(μJy)	32
Intensity	(μJy)	716

Determination: **OUT**
Comments: -

CIG 771

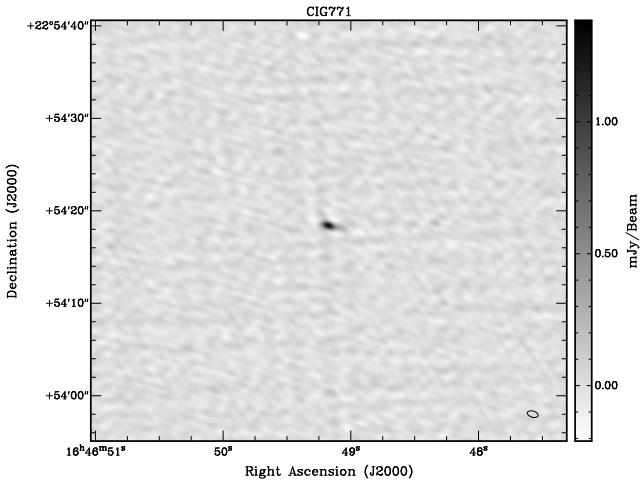

Galaxy name:		CIG 771
α (2000):	hh:mm:ss	16:46:49.14
δ (2000):	dd:mm:ss	22:54:18.5
Type		Control
Complete		No
Radio-excess		2.4

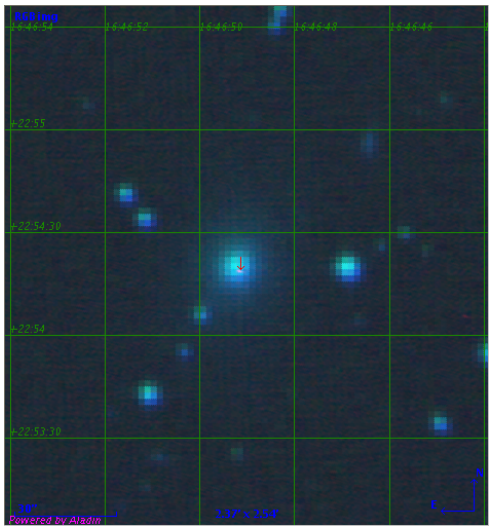

Source name:		a
α (2000):	hh:mm:ss	16:46:49.17
δ (2000):	dd:mm:ss	22:54:18.5
Distance	($''$)	0.7
RMS	(μJy)	43
Intensity	(μJy)	1381

Determination: **DET**
Comments:-

CIG 771B

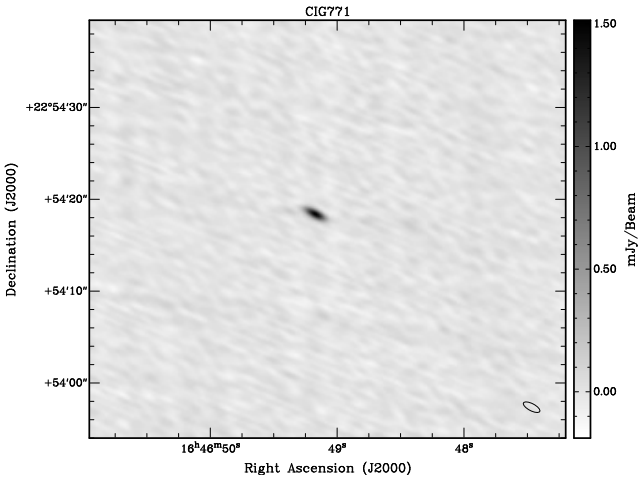

Galaxy name:		CIG 771B
α (2000):	hh:mm:ss	16:46:49.14
δ (2000):	dd:mm:ss	22:54:18.5
Type		Control
Complete		No
Radio-excess		2.4

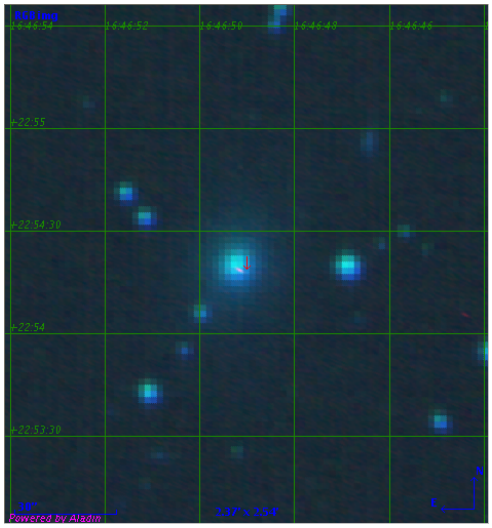

Source name:		a
α (2000):	hh:mm:ss	16:46:49.16
δ (2000):	dd:mm:ss	22:54:18.4
Distance	($''$)	0.7
RMS	(μJy)	32
Intensity	(μJy)	1511

Determination: **DET**
Comments: -

CIG 836

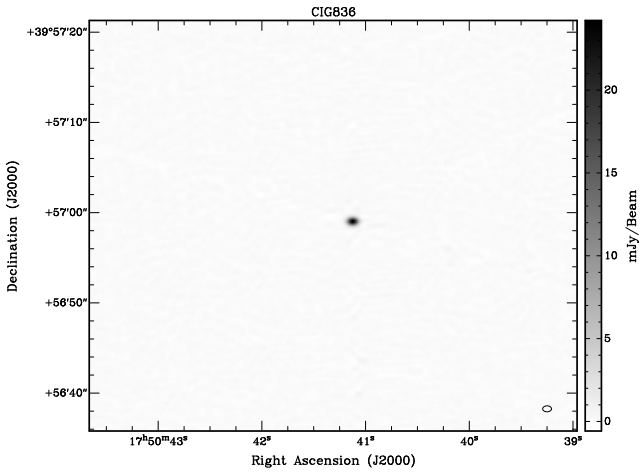

Galaxy name:		CIG 836
α (2000):	hh:mm:ss	17:50:41.23
δ (2000):	dd:mm:ss	39:56:59.8
Type		Factor 5
Complete		No
Radio-excess		29.7

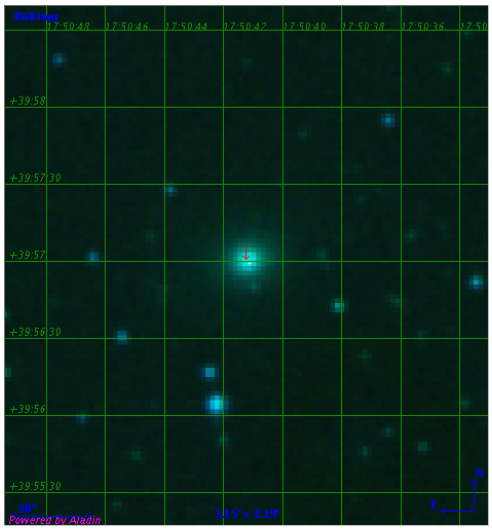

Source name:		a
α (2000):	hh:mm:ss	17:50:41.13
δ (2000):	dd:mm:ss	39:56:59.2
Distance	($''$)	1.3
RMS	(μJy)	76
Intensity	(μJy)	24149

Determination: **DET**
Comments: -

CIG 893

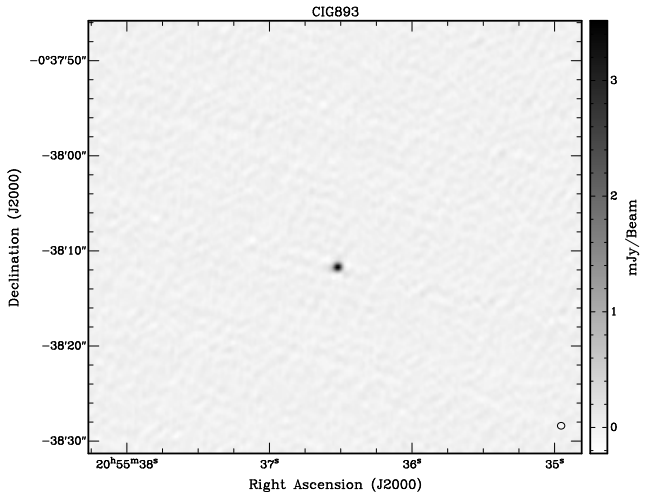

Galaxy name:		CIG 893
α (2000):	hh:mm:ss	20:55:36.51
δ (2000):	dd:mm:ss	−00:38:07.9
Type		Factor 3
Complete		Yes
Radio-excess		3.4

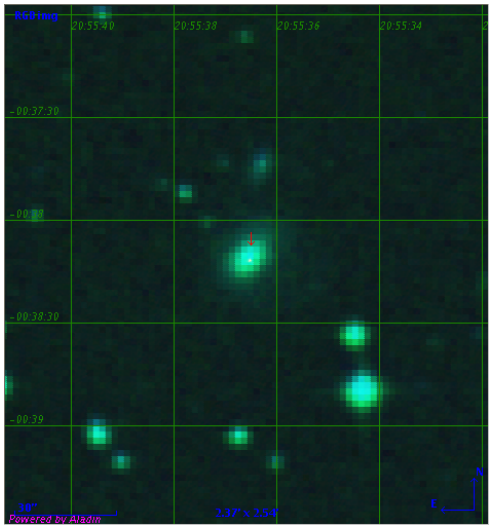

Source name:		a
α (2000):	hh:mm:ss	20:55:36.50
δ (2000):	dd:mm:ss	−00:38:11.7
Distance	($''$)	4.7
RMS	(μJy)	40
Intensity	(μJy)	3508

Determination: **OUT**
Comments: Classified as OUT but possible detection. Possible error in the position of the galaxy.

CIG 963

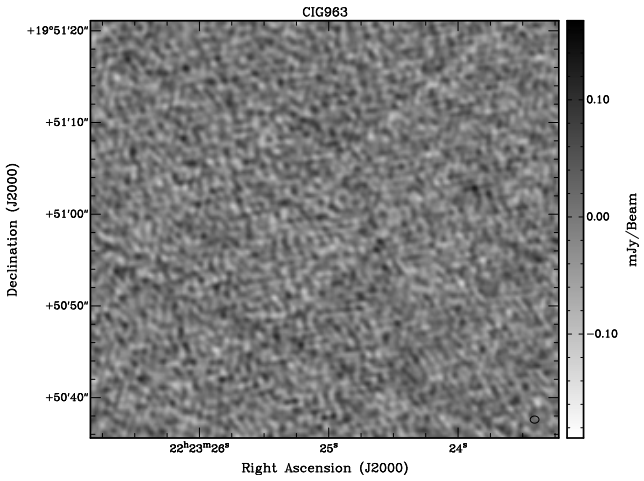

Galaxy name:		CIG 963
α (2000):	hh:mm:ss	22:23:25.44
δ (2000):	dd:mm:ss	19:50:58.6
Type		Control
Complete		No
Radio-excess		2.4

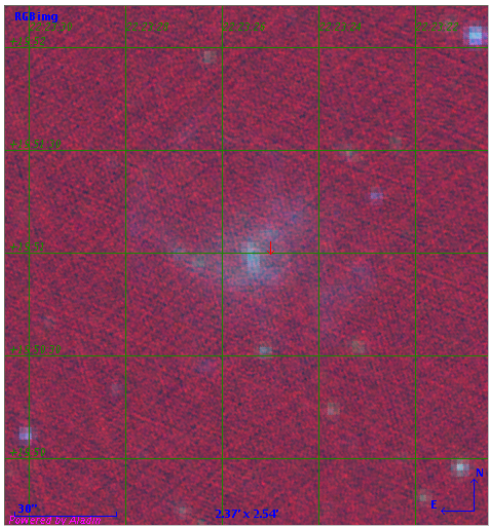

Source name:		-
α (2000):	hh:mm:ss	-
δ (2000):	dd:mm:ss	-
Distance	($''$)	-
RMS	(μJy)	136
Intensity	(μJy)	-

Determination: **NO**
Comments: Source not detected.

CIG 999

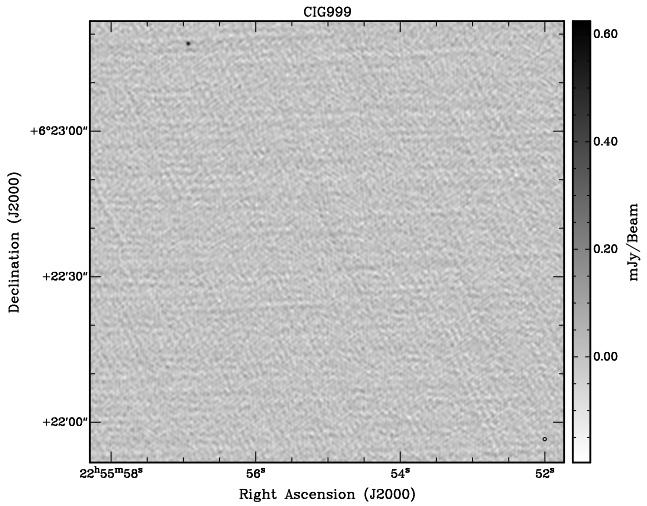

Galaxy name:		CIG 999
α (2000):	hh:mm:ss	22:55:54.96
δ (2000):	dd:mm:ss	06:22:38.2
Type		Factor 3
Complete		No
Radio-excess		3.5

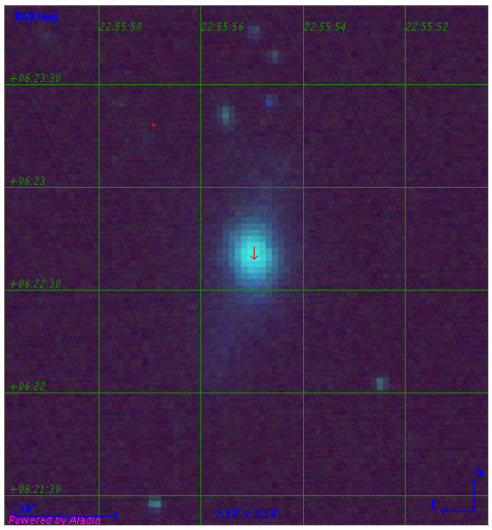

Source name:		a
α (2000):	hh:mm:ss	22:55:56.92
δ (2000):	dd:mm:ss	06:23:18.2
Distance	($''$)	49.7
RMS	(μJy)	34
Intensity	(μJy)	627

Determination: **OUT**
Comments: -

CIG 999B

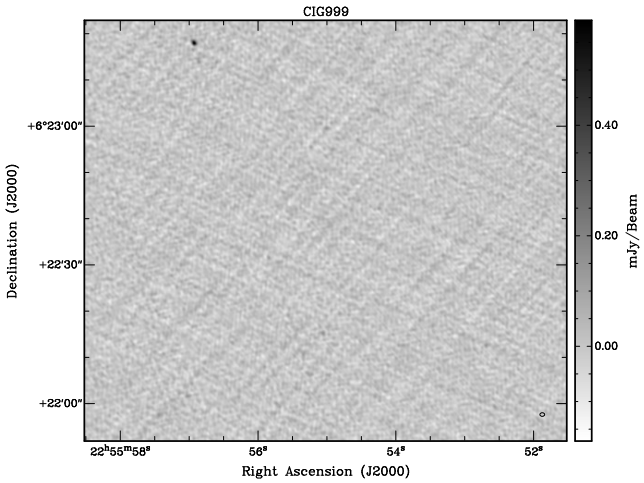

Galaxy name:		CIG 999B
α (2000):	hh:mm:ss	22:55:54.96
δ (2000):	dd:mm:ss	06:22:38.2
Type		Factor 3
Complete		No
Radio-excess		3.5

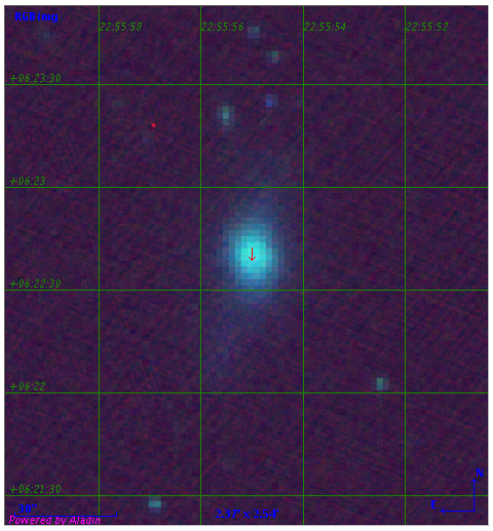

Source name:		a
α (2000):	hh:mm:ss	22:55:56.92
δ (2000):	dd:mm:ss	06:23:18.2
Distance	($''$)	49.7
RMS	(μJy)	115
Intensity	(μJy)	588

Determination: **OUT**
Comments: -

CIG 1004

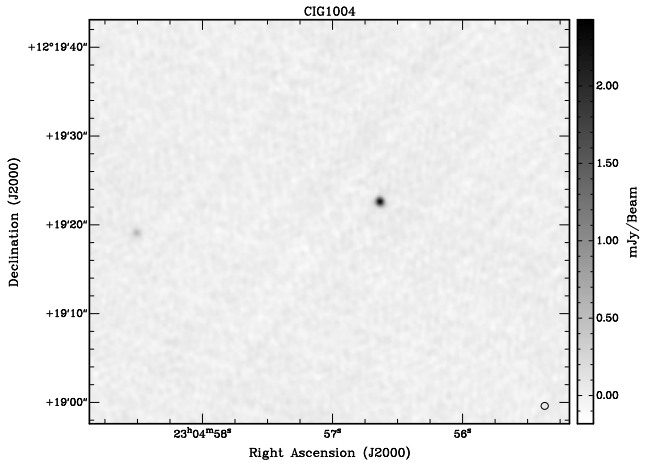

Galaxy name:		CIG 1004
α (2000):	hh:mm:ss	23:04:56.75
δ (2000):	dd:mm:ss	12:19:20.8
Type		Control
Complete		Yes
Radio-excess		1.0

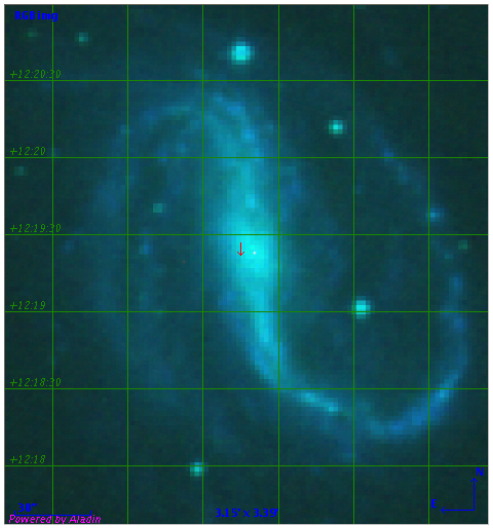

Source name:		a
α (2000):	hh:mm:ss	23:04:56.63
δ (2000):	dd:mm:ss	12:19:24.6
Distance	($''$)	4.0
RMS	(μJy)	35
Intensity	(μJy)	2422
Source name:		b
α (2000):	hh:mm:ss	23:04:58.50
δ (2000):	dd:mm:ss	12:19:19.2
Distance	($''$)	-
RMS	(μJy)	35
Intensity	(μJy)	553

Determination: **DET**
Comments: Possible error in the position of the galaxy. The coordinates of the source look accurate and in the center of the galaxy.

CIG 1045

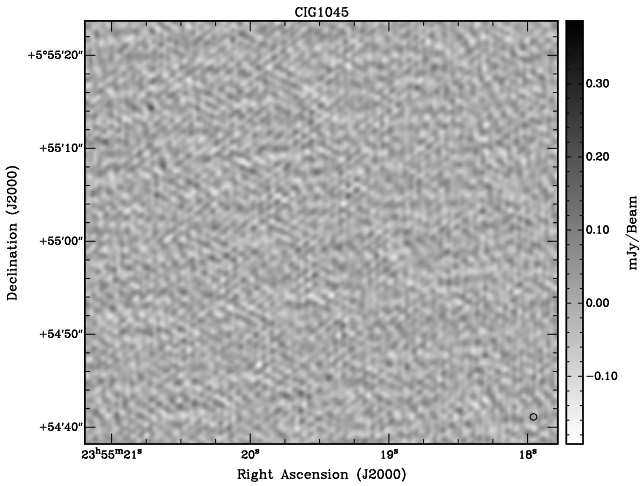

Galaxy name:		CIG 1045
α (2000):	hh:mm:ss	23:55:19.45
δ (2000):	dd:mm:ss	05:55:01.6
Type		Factor 5
Complete		Yes
Radio-excess		19.7

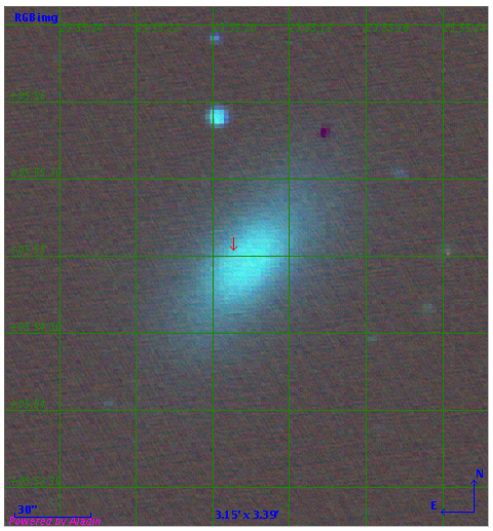

Source name:		a
α (2000):	hh:mm:ss	23:55:13.86
δ (2000):	dd:mm:ss	05:55:00.9
Distance	($''$)	83.4
RMS	(μJy)	36
Intensity	(μJy)	385

Determination: **OUT**
Comments: -

CIG 1045B

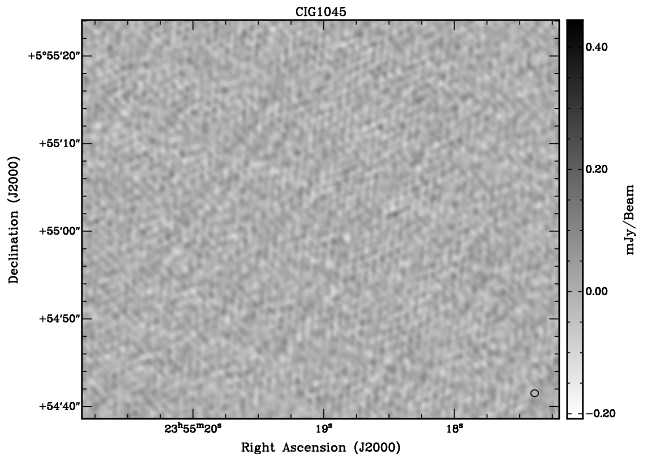

Galaxy name:		CIG 1045B
α (2000):	hh:mm:ss	23:55:19.45
δ (2000):	dd:mm:ss	05:55:01.6
Type		Factor 5
Complete		Yes
Radio-excess		19.7

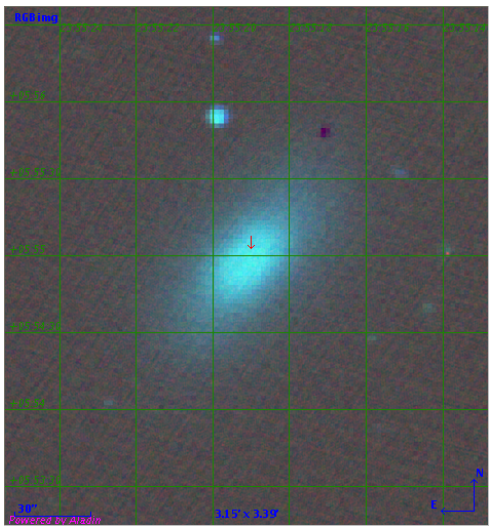

Source name:		a
α (2000):	hh:mm:ss	23:55:13.86
δ (2000):	dd:mm:ss	05:55:01.0
Distance	($''$)	83.4
RMS	(μJy)	29
Intensity	(μJy)	443

Determination: **OUT**
Comments: -

List of Figures

List of Tables

Bibliography

Adams, M. T., Jensen, E. B., & Stocke, J. T. 1980, AJ, 85, 1010 2.2

Adelman-McCarthy, J. K., Agüeros, M. A., Allam, S. S., et al. 2008, ApJS, 175, 297 7.1, 7.2

Akritas, M. G. & Bershady, M. A. 1996, ApJ, 470, 706 A.2

Akritas, M. G. & Siebert, J. 1996, MNRAS, 278, 919 A.3

Allam, S. S., Tucker, D. L., Lee, B. C., & Smith, J. A. 2005, AJ, 129, 2062 2.2

Alonso, M. S., Lambas, D. G., Tissera, P., & Coldwell, G. 2007, MNRAS, 375, 1017 1.2, 10.4

Andersen, V. & Owen, F. N. 1995, AJ, 109, 1582 10.1, 10.1, 10.1, 10.1, 10.2

Antonucci, R. 1993, ARA&A, 31, 473 1.1

Antonucci, R. R. J. & Miller, J. S. 1985, ApJ, 297, 621 1.1

Asari, N. V., Cid Fernandes, R., Stasińska, G., et al. 2007, MNRAS, 381, 263 7.4

Baade, W. & Minkowski, R. 1954, ApJ, 119, 206 1.1

Baldwin, J. A., Phillips, M. M., & Terlevich, R. 1981, PASP, 93, 5 7.6

Bertin, E. & Arnouts, S. 1996, A&AS, 117, 393 3.2

Best, P. N., Kauffmann, G., Heckman, T. M., et al. 2005a, MNRAS, 362, 25 10.2, 10.3, 10.3, 10.11

Best, P. N., Kauffmann, G., Heckman, T. M., & Ivezić, Ž. 2005b, MNRAS, 362, 9 10.3

Binette, L., Magris, C. G., Stasińska, G., & Bruzual, A. G. 1994, A&A, 292, 13 7.6

Blandford, R. D. & Rees, M. J. 1978, Phys. Scr, 17, 265 1.1

Bruzual, G. & Charlot, S. 2003, MNRAS, 344, 1000 7.4

Bushouse, H. A. 1986, AJ, 91, 255 1.2

Cardelli, J. A., Clayton, G. C., & Mathis, J. S. 1989, ApJ, 345, 245 7.4

Carter, B. J., Fabricant, D. G., Geller, M. J., Kurtz, M. J., & McLean, B. 2001, ApJ, 559, 606 10.2, 10.4

Cid Fernandes, R., Gu, Q., Melnick, J., et al. 2004, MNRAS, 355, 273 7.4

Cid Fernandes, R., Mateus, A., Sodré, L., Stasińska, G., & Gomes, J. M. 2005, MNRAS, 358, 363 7.4, 7.4

Condon, J. J. 1980, ApJ, 242, 894 4.4

Condon, J. J., Anderson, E., & Broderick, J. J. 1995, AJ, 109, 2318 10.1

Condon, J. J., Anderson, M. L., & Helou, G. 1991, ApJ, 376, 95 5.1, 10.2

Condon, J. J. & Broderick, J. J. 1991, AJ, 102, 1663 10.1, 10.1, 10.1, 10.1, 10.2

Condon, J. J., Cotton, W. D., & Broderick, J. J. 2002, AJ, 124, 675 2.3, 4.3, 4.1, 4.4, 4.4, 4.6, 5.2, 10.1, 10.1, 10.1, 10.2, 10.2

Constantin, A. & Vogeley, M. S. 2006, ApJ, 650, 727 10.4

Corbett, E. A., Norris, R. P., Heisler, C. A., et al. 2002, ApJ, 564, 650 10.1, 10.1, 10.2, 10.2, 10.2

Coziol, R., Iovino, A., & de Carvalho, R. R. 2000, AJ, 120, 47 1.2

Dahari, O. 1984, AJ, 89, 966 2.2

Dahari, O. 1985, AJ, 90, 1772 1.2

de Grijp, M. H. K., Keel, W. C., Miley, G. K., Goudfrooij, P., & Lub, J. 1992, A&AS, 96, 389 6.1

de Grijp, M. H. K., Lub, J., & Miley, G. K. 1987, A&AS, 70, 95 6.1

de Grijp, M. H. K., Miley, G. K., Lub, J., & de Jong, T. 1985, Nature, 314, 240 1.2, 6.1, 6.1

Decarli, R., Gavazzi, G., Arosio, I., et al. 2007, MNRAS, 381, 136 7.6

Dopita, M. A., Kewley, L. J., Heisler, C. A., & Sutherland, R. S. 2000, ApJ, 542, 224 7.6

Drake, C. L., McGregor, P. J., & Dopita, M. A. 2004, AJ, 128, 955 10.1

Drake, C. L., McGregor, P. J., Dopita, M. A., & van Breugel, W. J. M. 2003, AJ, 126, 2237 5.1, 10.1, 10.1, 10.1, 10.1, 10.2, 10.2

Dressler, A., Thompson, I. B., & Shectman, S. A. 1985, ApJ, 288, 481 10.4

Dultzin-Hacyan, D., Krongold, Y., Fuentes-Guridi, I., & Marziani, P. 1999, ApJ, 513, L111 1.2

Engelbracht, C. W., Rieke, M. J., Rieke, G. H., Kelly, D. M., & Achtermann, J. M. 1998, ApJ, 505, 639 7.4

Espada, D., Verdes-Montenegro, L., Huchtmeier, W., et al. 2009, In prep. 2.3

Espada, D. e. a. 2009a, In prep. 2.3

Espada, D. e. a. 2009b, In prep. 2.3

Falco, E. E., Kurtz, M. J., Geller, M. J., et al. 1999, PASP, 111, 438 2.2

Fath, E. A. 1909, Popular Astronomy, 17, 504 1.1

Feigelson, E. D. & Babu, G. J. 1992, ApJ, 397, 55 A.2

Feigelson, E. D. & Nelson, P. I. 1985, ApJ, 293, 192 A.1, A.3

Fioc, M. & Rocca-Volmerange, B. 1997, A&A, 326, 950 7.6

Focardi, P. & Kelm, B. 2002, A&A, 391, 35 10.4

Fuentes-Williams, T. & Stocke, J. T. 1988, AJ, 96, 1235 1.2

Gallazzi, A., Charlot, S., Brinchmann, J., White, S. D. M., & Tremonti, C. A. 2005, MNRAS, 362, 41 10.3

González-Martín, O., Masegosa, J., Márquez, I., Guerrero, M. A., & Dultzin-Hacyan, D. 2006, A&A, 460, 45 3.2

Hao, L., Strauss, M. A., Tremonti, C. A., et al. 2005, AJ, 129, 1783 7.4, 7.5, 10.4, 10.5, 10.4

Heckman, T. M. 1980, A&A, 87, 152 7.6

Helou, G., Khan, I. R., Malek, L., & Boehmer, L. 1988, ApJS, 68, 151 3.2

Helou, G., Soifer, B. T., & Rowan-Robinson, M. 1985, ApJ, 298, L7 5.1, 5.3

Hickson, P. 1982, ApJ, 255, 382 2.1

Ho, L. C. 1999, Advances in Space Research, 23, 813 3.2

Ho, L. C., Filippenko, A. V., & Sargent, W. L. W. 1997a, ApJS, 112, 315 7.4, 7.6, 7.6, 7.6, 10.4, 10.4

Ho, L. C., Filippenko, A. V., Sargent, W. L. W., & Peng, C. Y. 1997b, ApJS, 112, 391 10.5, 10.4

Ho, L. C. & Ulvestad, J. S. 2001, ApJS, 133, 77 1.2

Hooper, E. J., Impey, C. D., Foltz, C. B., & Hewett, P. C. 1995, ApJ, 445, 62 1.1, 5.1

Huchra, J. & Burg, R. 1992, ApJ, 393, 90 10.4

Impey, C. & Gregorini, L. 1993, AJ, 105, 853 5.1

Isobe, T., Feigelson, E. D., Akritas, M. G., & Babu, G. J. 1990, ApJ, 364, 104 5.2, A.2

Isobe, T., Feigelson, E. D., & Nelson, P. I. 1986, ApJ, 306, 490 5.2, A.3

Ivezić, Ž., Menou, K., Knapp, G. R., et al. 2002, AJ, 124, 2364 10.4

Kamp, I., Thompson, R., Conti, A., et al. 2004, ArXiv Astrophysics e-prints 2.5

Karachentsev, I. D. 1972, Soobshcheniya Spetsial'noj Astrofizicheskoj Observatorii, 7, 1 2.1

Karachentseva, V. E. 1973, Astrofizicheskie Issledovaniia Izvestiya Spetsial'noj Astrofizicheskoj Observatorii, 8, 3 2, 2.1, 3.1, 5.1

Karachentseva, V. E., Karachentsev, I. D., & Shcherbanovskii, A. L. 1979, Astrofizicheskie Issledovaniia Izvestiya Spetsial'noj Astrofizicheskoj Observatorii, 11, 3 2.1

Karachentseva, V. E., Lebedev, V. S., & Shcherbanovskij, A. L. 1986, Bulletin d'Information du Centre de Donnees Stellaires, 30, 125 2.2

Kauffmann, G., Heckman, T. M., Tremonti, C., et al. 2003a, MNRAS, 346, 1055 7.6, 7.6, 7.6, 10.2, 10.2

Kauffmann, G., Heckman, T. M., White, S. D. M., et al. 2003b, MNRAS, 341, 33 7.4, 10.3

Kauffmann, G., White, S. D. M., Heckman, T. M., et al. 2004, MNRAS, 353, 713 10.4

Keel, W. C., de Grijp, M. H. K., & Miley, G. K. 1988, A&A, 203, 250 6.1

Kellermann, K. I., Sramek, R., Schmidt, M., Shaffer, D. B., & Green, R. 1989, AJ, 98, 1195 1.1, 5.1

Kelly, B. C. 2007, ApJ, 665, 1489 A.2

Kennicutt, Jr., R. C., Roettiger, K. A., Keel, W. C., van der Hulst, J. M., & Hummel, E. 1987, AJ, 93, 1011 4.2

Kewley, L. J., Dopita, M. A., Sutherland, R. S., Heisler, C. A., & Trevena, J. 2001, ApJ, 556, 121 7.6, 7.12a, 7.12b, 7.12, 7.6, 7.6, 7.6, 10.4

Kewley, L. J., Groves, B., Kauffmann, G., & Heckman, T. 2006, MNRAS, 372, 961 7.6, 7.6, 7.6

Kolmogorov, A. 1933, Eng. Mat., 2 7.3

Krongold, Y., Dultzin-Hacyan, D., & Marziani, P. 2003, in Revista Mexicana de Astronomia y Astrofisica Conference Series, 105–105 1.2

Laurikainen, E. & Salo, H. 1995, A&A, 293, 683 1.2

Lavalley, M., Isobe, T., & Feigelson, E. 1992, 25, 245 4.3, A.3

Leitherer, C., Schaerer, D., Goldader, J. D., et al. 1999, ApJS, 123, 3 7.6

Leon, S. & Verdes-Montenegro, L. 2003, A&A, 411, 391 1, 2.2, 3.1

Leon, S., Verdes-Montenegro, L., Sabater, J., et al. 2008, A&A, 485, 475 1.3, 6, 2.3, 3.1, 3.2, 4, 5.1

Lisenfeld, U., Espada, D., Verdes-Montenegro, L., & et al. 2009, In prep. 2.3

Lisenfeld, U., Verdes-Montenegro, L., Sulentic, J., et al. 2007, A&A, 462, 507 4, 2.3, 3.1, 3.1, 3.2, 4.2, 4.3, 5.1, 5.4, 6.2

Lisenfeld, U., Voelk, H. J., & Xu, C. 1996, A&A, 314, 745 5.3

Low, F. J., Cutri, R. M., Huchra, J. P., & Kleinmann, S. G. 1988, ApJ, 327, L41 6.1

MacKenty, J. W. 1989, ApJ, 343, 125 1.2

MacKenty, J. W. 1990, ApJS, 72, 231 1.2

Maia, M. A. G., Willmer, C. N. A., Rossetto, B. M., & Machado, R. S. 2004, in IAU Symposium, Vol. 222, The Interplay Among Black Holes, Stars and ISM in Galactic Nuclei, ed. T. Storchi-Bergmann, L. C. Ho, & H. R. Schmitt, 435–438 10.4

Marcum, P. M., Aars, C. E., & Fanelli, M. N. 2004, AJ, 127, 3213 9.1

Martinez, M. A. 2008, PhD thesis, Instituto de Astrofísica de Andalucía 10.4, 10.3, 10.4

Martínez, M. A., del Olmo, A., Coziol, R., & Focardi, P. 2008, ApJ, 678, L9 7.5, 10.5, 10.4

Martinez, M. A., del Olmo, A., Focardi, P., & Perea, J. 2006a, ArXiv Astrophysics e-prints 1.2

Martinez, M. A., del Olmo, A., Perea, J., & Coziol, R. 2006b, ArXiv Astrophysics e-prints 1.2

Mateus, A., Sodré, L., Cid Fernandes, R., et al. 2006, MNRAS, 370, 721 7.4

Mauch, T. & Sadler, E. M. 2007, MNRAS, 375, 931 5.2

Menon, T. K. 1995, MNRAS, 274, 845 4.5, 4.9

Miller, C. J., Nichol, R. C., Gómez, P. L., Hopkins, A. M., & Bernardi, M. 2003, ApJ, 597, 142 1.2, 7.6, 10.4

Miller, N. A. & Owen, F. N. 2001, AJ, 121, 1903 1.2, 10.1, 10.1, 10.1, 10.2, 10.2

Montero-Dorta, A. D., Croton, D. J., Yan, R., et al. 2009, MNRAS, 392, 125 10.4

Morton, D. C. 1991, ApJS, 77, 119 7.4

Moultaka, J., Ilovaisky, S. A., Prugniel, P., & Soubiran, C. 2004, PASP, 116, 693 7.2

Niklas, S. 1997, A&A, 322, 29 5.1

Niklas, S., Klein, U., & Wielebinski, R. 1995, A&A, 293, 56 5.2, 10.1, 10.1, 10.1, 10.2

Odewahn, S. C. 1995, PASP, 107, 770 2.2

O'Donnell, J. E. 1994, ApJ, 422, 158 7.4

Omar, A. & Dwarakanath, K. S. 2005, Journal of Astrophysics and Astronomy, 26, 89 10.1, 10.1, 10.1, 10.1, 10.2

Osterbrock, D. E. & Ferland, G. J. 2006, Astrophysics of gaseous nebulae and active galactic nuclei (Astrophysics of gaseous nebulae and active galactic nuclei, 2nd. ed. by D.E. Osterbrock and G.J. Ferland. Sausalito, CA: University Science Books, 2006) 7.5, 7.6

Petrosian, A. R. 1982, Astrofizika, 18, 548 1.2

Rafanelli, P., Violato, M., & Baruffolo, A. 1995, AJ, 109, 1546 1.2

Reddy, N. A. & Yun, M. S. 2004, ApJ, 600, 695 1.2, 6.1, 10.1, 10.1, 10.1, 10.1, 10.2, 10.2

Reviglio, P. & Helfand, D. J. 2006, ApJ, 650, 717 10.4

Richards, G. T., Fan, X., Newberg, H. J., et al. 2002, AJ, 123, 2945 7.1

Rowan-Robinson, M. 1977, ApJ, 213, 635 1.1

Roy, A. L., Norris, R. P., Kesteven, M. J., Troup, E. R., & Reynolds, J. E. 1998, MNRAS, 301, 1019 5.1

Sandage, A. 1965, ApJ, 141, 1560 1.1

Sanders, D. B., Mazzarella, J. M., Kim, D.-C., Surace, J. A., & Soifer, B. T. 2003, AJ, 126, 1607 2.10

Sanders, D. B., Soifer, B. T., Elias, J. H., Neugebauer, G., & Matthews, K. 1988, ApJ, 328, L35 6.1

Schechter, P. 1976, ApJ, 203, 297 2.3

Schlegel, D. J., Finkbeiner, D. P., & Davis, M. 1998, ApJ, 500, 525 7.4

Schmidt, M. 1968, ApJ, 151, 393 3.1

Schmitt, H. R. 2001, AJ, 122, 2243 1.2

Schmitt, H. R., Ulvestad, J. S., Antonucci, R. R. J., & Kinney, A. L. 2001, ApJS, 132, 199 9.1

Schmitt, J. H. M. M. 1985, ApJ, 293, 178 5.2, A.3

Seyfert, C. K. 1943, ApJ, 97, 28 1.1

Shimada, M., Ohyama, Y., Nishiura, S., Murayama, T., & Taniguchi, Y. 2000, AJ, 119, 2664 1.2

Smirnov, N. V. 1936, C. R. Acad. Sci. Paris, 202, 449 7.3

Smith, F. G. 1951, Nature, 168, 962 1.1

Sopp, H. M. & Alexander, P. 1991, MNRAS, 251, 14P 5.1

Sorrentino, G., Radovich, M., & Rifatto, A. 2006, A&A, 451, 809 10.4, 10.5, 10.4

Stasińska, G., Asari, N. V., Fernandes, R. C., et al. 2008, MNRAS, 391, L29 7.6, 7.13b, 7.13

Stasińska, G., Cid Fernandes, R., Mateus, A., Sodré, L., & Asari, N. V. 2006, MNRAS, 371, 972 7.6, 7.13a, 7.13

Strauss, M. A., Weinberg, D. H., Lupton, R. H., et al. 2002, AJ, 124, 1810 7.1

Sulentic, J. W., Verdes-Montenegro, L., Bergond, G., et al. 2006, A&A, 449, 937 3, 2.1, 2.2, 2.1, 2.3, 3.1, 3.1, 4.2, 5.1, 10.1, 10.2

Sulentic, J. W., Zamfir, S., Marziani, P., et al. 2003, ApJ, 597, L17 4.3

Van Duyne, J., Beckerman, E., Salzer, J. J., et al. 2004, AJ, 127, 1959 4.4

Veilleux, S. & Osterbrock, D. E. 1987, ApJS, 63, 295 7.6, 7.6

Verdes-Montenegro, L., Sulentic, J., Lisenfeld, U., et al. 2005, A&A, 436, 443 1.2, 2, 2.1, 2.2, 2.3, 3.1, 3.1, 3.2, 4.2, 4.3

Verley, S., Combes, F., Verdes-Montenegro, L., Bergond, G., & Leon, S. 2007a, A&A, 474, 43 2.3

Verley, S., Leon, S., Verdes-Montenegro, L., et al. 2007b, A&A, 472, 121 5, 2.2, 3.1, 4.4, 10.1

Verley, S., Odewahn, S. C., Verdes-Montenegro, L., et al. 2007c, A&A, 470, 505 5, 2.2, 3.1, 4.4

Véron-Cetty, M.-P. & Véron, P. 2006, A&A, 455, 773 3.2

Wada, K. 2004, Carnegie Observatories Astrophysics Series, Vol. 1, Fueling gas to the central region of galaxies., ed. L. C. Ho (Observatories of the Carnegie Institution, California), coevolution of Black Holes and Galaxies 1.1

Xinfa, D., Xinsheng, M., Chenghong, L., Qun, Z., & Ji-zhou, H. 2005, ArXiv Astrophysics e-prints 2.2

Xu, C., Hacking, P. B., Fang, F., et al. 1998, ApJ, 508, 576 6.1

Xu, C., Lonsdale, C. J., Shupe, D. L., O'Linger, J., & Masci, F. 2001, ApJ, 562, 179 6.1

Xu, C. & Sulentic, J. W. 1991, ApJ, 374, 407 2.10

York, D. G., Adelman, J., Anderson, Jr., J. E., et al. 2000, AJ, 120, 1579 7.1

Young, J. S. & Knezek, P. M. 1989, ApJ, 347, L55 4.2

Yun, M. S., Reddy, N. A., & Condon, J. J. 2001, ApJ, 554, 803 5.1, 5.2, 5.3, 6.1, 10.1, 10.1, 10.1, 10.1, 10.2

Zwicky, F., Herzog, E., & Wild, P. 1961, Catalogue of galaxies and of clusters of galaxies, Vol. I, ed. F. Zwicky, E. Herzog, & P. Wild 2.1

Zwicky, F., Herzog, E., & Wild, P. 1963, Catalogue of galaxies and of clusters of galaxies, Vol. 2, ed. F. Zwicky, E. Herzog, & P. Wild 2.1

Zwicky, F., Herzog, E., & Wild, P. 1966, Catalogue of galaxies and of clusters of galaxies, Vol. 3, ed. F. Zwicky, E. Herzog, & P. Wild 2.1

Zwicky, F., Herzog, E., & Wild, P. 1968, Catalogue of galaxies and of clusters of galaxies, ed. F. Zwicky, E. Herzog, & P. Wild 2.1

Zwicky, F., Karpowicz, M., & Kowal, C. T. 1965, "Catalogue of Galaxies and of Clusters of Galaxies", Vol. V, ed. F. Zwicky, M. Karpowicz, & C. T. Kowal 2.1

Zwicky, F. & Kowal, C. T. 1968, "Catalogue of Galaxies and of Clusters of Galaxies", Volume VI, ed. F. Zwicky, E. Herzog, & P. Wild 2.1